Department of Precision and Microsystems Engineering

Design and Validation of Steer, Roll, Yaw and Sway Motion of a Kinematics-Based Bicycle Simulator

Jelle Haasnoot

Report no	: 2021.074
Coach	: Dr.ir. Volkert van der Wijk
Professor (chair)	: Prof.dr.ir. Arend L. Schwab
Professor	: Dr.ir. Riender Happee
Company supervisor	: Martin Smits
Specialisation	: Mechatronic System Design
Type of report	: MSc Thesis
Date	: 25 October 2021

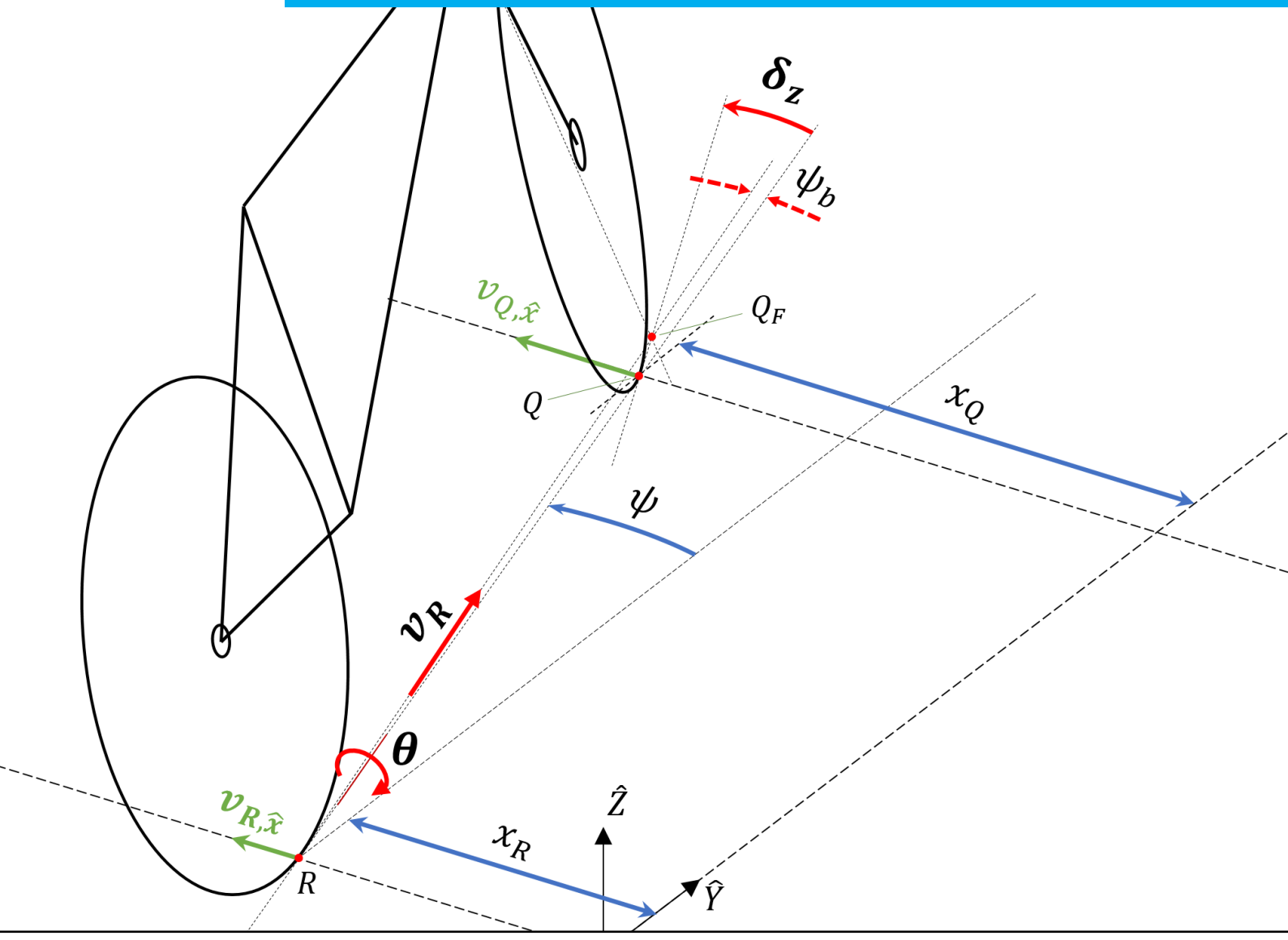

TU Delft Delft University of Technology

Challenge the future

Contents

List of Figures

List of Tables

Abstract

Bicycle simulator research has been the subject of considerable research, however, few of these attempts have integrated direct balance control and enough freedom of motion to deliver a real-world kinematic cycling experience. In this study, the B.I.K.E. (Bicycle Intrinsic Kinematics Emulator) system, a kinematic bicycle simulator, is developed with the purpose of letting its users experience realistic kinematic motion, which are: steer, roll, yaw and sway motions. This study validates the developed simulator by performing a kinematic comparison of bicycle motion among 15 participants of varying age and mass, and performs an initial subjective study to investigate effects common to indoor vehicle simulation. Manoeuvres performed by the participants are straight-line cycling, at low (5 km/h) to high (40 km/h) velocities, as well as performing a zig-zagging motion. The results show that users can successfully rely on existing bicycle skills to use the simulator. They also show that, in the kinematic sense, the simulator performs similarly to an outdoor bicycle, particularly at velocities below 35 km/h, but more work is needed in improving the vehicle model and control algorithm to accurately cover low to high-velocity cycling. Subjectively speaking, the simulator performs better than existing static solutions, but more work will be required to make the riding experience feel like real outdoor cycling.

Chapter 1

Introduction

In recent years, indoor cycling simulators (or 'trainers', used as exercising equipment) have undergone great technical improvement. These devices, which allow their users to exercise cycling indoors, provide braking resistance to an eager athlete, similar to spinning bikes and ergometers in gyms. They do so at increasingly higher accuracy and power levels with each new generation of indoor trainer. It has now become a trend among manufacturers of these personal simulators to strive for adding increasingly accurate representations of (both virtual and mechanical) bicycle motion, with some products already available on the market ([38], [23], [51]). Tacx, an experienced manufacturer of indoor cycling trainers, being no different. They initiated the study described in this report, with a request for the development of a bicycle simulator incorporating more realistic phyisical motion, allowing for a more natural recreation of a cyclist's balancing behaviour and power delivery indoors.

1.1 State of the Art: Simulators and Bicycles

Looking back at the history of studies on bicycle simulators, several of attempts at designing of a bicycle simulators incorporating physical motion have been made. Static setups with two controllable mechanical degrees of freedom on the bicycle ([15], [39], [8], [45], [30], [42], [33], [18]) appear to be the most prevalent, where usually only the rear-wheel velocity and steering angle are left as controllable to the user. Full-fledged Stewart platform-based simulators, with six or more degrees of freedom of the bicycle ([50], [14], [40], [22]) have been developed as well, but are rarer.

The focus of these simulators appears to lie with the development of a realistic virtual environment through visual input and modelled control features based on either one input (usually the bicycle's steering angle), or force-based measurements (usually the applied steering torque). None of the attempts at a realistic bicycle simulator (save for [30], [14]) report on the (lack of) kinematics or degrees of freedom of their simulators, and compared it to real-world cycling. For as far as the author's knowledge, no study has ever attempted to design a bicycle simulator with physically accurate bicycle kinematics where the rider is able to balance the bicycle directly.

The knowledge on how this balancing act works and how humans control bicycles has been around quite awhile. Schwab ([41]) provides a summary, paraphrased in this paragraph. In the past, in as early as 1820, it was found that to balance a bicycle, one had to steer into an undesired fall ([10]). Laterally accelerating the support line of the bicycle is what primarily rights it, the acceleration generated by steering the front wheel of the bicycle ([35]). In [35], it was also found that to exert a lateral force with the bicycle in turning a corner (counteracting the centripetal force in performing a circular motion), riders must also be able to lean the bicycle to compensate for this force, then afterwards compensate for this lean by steering. Upper-body lean actually contributes very little to a person stabilising a bicycle, and the largest contributor to bicycle stability is considered to be the steering input. However, at very low speeds, knee-movements also aid in the stabilisation of the bicycle ([20], [29]). Thus, the focus of this simulator's motion will lie with the integration and enactment of the degrees of freedom required for the balance of a bicycle: steer into an undesired fall (roll), resulting in lateral (sway) and yaw motion, hence accelerating the bicycle's support line and letting the cyclist balance himself.

Kinematically speaking, adopting the requirements for the motions on the to-be developed simulator from state-of-the-art knowledge on human bicycle control and providing a cyclist with the necessary tools to balance the simulator seems very feasible. However, a simulator's quality is heavily influenced by the shape and form of visual motion cueing, level of user involvement and task difficulty as well. A literature study performed by the author (Appendix F) provides insight into the influence of motion perception, visualisation and simulator application. In short, usability, quality and immersion levels of a simulator depend on these matters, with emphasis of the congruence level between visual and physical simulator motion. Including the necessity to balance the bicycle in the to-be designed bicycle simulator, as well as the addition of realistic physical bicycle motion is expected to increase the subjective realism of the simulator. Subjective quality of the simulator is not a prime concern in its development, but recording it in experiments can point us in directions of improvement and relate any usability issues to subjective matters, if and when they arise.

1.2 Goal of this Study

With the background provided above, this study will propose a development method and prototype for a bicycle simulator, where its user will be given the freedom to balance the bicycle with direct kinematic control. Concretely, the following question will be answered in this study:

How accurately does a bicycle simulator, designed for the user to balance while adopting a kinematic vehicle model, perform when compared to real-world outdoor cycling?

Where focus lies with steer, roll, yaw and sway motion, as discussed. Sustained cornering behaviour and forward accelerations are, as a result, not part of the development focus in this study. In support of the research question, an additional matter to be evaluated in this study is how a cyclist usually performs during normal, outdoor cycling for an evaluation of the performance of the prototype.

I hope to contribute to the current state-of-the-art of bicycle simulators and bicycle dynamics by proving that bicycle simulation where the balancing task of the bicycle is relayed to the user is possible. Additionally, the accuracy of existing and new bicycle models can be validated with data recorded in this study, and other new areas of exploration on the topic of bicycle simulation are provided with the results of this study.

1.3 Outline

Starting the development of the simulator, the full requirements of it are presented in chapter 2. A kinematic bicycle vehicle model will be derived based on the required motions, implemented through an actively-controlled setup, including a visualisation for the user. The steps in these developments are demonstrated in section 2.1. An independent sensor system and data analysis method will be developed as well in order to validate the kinematics of the prototype of the bicycle simulator in section 2.2.

Experiments covering a range of usual manoeuvres performed by a larger number of cyclists should provide the data required to validate the prototype. The experiments, participant demographics and procedures are outlined in chapter 3. These experiments include the recording of subjective data on the simulator's performance.

Results from experiments are shown and discussed in chapter 4, both in the kinematic and subjective sense. Finally, chapter 5 will provide conclusions based on the performed study and outline future areas of exploration based on the results that were found.

Chapter 2

Simulator Design & Validation Method

This chapter will describe the simulator design process, by starting with a definition of the simulator's requirements directly below. Following that, the kinematic vehicle model of the bicycle will derived, its implementation described and the system realisation outlined in section 2.1. The kinematic validation method, using an array of sensors, and their role in the validation of the simulation are described in section 2.2.

To rephrase the research question and reiterate the purpose of the simulator, it has to:

- Let the user have the kinematic freedom and control of the inputs of a bicycle he would have on a real road, in terms of steer, roll, yaw and sway motions.
- Defer the balancing task of the bicycle to the user, which he should be able to do similarly to when cycling on a real road.

Using the knowledge from chapter 1, these statements are transformed into concrete requirements, based on the kinematics a bicycle is subject to and a human controller acts on and with. Concretely, the requirements for the simulator and vehicle model are the following:

1. The simulator should be designed with the degrees of freedom necessary to not restrict the mechanical freedom for balancing and pedalling manoeuvres as during outdoor cycling. This means that rear-frame roll, yaw and front-fork steer should remain free to move in the simulator. Surge, heave and pitch motions are beyond the scope of this study.
2. The simulator should respond kinematically to a cyclist's control actions, through sensor-based input and state measurements, similar to how a real bicycle would on the road outdoors. The inputs are the steer angle and rear-wheel velocity of the bicycle. A motion response should follow according to a vehicle model derived from a real bicycle's geometry and no-slip boundary conditions.
3. As an input, the rear-wheel velocity of the simulator should be determined by the user and approximated forward dynamics. A braking unit should fulfil this requirement, such that a proper simulation of resistance can be provided to the user. The power required to maintain a certain velocity should be similar to what is required outdoors, although the main focus of simulator quality lies with its kinematics, rather than its kinetics.
4. A visualisation system should, coupled with the braking unit resistance and rear-wheel velocity, give the user of the simulator a sense of forwards velocity.

Additional boundary conditions are, per company requirements and wishes:

1. The simulator should support rider masses of up to 120 kgs.
2. The simulator should, in the least, approximate outdoor roll, yaw and sway motion more than the current high-end static solution produced by Tacx does.
3. The simulator should allow for a user to use his own bicycle, and accommodate most common racing bicycle frame dimensions.

The simulator system, of which the development starts in subsection 2.1.1 with the derivation of the vehicle model, will be donned the B.I.K.E. system (Bicycle Intrinsic Kinematics Emulator), and referred to as such.

2.1 Simulator Design

2.1.1 Vehicle Model

The outputs of the vehicle model, thus the (intended) motions of the simulator, will be dependent only on the kinematic states and inputs of the bicycle and of the simulator system itself. It will not implement a dynamic bicycle-rider model[1] dependent on the bicycle's and rider's masses and forcing terms, and try to stabilise that model. The balancing actor of the simulator will be the human, in order to simulate the balancing behaviour and effort humans usually employ on a bicycle (see chapter 1).

We start with the definition of a coordinate system and variables for the vehicle model in Figure 2.1. Boldfaced variables denoted with red arrows are (direct or indirect) inputs of the vehicle model. Dashed variables, such as ψ_b and δ, are directly related to other inputs by geometry. Blue arrows denote additional states of the bicycle, becoming important during the implementation stage of the vehicle model. Green arrows are the outputs of the bicycle states and inputs, i.e. the to-be controlled contact points of the bicycle with the ground.

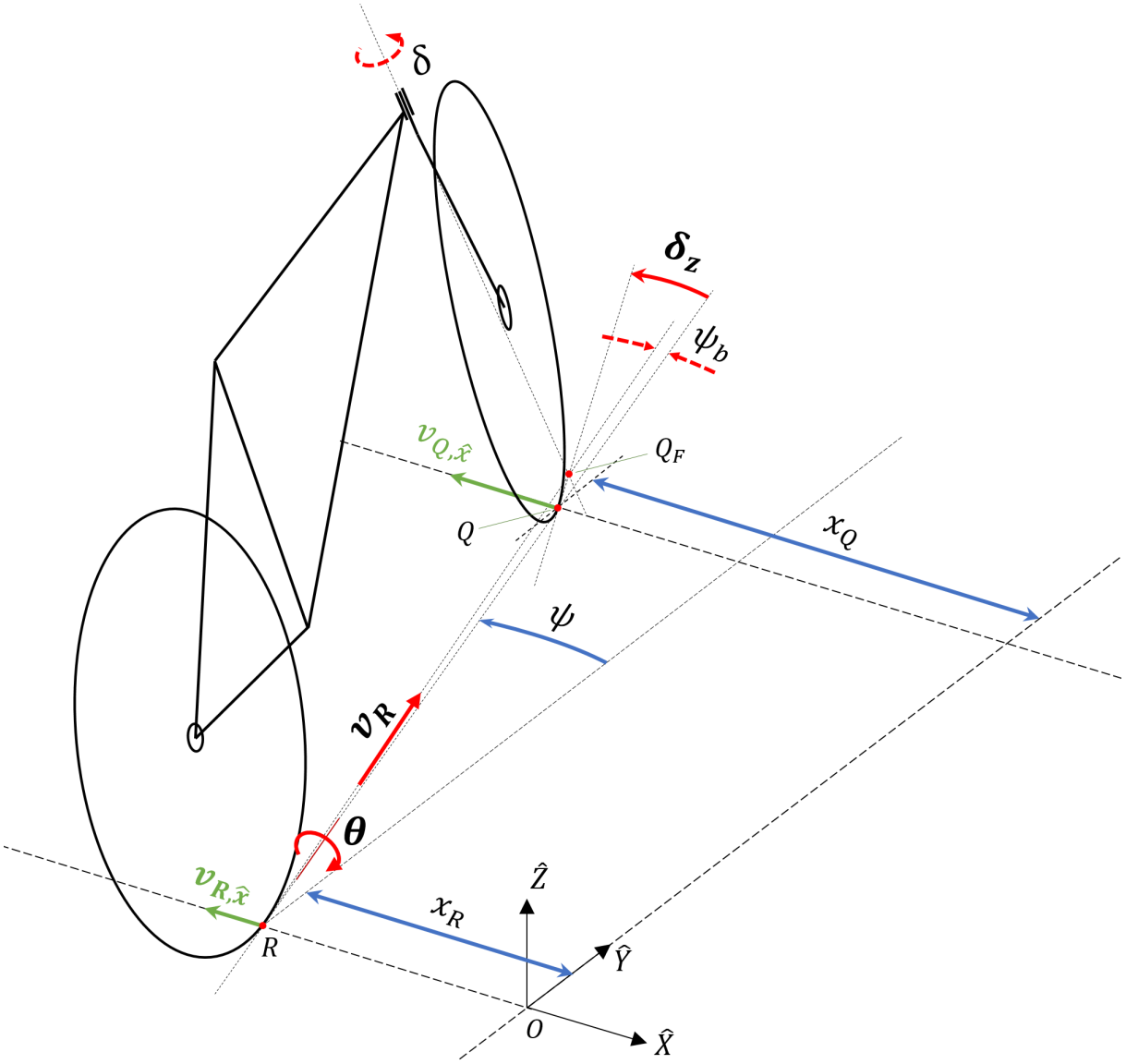

Figure 2.1: Bicycle definition of variables. Colours indicate variable types. R denotes the rear-wheel contact point with the ground, Q the front. O is the origin of the frame $\hat{X}\hat{Y}\hat{Z}$, fixed in orientation but moving along the $\hat{Y}$-axis with point R.

[1]Dynamic bicycle-rider model, a full set of the equations of motion of a combined bicycle-rider system. The Whipple model is an example, with a fixed-rider assumption and a subdivision of the bicycle into a multibody system of four parts, each with their own mass, inertia and forcing terms (see [3] for a recent review on bicycle dynamics and modelling, including the Whipple model)

In Table 2.1, the declared variables are given a description and symbol. These variables will be used in the derivation of the controlled outputs of the simulator, as well as the description of the controller.

Table 2.1: Description of variables. Indicated are the variable symbol, its unit and a description of the variable

Symbol	**Units**	**Description**
δ	rad	Steer angle steer axis
δ_z	rad	Steer angle $\hat{X}\hat{Y}$-plane
θ	rad	Roll angle, around $R \rightarrow Q$-axis
ψ	rad	Bicycle yaw angle
ψ_b	rad	Steer-caused yaw angle
v_R	m/s	Rear-wheel velocity, along $R \rightarrow Q_F$
$x_R,\ x_Q$	m	Position along $\hat{X}$ points R, Q
$v_{R,\hat{x}},\ v_{Q,\hat{x}}$	m/s	Velocity along $\hat{X}$ points R, Q

The given description of the bicycle states and controlled outputs depend on, in addition to the restrictions and boundary conditions assumed in section 2.1, the dimensions of the bicycle the simulator is used with. These are visualised in Figure 2.2:

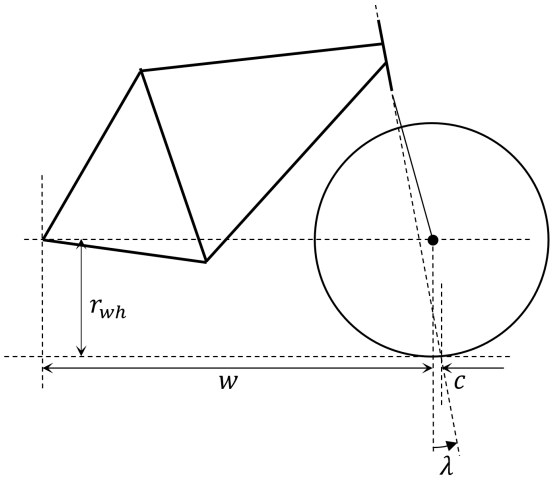

Figure 2.2: General dimensions of a bicycle. Indicated are the bicycle's wheel radius r_{wh} [m], the wheelbase of the bicycle w [m], the trail length of the bicycle c [m] and the head angle of the bicycle λ [rad].

Assuming a rigid-body model and no-slip boundary conditions for the wheel-ground interactions, the derived outputs of the rear and front wheel lateral velocity $v_{R,\hat{x}}$ and $v_{Q,\hat{x}}$, computed from the bicycle states v_R, δ_z and ψ, are the following for the rear and front wheel ground contact points, R and Q, respectively:

$$\vec{\mathbf{v}}_{R,\hat{x}} = -\sin(\psi_b + \psi) v_R \tag{2.1}$$

$$\vec{\mathbf{v}}_{Q,\hat{x}} = \frac{-\sin(\delta_z + \psi) v_R}{\cos(\delta_z)} \cos(\psi_b) \tag{2.2}$$

Where the nonlinear term ψ_b is a derived value from δ_z, w and c. δ_z is used for convenience, since the sensor implementation of the simulator will be oriented as such. The full derivation of ψ_b, Equation 2.1 and Equation 2.2 and the relation between δ and δ_z are given in Appendix B.

In literature, a set of kinematic equations for a bicycle are presented in [26]. Another common model is the inverted pendulum bicycle model, described in [3]. These kinematic descriptions are usually linearised for subsequent analyses and simplified mathematics. Here, the equations derived by the author are left as-is, for now, since no full analysis of the model is performed beyond its implementation, and the digital implementation of the model allows for nonlinear terms. Chapter 4 will show a comparison between these models and results measured. The author's model, when linearised, is identical to the inverted-pendulum model (save for the ψ_b correction), but uses δ_z instead of δ, which is oriented differently.

2.1.2 Simulator Control Structure

Now the basic structure and dependencies for the required motion of the B.I.K.E. system is present in its vehicle model, we can take a step back and take a look at all the elements required in the simulator from chapter 1. More subsystems are added to satisfy the set requirements and to close the loop between the drive algorithm, the cyclist's actions and the simulator's motions and states, for a safer, less intrusive and more intuitive simulator experience for the user.

The complete functioning of the B.I.K.E. system (with a physical rider-cyclist combination in the loop) will, in basic terms, be structured as in Figure 2.3, with a description of the added elements below it. Note the reference to the control of the front support point not being denoted with Q, but F. This is due to the fact that in the electromechanical system, the point where the front of the bicycle is actuated and point Q do not correspond. Equation 2.3 compensates for this difference.

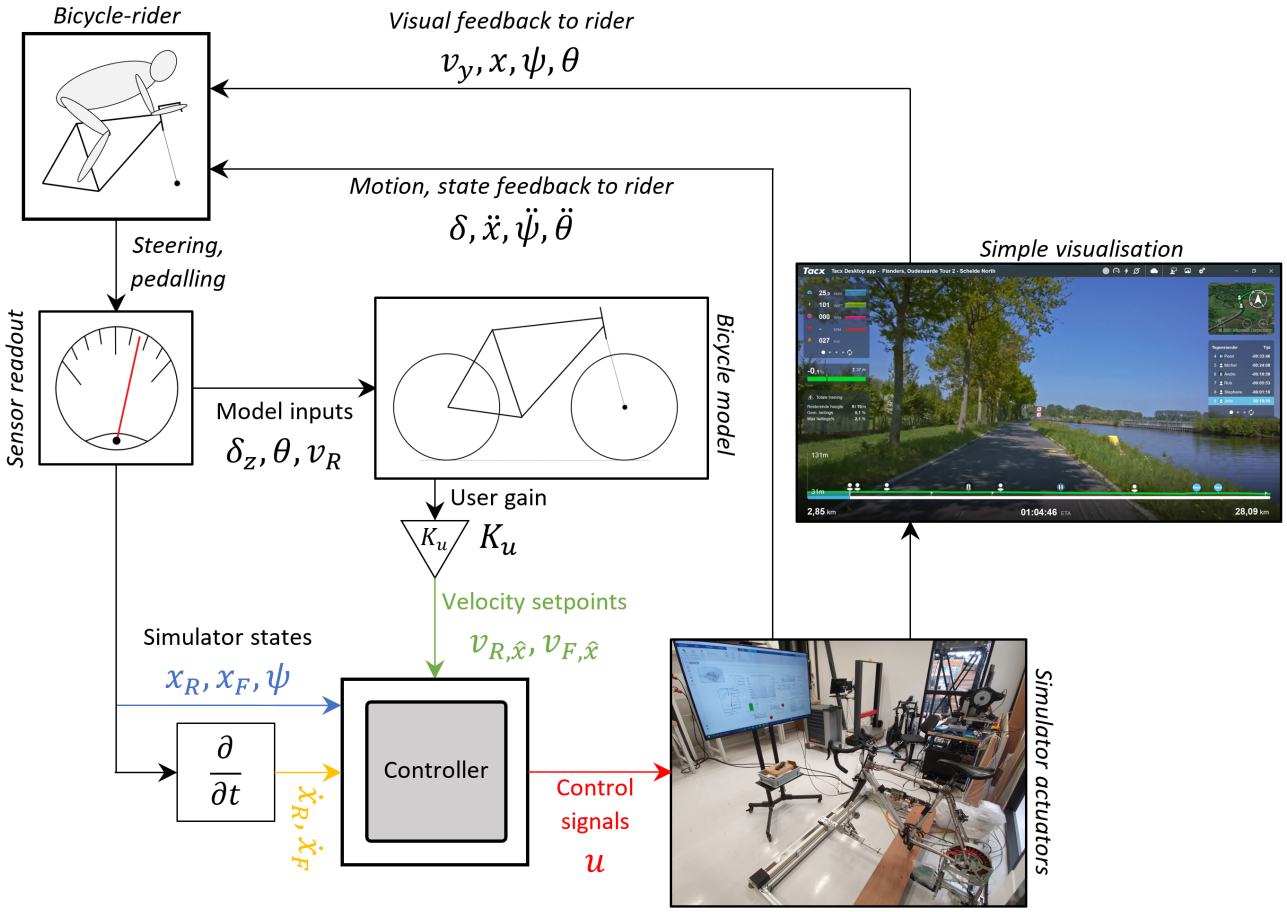

Figure 2.3: Basic controller scheme of the bicycle setup. $v_{R,\hat{x}}$ and $v_{F,\hat{x}}$ indicate the generated setpoints for velocity, $\dot{x}_R$ and $\dot{x}_F$ the actual physical motion. Arrows indicate information streams, and are given with a description.

The controller block in Figure 2.3 enacts the bicycle model, but it also has to inhibit this motion in order to not let the user reach the ends of the operating range of the simulator. It consists of a dual P-controller, one of which reduces the actuator velocity error, and the other controls the actuator position as a return-to-zero enforcer. This position controller acts on the displacement between a desired and actual position of either point R or Q. A schematic representation of the controller block from Figure 2.3 is shown in Figure 2.4. Coloured arrows refer to the connections in the main control algorithm in Figure 2.3.

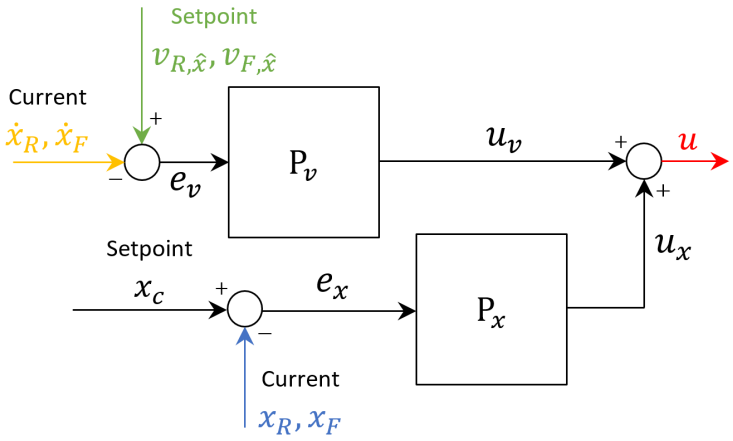

Figure 2.4: P-controllers of the simulator control algorithm. Note: these controller schemes apply to both the rear and the front actuators.

P_v is the proportional controller that will act upon the difference between the setpoint and actual actuator velocity $v_{R,\hat{x}} - \dot{x}_R$ (similarly to the front $v_{F,\hat{x}} - \dot{x}_F$). This difference could, for example, originate from the added dynamics of the actuator and simulator hardware. P_x is the proportional controller which acts on the error between $x_c - x_R$ (similarly, $x_c - x_F$), where x_c is a constant position setpoint. The resulting control signal u is converted to a voltage and sent to the respective actuators of the electromechanical system (fully described in subsection 2.1.3).

Studies describing vehicle simulator dynamics usually incorporate a washout algorithm[2] in addition to the return-to-zero algorithm (e.g. [13], [7], [43], [46]). In the B.I.K.E. system, the washout algorithm will be implemented only if and when a lack thereof will make the simulator unusable for participants, leaving the initial control scheme as free as possible.

Since the vehicle model only has the increasing sensitivity to a steering input and increasing rear-wheel velocity with an increasing virtual velocity to indicate to the user what his forwards velocity is (thus making external visualisation a requirement of the simulator), the final added element to the simulator will be a visualisation of an outdoor environment, to present the user of the simulator with a sense of forwards motion. When v_R increases, the visualisation also speeds up its display of the environment. More details on this visual system are given in subsection 2.1.4.

Thus, information provided to the user about the bicycle he is currently controlling is two-fold: on the one hand, the user is now provided with visual information in multiple regards; by what is visible on the screen, and by what is stationary around it. A human's peripheral vision, using the concept of optic flow[3] is used for an estimation of forward velocity v_y (not necessarily an accurate estimate of v_R, see Appendix F for a description of limitations). At the same time, using the monitor outline and the world around it, the user of the simulator is also provided with external reference of how he and the bicycle are located (x) and oriented (ψ, θ) with respect to the screen. These visual elements are provided to the bicycle-rider system from the visualisation block in Figure 2.3.

On the other hand, the user is physically actuated externally, where he can use his physical motion sensors to obtain information to act upon. A cyclist usually uses proprioceptive[4] and vestibular[5] sensors to obtain information on the current steering angle δ from proprioception, and sideways acceleration $\ddot{x}$, yaw angular acceleration $\ddot{\psi}$ and roll-rate $\dot{\theta}$ in a bicycle from the vestibular sensors (cycling control loop modelled by [28]).

[2] A washout algorithm removes low-frequency content from motion control signals of a vehicle simulator. Usually applied when perceptive realism of the simulated vehicle is required (e.g. flight simulation). See Appendix F for an overview.

[3] Optic flow is the "flow" of the outside world along a human's eye, and generally used for a velocity estimate, although there are limitations. See Appendix F for an overview.

[4] Proprioceptive sensors are sensors in the body related to sensing force and displacement; an example are the muscle spindles, which sense muscle length and velocity. See Appendix F for an overview.

[5] The inner-ear vestibular sensors provide linear and angular acceleration information to the brain the head is currently undergoing. A human is able to integrate those acceleration signals to obtain a velocity estimate. See Appendix F for an overview.

2.1.3 Electromechanical Design

The electromechanical implementation of the control scheme of subsection 2.1.2 should fulfil the requirements set in chapter 1. Mechanically speaking, the B.I.K.E. system should allow the user freedom in rolling, steering his bicycle. The mechanical mounting system for the bicycle frame is designed as such, leaving the bicycle free to roll and steer, and directly measuring those rotations as well. The mounted bicycle is to be connected to a resistance unit (a disassembled Tacx Neo 2T indoor trainer, functioning as a standalone braking unit), which applies a certain braking power related to the user's pedalling power and rear-wheel velocity, providing a sense of velocity to the user and requiring a relatively realistic effort from the user.

A twin-railed actuator configuration was picked for its independent controllability, should individual augmentations need to be made to only the front or rear actuator. A minimum performance is required for each of them, when driving points R and F. Pilot measurements (performed with the system described in Appendix A) combined with the maximum allowed rider mass requirement of 120 kg prescribes the minimum actuator performance in terms of force, acceleration and velocity. A design safety factor of approximately 2.3 is used for the lateral force. Having picked and designed custom parts based on these and other company requirements (set in chapter 2), waited for the orders to arrive and assembled the mechanical parts, the B.I.K.E. system ended up as in Figure 2.5.

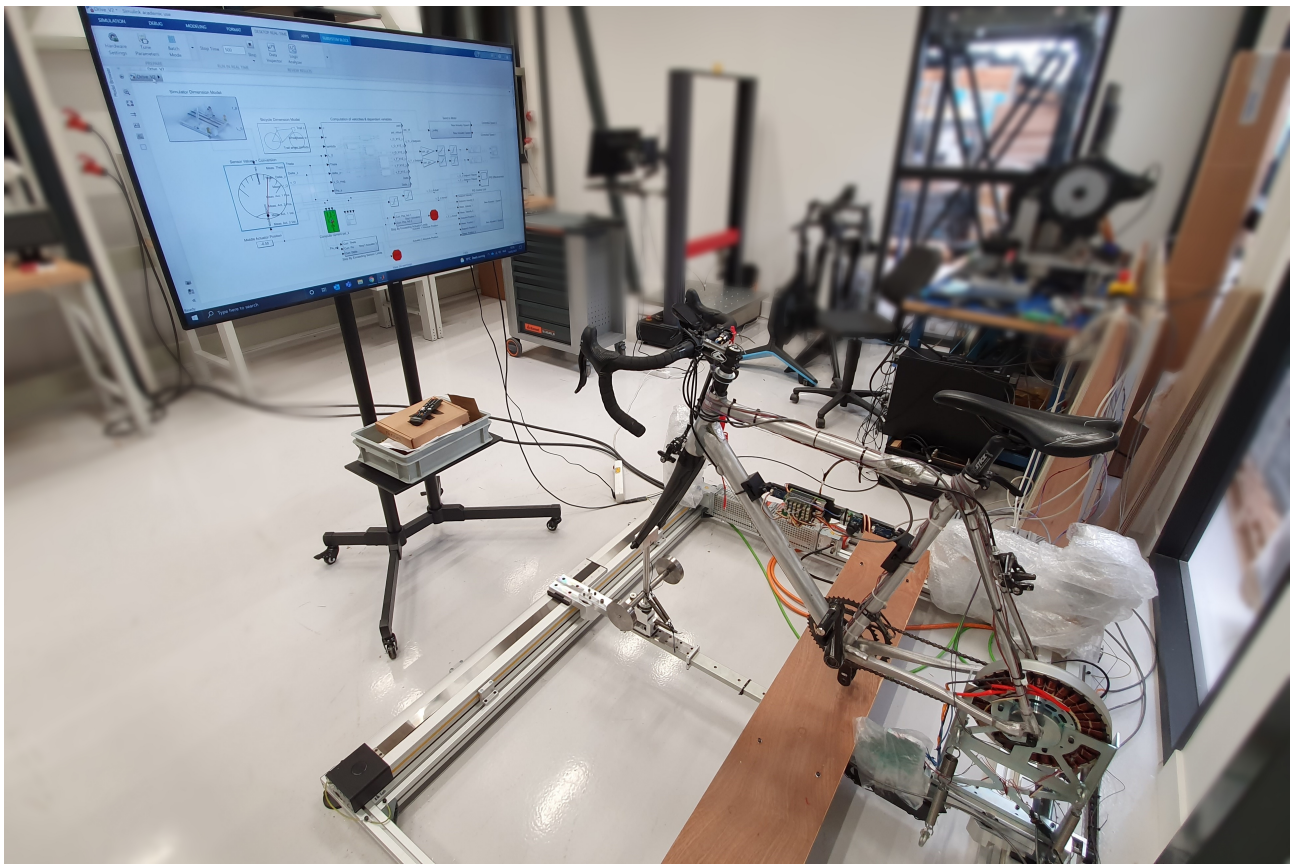

Figure 2.5: Bicycle simulator, realised. The visualisation screen, the used bicycle frame and the electromechanical system are visible. Springs at the rear of the bicycle keep the bicycle in its upright position, and a mass-spring combination at the front of the bicycle provides steering resistance to the user.

The actuators which were picked based on the force-acceleration requirements are a set of Parker OSPE32BHD linear positioners ([31]). In section E.6, the properties of the electromechanical components of the bicycle simulator are described in more detail, as well as the safety functions that were implemented with it.

Beneath the front fork support, a linear guide is used to allow bicycles with different wheelbases to be mounted. To the front fork support, additional masses and springs are attached to simulate an approximated inertia and gyroscopic torque normally generated by an aluminium front wheel at standstill. The accuracy of the torque generated by the springs is not expected to be high, and not validated, since producing accurate steering kinetics is outside of the scope of this study. It purely serves as a stabilising torque for the front fork here, and provides resistance for the user to feel to make the steering response feel a bit more natural and stable. Another set of springs at the rear of the bicycle keep it upright without a rider, and compensate for the weight of the resistance unit, but only just, to minimise interference with the rolling behaviour of the user. A slight roll angle of $\theta \approx 5^{\circ}$ is sufficient to knock it over its balancing point.

The vehicle model from subsection 2.1.1 is implemented in this mechanical setup with the direct measurement of δ_z and θ with potentiometer rotation sensors. Conveniently, the resistance unit uses permanent magnets in its rotor, of which the change in magnetic field can be measured with a HALL-sensor. Thus, a direct measurement of the rear-wheel velocity v_R is available as well. All sensor signals are filtered, using low-pass filters of different passbands frequencies and order, optimising the trade-off between remaining signal noise and filter group delay.

The only required change to the derived bicycle model is the extrapolation of the velocity of point Q to the point of actuation on the front actuator, point F, since the bicycle is not directly supported with an actuator at point Q (see Figure 2.1). Using Equation 2.2, the derived yaw-rate as a result of the geometric relation between the rear and front wheels, and a set distance between the front and rear mounting points R and F along the $\hat{Y}$-axis (denoted L_0, the distance between the mounting points of the front and rear actuators), we obtain the controlled velocity at point F in Equation 2.3. The full derivation is outlined in Appendix B.

$$\vec{\mathbf{v}}_{F,\hat{x}} = -\frac{L_0 \sin(\delta_z - \psi_b) v_R}{w \cos(\theta) \cos(\delta_z)} - \sin(\psi_b + \psi) v_R \tag{2.3}$$

With this augmentation, the control algorithm is ready to be implemented using National Instruments PCIe-6353 I/O hardware, running on MATLAB Version 2020b on a Dell Precision 5820 workstation. This workstation uses an Intel i9-10920X 12-core CPU and 128GB of DDR4 RAM. Using MATLAB's SIMULINK Desktop Real-Time extension, real-time, high-speed communication with the hardware is possible. For a visualisation of the layout and exact components of this algorithm, please refer to section E.6.

2.1.4 Visualisation

A component of the full system loop that needs to be emphasised is the visual system, due to its potential influence on the usability of the simulator. To mimic a visual environment experienced by the participants of this study outdoors, we opt to use a visualisation system displaying a prerecorded activity. Using an external display[6], placed centred with the linear actuators (see Figure 2.6 for a representation). The middle of the screen is at $y_c = 1.29$ m from point Q, vertically. The participants' eyes are offset with $y_o = 0.32$ m vertically, $x_c = 1.09$ m horizontally. This creates a horizontal field of view of $F_h = 58.8°$ (when the participant is centred with the middle of the screen), and a vertical field of view of $F_v = 33.3°$, rotated downwards approximately 15.9° with respect to the horizontal view.

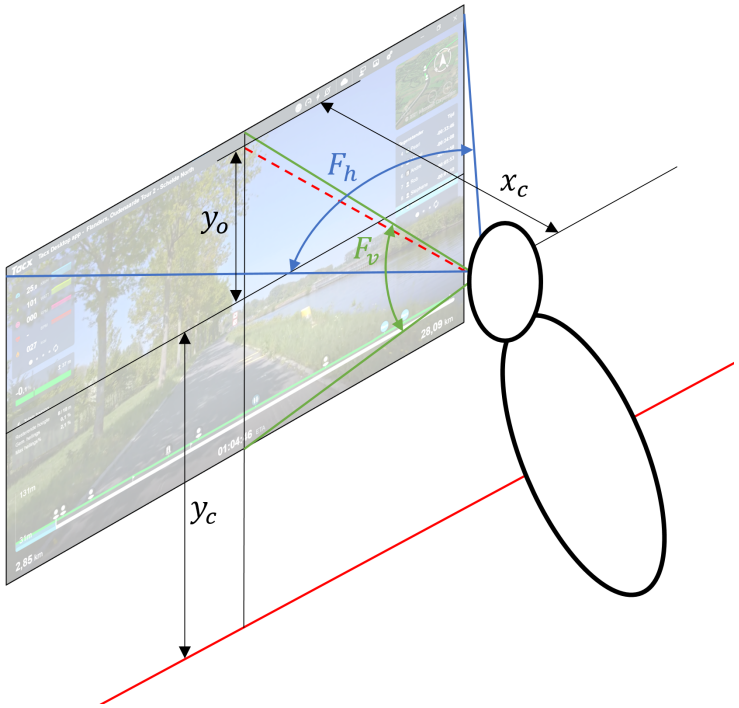

Figure 2.6: Schematic representation of visual system of bicycle simulator (not to scale). Indicated are the vertical and horizontal fields of view, as well as the vertical offset of the screen. The dashed red line indicates viewer's eye-level.

The current visualisation software ([44]) was picked for its availability, its resemblance to the outdoor experimentation environment and its ease of application with the used resistance unit. More abstract, third-person view options exist (e.g. [51]), and since no attempt is made in this study to really immerse the user of the simulator in the virtual environment, creating a deliberate disconnect between the simulator's motion and the visual system may immerse the user just as well or better than the current solution.

An external monitor was preferred over a head-mounted display, since a head-mounted display brings a number of challenges to overcome in developing the simulator. First of all, a virtual reality environment would have to be developed, taking up a large amount of time. Moreover, the vehicle model would have to be augmented to allow for a sustained yaw angle ψ, also requiring a change of the return-to-zero controller to allow for this sustained orientation change.

Furthermore, incongruousness between visual and (a lack of) physical motion in a vehicle simulator can incite high levels of simulator sickness. This could be due to the motion not being the same as the expectation from previous experiences ([36]), or the frequency content of the incongruence between visual and physical motion being in the same frequency range as human postural control ([11]). Even just the lack of motion can cause simulator sickness, although this is dependent on the person ([48]). Using an external monitor over a head-mounted display generally decreases simulator sickness incidence, but also sense of immersion and realism ([13], [27]). Using an external display gives the participant solid visual reference for his actual motion, largely eliminating the mismatch between visual and physical motion ([13], [34]).

[6]External 55" monitor, 4K resolution monitor (outline 1.228 × 0.702 m, width by height)

2.2 Measurement Design

Completing the vehicle model, control scheme and hardware implementation of the simulator system is half the battle in completing this study. The simulator is validated by comparing how cyclists ride it with how they ride a bicycle outdoors. The foundation for this comparison lies with the kinematics of the bicycle. The control system of the bicycle simulator is kinematics-based, thus comparing kinematic properties instead of forces is expected to be easier. A measurement of the (coupling of a) bicycle's states during a certain manoeuvre is used to compare outdoor cycling, the simulator and, per the minimum performance requirement of the company (chapter 2), a static setup.

2.2.1 Sensors and Implementation

Due to time constraints, and it also not being an intrinsic part of this study, the measurement system for collecting this data is largely based on tried-and-true iterations of such a system ([28], [4], [5], [47], [9], [37] and [21]) with the omission of steer-torque measurements and addition of crank torque, crank velocity and rotation angle measurements. In Appendix A, the sensor system and basic data processing of the used measurement system is described. The measurement system is available visually in Figure 3.2. In this section, data will be considered as if it were measured in bicycle-fixed coordinate system, in the correct units and pre-filtered. The sensors used to collect kinematic data are the following:

1. Two 6-axis Inertial Measurement Units (IMU's), which measure acceleration and angular rates in a 3D coordinate system ($\vec{\mathbf{a}}_{I,r}, \vec{\mathbf{a}}_{I,f}, \vec{\boldsymbol{\omega}}_{I,r}, \vec{\boldsymbol{\omega}}_{I,f}$, subscripts indicating rear and front IMU's). The IMU's are located at the red squares in Figure 2.7:

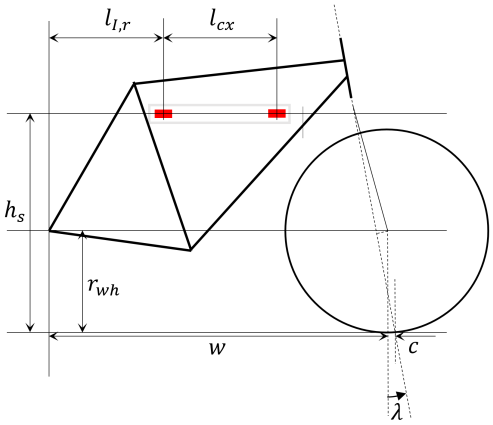

Figure 2.7: IMU placement within bicycle, as red squares. Oriented with one measurement axis aligned with gravity, when bicycle is level. More base bicycle and placement dimensions given, as well.

2. One measurement potentiometer, which measures the steering angle of the bicycle front frame (δ).
3. One Hall-effect sensor, which detects changes in magnetic field caused by magnets fixed to a bicycle wheel's, which in turn can be turned into a velocity measurement (v_R).
4. One set of Garmin Rally 200 measurement pedals, which, in a specific debugging configuration, record raw pedal angular acceleration, angular velocity, crank angle and crank torque values ($\alpha_T, \omega_T, \theta_T, T$). Limited memory is available on the bicycle pedals, which limits the experiment duration to about one hour, requiring the sets of pedals to be switched out between experiments if they get close to filling up the memory.

The sensors used provide, after data processing, an estimate of the orientation, velocity and accelerations the bicycle is undergoing at a certain time (see Appendix A for the data processing steps). These include the vehicle model inputs and states used in the vehicle model described in subsection 2.1.1: steer angle δ[7] and rear-wheel velocity v_R. With this data, we can obtain an estimate of the relations between these inputs, and the resulting bicycle states in terms of roll, sway and yaw motions. The process of obtaining this relation is described in subsection 2.2.2.

[7]Note: not the same as the used δ_z, but related to δ through bicycle geometry (see Appendix B for a mathematical definition).

2.2.2 System Identification & Comparison

As kinematic data on the bicycle's motions is generated for a certain cycling experiment, we can use this data to compare different cycling situations (for example, outdoor cycling and using the bicycle simulator). We measure only the bicycle's motions and orientation, but we have to consider the bicycle's motion to be a product of the bicycle's geometry and the person who is using it.

With this notion, we are able to verify whether the kinematics of the bicycle-rider combination, during several manoeuvres, show similar behaviour when performing these manoeuvres outdoors or when we add the dynamics of the vehicle model and electromechanical actuators to it. The comparison between datasets, recorded for a certain participant performing a certain cycling manoeuvre, is based on the following two mathematical measures:

1. **Frequency-Dependent Model Estimation**: For all manoeuvres and cycling situations, a certain linear relation can be derived for a bicycle-rider combination which approximates the kinematics fairly accurately. This linear relation uses the description of a discrete-time State-Space model. This method has been used in the past, and lower-order models are still able to approximate bicycle dynamics fairly accurately ([28]). Focusing on the kinematic behaviour of this system, we need to select a number of measurable in- and outputs measured on the bicycle to be able to predict and reproduce the behaviour of the bicycle-rider system from the inputs. Observing differences between approximated systems in different cycling situations shows whether or not the bicycle-rider system behaves similarly to outdoor cycling, and whether frequency-dependent anomalies exist between situations. The bicycle model is derived using a grey-box estimation algorithm, MATLAB's SSEST function.
2. **Frequency-Dependent Coherence Between Measured Variables**: The magnitude-squared coherence is an indicator of how two signals are correlated by comparing the spectral decomposition of those two signals. With this, we can compare how well in- and outputs are correlated with a simple frequency-dependent metric. The coherence is obtained using MATLAB'S MSCOHERE function.

A full description of the method, initialisation and mathematics involved with the above two metrics, refer to Appendix C.

It is not possible (in the current study configuration) to robustly quantify a participant's performance of a certain balancing task during a certain manoeuvre, since there is no quantifiable external disturbance or task presented to the participant (except for just that: balancing the bicycle and maintaining a certain velocity). It *is* possible to observe differences in the response of the bicycle-rider system when considering measurable inputs, states and outputs of the bicycle, controlled by the rider.

Two sets of inputs and outputs are picked, to relate information on bicycle-road interactions as well as internal kinematics of the bicycle. The first set, because this study focuses on the kinematic sway, yaw and roll motion, considers the following inputs and outputs:

Table 2.2: Input and output signals for the system identification of intrinsic bicycle-rider kinematics. See Figure 2.1 for definition of these variables.

Parameter	**I/O**	**Description**
δ	Input	Steering angle $[rad]$
$a_{R,\hat{x}_P}$	Output	Lateral Acceleration R $\left[\frac{m}{s^2}\right]$
ψ	Output	Yaw angle $[rad]$
$\dot{\psi}$	Output	Yaw rate $\left[\frac{rad}{s}\right]$

$a_{R,\hat{x}_P}$ (referred to as $a_{O,\hat{x}_P}$ in Appendix C) considers the lateral acceleration of point R, perpendicular to the travelling direction of the rear wheel.

The second set of inputs and outputs is the roll-steer relation (input δ to output θ). These comparisons can tell us whether, mechanically, the bicycle-rider system still acts like one on the simulator, or that the simulator induces a large enough change in control behaviour that we can observe it in this relation. Humans have been found to operate bicycles differently based on level of experience ([4]).

All recorded datasets are sliced between certain timestamps where the velocity of the cyclist is within the range of the current to-be attained velocity, or is at least constant for the duration of the manoeuvre. The δ input and $a_{R,\hat{x}_P}, \psi$ and θ outputs are de-trended with a linear relation (as in $y = ax + b$) over a certain manoeuvre window, to remove drift or offset effects, as well as improve the state-space estimation accuracy. This alteration is justified with the notion that higher-frequency signal content (> 0.5 Hz, observed from experiments, increasing with cycling cadence) relates to the balancing kinematics of the bicycle-rider system, and we are not interested in very low-frequency (< 0.1 Hz) content of these signals (since those cannot be reproduced on the simulator). Input and output signals are always visually inspected before the derived signals and systems are approximated, to verify the effect of the above operations. Bad or incomplete data are omitted from results.

Chapter 3

Experiments

The functioning of the simulator and the implementation of a measurement system with its related data analysis methods have been clarified. Pilot experiments have shown that the simulator works and is usable for cyclists after a brief introduction and accustomisation period with the simulator. A report on how participants responded is present in chapter 4.

In order to obtain data on how well the simulator performs, and in which regards it is still lacking, experiments are performed with a subject pool of 15 participants. This chapter describes the experimental procedures for all participants. We focus on the participants, the experiments themselves, the subjective data that is recorded and the processing of that data afterwards.

3.1 Participants

15 participants are invited based on outdoor and indoor cycling experience, as well as availability both in and outside the graduation company, to try and obtain a larger pool of cyclist ability since it has been shown that cyclists control bicycles differently based on experience ([6]). A participant's cycling experience is categorised with the yearly average distance travelled on any bicycle. With the recording of this data, subjective scores, as well as differences in kinematic cycling behaviour may be explained in the results. The participants are not compensated for the experiment, and their personal data (age, gender, bicycle type, cyclist experience) are pseudonymised. The following table represents participating pool of subject demographics:

Table 3.1: Participants for the experiments, their age, sex, cycling experience and mass indicated. (*): Additional dataset available from the author in pilot experiments.

Participant number	**Age**	**Sex**	**Cycling Experience**		**Mass (kg)**
			Indoors	Outdoors	
001	24	M	1	4	80.5
002	26	M	3	4	79
003	31	M	3	4	74
004	28	M	2	1	104
005	24	M	1	2	73
006	25	M	1	3	69
007	23	M	1	2	86
008	25	M	1	2	83
009	23	M	1	3	103
010	27	M	1	2	94
011	21	M	1	4	73
012	28	M	1	1	88
013	26	M	1	1	105
014	24	M	1	5	69
015	39	F	1	3	60.5
016*	23	M	2	2	70.5

The participants' cycling experience levels are subdivided into 5 groups, with Table 3.2 showing the average travelled distance limits per level. The levels are referred to in Table 3.1.

Table 3.2: Cyclist experience levels, travelled kilometres per year. Applies to both indoor and outdoor cycling.

Level 1	0 - 1000 km/year
Level 2	1001 - 2000 km/year
Level 3	2001 - 4000 km/year
Level 4	4001 - 8000 km/year
Level 5	8001+ km/year

All participants are presented with an Informed Consent form (supplemented in section E.3) and can only participate if it is clear to the subject what is expected of him. In the Informed Consent form, the experiments are described, as well as the inherent risks and required data processing. These forms are signed by the experiment supervisor and each test subject and kept for three months in administration after the conclusion of the experiments. After that, they are destroyed. See section E.4 for a full description of how participant data is handled.

3.2 Experiment Design

Based on requirements set in chapter 2, the experiments cover the data collection during three main cycling situations: performing a set of manoeuvres during outdoor cycling, during use of the B.I.K.E. system and during use of a static setup. The experimental procedure every participant undergoes is summarised in Figure 3.1 (fully described in Appendix D).

	Participant introduction	10 min.	Fill out IC form. Explain experiment procedures. Verify empty pedals.
Outdoor experiments	Prepare bicycle	5 min.	Startup RPi. Connect pedals. Fill out Q-forms
	Go-to outdoor experiment loc.	10 min.	Ride to experiment location.
	Outdoor experiments	14 min.	Start RPi meas. Start pedal meas. Calibrate pedals
	8 velocities	10 min.	5, 10, ..., 40 km/h straight
	Zig-zag	2 min.	Appr. 20 km/h, 1 m width
	Stand-up sprint	2 min.	No max. velocity
	Return ride	10 min.	Fill out Q-forms Stop RPi meas. Stop pedal meas.
Bicycle sim. experiments	Prepare bicycle	15 min.	Fill out Q-forms Change pedals. Start download pedals. Prepare bicycle sim.
	Bicycle simulator experiments	25 min.	Fill out Q-forms Start RPi meas. Start pedal meas. Calibrate pedals
	Accustomization	10 min.	80% sim. accuracy
	8 velocities	10 min.	5, 10, ..., 40 km/h straight
	Zig-zag	2 min.	Appr. 20 km/h, 1 m width
	Stand-up sprint	2 min.	No max. velocity (opt.)
Static sim. experiments	Prepare bicycle	15 min.	Fill out Q-forms Change pedals. Start download pedals. Prepare static sim.
	Static simulator experiments	15 min.	Start RPi meas. Start pedal meas.
	8 velocities	10 min.	5, 10, ..., 40 km/h straight
	Stand-up sprint	2 min.	No max. velocity
	Experiment roundup	15 min.	Fill out Q-forms Fill out Q-forms +15 min.

Figure 3.1: Full experimental procedures with short descriptions of each experimental phase. Denoted are the outdoor, simulator and static setup measurement phases, as well as each to-be performed manoeuvre and action per phase.

The rest of this section outlines the used experimental setups, the manoeuvres performed during experiments and the subjective data collected from participants.

3.2.1 Cycling Setups

The experiments are sectioned in three cycling situations; cycling outdoors, cycling on the B.I.K.E. system and cycling on a static setup. Each of these setups allows for an existing racing bicycle to be used, which is the same bicycle for all participants across all experiments. Cyclists are allowed to set the saddle height, but other than that, the bicycle remains the same. This decision was made to eliminate free variables that would be introduced with using different bicycles. It also decrease experiment duration times. The removal and re-installation of the measurements system between bicycles could also introduce systematic errors with incorrect, or slightly offset mounting of the measurement board.

Below, the cycling setup used in each of the experiment phases is outlined.

Outdoor Cycling Experiment Setup

The bicycle to be used for outdoor cycling experiments (and its frame for the other experiments, as well) is shown in Figure 3.2. The frame is a mid-sized aluminium frame to make it accessible to participants of different sizes. This may interfere with how the participants usually control a bicycle, but this interference is the same for each participant across experiments.

Figure 3.2: Measurement bicycle with measurement board (see Appendix A) attached to its frame. Remnants of previous studies are still present in the form of strain gauges and wires, which could not be removed.

Tyre pressure will be consistent across experiments, at 7.5 bar. The bicycle frame is an older Jan Janssen model, although the exact type could not be recovered due to the absence of paint and a model sticker. Measured frame dimensions are given in Table 3.3 below, referring to Figure 2.2's notation:

Table 3.3: Jan Janssen bicycle basic dimensions.

Symbol	Value
w	0.995 m
c	0.06 m
λ	18.6°
r_{wh}	0.35 m

Bicycle Simulator Experiment Setup

The B.I.K.E. system adopts the same bicycle frame from outdoor experiments. Figure 3.3 shows the simulator, now in use by a participant, with the visualisation active in the background as well. The visualisation shows to the participant a numerical representation of the velocity he is currently travelling at, as well as a timer (alternating with estimated time of arrival for the displayed route). These aid in letting the participant complete a certain manoeuvre in a required amount of time.

Figure 3.3: Simulator setup to be used for bicycle simulator experiments. Visible are the same bicycle as in outdoor experiments, the simulator, and the visual representation of an outdoor cycling environment. On the left, with a participant, on the right, a front view.

Added to the simulator are foam patches to reduce vibrations caused by the simulator and the motions of the participant, as well as inhibit the flexing of the simulator by some regard. Improvements for a following iteration in terms of stiffness of the support frame are certainly possible, but the current configuration does not interfere with the functioning of the device.

Cyclists are allowed to warm up and get used to the simulator for a period of approximately 10 minutes, before experiments are initiated, although if a participant requires longer to get used to the simulator, he is provided with additional time. A participant is considered “used to the simulator” when starting up from standstill costs little effort, since that is believed to be the most difficult part of using the simulator. After the accustomisation period, experiments are inititated and the participant is asked to keep his mind on the manoeuvre at hand.

A full description of the design and functioning of the device is present in chapter 2, and the safety features for the participant are outlined in section E.6.

Static Experiment Setup

The static setup is similar to the bicycle simulator setup. The front wheel will be locked for steering, since on the one hand, steering has a little to no expected effect on the motion of the static setup, and on the other, this is also how the setup is intended by the manufacturer. Differences in the appliance of forces and torque on the steering wheel could be observed in future studies if they were recorded.

Figure 3.4: Simulator setup to be used for fixed bicycle simulator experiments. Visible are the same bicycle as in outdoor experiments, the simulator, and the visual representation of an outdoor cycling environment, on the left. On the right, the setup without a mounted bicycle is visible.

The visualisation of the static setup is exactly the same as the one used during the bicycle simulator experiments. It is verified that the screen is positioned at the same distance from the bicycle's steering handles as in the bicycle simulator experiments.

3.2.2 Cycling Manoeuvres

There are a number of manoeuvres to be performed by the participants across experimental setups. These are performed, in order, as:

1. Constant cycling on a straight, flat road at incrementally increasing velocities: 5, 10, 15, 20, 25, 30, 35, 40 km/h, while remaining seated on the bicycle. Do this for about one minute per velocity instance, not counting the acceleration time between velocities. Elapsed time and current velocity can be monitored by the cyclist on the Garmin Edge 530 device screen, or on the visualisation screen during indoor experiments.
2. Zig-zagging at a velocity of approximately 20 km/h, to obtain information on evasion manoeuvring and cornering behaviour for small cornering angles. The maximum width of the motion is 1 m, to remain between simulator bounds. This width is indicated to the participant as the half-width of the road where tests are conducted. This manoeuvre is not performed on the static setup, due to the impossibility of steering and controlling the bicycle.
3. The performing of a standing-up cycling manoeuvre, with no required velocity, other than that the subject should be able to maintain the velocity he picks for standing-up cycling for one minute.

With the first manoeuvre, we try to obtain differences in the bicycle's kinematics due to the differences in travelling speed. Bicycle dynamics are closely related to its travelling velocity ([26], [19], [28]), hence the bicycle-rider interaction is recorded at eight different velocities. Participants are allowed to skip higher velocities if they reckon it will become too unsafe, misjudged the time they could maintain a velocity, or the participants cannot deliver the power required. It can be decided after the fact whether the recorded data will be used in the subsequent analyses. All manoeuvres are performed in a straight line, due to sustained cornering behaviour not being a part of the scope of this study, as well as the vehicle model not being configured for such sustained motions.

The second manoeuvre could show differences in control behaviour of the cyclist during outdoor zig-zagging in terms of how far and fast the user dares to go, and whether the bicycle-rider system reacts differently on the simulator. During zig-zagging, more defined sensor data (i.e., larger amplitudes, disturbed less by vibrations) are obtained, which may improve state-space approximation accuracy in later stages of the data analysis.

The final manoeuvre should tell us differences in the dynamics of the bicycle when standing up. Since during normal cycling, the bicycle rider's body and the bicycle frame are more or less attached (often approximated through rigid-rider models, see [28] for an experimental implementation). When standing up, this fixation is lifted and the bicycle is allowed more freedom of motion, thus the stabilisation dynamics of the bicycle-rider system change. Reducing the mass of the actuated bicycle, but still applying relatively similar steering and pedalling torque, should, intuitively (and from experience), increase the amplitude of the resulting motion of the bicycle. Verifying whether standing up on the simulator is still safely possible, should give an indication whether the simulator can handle these increased amplitude of kinematics.

Kinematic data will be recorded with the performance of the above manoeuvres using the Raspberry Pi-based measurement system and Garmin Rally 200 pedals, described in Appendix A.

3.2.3 Subjective Measurements

In order to evaluate what cyclists experience as realistic cycling, and to find out whether the bicycle simulator was disruptive compared to their usual outdoor cycling experience as well as an improvement over static cycling, a number of questions will be asked to them. The possible answers consist of a score between 1 and 10, whole-numbers only. The questions are presented at the start of all experiments, for the subject to keep in mind during the experiments, and answered at different times.

The questions asked are subdivided into two categories; questions related to the current experiment, not comparative to other situations, and questions specifically touching upon differences between the simulator and outdoor cycling. Questions of the first category are asked after every cycling situation; outdoor, simulator and static setup. These are:

1. "*I felt like I was riding a bicycle*"
2. "*I felt like I was riding* my *bicycle*"
3. "*Steering felt natural during the ride*"
4. "*Maintaining control of the bicycle was effortless*"
5. "*Balancing the bicycle felt natural during the ride*"
6. "*I felt I was not restricted in rolling the bicycle beneath me*"
7. "*The forwards motion I experienced felt coupled to my pedalling cadence and power*"
8. "*I was focused more on the mechanical aspects and limitations of the bicycle, than on the actual cycling*"
9. "*The velocity I was cycling at felt the same as the velocity of what I was seeing*"
10. "*I felt like I could ride the bike wherever I wanted on the road that I could see*"
11. "*I felt like I was in control of the bicycle*"
12. "*I felt comfortable during cycling*"
13. "*I felt safe during the ride*"
14. "*The ride was enjoyable.*"
15. "*During cycling, I felt as if there was some aspect of cycling missing. If scored above 1, this was missing in my view: "*

Several questions investigate several different aspects of cycling and vehicle simulation in general; questions 1 through 8 relate to the physical motion experienced by the participant. How well is the physical motion of the system in question representative of the participant's idea of cycling? Did he experience the activity as a cycling activity, or a mechanical concoction which only partially feels like a bicycle? What we hope to learn from these questions is how accurate the simulator represents an outdoor cycling activity, the level of intrusion on a participant's usual cycling behaviour and whether the solution is viable as an alternative to outdoor cycling in the subjective sense.

Questions 9 and 10 relate to the visual aspect of the simulator; did the participant feel like the visual and physical motions of the particular cycling situation matched? Did he feel like the visual environment was part of the available mechanical space of the simulators? With these questions, we can determine what the importance and level of disruption is the visual solution incurs in the simulator and static setup solutions.

Questions 10 through 15 cover the overall experience of the cycling activities. Was the participant frightened or feeling out-of-control during the experiments? Did the participant control the simulator, or the other way around? Or did the cycling situation not matter at all? Answers to these questions provide insight and possible explanations for differences in control behaviour, with for example the rider's arms stiffening up due to a frightened response to the motion or lack of motion in a certain cycling activity, or changing his balancing input from mainly steering to increasingly using upper-body leaning motions.

Questions of the second category, which compare different situations or are specific to the B.I.K.E. system are answered after all experiments are completed. They are:

1. "*Balancing cost more effort on the simulator than outside*"
2. "*Delivering pedalling power cost more effort on the simulator compared to outside*"
3. "*Steering the bicycle had the same result on the simulator, as outside*"
4. "*The sideways velocity of the simulator felt natural, compared to outside*"
5. "*The physical motion of the simulator influenced my cycling positively*"
6. "*The visualisation presented on the simulator influenced my cycling positively*"

The scores to these questions will not be compared between situations, since they will only be answered once. The phrasing of these questions is what differentiates them from questions asked after each cycling situation, but similarities in scores can be observed between these six and the questions of the first category.

An additional metric which is going to be evaluated with the simulator, is simulator-induced motion sickness, or simulator sickness. Simulator sickness is a separate category which will be based on the Simulator Sickness Questionnaire (SSQ) method proposed by Kennedy & Lane [17]. This method is widely applied in studies on simulator sickness occurring in vehicle simulators (for example, [13], [12], [49]), thus it will be applied here as well. What is important to note is that in the simulator presented in this study, physical exertion is a large part of the usage of the simulator, so results from the statistical scores will have to be interpreted accordingly.

What we expect for the incidence of simulator sickness, is that simulator sickness incidence can increase going from outdoor to indoor cycling experiments, but that the incidence will remain small among participants. This is due to the use of an external monitor (see subsection 2.1.4), as well as due to cycling being a high-involvement activity. Balancing and controlling a bicycle costs effort, which requires one's concentration and focus. Increased effort and focus on a certain controlling task have been shown to decrease simulator sickness incidence ([25], [2], [49]).

Participants fill out three columns of SSQ scores relating various bodily symptoms (listed in section 3.3) to a certain cycling experiment. The first is filled out fifteen minutes before the experiment starts, the second is filled out directly after the performing of an experiment and the final one is filled out after fifteen minutes has passed after completing an experiment. The first column and third column of two consecutive experiments may correspond, due to the experiments usually taking place in one go.

Randomisation of the order of experiments (outdoor, simulator and static cycling) may improve the basis on which we draw conclusions in terms of simulator sickness, but for convenience, as well as letting participants directly experience the difference in kinematics between outdoor cycling and the B.I.K.E. system, the order of experiments is kept the same for all participants.

3.3 Subjective Data Analysis

Scores given as answers to questions will be compared on both a within-subject and between-subject basis. Scores given by participants are compared between cycling situations, but also compared to other participants, to see whether we can derive causes for changes in kinematic behaviour between subjects, since the bicycle and simulator configuration is the same across participants.

A statistical paired t-test will be performed on the means of scoring results from the first category of questionnaire, to try to indicate a significant difference between question scoring of static/simulator and outdoor cycling. The standard deviation will be computed for questions of the second category, to see how much participants agreed on a certain score.

Using SSQ, participants are able to score how they feel and what symptoms from simulator sickness they are experiencing beforehand and after the cycling experiments (both indoor and outdoor, to obtain a baseline). [17] also proposes a standardised weighing of the scores, such that categorisation of symptoms is possible. The symptoms are categorised in three categories; *Disorientation*, *Nausea* and *Oculomotor*, and symptom scores (0, 1, 2, or 3) are weighted in one or more of these categories as in Table 3.4:

Table 3.4: Simulator sickness scoring table, adopted from [17].

SSQ Symptom	**Weight**		
	Nausea N	Oculomotor O	Disorientation D
General discomfort	1	1	0
Fatigue	0	1	0
Headache	0	1	0
Eyestrain	0	1	0
Difficulty focusing	0	1	1
Increased salivation	1	0	0
Sweating*	1	0	0
Nausea	1	0	0
Difficulty concentrating	1	1	0
Fullness of head	0	0	1
Blurred vision	0	1	1
Dizzy (eyes open)	0	0	1
Dizzy (eyes closed)	0	0	1
Vertigo	0	0	1
Stomach awareness	1	0	0
Burping	1	0	0
Total	Sum $N \times 9.54$	Sum $O \times 7.58$	Sum $D \times 13.92$

Where participants of this study were instructed to give scores on a 1 to 10 range, scores are re-weighted such that they fall within the range of 0 to 3, as [17] requires. Scores and significant differences in score averages between cycling situations will be compared based on a paired t-test, comparing the results from the bicycle simulator and static cycling with outdoor cycling.

Chapter 4

Results

In this chapter, the processed results of rides from test subjects will be described. In section 4.2, the kinematic data recorded from participants will be compared on a manoeuvre-by-manoeuvre basis. First in terms of the time-domain response during several manoeuvres, and after in terms of the approximated State-Space systems. The observed results in terms of kinematics are discussed there, as well. In the latter part of this chapter (section 4.3), subjective results recorded during outdoor cycling, cycling on the simulator and cycling on the static setup will be compared. Questions from the first and second category (see subsection 3.2.3) as well as the Simulator Sickness Questionnaire are shown and discussed.

4.1 Conducting the Experiments

Overall, the experiments have provided a broad set of data both in the kinematic and subjective areas. All participants were able to use the bicycle provided to them, and perform almost all manoeuvres on it. Participants seemed to cope well with the B.I.K.E. system as a whole. All of the participants were able to get used to the simulator's motion within a reasonable amount of time, where the person who struggled most took approximately ten minutes to start up from standstill, and another ten to relax and use the simulator as intended.

During experiments, three participants were not able to reach the prescribed velocity of 40 km/h on the road due to the required effort involved (participants 008, 010 and 015). Only one participant was not able to perform higher-velocity manoeuvres on the simulator due to the motions being too jittery and unstable for him to continue (participant 008). This was attributed during experiments to tension in the arms of the participant resulting from increased nerves and very little experience with racing bicycles. Other participants, with more cycling experience, showed more relaxed behaviour on the simulator and did not experience instability problems at all. However, almost all participants showed difficulty with attaining the lowest velocity (5 km/h) on the simulator. So some performed the first manoeuvre at a slightly higher velocity.

The standing-up manoeuvre was not performed on the simulator, since the behaviour of the simulator was experienced as too jittery while participants stood up from the saddle. Larger excitations of the steering angle during standing up, as well as an undamped steering response may have been the cause of this instability. For safety's sake, participants were instructed not to perform the manoeuvre.

Participants with previous experience with using highly-kinematic indoor training solutions, like the Tacx Magnum belt-driven trainer, or the Tacx Antares roller-based trainer, tended to show immediate aptitude for the simulator and required little or no coaching on how to get used to the simulator's motions. Although the number of participants with this previous experience was small (participants 2, 3, 11), this was a recurring theme among them. As an additional experiment, the final participant (15) was instructed to ride the simulator without any helpful tips on how to get used to the simulator easily during the first three attempts to start up from standstill. She showed much difficulty initially, but after receiving the note that gaining some velocity while not lifting both legs immediately, the participant managed to get moving the subsequent attempt.

It became clear that during the experiments, the focus of the participants lied with the speed reading on either the screen the Edge device or the visualisation presented during indoor experiments. This notion should be taken into account while interpreting the subjective results.

4.2 Kinematics

4.2.1 Time-domain Response

A first look at the kinematic data recorded during the experiments gives insight in the performance of the simulator, as well as the measurement system that records the kinematics of the bicycle while cycling. Figure 4.1 shows samples of the recorded data from four participants, during four manoeuvres. Shown are raw signals for the common kinematic input for bicycle control, steer angle δ, and one of the outputs we can directly measure, yaw-rate $\partial\psi/\partial t$ for outdoor and simulator measurements. Results from static cycling experiments are omitted here, since they remain near-zero and seemingly uncorrelated across manoeuvres.

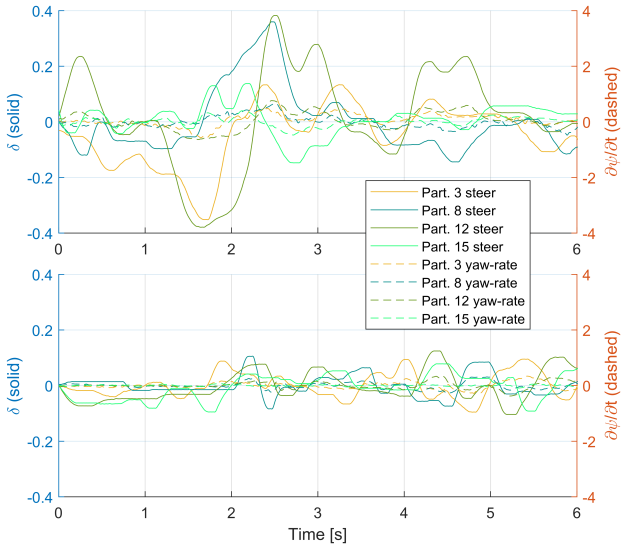

(a) Timeseries comparison between outdoor (top) and simulator (bottom), a startup manoeuvre. With legend.

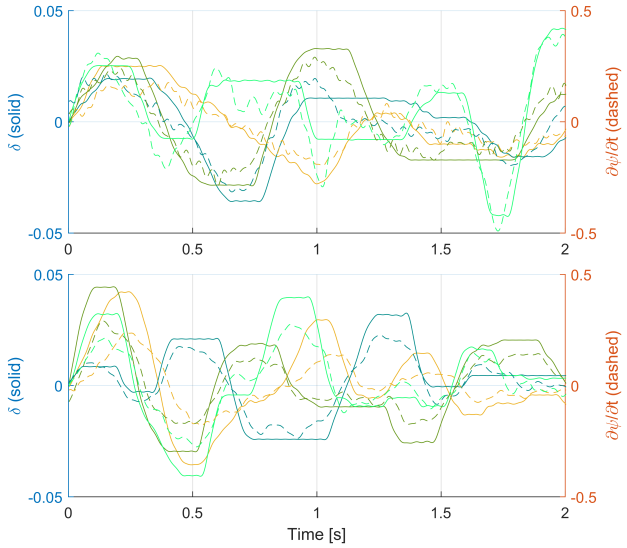

(b) Timeseries comparison between outdoor (top) and simulator (bottom), at 20 km/h.

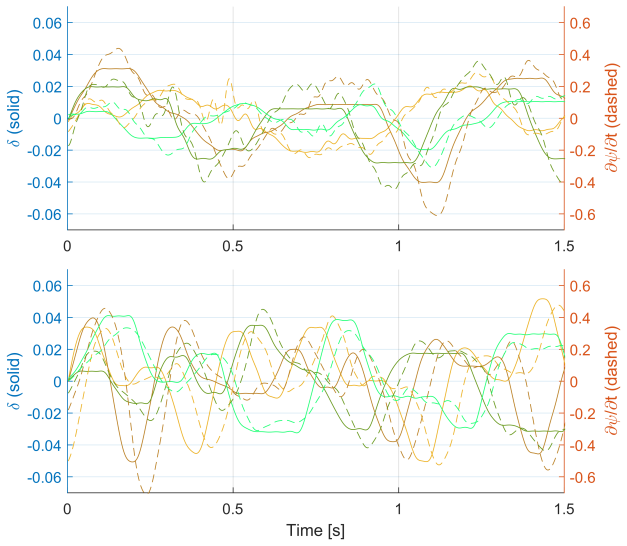

(c) Timeseries comparison between outdoor (top) and simulator (bottom), at 40 km/h.[1]

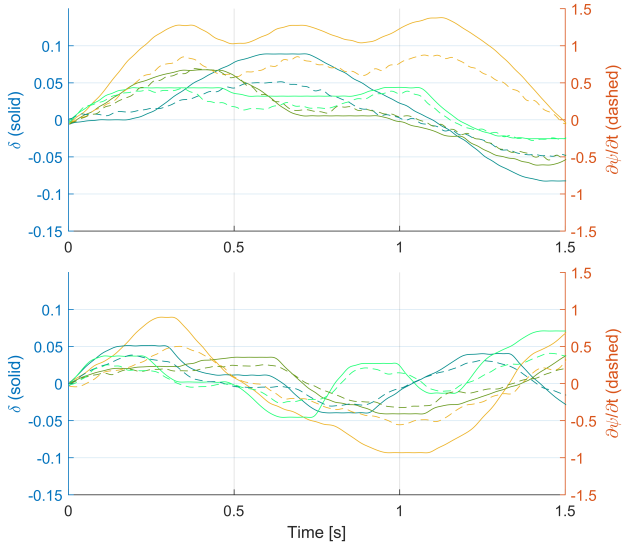

(d) Timeseries comparison between outdoor (top) and simulator (bottom), during a zig-zagging motion.

Figure 4.1: Time-domain representation of four manoeuvres from four test subjects, shown are δ, $\partial\psi/\partial t$. Participants shown are 3, 8, 12 and 15. In each subplot, the upper graph shows the outdoor response, the lower shows the bicycle simulator response. Note the changing scales on the y-axes, and that the left and right axes are always related as the right being tenfold the range of the left axis.

[1]Note: participant 9 was used instead of 8, since sensor data appeared corrupt during this manoeuvre with 8.

What is directly apparent in these figures is that the steering sensor expresses some unexpected behaviour while being actuated by the bicycle's user. This manifests itself in the horizontal plateau after each steering action of the bicycle. This is either a consequence of the toothed belt used to connect the steering axis and the potentiometer axis, or the limited precision of the analogue-to-digital converter used for the voltage measurement. Measures were taken to pretension the belt to minimise play, but there still remains some.

All measurements recorded outdoors show more signal noise than those recorded indoors, likely due to increased vibrations on outdoor roads. This becomes especially visible during higher velocities, where the measured yaw-rate $\partial\psi/\partial t$ shows more high-frequency behaviour unrelated to the steering angle during outdoor measurements. The same manoeuvre performed on the simulator appears more stable and smooth. The data shown was only filtered with a low-pass IIR filter with passband 30 Hz, no other processing was applied (other than de-trending the signals such that any drifting over the signal section range was counteracted).

Moreover, a participant's behaviour during startup manoeuvring (Figure 4.1a) changes significantly between outdoor cycling and on the simulator, where the steer input is used much more conservatively. Much larger steering angles were recorded for outdoor cycling than during simulator attempts.

The simulator seems to respond similarly to a steer angle input during lower-speed manoeuvring when compared to outdoor cycling, but starts to differ with increasing velocity. From visual inspection, Figure 4.1b already shows a slight delay between an applied steer angle and the resulting yaw-rate. This difference becomes even more apparent during high-velocity cycling (40 km/h). This delay introduced by the electromechanical system (vehicle model-actuator combination) is evident in Figure 4.1c, independent of the participant using the simulator. We do not observe this delay during the same manoeuvre, but performed outdoors. The approximated state-space models should provide more information on this phenomenon across all participants.

4.2.2 State-Space Approximations & Coherence

As described in subsection 2.2.2, the main comparative factor of differences in kinematics between cycling situations will be the state-space representation of the observed bicycle-rider behaviour during a certain manoeuvre. Considering the two sets input-output combinations described in subsection 2.2.2, a relation between each input and output is determined for each set.

With the state-space representation, the contributing result for each participant is shown as well. In a later stage, differences in participant results could be correlated to their demographics or subjective results. Figure 4.2 indicates the marker type and corresponding participant number, mass and cyclist level. The colours in Figure 4.3d indicate the performed manoeuvre velocity.

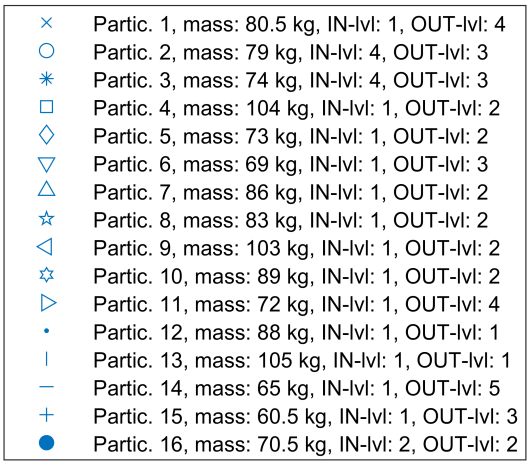

Figure 4.2: Indicated are subject masses, and the recorded cyclist levels, so that dependencies of cycling behaviour may be derived later.

One extra dataset for kinematic measurements was available recorded by the author, during a validation session of experiments. This set is indicated as the sixteenth participant. Models for a certain participant, manoeuvre and cycling setup with bad/insufficient sensor data were omitted.

To increase the robustness of the state-space approximation, all input and output signals, for both sets of state-space models, were filtered with an IIR-lowpass filter with a passband frequency obtained from the coherence between the input δ and the first output ($a_{R,\hat{x}_P}$ and θ). This passband was twice the frequency where the coherence first dropped below 0.7, with increasing frequency above 0.5 Hz (usually where the pedalling frequency becomes less influential on the cycling dynamics). This improves the quality of the approximated models, while not removing the fundamental signal dynamics for cycling of the manoeuvre at hand. As discussed in subsection 2.2.2, in- and output signals are de-trended as well.

To give a comprehensive overview of state-space approximations, the average gain for each input-output relation was extracted from the state-space frequency response between half and double the pedalling frequency of a certain manoeuvre, since all derived models produced a linear gain-frequency relation over the frequency range of interest (and signal coherence is high between 0.2 and 3 Hz, see Figure 4.3c): slope 0 dB/dec for $a_{R,\hat{x}_P}$ and $\partial\psi/\partial t$, and slope -20 dB/dec for ψ due to it being a result of numerical integration from $\partial\psi/\partial t$.

In the now following results, the static setup is omitted entirely. State-space approximations showed near-zero gain and random phase, and coherence levels were very low. An intuitive result, since the static setup has no steer input to couple to model outputs, due to the absence of freedom of steering and the lack of a forward velocity resulting in sway and yaw motion. Figure 4.3 shows the results of the full set of input-output relations: δ to $a_{R,\hat{x}_P}, \psi$ and $\partial\psi/\partial t$ in terms of average gain (Figure 4.3a), phase (Figure 4.3b) and signal coherence (Figure 4.3c). Potential extra data processing is discussed with each figure. Blue symbols and text indicate data recorded outdoors, red symbols data recorded during use of the B.I.K.E. system.

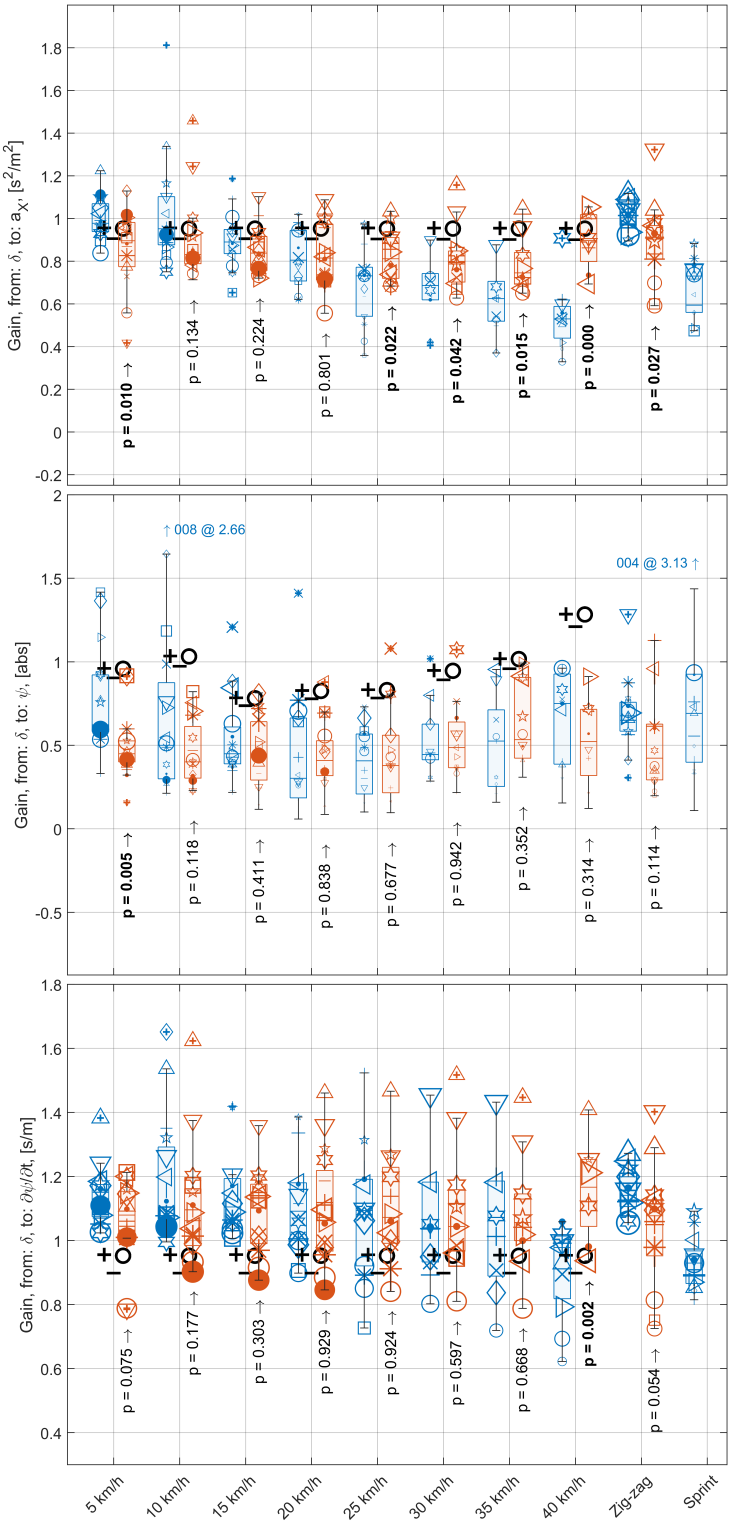

(a) Gains from approximated (blue = outdoor, red = simulator) and existing models (black, see main text body), obtained for each participant at every velocity. With boxplot distributions and t-test p-values, comparing gain means between manoeuvres. Smaller markers indicate worse state-space approximation. Outliers are indicated through text notes. Note the changing units on the vertical axis, due to the velocity-normalisation.

Since we built up an expectation for the approximated input-output relations with the vehicle model derived by the author (Appendix B) and existing models ([26], [3]), and we know that the kinematic behaviour of a bicycle is heavily velocity-dependent ([26], [19], [28]), the gains resulting from the approximated state-space systems are normalised with $v_R^2, 1$ and v_R for outputs $a_{R,\hat{x}_P}, \psi$ and $\partial\psi/\partial t$, respectively. Note the changing y-axes in Figure 4.3a.

In terms of vehicle model accuracy, we are able to make a comparison with the same normalised models. The models (adapted for comparative purposes) from the author en literature were numerically simulated with θ and $\dot{v}_R$ set to 0, since those were no inputs in the approximation of the current state-space models. The obtained, normalised gains are given in Figure 4.3a as well with the following symbols (mathematical expressions given):

– Auth.: $a_{R,\hat{x}_P} = -\sin(\psi_b + \psi)\dot{v}_R - \cos(\psi_b + \psi)v_R(\dot{\psi}_b + \dot{\psi})$
$\dot{\psi} = \frac{v_R \sin(\delta_z - \psi_b)}{w \cos(\theta)\cos(\delta_z)} \cos(\lambda)$

\+ [26]: $a_{R,\hat{x}_P} = -\frac{v_R^2\delta + v_R c\dot{\delta}}{w} \cos(\lambda)$
$\dot{\psi} = \frac{v_R\delta + c\dot{\delta}}{w} \cos(\lambda)$

∘ [3]: $a_{R,\hat{x}_P} = -\dot{v}_R \sin(\psi) - \cos(\psi)v_R\dot{\psi}$
$\dot{\psi} = \frac{v_R \tan(\delta)}{w\cos(\theta)}$

State-space approximations which produced a 10% or worse reproduction of either $a_{R,\hat{x}_P}$ or $\partial\psi/\partial t$ from original input data are omitted from results. Boxplot distributions in Figure 4.3a show the grouping of gains from participants, and p-values resulting from two-sided t-tests between the means of plotted gains of simulator and outdoor cycling per manoeuvre are shown as well. Bold-faced p-values indicate a value smaller than 0.05. Larger marker sizes in Figure 4.3a indicate a better model approximation, the largest markers showing a model quality of $> 90\%$.

Evidently, an outdoor bicycle experiences a non-linear decrease in its dependency of $a_{R,\hat{x}_P}$ on velocity above 20 km/h, while the simulator, as its model dictates, behaves more constantly with increasing velocity. This is also the case for $\partial\psi/\partial t$, although only significantly present above 40 km/h.

Figure 4.3b shows the phase response of the same systems, although the phase value was now obtained exactly at pedalling frequency instead of between half and double the pedalling frequency. This is due to the phase response in the approximated models being non-linear as opposed to the gain. The phase was wrapped with steps of 360° for improved comparability in Figure 4.3b, and the wrapped model phase should still produce identical results to the unwrapped one.

It appears that the largest differences between the simulator and outdoor cycling become evident when considering the phase. Almost all manoeuvres show a significant phase delay of the simulator response with respect to outdoor cycling as a result of an input δ. This delay is almost certainly originating from the delays introduced to the simulator through the vehicle model-actuator combination, and we have observed this delay in Figure 4.1 as well. However, the bicycle-rider system by itself, during outdoor cycling, also appears to have an intrinsic phase lead at lower velocities for $a_{R,\hat{x}_P}$, which turns into a delay once manoeuvre velocity starts to go up. For ψ and $\partial\psi/\partial t$, a phase delay during outdoor cycling is immediately present (albeit very small), which increases with increasing velocity.

Again, existing mathematical vehicle models have been plotted again, see the previous page for model mathematics. The model by [26] appears to always have a phase lead across all velocities, but this is likely to be an artefact of the numerical simulation of the presented models, since the model computation included a numerical differentiation step, which alters the phase response as well. The same goes for the computation of the model derived by the author, albeit not for all outputs.

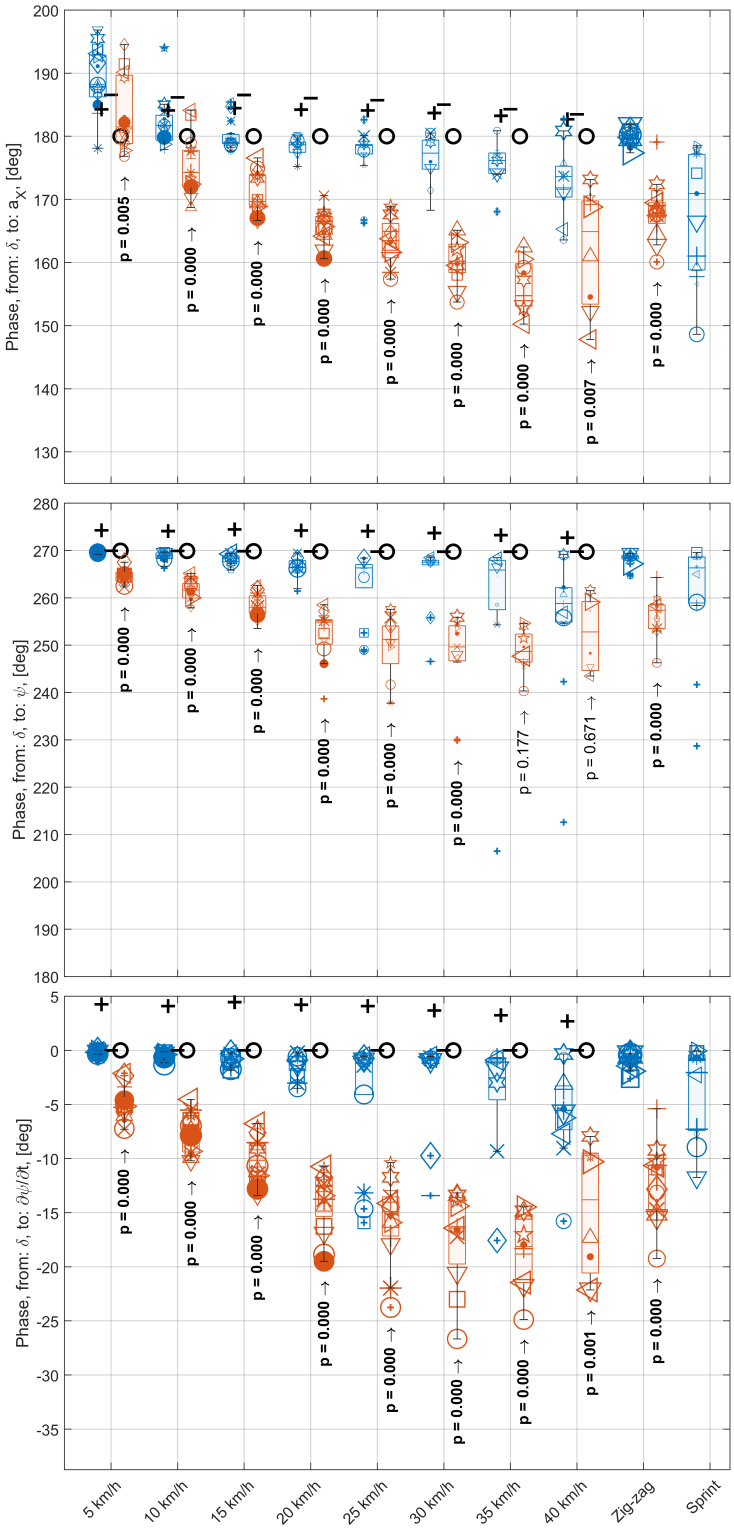

(b) Phases from approximated (blue = outdoor, red = simulator) and existing models (black, see main text body), obtained for each participant at every velocity. With boxplot distributions and t-test p-values, comparing phase means between manoeuvres. Smaller markers indicate worse state-space approximation.

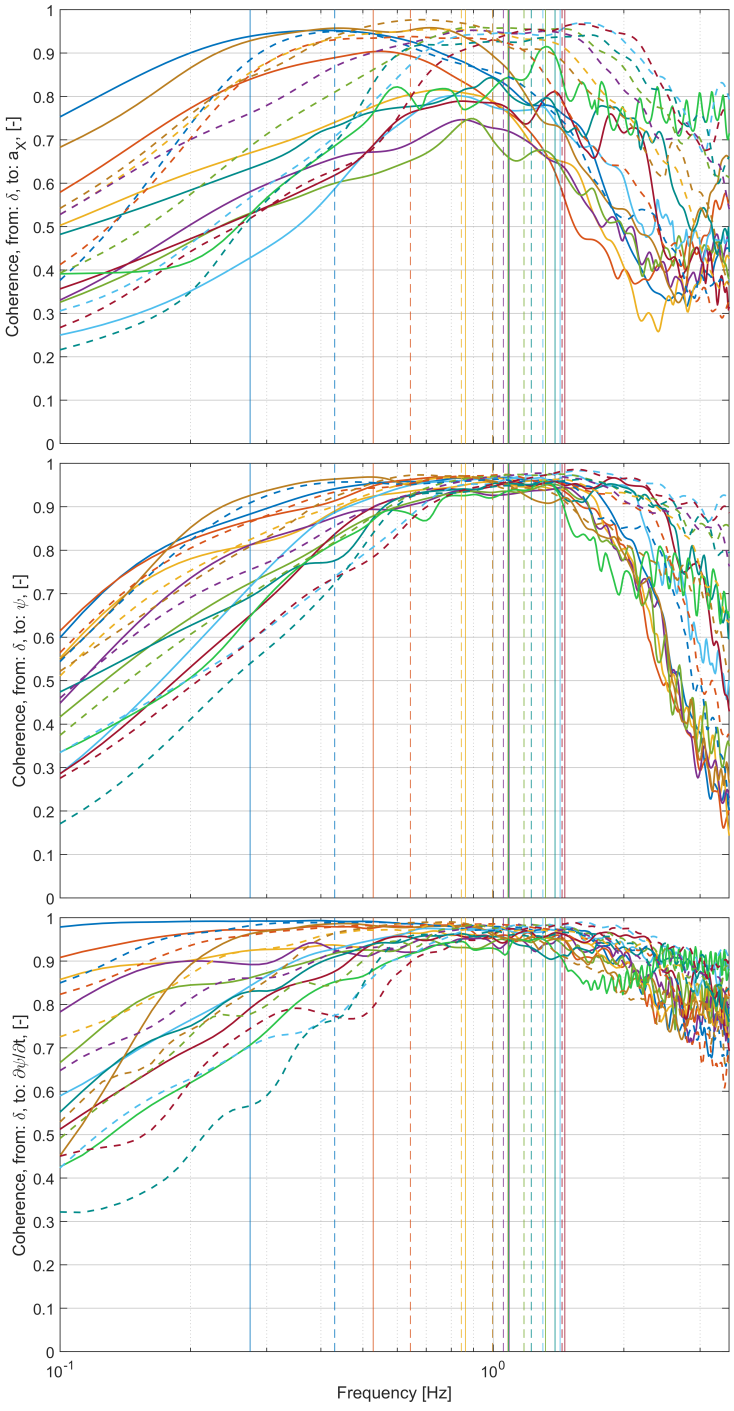

(c) Coherence of experiments, averaged across participants for every cycling manoeuvre. Vertical lines indicate the average pedalling frequency for that particular manoeuvre. Solid lines indicate outdoor cycling, dashed lines indicate simulator cycling. Colours indicate the performed manoeuvre, see Figure 4.3d.

Finally, Figure 4.3c shows the coherence between input and output signals, averaged across participants, as well as the average pedalling frequency of that particular cycling manoeuvre as vertical lines. Figure 4.3d shows the legend in terms of line colour.

(d) Colour legend for coherence responses. Different colours indicate different manoeuvres.

On average, all input-output relations show coherence values above 0.8 between half and double the average cadence of that particular manoeuvre, although less so at higher manoeuvre velocities in the $\delta - a_{R,\hat{x}_P}$ relation (see Figure 4.3d for a description of colours). To obtain the gain and phase around these frequencies seems to have been a robust strategy of simplifying the comparison between outdoor and indoor cycling.

During outdoor cycling, the coherence seems to decrease as the velocity of a certain manoeuvre increases. This is likely to be the result of increased signal noise due to increased vibrations at higher frequencies, but may also be a result of increased dependencies on other dynamics within the bicycle at higher velocities. The reduction of the amplitude of the steer signal may have an influence as well, since this can increase the influence of plateauing effects as shown in Figure 4.1.

The bicycle simulator shows a higher coherence rate across manoeuvres at higher frequencies as well, but less at lower frequencies. This is likely due to the absence of low-frequency manoeuvres on the simulator due to the limited width of the simulator, and the current configuration of the drive algorithm. This difference is clearest at low velocities with the $\delta - \partial\psi/\partial t$-relation, where low frequency motions are most common.

Figure 4.3: Full model results: state-space approximations at pedalling frequency and coherence between inputs and outputs for full system, i.e. in terms of steer, lateral acceleration, yaw and yaw-rate.

For the second set of in- and outputs defined in subsection 2.2.2, the steer-roll relation, these same gain, phase and coherence metrics are computed and shown in Figure 4.4.

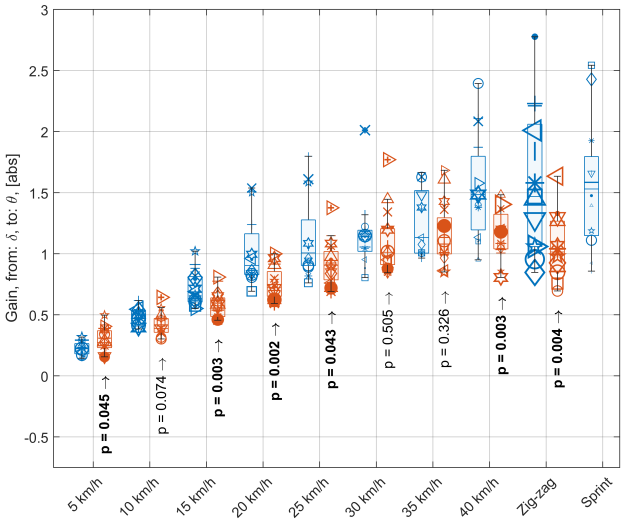

(a) Gains from approximated (blue = outdoor, red = simulator) model, obtained for each participant at every velocity. With boxplot distributions and t-test p-values, comparing gain means between manoeuvres. Smaller markers indicate worse state-space approximation.

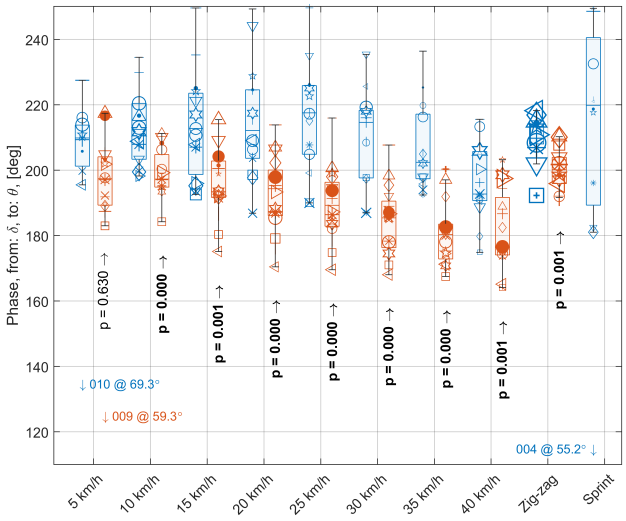

(b) Phases from approximated (blue = outdoor, red = simulator) model (black, see main text body), obtained for each participant at every velocity. With boxplot distributions and t-test p-values, comparing phase means between manoeuvres. Smaller markers indicate worse state-space approximation. Outliers are indicated through text notes.

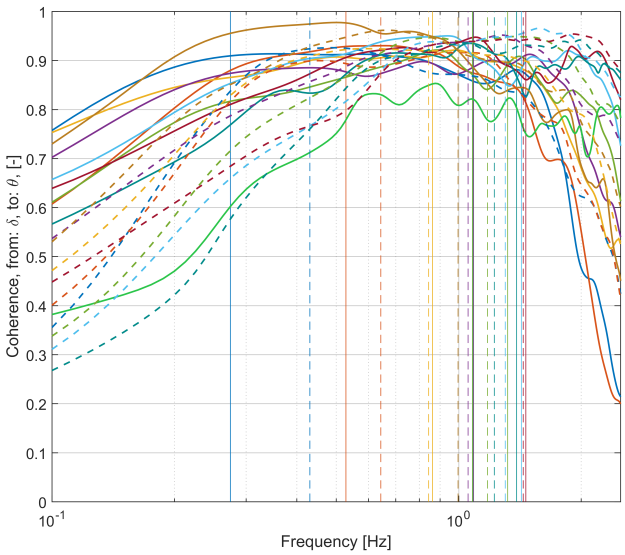

(c) Coherence of experiments, averaged across participants for every cycling manoeuvre. Vertical lines indicate the average pedalling frequency for that particular manoeuvre. Solid lines indicate outdoor cycling, dashed lines indicate simulator cycling. Colours indicate the performed manoeuvre, see Figure 4.4d.

(d) Colour legend for coherence responses. Different colours indicate different manoeuvres.

Figure 4.4: Steer-roll model results: state-space approximations at pedalling frequency and coherence between input and output, i.e. in terms of steer and roll angles.

Here, again, model predictions with an accuracy below 10% are omitted from the results. Overall, the model predictions were consistently around 50%, which is sufficient for capturing the steer-roll kinematics related to the pedalling frequency. The in- and output signal were again filtered with an IIR low-pass filter dependent on where the coherence dropped below 0.7 above 0.5 Hz. The gains were obtained similarly as with the full model description, around and at the pedalling frequency for the gain and phase, respectively. Gains were now not normalised with velocity, since a dependency may also exist upon bicycle states other than the rear-wheel velocity.

What we observe is that the steer-roll relations, comparing outdoor and simulator results, are relatively similar in terms of gain, although the gains observed on the simulator are somewhat lower, on average and across all manoeuvres.

The phase recorded for the steer-roll relation shows a constant phase during outdoor cycling with increasing manoeuvre velocity, whereas the phase of the bicycle simulator decreases with increasing velocity. This behaviour for phase is similar to what the full system description showed (see Figure 4.3b), so this could again be a result from increasing time-delays with higher velocities. The coherence between roll and steer shows a higher correlation around the pedalling frequency, as did the first state-space model in Figure 4.3a. The coherence of the simulator appears to have shifted to higher frequency compared to the outdoor cycling.

4.2.3 Discussion

To validate the design and control algorithm of the B.I.K.E. system, kinematic data was obtained during straight-road cycling manoeuvres during outdoor cycling, on the simulator and on a static setup. In terms of amplitude, the kinematic data seems to be in the same order of magnitude as other studies ([5]). At lower speeds the steer angle amplitude is high, to decrease with increasing velocity, as we see happening with bicycle-rider control in other studies as well ([28]). Although experimental data on bicycle kinematics is readily available, (e.g. [4], [5], [47], [9], [37] and [21]), as far as the author's knowledge, none have attempted to use and approximate the data through the modelling as in this study, making it tougher to make a qualitative comparison between the presented and existing results.

Confirming what we expect from literature is that a bicycle's kinematics are heavily dependent on velocity ([26], [19], [28]). Only with the velocity-normalisation as applied are the gains of the full kinematics somewhat behaving linearly with increasing velocity. But we observe that a nonlinear relation exists with increasing forwards velocity in terms of $a_{R,\hat{x}_P}$ and $\partial\psi/\partial t$. However, with increasing velocity, model approximation declined, especially for outdoor cycling. A more robust method of data processing and state estimation of the bicycle from sensor data (such as with Kalman filtering), as well as the sensor data itself (to remove for example the plateau-effect observed in δ) could improve the estimated model quality, thus increasing our confidence in the results we found here.

The vehicle models derived by the author (see Appendix B) and others ([26], [3]) do not entirely cover the response we observe in the results. In terms of gain, for $a_{R,\hat{x}_P}$ all models are relatively accurate, but the outdoor response to the steer input δ drops with increasing velocity, whereas the vehicle models (and simulator response) remain largely constant. For $\partial\psi/\partial t$, it is the other way around, where the models are inaccurate initially, at low velocity, but tend to be more correct at higher velocities. Further developments in the vehicle model (including tyre dynamics, tyre side-slip (see [3] for a review) combined with the reduction in phase delay, could result in a more realistic motion and experience for the user.

Another trend was observed (both outdoors and on the simulator) when looking at how individual subjects performed kinematically; not all participants produced the same models, even where model estimation quality is high. This infers the same bicycle is controlled differently when changing the person using it. This is in line with the notion that cyclists control bicycles differently based on experience level ([6]). Cain ([6]) states that experienced cyclists use less steering control input, and especially at higher speeds, apply rider lean control more to balance oneself on the bicycle. This tends to hold true for some participants (e.g. 2, 3, 4, high experience level), but not for others (e.g. 1, 11, 14, low experience level, who tend to apply higher gains in the steer to roll relations than others).

The differences in bicycle-rider gains could also be an effect of cyclist mass when considering this effect on the simulator. We seem to, however, observe control differences both on the simulator and outdoors. A focused study, which focuses on bicycle control, incorporating upper-body lean as well as steering torque, which categorises cyclists more accurately based on experience levels and classifies with which type of bicycle, could provide more insight in the differences between riders. However, subjective scores could explain the differences in bicycle-rider behaviour as well. section 4.3 should provide insight in that regard.

In terms of pure simulator performance, the current configuration of control model and electromechanical actuators limits the bandwidth of the actuators. A substantial increase of phase delay with respect to outdoor cycling seems to point in that direction. Instability experienced by some participants at higher velocity could, as opposed to what was hypothesised early in chapter 4, also have been a result of the simulator not being able to keep up with the required motion, instead of just being caused by the stiffness of the rider on the bicycle. Another possible cause is the flexibility of the bicycle frame starting to play a part in the dynamics of the actuators, either by increased flexing due to the rider's forces or increasing frequencies the bicycle frame might be susceptible to.

4.3 Subjective Influences

4.3.1 Questionnaire Responses

For the subjective responses of the test subjects, the scores to the questions posed in subsection 3.2.3 of the first and second category are the following:

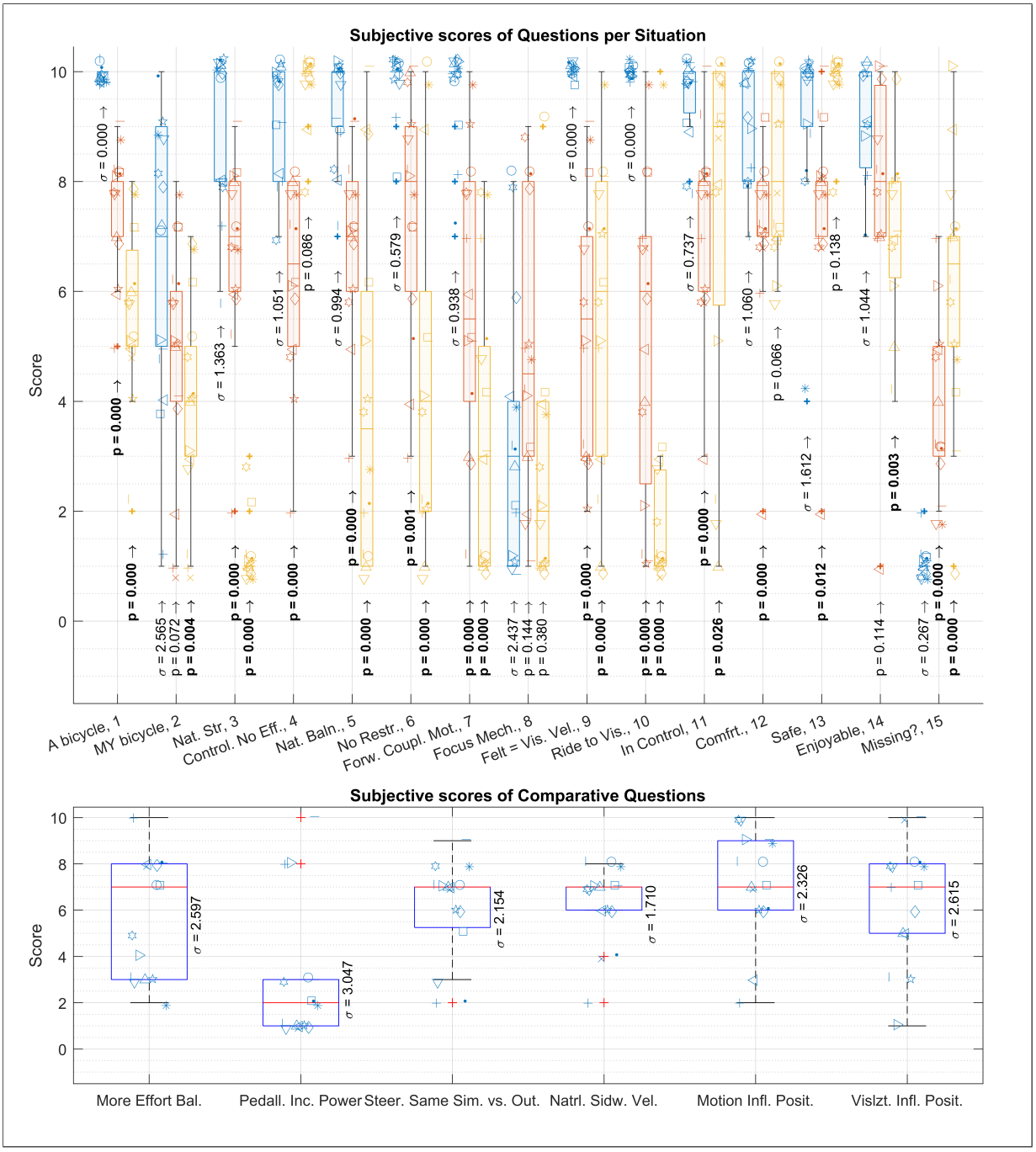

Figure 4.5: Subjective scores. p-values refer to a two-tailed t-test, comparing the means of scores of simulator and static cycling to the mean of the outdoor question responses. A p-value lower than 0.05 is boldfaced. The σ indicates the standard deviation of the scores. Individual responses are visible with markers according to Figure 4.2.

Considering questions 1 through 8, those regarding the simulator's quality of bicycle simulation (see subsection 3.2.3 for the questions), there appears to be a trend of outdoor cycling being scored the highest, the simulator performing worse (lower scores for questions 1 through 7, higher in question 8) and the static setup performing the worst. Except for the required control effort of the bicycle, which is scored lowest for the simulator and highest for the static setup, which is to be expected since no real control effort is required there. Apparently, most participants still experienced a restriction in rolling the bicycle while riding the simulator, compared to riding outdoors (question 6). But, interestingly, when asked how the participants felt the forwards motion they experienced on the simulator was coupled to their cadence and power application (question 7), they picked an average score of approximately 6. This is not an intuitive result, since the simulator is fixed in terms of forwards motion, but apparently participants experienced there being some.

Questions regarding the visual implementation of the simulator (9 and 10) were answered with largely deviating answers. During experiments, this question had to be reexplained the most, which could be an indication that the wording of the questions was not clear enough to provide a clear understanding of it within the participant. According the scores that were given, some participants experienced enough freedom to perceive it as free enough to ride the bicycle where they wanted (on the simulator), and some did not experience this freedom at all. The same goes for the perception of forwards velocity through the visualisation. Test subjects with more outdoor cycling experience tended to score questions 9 and 10 higher (participants 2, 3, 4, 6, 14), but the amount is too little to state a clear correlation.

Finally, questions regarding the overall subjective experience of the participant (11 through 15) were scored relatively high overall (except question 15, where a low score is a positive outcome). Most participants felt safe, comfortable and found the ride enjoyable on the simulator, but not as much as during outdoor cycling. Participants felt safest during the use of the static setup, which grants people the most stability and stiffness, so this result can be expected. One participant found the experience the opposite of safe, fun and comfortable (participant 9), although that participant did finish all experiments and did not seem to struggle much with getting used to the simulator motion. When participants were asked what they were missing on the setup they were riding, forwards motion of the setup was a common answer on the simulator ($n = 5$), as well as flow of wind ($n = 5$). On the static setup, freedom of steering ($n = 7$) and overall freedom of motion ($n = 10$) were common answers.

The second category of questions relate the simulator to outdoor cycling more directly. Participants are divided whether using the simulator increased the required effort to balance the bicycle; however, participants disagree with the notion that using the simulator cost increased power compared to outdoor cycling. Participants were also divided when asked whether the steering responses felt similar, comparing outdoor to simulator cycling. "Not entirely" seems to be a safe interpretation, considering the median of a score of 7. The same goes for whether sideways motion felt natural on the simulator comparing outdoor cycling. Participants tend to agree more here, with a lower standard deviation, and the score also corresponds with the scoring of question 3 of the questions of the first category. The average scoring when asked whether the motion influenced the participant's cycling positively, is pretty high, but participants do not all agree there, with a higher standard deviation. The same goes for the question regarding whether the visualisation influenced the participant's cycling positively.

4.3.2 Simulator Sickness Incidence

In terms of simulator sickness, participants showed no particular physical response to the combination of the visual system and the simulator. The highest scores on the SSQ spectrum were given during indoor cycling (either simulator or static setup) on the *fatigue* and *sweating* scores, most likely due to the intensity of experiments performed on the simulator. After 15 minutes, the intensity of these (and other) symptoms usually reduced to the level the participants experienced 15 minutes before undertaking the experiment. See Figure 4.6 for the scores given by participants, adapted for the usual 0 to 3 scoring range of [17].

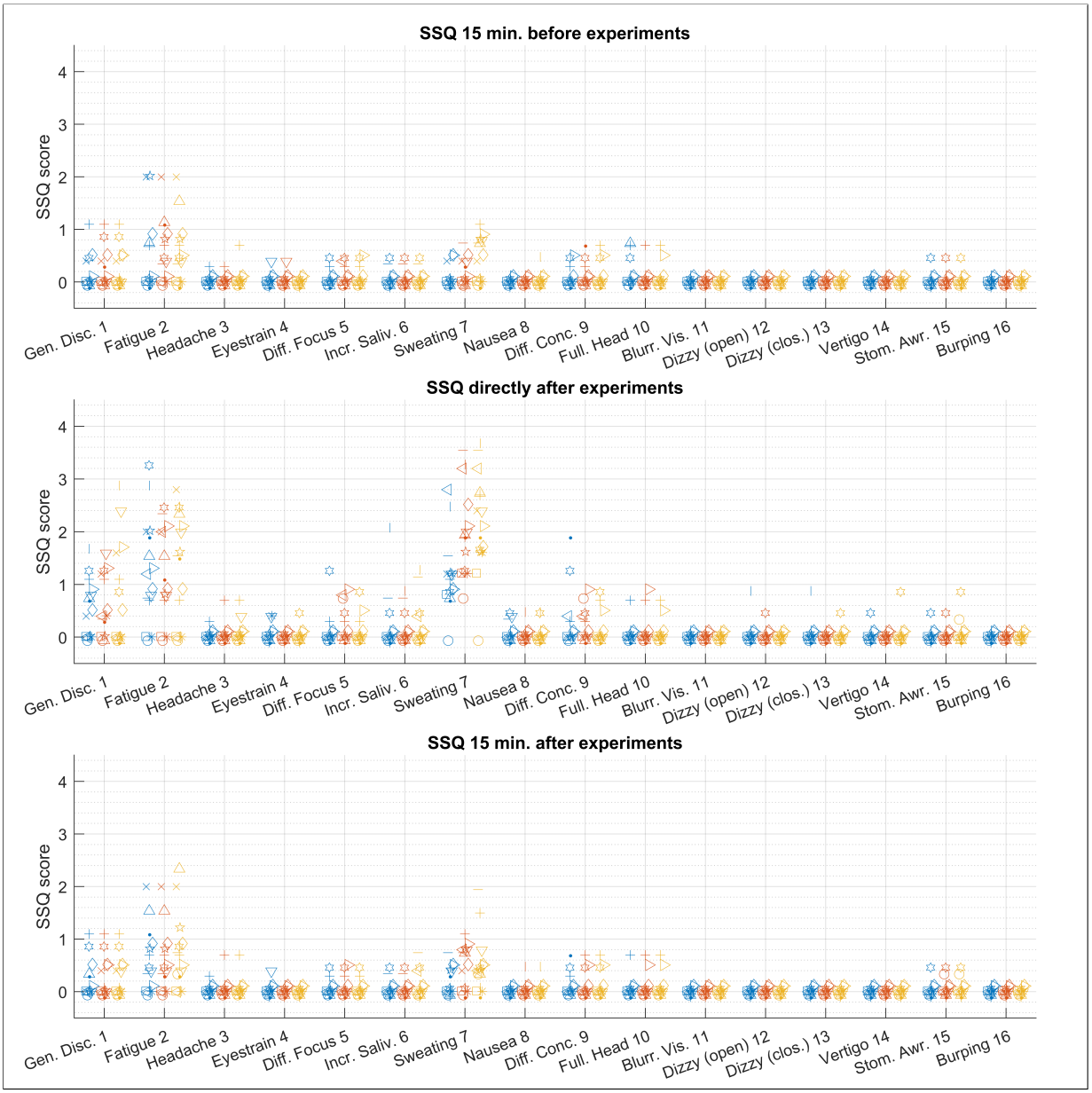

Figure 4.6: SSQ scores of participants before, directly after and after 15 minutes during experiments. Blue, red and yellow indicate outdoor, simulator and static cycling, respectively. Markers indicate participants.

Especially fatigue and sweating seemed to occur a lot during cycling, sweating even more so indoors, which are all assumed to relate to the physical exertion participants underwent, and the toughest manoeuvres coming last during experiments on a certain setup. The processing proposed in section 3.3 is heavily swayed due to the sweating and fatigue scores, thus the processed results are not shown here, since all other scores remained low as well.

4.3.3 Discussion

On the subjective side of the simulator, participants appeared to be fairly certain they were riding a bicycle. Questions regarding the control and quality of the motion of the simulator were scored close but still lower than outdoor cycling, relatively consistently, indicating that the subjective experience of the simulator is not yet what it could be. However, when queried what was missing in the simulator, participants also pointed to elements not considered in the design now, like wind and forwards motion, which could be included in future studies. Although maybe through advanced motion cueing, the motion profile of the simulator could be altered in such a way that its users could be tricked into perceiving forwards motion, since there already was some according to the participants.

Questions regarding the visualisation of the simulator produced widely varying scores, which could be due to the fact that the visualisation presented provides little immersion, or that the focus of the participant clearly lied more with maintaining the correct velocity than observing the scenery presented on the screen. During experiments, it became apparent that the wording of the questions regarding the visualisation seemed to cause confusion with the participants in some cases. The distribution of the scores could also be due to the participants not speaking out this confusion, leaving the interpretation of the question to maybe be incorrect.

Most participants appeared to experience being in control of the simulator, and felt safe and comfortable during the ride, although this was true more so in the case of outdoor cycling, and scores also did not differentiate much from scores of the static setup.

Comparative questions provide confirmation of that the subjective steer response lies close to outdoor cycling, as well as a natural sideways velocity, although scores were not a perfect 10 throughout. Participants were divided more on the matter of whether the provided motion, and the provided visualisation in particular, improved their cycling performance positively. This is in accordance with the question regarding whether participants experienced an increased effort trying to balance the bicycle, compared to outdoor cycling. On average, most participants agree that they did, although opinions were divided here as well.

Overall, the questionnaire scores from participants represent what kinematic measurements have indicated. The B.I.K.E. system approximates the behaviour of an outdoor bicycle, but is not yet realistic enough to produce the same sense of subjective realism experienced outdoors. Measurements on the kinematics of the bicycle indicate the same. In many regards, the kinematics of the bicycle come close to what happens outdoors, but lack the final push towards realism. Subjective scoring indicate a close-but-not-identical steering response of the simulator, which seems a logical result of there not being an actively controlled steering column with a correct steering torque and rotation response, dependent on forwards velocity.

As was the expectation from earlier studies, no real incidence of simulator sickness can be attributed to be a direct effect of the visualisation used in the simulator. As other studies have shown, a high involvement task, such as balancing a bicycle, reduces the risk for simulator sickness ([25], [2], [49]). A study ([27]) with a (static) bicycle ergometer and external monitor also investigated sickness effects, where more incidence of simulator sickness was recorded, but this setup did not include physical motion other than pedalling. Adding motion in a simulator, and letting that motion be similar to what you'd expect (from a bicycle, in this case) also reduces simulator sickness incidence ([36]). However, where there was no motion, i.e. with the static setup, no increase in simulator sickness incidence was observed. This could be due to the fact that participants were very focused on maintaining the correct velocity, or that they were not really immersed in the visual environment. A large field of view is required to induce a sense of immersion with the viewer (approximately 120°, [16]), which was also not present in the bicycle simulator.

Chapter 5

Conclusion & Future Work

5.1 Conclusion

In this study, I set out with the ambitious task of developing a bicycle simulator which simulates the roll, yaw and sway motion experienced by cyclists outdoors on an indoor setup, and validating this design through experiments. The main goal was to find out how accurately the developed bicycle simulator, which allows the user to balance it and which uses a kinematic vehicle model, compared to real-world outdoor cycling. The simulator design was based on the notion that cyclists normally control the support line of the bicycle by steering, and balance themselves and the bicycle as a result. The focus of studied motions lied with steer, roll, yaw and sway motions. A bicycle model was developed using bicycle geometry and kinematics and a measurement system was designed with the purpose of validating the simulator in mind. The minimal requirement for the performance of the simulator was to surpass existing static solutions in its realism of kinematic motion, compared to outdoor cycling.

Success was achieved in developing such a simulator. The simulator has the required degrees of freedom, response to cycling inputs, incorporates a resistance unit and uses a basic visualisation system. The B.I.K.E. system is, for a subject pool of 15 participants, usable and requires less than 15 minutes to get used to, in its current state. Users do not require preexisting experience with racing bicycles to be able to use this simulator, but cycling experience aids in the ease of getting used to the simulator. The model developed for the simulator is accurate in terms of the sway and yaw motions of the bicycle, with an exception for high-velocity ($> 35km/h$) riding, where a lack of damping, a lack of an active steering assembly and deviations between the vehicle model and reality increases the sensitivity of the simulator. The simulator is validated with a developed remote measurement system and newly proposed data analysis method, as well. It has been proven, through objective and subjective measures, that the steering response and applied balancing behaviour of cyclists on the simulator strongly resemble those taking place outdoors, but does not yet behave one-to-one.

As such, there is room for improvement on the simulator. The steering response could be controlled actively, to increase kinematic accuracy of the simulator as well as subjective realism. The visualisation's effect on subjective realism and immersion, and general usability of the simulator, appears to be low. If achieving subjective realism of the simulator becomes a goal in the future, the visualisation seems a good place to start.

In conclusion, with the B.I.K.E. system, I hope to have opened up the path towards a new method of bicycle simulation, which in the future could in turn open up research into simulator design, cyclist stabilisation and balancing behaviour, bicycle design and modelling, human controller metrics and high-involvement human-machine interaction, among others. Practically, the simulator as proposed could be used as a more kinematically free solution over existing ones for training purposes, but due to its adaptability, could be used in medical rehabilitation as well. A first step towards reproducing outdoor cycling balancing behaviour through kinematic modelling has been made.

5.2 Future work

Results from the present work point the way to numerous possible improvements. First of all, the quality of the kinematics of the bicycle could be improved, in multiple ways. As results show, non-linearities exist in the behaviour of a bicycle out on the road and its dependency on velocity. Using the found results in the vehicle model could already improve the kinematic response of the simulator. Another possibility in the improvement of the kinematics of the bicycle is the addition of realistic steering dynamics, where the torque-velocity response is closer to outdoor cycling than it currently is, with the mass-spring torque resistance. Not only could this improve kinematics of the bicycle in terms of accuracy and stability, but subjective realism as well. These and other improvements, like adding other physical elements to the simulator such as forwards motion, wind simulation or incline motion, could all improve the kinematic accuracy of the simulator, but improve on the subjective realism of it as well.

The kinematic vehicle model derived from bicycle geometry could also be improved with including tyre geometry, sideslip and deformation and also flexibility of bicycle parts (including the tyres), by for example linking those qualities experimentally to the bicycle's states as well as the rider's mass properties. An additional validation method of the used vehicle model could be the performing of an experimental stability analysis using perturbation methods with an uncontrolled bicycle on the simulator.

Improving the drive algorithm, which incorporates the vehicle model, of the simulator in terms of acceleration and control accuracy could decrease time delays inherent to the simulator. Should that not be enough to let the simulator perform better at increasing velocities, actuator qualities could be improved to match the required dynamics of the system, although much can be achieved by optimisation of the current control loops.

The measurement system and data processing algorithm are open to improvement and increase of robustness. Reducing influences of play, drift and limited accuracy of sensors is a first step there. Obtaining the states of the bicycle in a more robust manner from these sensors, with for example Kalman filtering, could as a consequence improve the model approximation from this data. On the topic of modelling, a non-linear model instead of the current linear state-space model, or an increase of bicycle states and input signals could improve the quality of the resulting models, such that they more accurately represent the kinematics of the bicycle.

Finally, more experiments are necessary for a more complete subjective analysis of the simulator, where the focus of the experiments only lies with the subjective experience. Improving the quality of the visual system, drawing the focus of the user to the virtual environment either by changing what is currently displayed or changing the visualisation system entirely, to a head-mounted display, or even larger (spherical) projection screens. In combination with the rebuilding of the control algorithm to allow for sustained cornering while using the bicycle simulator, an upgrade of the visual system could improve the immersion factor of the simulator greatly.

Bibliography

[1] Bendat, J. and Piersol, A. (1986). *Random Data: Analysis and Measurement Procedures*. Wiley-Interscience.

[2] Bos, J. (2015). Less sickness with more motion and/or mental distraction. *Journal of Vestibular Research*, 25(1):23–33.

[3] Bruni, S., Meijaard, J., Rill, G., and Schwab, A. (2020). State-of-the-art and challenges of railway and road vehicle dynamics with multibody dynamics approaches. *Multibody System Dynamics*, 49(3).

[4] Cain, S. (2013). An experimental investigation of human/bicycle dynamics and rider skill in children and adults. *Doctoral dissertation. Ann Arbor, MI: University of Michigan.*

[5] Cain, S. (2016). Measurement of bicycle and rider kinematics during real-world cycling using a wireless array of inertial sensors. In *Proceedings, Bicycle and Motorcycle Dynamics 2016, Symposium on the Dynamics and Control of Single Track Vehicles, 21–23 September 2016, Milwaukee, Wisconsin USA*.

[6] Cain, S., Ashton-Miller, J., and Perkins, N. (2016). On the skill of balancing while riding a bicycle. *PLoS ONE*, 11(2):e0149340.

[7] Cleij, D., Venrooij, J., Pretto, P., Pool, D., Mulder, M., and Bülthoff, H. (2018). Continuous subjective rating of perceived motion incongruence during driving simulation. *IEEE Transactions on Human-Machine Systems*, 48(1).

[8] Dialynas, G., Schwab, A., and Happee, R. (2019). Design and hardware selection for a bicycle simulator. *Mechanical Sciences*, 10:1–10.

[9] Dozza, M. and Fernandez, A. (2014). Understanding bicycle dynamics and cyclist behaviour from naturalistic field data. *IEEE Transactions on Intelligent Transportation Systems*, 15(1).

[10] Goetz, T. and von Drais von Sauerbronn, K. (1820). Draisinen. *Journal für Literatur, Kunst, Luxus und Mode*, 35.

[11] Groen, E. and Bos, J. (2008a). Simulator sickness depends on frequency of the simulator motion mismatch: An observation. *PRESENCE: Teleoperators and Virtual Environments*, 17(6):584–593.

[12] Groen, E. and Bos, J. (2008b). Simulator sickness depends on frequency of the simulator motion mismatch: An observation. *Presence*, 17(6):584–593.

[13] Grottoli, M. (2020). *Development and Evaluation of a Motorcycle Riding Simulator for Low Speed Maneuvering*. PhD thesis, Delft University of Technology.

[14] He, Q., Fan, X., and Ma, D. (2005). Full bicycle dynamic model for interactive bicycle simulator. *Journal of Computing and Information Science in Engineering*, 5(4).

[15] Hernández-Melgarejo, G., Flores-Hernández, D., Luviano-Juárez, A., Castañeda, L., Chairez, I., and Di Gennaro, S. (2019). Mechatronic design and implementation of a bicycle virtual reality system. *ISA Transactions*, 97:336–351.

[16] Jamson, H. (1996). Driving simulation validity: issues of field of view and resolution. *Proc. Driving Simul. Conf.*, pages 57–64.

[17] Kennedy, R., Lane, N., Berbaum, K., and Lilienthal, M. (1993). Simulator sickness questionnaire: An enhanced method for quantifying simulator sickness. *The International Journal of Aviation Psychology*, 3(3):203–220.

[18] Kikuchi, T. (2012). Development of virtual reality bike with cylindrical mr fluid brake. In *Proceedings of the 2012 IEEE International Conference on Robotics and Biomimetics, December 11-14, 2012, Guangzhou, China*.

[19] Kooijman, J., Meijaard, J., Papadopoulos, J., Ruina, A., and Schwab, A. (2011). A bicycle can be self-stable without gyroscopic or caster effects. *Science Magazine*, 332(6027):339–342.

[20] Kooijman, J., Schwab, A., and Moore, J. (2009). Some observations on human control of a bicycle. In *Proceedings of the ASME 2009 Internation Design Engineering Technical Conferences and Computers and Information in Engineering Conference, IDETC/CIE 2009 (August 30-September 2, San Diago, CA)*, page 8. American Society of Mechanical Engineers, New York. Paper No. DETC2009-86959.

[21] Kovácsová, N., de Winter, J., Schwab, A., Christoph, M., Twisk, D., and Hagenzieker, M. (2016). Riding performance on a conventional bicycle and a pedelec in low speed exercises: Objective and subjective evaluation of middle-aged and older persons. *Transportation Research Part F*, 42:28–43.

[22] Kwon, D., Yang, G., Lee, C., Shin, J., Park, Y., Jung, B., Lee, D., Lee, K., Han, S., Yoo, B., Wohn, K., and Ahn, J. (2001). Kaist interactive bicycle simulator. *Proceedings - IEEE International Conference on Robotics and Automation*, 3.

[23] LifeLine (2021). Lifeline rocker plaat. Last accessed on October 23rd, 2021.

[24] Ljung, L. (1999). *System Identification: Theory for the User*. Pearson.

[25] Matsangas, P., McCauley, M., and Becker, W. (2014). The effect of mild motion sickness and sopite syndrome on multitasking cognitive performance. *Human Factors*, 56(6).

[26] Meijaard, J., Papadopoulos, J., Ruina, A., and Schwab, A. (2007). Linearized dynamics equations for the balance and steer of a bicycle: a benchmark and review. *Proceedings of the Royal Society A*, 463:1955–1982.

[27] Mittelstaedt, J., Wacker, J., and Stelling, D. (2018). Effects of display type and motion control on cybersickness in a virtual bike simulator. *Displays*, 51:43–50.

[28] Moore, J. (2012). *Human Control of a Bicycle*. PhD thesis, University of California.

[29] Moore, J., Kooijman, J., Schwab, A., and Hubbard, M. (2011). Rider motion identification during normal bicycling by means of principal component analysis. *Multibocy System Dynamics*, 2(25):3–4.

[30] O'Hern, S., Oxley, J., and Stevenson, M. (2017). Validation of a bicycle simulator for road safety research. *Accident Analysis and Prevention*, 100:53–58.

[31] Parker (2021). Ospe32-bhd belt driven, square rail bearing, rodless linear actuator. From: https://ph.parker.com/us/en/ospe32-bhd-belt-driven-square-rail-bearing-rodless-linear-actuator, Retrieved on: August 30th, 2021.

[32] Penny, W. (2000). Signal processing course.

[33] Powell, J. (2017). Hardware design for an electro-mechanical bicycle simulator in an immersive virtual reality environment. Master's thesis, University of Iowa.

[34] Prothero, J. (1998). *The role of rest frames in vection, presence and motion sickness*. PhD thesis, University of Washington.

[35] Rankine, W. (1869, 1870). On the dynamical principles of the motion of velocipedes. *Engineer*, 28, 29:79, 129, 153, 175, 2.

[36] Reason, J. and Brand, J. (1975). *Motion sickness*. Academic Press.

[37] Sanjurjo, E., Naye, M., Cuadrado, J., and Schwab, A. (2019). Roll angle estimator based on angular rate measurements for bicycles. *Vehicle System Dynamics*, 57(11):1705–1719.

[38] Saris (2021). Mp1 nfinity trainer platform. Last accessed on October 23rd, 2021.

[39] Schramka, F., Arisona, S., Joos, M., and Erath, A. (2018). Development of virtual reality cycling simulator. *JCP*, 13(6):603–615.

[40] Schulzyk, O., Bongartz, J., Bildhauer, T., Hartmann, U., Goebel, B., Herpers, R., and Reinert, D. (2007). A bicycle simulator based on a motion platform in a virtual reality environment. *Advances in Medical Engineering. Springer Proceedings in Physics, vol. 114. Springer, Berlin, Heidelberg.*

[41] Schwab, A. and Meijaard, J. (2013). A review on bicycle dynamics and rider control. *Vehicle System Dynamcics: International Journal of Vehicle Mechanics and Mobility*, 7(51):1059–1090.

[42] Shoman, M. M. and Imine, H. (2021). Bicycle simulator improvement and validation. *IEEE Access*, 9.

[43] Smaili, M., Jansen, H., Naseri, A., Groen, E., and Stroosma, O. (2017). Pilot motion perception and control during a simulated decrab maneuver. Technical Report NLR-TP-2017-097, Netherlands Aerospace Centre (NLR).

[44] Tacx (2021). Tacx desktop app. From: https://www.microsoft.com/nl-nl/p/tacx-desktop-app/9nln5vxq40kx?activetab=pivot:overviewtab, Retrieved on: August 24th, 2021.

[45] Tang, Y., Tsoi, M., Fong, D., Lui, P., Hui, K., and Chan, K. (2007). The design of a virtual cycling simulator. *Lecture Notes in Computer Science*, 4469:162–170.

[46] Valente Pais, A. (2013). *Perception Coherence Zones in Vehicle Simulation*. PhD thesis, Delft University of Technology.

[47] Wang, P. and Yi, J. (2015). Dynamic stability of a rider-bicycle system: Analysis and experiments. In *2015 American Control Conference, Palmer House Hilton, July 1–3, 2015. Chicago, IL, USA*.

[48] Westerhof, B. (2018). Evaulation of the cruden motorcycle simulator. Master's thesis, Delft University of Technology.

[49] Wilson, M., Beadle, S., Kinsella, A., Mattfield, R., Hoover, A., and Muth, E. (2020). Task performance in a head-mounted display: The impacts of varying latency. *Displays*, 61:101930.

[50] Yap, H., Tan, C., Taha, Z., Chang, S., Sivadas, C., and Wan, W. (2018). Design and development of a spatial immersive track cycling simulator. *Journal of Movement, Health & Exercise*, 2(7):39–52.

[51] Zwift (2020).

Appendix A

Measurement System

In this appendix, the full hardware of the used measurement system in this study will be described. On a hardware level, the choice of sensors and their properties are given, and on a software level, the data acquisition as well as data processing algorithms are given.

A.1 Measurement Hardware

Based on earlier studies (see main document for references), the main method of obtaining the orientation and acceleration of a bicycle frame is through the use of Inertial Measurement Units, or IMU's. These often include an accelerometer and a gyroscope, of which the data streams can be combined to obtain a fairly accurate estimate of the bicycle's orientation. Existing studies often include a method of measuring the steering angle of the bicycle, as well as the velocity of the bicycle, which are both properties which change the kinematic behaviour of a bicycle.

One aspect which is not often recorded when experiments are performed on measuring the bicycle's kinematics, is the orientation and force exerted on the crank arms of the bicycle. In accordance to personal experience, as well as the analysis of existing higher degree-of-freedom indoor cycling setups, the coupling of the cyclist's cadence and the orientation of the bicycle are coupled quite extensively. A number of reasons can exist as to why these properties have not been recorded extensively;

- The measurement of the crank and pedal orientation, while not in a static indoor cycling environment, can be impractical due to moving components and data transmission in close proximity.
- Existing wireless crank sensors transmit data too slowly to be useful.
- The high-end equipment is very expensive, and not very open in its application.

In this study, we try to overcome these limitations by making use of Tacx's association with Garmin, and Garmin's enabling of developer modes on existing torque and crank orientation sensors, which in turn enable them to produce raw, high-frequency data while not producing large costs. Based in literary examples, and requirements set for the measurement system, the following sensors have been selected in the early phases of this study:

Table A.1: Sensor selection for the measurement of bicycle states, and their properties

Measured variable	**Sensor type**	**Symbol**	**Name**	**No.**
Angular velocity	HALL sensor	ω_R	Grove HALL Sensor	
Rear frame acceleration & angular velocity	IMU	$\vec{\boldsymbol{a}}_R, \vec{\boldsymbol{\omega}}_R$	Grove 6-axis IMU	
Steering angle	Potentiometer	δ_F	Vishay Model 132	
Crank angle & torque	Smart pedals	α_T, T_T	Garmin Rally 200	

Below, the main and relevant characteristics of these sensors are given. Due to confidentiality with Garmin's measurement pedals, those have been left out.

Table A.2: Grove HALL sensor (based on the Allegro A1101 HALL effect sensor) basic capabilities. Full capabilities described in Allegro's documentation[1].

Sensor quality	**Value and units**
Transition period	400 ns

Table A.3: Grove 6-axis IMU (based on the Bosch BMI088 sensor) basic capabilities. Full capabilities described in Bosch's documentation[2].

Sensor quality	**Value and units**
ADC Precision	15-bit
Gyroscope full-range (selectable)	$\pm 125 \frac{deg}{s}$
Accelerometer full-range (selectable)	$\pm 3g$
Gyroscope output datarate (selectable)	400 Hz
Accelerometer output datarate (selectable)	800 Hz
Gyroscope low-pass filter bandwidth (selectable)	...
Accelerometer low-pass filter bandwidth (selectable)	...

Table A.4: Vishay Model 132 basic capabilities. Full capabilities described in Vishay's documentation[3].

Sensor quality	**Value and units**
Linearity	$\pm 1.0\%$
Mechanical rotation freedom	$340^\circ \pm 5^\circ$
Power rating	2.75 W

The placement of the measurement board, with the above sensors attached to them, within the bicycle frame is given below:

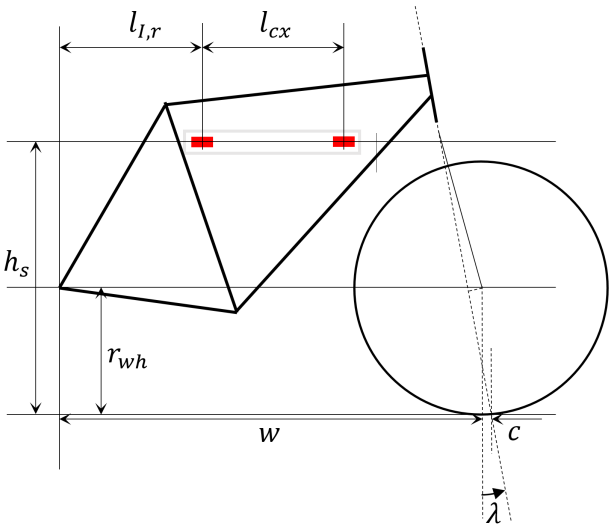

Figure A.1: Location of the front and rear IMU's with respect to the bicycle. Sensors are placed such that accelerometer x-axis aligns with the negative gravity vector in rest. Some common geometric bicycle parameters are indicated, as well.

[1]Allegro A1101 documentation: `https://www.allegromicro.com/~/media/Files/Datasheets/A110x-Datasheet.ashx`, last viewed on October 21st, 2021

[2]BMI088 documentation: `https://www.bosch-sensortec.com/products/motion-sensors/imus/bmi088/`, last viewed on October 21st, 2021

[3]Vishay Model 132 documentation: `https://www.vishay.com/docs/57096/132.pdf`, last viewed on October 21st, 2021

In its implementation, the measurement board looks as follows:

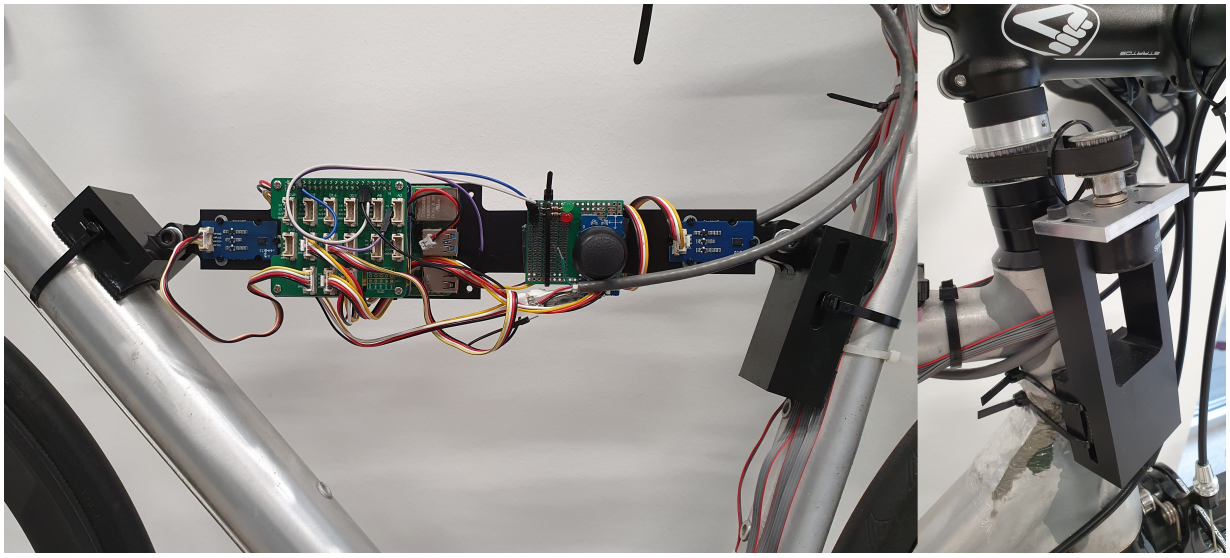

Figure A.2: Measurement board used to capture the dynamics and states of the bicycle, as well as the steering sensor attached to the bicycle steering column.

The data of this array of sensors is collected on an on-board Raspberry Pi 4B 8GB, with an approximate data rate of 207 Hz. For software implementation, refer to the supplemented Python scripts.

The main communication between the sensors is based on the I^2C[4] protocol, which allows multiple sensors to use the same clock signal during each measurement cycle. For this purpose, an expansion board was added to the Raspberry Pi to allow for more sensors to be connected. A battery, a control joystick and control LEDs are used as well.

[4]See `https://en.wikipedia.org/wiki/I%C2%B2C` for an overview.

A.2 Data Analysis & Comparison

We are looking for a relation between certain measurable variables in a bicycle which define someone's cycling pattern, comparable to how someone has a certain gait when walking. Since a bicycle is driven by an oscillating force and bicycle crank angle input, a relation can be made in the frequency domain between those and the orientation and angular rate data from the bicycle frame in terms of a frequency response function. In addition to the frequency response, the frequency-dependent coherence between bicycle states should also give an indication whether certain states are closely related in a certain cycling situation.

A.2.1 Data Recording - On Raspberry Pi

There are two Python scripts which are of importance in the measurement procedure taking place on the Raspberry Pi. Both are discussed in broad terms. The scripts are created using Python version 2.7.

InitialBalancer.py

Script for calibration and positioning of measurement board. In this script, the packages that are of importance to the script are first imported.

The addresses for the connections with the sensors and control units are then defined; in the case of I2C, the sensor addresses are board-determined, and for the digital pins, the address is dependent on the connected GPIO pin. Within the I2C protocol, registers are used to store data from different origins (for example accelerations in three directions). For the used sensors, the registers addresses are available in the documentation (see section on hardware above).

The I2C interface accepts control messages to certain registers. In *InitialBalancer.py*, there are several function created to convert bit-wise configuration messages to configuration information as text, as well as functions to read out raw data from the sensors for debugging purposes. At each startup, both sensors are reconfigured to the settings defined in the Python script. This way, they record data as in the previous experiments.

In the bottom part of the script, a loop within a function is created. The inner loop is for the recording of a number of samples which are averaged to remove noise components near zero. The orientations of the sensors are estimated using Equation A.23 and Equation A.24. In the function definition, the lines which are going to be plotted are created and shown shown using a MATPLOTLIB.PYPLOT object. Running this script will create a graph showing four lines, two of which are the roll and pitch angles of the front sensor, and the other two are the same angles from the rear sensor. With this visualisation, we verify the measurement board is affixed to the frame such that pitch and roll angles are zero when the bicycle is in the upright position.

MainMeasurement.py

Script for collecting and storing data from the measurement board. A lot of the initial procedures from *Initial-Balancer.py* are identical in this script. Here, the same I2C sensors and GPIO pins are initialized using their regular addresses and registers. The main workflow of the data storage is the following:

1. Turn on system, enable sensors and check for errors.
2. Create working directory for current experiment series.
3. In case of no errors, wait for the user to give the start signal (hold down joystick for four seconds = four green LED blinks).
4. When start signal is given, raw data from the sensors is stored in a new subfolder, named after the measurement number. Only green LED on.
5. When loop count surpasses the intermediate save limit (usually after 5 minutes), measurements are suspended for a short while while the data is stored (red LED on). Measurements continue after storage, and the red LED is off again.
6. During operation, the system continually checks for a stop signal (hold joystick sideways for four seconds = four red LED blinks). When it is given, the current measurement file is stored and all intermediate files are combined, converted to integers and stored as one .csv file.
7. Once done storing, the system is ready (both red and green LEDs on) for the next measurement in the experiment.

Once measurements are finished, the file can be accessed by connecting the Raspberry Pi to a display and input devices, and copying or e-mailing the measurement folder to the analysis PC. What happens after, is discussed in subsection A.2.3.

A.2.2 Data Recording - On Rally 200 + Garmin Edge 830

Another set of sensors which records and stores data during the experiments, are the Rally 200 Pedals. The procedure of enabling raw data measurements is only available for Garmin employees, or those granted access. In essence, this function on the Edge 830 enables the user to let the pedals store their raw data on the pedals themselves, after which the pedals have to be emptied wirelessly using software tools created by Garmin. In Appendix D, the steps for obtaining, storing and using this data is described, assuming the user has access to the proprietary software tools.

A.2.3 After-the-fact Data Processing

In general, the workflow from data processing can be divided in a number of discrete steps:

1. Time-alignment and resampling to universal sampling rate of data streams
2. Conversion from data streams to correct quantity and units
3. Performing calculations to obtain orientation, velocity and projected accelerations

These steps will be described below. In principle, all functions and methods are applied to all data streams, unless specified otherwise. Use of the data after step 3 is described in the main document this Appendix is attached to, and in other Appendices.

1: Time-alignment and resampling

With the current measurement system design, we obtain data from two sensor systems: the Raspberry Pi, producing accelerometer, gyroscope, digital Hall-effect pulses and potentiometer voltage data, and the Rally pedals, producing force and acceleration data for each pedal. This means two different recorded time series, sample rates, and different starting and ending times of the measurements (Raspberry, Left and Right pedal). A compensation for this is required. For now, this is done on a graphical basis. Each measurement is started with a calibration "bump", or in other words, a short burst of force on the right pedal, which also results in a accelerometer measurement peak. These are aligned by adding a delay to the time series of the pedals, since that measurement was started latest (as described in the experimental procedures, see Appendix D.). This procedure is done first to the recorded time series of each pedal as well, since those are often misaligned seemingly randomly.

Because all data sources have a different time series length, trailing and leading zeros are added to the Raspberry Pi data, such that they have the same starting and ending point as the pedal data.

Another necessary evil that has to be resolved, is that the Raspberry Pi has intermediate saving points, which act as a backup, to increase reliability of the measurement system and have a buffer when for whatever reason, the measurement system stops working. These points can be recognised in the time series of the Raspberry Pi by a sudden large timestep (several Δt's long). To increase the stability of the signal and the filters that are applied in a later stage, these gaps in data are filled up with data as if the sensor were perfectly horizontal and still.

When the time series have been aligned properly, the resampling of data commences. The goal is to make sure all data streams from all sensors are sampled at the same points as well as provide a uniformly distributed time series, to remove the need for accounting for this difference in a later stage. This is done using MATLAB's INTERP1 function, which is able to resample data with an existing time series, on a new time series. All data is truncated to a certain ending index, determined based on the shortest data length, since INTERP1 does not always produce the same length signal if based on two different time series. This truncation length is also based on the settling time of the applied filters, to remove oscillation in signals those might cause. Once this is done, and the signals have been assigned proper names, we can move on to the second step of data processing.

2: Conversion to useful data

The data that comes in from the sensors have the following names and units. They are described in Table A.5 and Table A.6.

Table A.5: Data produced by the measurement board connected to the Raspberry Pi. Given are the names as in the script *MainMeasurement.py*, the signal precision, a description of the obtained signal value and the symbol referred to in subsequent math operations.

Variable name (Pi)	Precision (Pi)	Description	Variable (math)
acc_rX	INT16	x Acceleration rear accelerometer	$a_{r,x}$
acc_rY	INT16	y Acceleration rear accelerometer	$a_{r,y}$
acc_rZ	INT16	z Acceleration rear accelerometer	$a_{r,z}$
acc_fX	INT16	x Acceleration front accelerometer	$a_{f,x}$
acc_fY	INT16	y Acceleration front accelerometer	$a_{f,y}$
acc_fZ	INT16	z Acceleration front accelerometer	$a_{f,z}$
gyr_rX	INT16	x Angular rate rear gyroscope	ω_x
gyr_rY	INT16	y Angular rate rear gyroscope	ω_y
gyr_rZ	INT16	z Angular rate rear gyroscope	ω_z
gyr_fX	INT16	x Angular rate front gyroscope	ω_x
gyr_fY	INT16	y Angular rate front gyroscope	ω_y
gyr_fZ	INT16	z Angular rate front gyroscope	ω_z
delta_sens	UINT16	Steer angle sensor	δ
HALL_sens	INT16	Rear wheel rotation rate	ω_R
T	DOUBLE	Pi timestamp	t_{Pi}

Table A.6: Data produced by the left measurement pedal. Given are the names, the signal precision, a description of the obtained signal value and the symbol referred to in subsequent math operations. These descriptions apply to the right pedal as well, changing the "L" notation to "R" in each signal name and math symbol.

Variable name (L Pedal)	Precision (L Pedal)	Description	Variable (math)
a_rad_L	INT8	Radial acceleration left pedal	$a_{rad,L}$
a_tan_L	INT8	Tangential acceleration left pedal	$a_{tan,L}$
F_plan_L	DOUBLE	Planar applied force left pedal axis	$F_{rad,L}$
F_norm_L	DOUBLE	Normal applied force left pedal axis	$F_{tan,L}$
sin_TL_raw_dat	DOUBLE	Sine of estimated crank angle	$\sin\theta_R$
cos_TL_raw_dat	DOUBLE	Cosine of estimated crank angle	$\cos\theta_R$
T_L	DOUBLE	Left pedal timestamp	t_L

We assume here that the time-alignment and resampling process have been completed successfully, so we can disregard any time differences or effects of misalignments in the processing of the data. The new, uniform time series will be denoted t, with a sampling frequency of $F_s = 400$ Hz.

We start with the computation of the acceleration vector of the accelerometers. This means converting the signed integer data into actual acceleration values, which is dependent on the accelerometer range and binary precision. The accelerometer has a 16-bit precision output, so a 15-bit precision for signed values. The accelerometer range is configurable on the accelerometer, and is currently set to ±3 g, based on pilot experiments. For each of the accelerometers, and their axes, the acceleration for one axis on the rear accelerometer is defined as in Equation A.1:

$$a_{r,x} = \text{ACC\_RX} * \frac{3}{32768} \frac{m}{s^2} \tag{A.1}$$

The acceleration vector for the front and rear accelerometers are defined as:

$$\vec{\mathbf{a}}_r = \begin{bmatrix} a_{r,x} \\ a_{r,y} \\ a_{r,z} \end{bmatrix} \quad \vec{\mathbf{a}}_f = \begin{bmatrix} a_{f,x} \\ a_{f,y} \\ a_{f,z} \end{bmatrix}$$

The same procedure is valid for the gyroscopes, which have a range of $\pm 125 \ \frac{^\circ}{s}$. The angular rate for one axis on the rear gyroscope is defined as in Equation A.2:

$$\omega_{r,x} = \text{GYR\_RX} * \frac{125}{32768} * \frac{\pi}{180} \ \frac{rad}{s} \tag{A.2}$$

The angular rate vectors for the front and rear gyroscopes are defined as:

$$\vec{\boldsymbol{\omega}}_r = \begin{bmatrix} \omega_{r,x} \\ \omega_{r,y} \\ \omega_{r,z} \end{bmatrix} \quad \vec{\boldsymbol{\omega}}_f = \begin{bmatrix} \omega_{f,x} \\ \omega_{f,y} \\ \omega_{f,z} \end{bmatrix}$$

A velocity estimation is obtained from the Hall sensor, mounted to the seatstay tubes. A pulse is obtained from the sensor every full rotation of the rear wheel, so it is possible to calculate an estimation for the angular velocity of the rear wheel. The indices on which a rise is detected in the sensor signal is stored, and the time difference between them is used to compute an estimate of the rear-wheel velocity. The following conditions are used to detect a rising signal:

$$p_{i-1} \neq 1 \text{ AND } p_i = 1$$

Where p_i is the i-th value in HALL_SENS. When either of the above two conditions is true, the index is stored and the accompanying timestep is recorded. Let k be the index of a recorded rise in the signal produced by the Hall sensor, and n be the number of magnets measured per revolution. The approximated velocity is then:

$$\omega_R = \frac{2\pi}{n\,(t_k - t_{k-1})} \ \frac{rad}{s} \tag{A.3}$$

Due to data sometimes being missed by vibration or sensor misalignment, an additional algorithm is used to compensate for missed data based on the signal that was produced in Equation A.3. The second order derivative is used to detect sudden drops in the velocity signal. The average amount of pulses during a certain window before that drop is then used to fill the missing pulses in the signal. This solution is not completely robust, but improves signal quality especially at higher velocities.

Where r_{cr} is the crank length from rotation axis to pedal axis. The acceleration data from the individual pedals is also computed, since this may prove to be useful as an input to compare different cycling situations with. First, the angular acceleration of a crank is computed with the radial and tangential acceleration readings from both pedals. Here, the signals are again produced in opposing coordinate systems, thus the signs of the signals might be unexpected. To bypass the pedal's own filtering for this estimate, we do our own processing of the raw data with the installation angles of the pedals with respect to the bicycle cranks. The below processing applies to the right pedal, as well.

$$\begin{bmatrix} a_{r,L} \\ a_{t,L} \end{bmatrix} = -\begin{bmatrix} \cos(\theta_{inst,L}) & -\sin(\theta_{inst,L}) \\ \sin(\theta_{inst,L}) & \cos(\theta_{inst,L}) \end{bmatrix}^{-1} \begin{bmatrix} a_{rad,L} \\ a_{tan,L} \end{bmatrix} \tag{A.4}$$

And similarly, torque:

$$\begin{bmatrix} F_{r,L} \\ F_{t,L} \end{bmatrix} = -\begin{bmatrix} \cos(\theta_{inst,L}) & -\sin(\theta_{inst,L}) \\ \sin(\theta_{inst,L}) & \cos(\theta_{inst,L}) \end{bmatrix}^{-1} \begin{bmatrix} F_{plan,L} \\ F_{norm,L} \end{bmatrix} \tag{A.5}$$

From these rotated values, we can obtain the instantaneous angular acceleration of the cranks:

$$\alpha_T = -\frac{a_{r,R} - a_{r,L}}{2} * \frac{1}{256 * r_{cr}} \tag{A.6}$$

And the instantaneous torque exerted on the crank axis. The applied torques to each pedal are computed and combined into a net torque as follows:

$$T_L = r_{cr} * F_{t,L} \tag{A.7}$$
$$T_R = r_{cr} * F_{t,R} \tag{A.8}$$
$$T_{tot} = T_L - T_R \tag{A.9}$$

Since the pedals produce data in opposed coordinate systems, the combination of this data is different from what one might expect. In addition to the angular acceleration, the instantaneous crank angles and angular velocity of the crank can be computed as well:

$$\theta_{T,R} = \text{ATAN2}\left(\frac{a_{r,R} - a_{r,L}}{2},\ \frac{a_{r,R} + a_{r,L}}{2}\right) \tag{A.10}$$
$$\theta_{T,L} = \theta_{T,R} + \pi \tag{A.11}$$
$$\omega_T = \sqrt{-\frac{a_{r,R} + a_{r,L}}{2} * \frac{1}{256 * r_{cr}}} \tag{A.12}$$

Considering the steer sensor, the conversion from sensor data to steering angle is dependent on several variables. Firstly, the voltage from the potentiometer (V_δ) is converted into a 12-bit signal, giving it a precision of $\frac{1}{4096}\ \frac{V}{bit}$. The analogue-to-digital converter uses an internal reference voltage of $V_{ref} = 3\ V$, while the potentiometer is fed with $V_{max} = 3.3\ V$. By experimentation, the minimum and maximum voltages were obtained, giving the sensor a conversion ratio of $V_{conv}\ \frac{V}{deg}$. Secondly, the signal is offset by a certain value, due to initial mounting of the gears on both the steering and potentiometer axes. $\delta_G\ deg$ is used to compensate for the offset. This value can be obtained by keeping the bicycle steering wheel straight in the initial stage of the measurements. Thirdly, the measurement potentiometer has a certain maximum mechanical angle over which it can measure, $\delta_{max}\ deg$, which acts as the scaling for the voltage to an angle value. Finally, there exists a transmission ratio i_δ between the steering and potentiometer axes due to the gears used. This brings the computation of the steering angle down to:

$$\delta = \left(V_\delta * \frac{2 * V_{ref}}{4096} * \frac{1}{V_{max} * V_{conv}} * \delta_{max} - \delta_G\right) \frac{1}{i_\delta} * \frac{\pi}{180} \tag{A.13}$$

For situations in which the cyclist keeps his bicycle chain under tension (in other words, directly coupled with the rear wheel velocity), we can obtain an estimate for the transmission ratio between the cranks and the rear wheel, caused by the bicycle chainset. This is now done by checking the velocity of the cranks and making sure it is above a certain limit. Then, dividing it by the rear wheel velocity obtained from the Hall sensor, we obtain a transmission ratio, which can be used to compare data from different cyclist when they prefer different transmissions for a certain manoeuvre.

Finally, the raw data (with low-pass filtering of passband frequency of 30 Hz already applied to them), are plotted in one large figure, for visual review and for spotting discontinuities. Such a figure may look like Figure A.3:

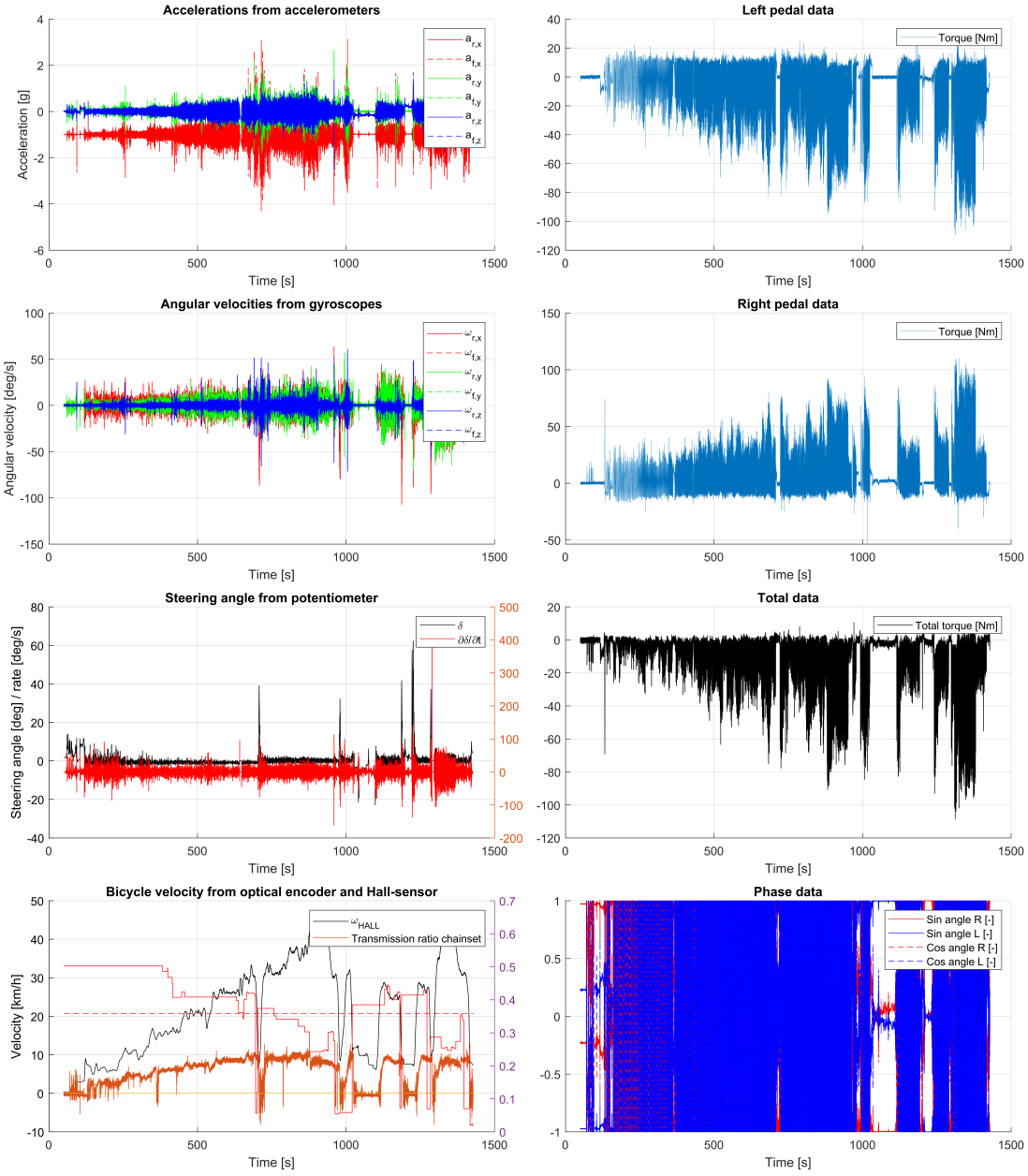

Figure A.3: Raw data obtained from sensors. Subfigures show data originating from different sensors, including rotation rate, acceleration, pedal torque and crank and rear-wheel velocity.

Performing calcultions to obtain orientation data

One of the aims of the measurement system is to obtain the geometric orientation of the bicycle with respect to a fixed world frame. This world frame is indicated in Figure A.4 as the $\hat{x}\hat{y}\hat{z}_{ac,O}$ coordinate system. Several other coordinate systems are defined, which will be discussed once they become relevant.

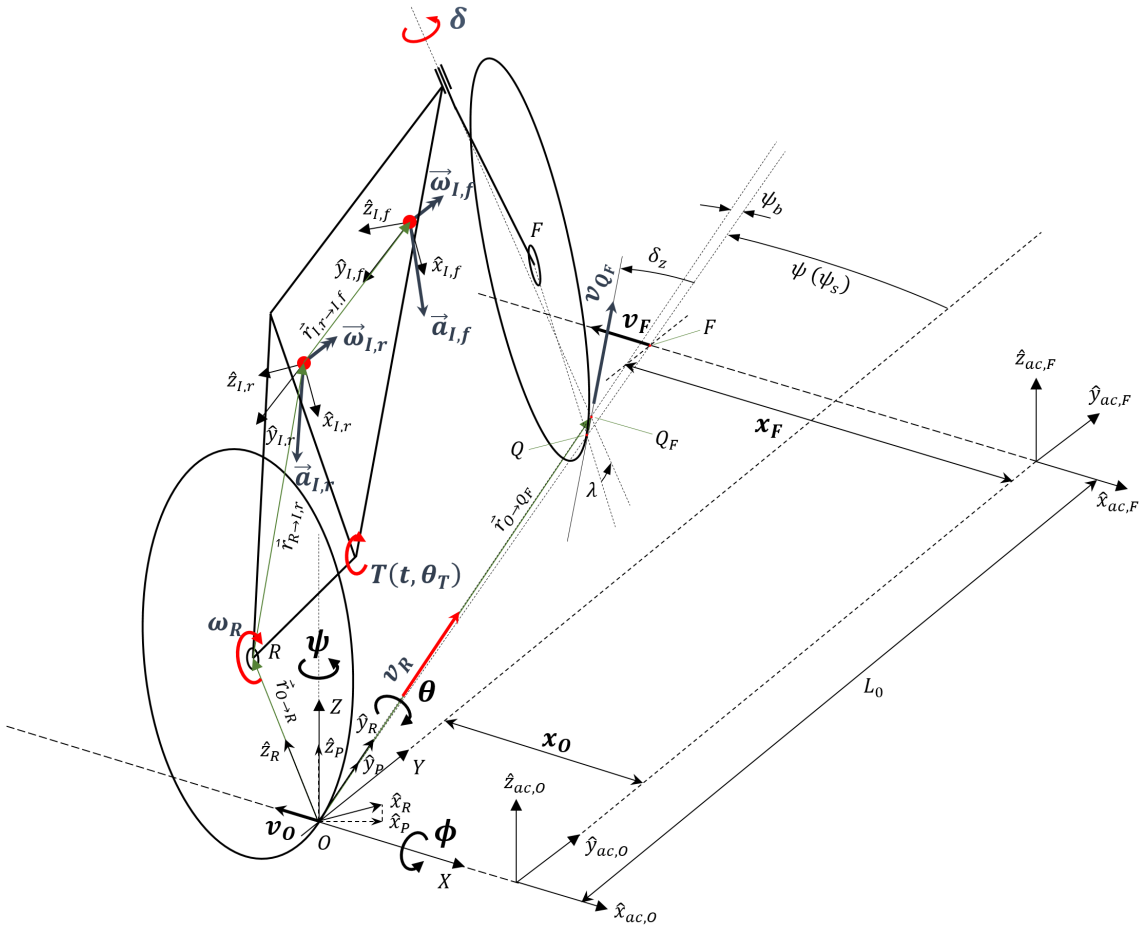

Figure A.4: Coordinate system, with sensors placed in the bicycle. Indicated are several coordinate systems, observed sensor values and coordinates of the simulator as well.

The orientation angles ϕ, θ and ψ are defined as the rotations about the $X, \hat{y}_R$ (pointing from point O to Q_F) and Z axes. The $\hat{x}_R, \hat{y}_R, \hat{z}_R$ coordinate system is a bicycle rear frame-fixed coordinate system, where $\hat{z}_R$ is aligned with the rear wheel vertical axis, and $\hat{y}_R$ is aligned with the bicycle wheel base (between points O and Q). Two sources exist for the obtaining of the orientation angles of an IMU. On the one hand, an accelerometer can be used to obtain its own rotation by measuring the gravity vector on its own three axes, but there are limitations. Only two angles can be determined, due to ambiguity in 3D rotations, and orientation estimations from accelerometers are generally very sensitive to vibration. On the other hand, a gyroscope can integrate the measured angular rate into a rotation as well, with the downside that gyroscopes are subject to drift - a problem which is amplified when numerically integrating the angular rate.

Combining the sensor readings from both an accelerometer and a gyroscope is a well-known strategy, with methods such as static selective combination (known as complementary filtering[5].), or highly advanced Kalman-based filters[6]. This study proposes a method in-between to obtain better results than using one source for the orientation of the bicycle, but not have to use such an advanced method as Kalman filtering. In the proposed method, the current state of accelerometer readings is the basis for a weighing factor, which selects a (combination of) geometric orientation source(s). This method, adjusted for this measurement system, first rotates the coordinate system of both IMU's ($\hat{x}_{I,r}, \hat{y}_{I,r}, \hat{z}_{I,r}$ and $\hat{x}_{I,f}, \hat{y}_{I,f}, \hat{z}_{I,f}$ for the rear and front, respectively) such that they would align with the world X, Y, Z coordinate system if the bicycle would be upright with a zero rotation angles ($\psi = \theta = \delta = 0$). For this, we need a rotation matrix which rotates the certain three-axial sensor readings to the new coordinate system:

$$\begin{aligned}\vec{\mathbf{R}}_{sens} &= \vec{\mathbf{R}}_x^{-1}(-\pi)\vec{\mathbf{R}}_y^{-1}\left(\frac{\pi}{2}\right)\vec{\mathbf{R}}^{-1}{}_z(0) \\ &= \begin{bmatrix}1 & 0 & 0\\ 0 & \cos(-\pi) & -\sin(-\pi)\\ 0 & \sin(-\pi) & \cos(-\pi)\end{bmatrix}\begin{bmatrix}\cos\left(\frac{\pi}{2}\right) & 0 & \sin\left(\frac{\pi}{2}\right)\\ 0 & 1 & 0\\ -\sin\left(\frac{\pi}{2}\right) & 0 & \cos\left(\frac{\pi}{2}\right)\end{bmatrix}\begin{bmatrix}1 & 0 & 0\\ 0 & 1 & 0\\ 0 & 0 & 1\end{bmatrix}\end{aligned} \tag{A.14}$$

Where $\vec{\mathbf{R}}_x, \vec{\mathbf{R}}_y, \vec{\mathbf{R}}_z$ are standard right-handed Cartesian coordinate system rotation matrices, with the rotation axis being denoted by the subscript. All IMU measurements at a certain measurement interval are pre-multiplied with Equation A.14's rotation matrix. In general, for a relative-motion analysis in 3D, the following equation holds true for certain points A and B in 3D space, moving and accelerating with respect to each other:

$$\vec{\mathbf{a}}_B = \vec{\mathbf{a}}_A + \vec{\boldsymbol{\alpha}} \times \vec{\mathbf{r}}_{A\to B} + \vec{\boldsymbol{\omega}} \times (\vec{\boldsymbol{\omega}} \times \vec{\mathbf{r}}_{A\to B}) + 2\vec{\boldsymbol{\omega}} \times \left(\vec{\mathbf{v}}_{B/A}\right)_{xyz} + \left(\vec{\mathbf{a}}_{B/A}\right)_{xyz} \tag{A.15}$$

We can use Equation A.15 to compensate for angular accelerations picked up in the IMU accelerometers, due to an angular acceleration of the bicycle frame in the $\hat{x}_R, \hat{y}_R, \hat{z}_R$ coordinate system. We can substitute A with O, and B with I, r for the rear accelerometer, I, f for the front one, in Equation A.15. $\vec{\mathbf{v}}_{B/A}$ and $\vec{\mathbf{a}}_{B/A}$ can be set to zero, since no relative motion exists between the accelerometers and point O, assuming the accelerometers and bicycle frame are rigidly connected. So:

$$\vec{\mathbf{a}}_{I,r} = \vec{\mathbf{a}}_{O,r} + \vec{\boldsymbol{\alpha}}_{O,r} \times \vec{\mathbf{r}}_{O\to I,r} + \vec{\boldsymbol{\omega}}_{O,r} \times (\vec{\boldsymbol{\omega}}_{O,r} \times \vec{\mathbf{r}}_{O\to I,r}) \tag{A.16}$$

Where $\vec{\mathbf{a}}_{O,r}$ consists of only linear accelerations and $\vec{\mathbf{a}}_{I,r}$ measures both linear accelerations not originating from the angular velocities and accelerations of the bicycle frame, as well as acceleration due to angular accelerations. $\vec{\mathbf{a}}_{O,r}$ is obtained by rearranging Equation A.16:

$$\vec{\mathbf{a}}_{O,r} = \vec{\mathbf{a}}_{I,r} - \vec{\boldsymbol{\alpha}}_{O,r} \times \vec{\mathbf{r}}_{O\to I,r} - \vec{\boldsymbol{\omega}}_{O,r} \times (\vec{\boldsymbol{\omega}}_{O,r} \times \vec{\mathbf{r}}_{O\to I,r}) \tag{A.17}$$

Since the coordinate system $\hat{x}_R, \hat{y}_R, \hat{z}_R$ is now aligned with the IMU coordinate systems (due to rotating with Equation A.14), point O now undergoes the same the angular velocity $\vec{\boldsymbol{\omega}}_{I,r}$ and acceleration $\vec{\boldsymbol{\alpha}}_{I,r}$. $\vec{\boldsymbol{\alpha}}_O$ is obtained trough the numerical differentiation of $\vec{\boldsymbol{\omega}}_{I,r}$, using the a higher-order numerical differentiation method, looking only at past samples:

$$\vec{\boldsymbol{\alpha}}_O = \frac{\partial \vec{\boldsymbol{\omega}}_{I,r}}{\partial t} \approx \frac{-2\vec{\boldsymbol{\omega}}_{I,r,t_{i-3}} + 9\vec{\boldsymbol{\omega}}_{I,r,t_{i-2}} - 18\vec{\boldsymbol{\omega}}_{I,r,t_{i-1}} + 11\vec{\boldsymbol{\omega}}_{I,r,t_i}}{6\Delta t} \tag{A.18}$$

With $\vec{\boldsymbol{\omega}}_{I,r,t_{i+1}}$ a measurement of angular velocity at time instance t_{i+1}, and Δt is the timestep between measurements. The obtained signal is low-pass filtered to reduce the differentiation noise, with a passband frequency of 6 Hz. $\vec{\boldsymbol{\omega}}_O$ is equal to $\vec{\boldsymbol{\omega}}_{I,r}$. Using the definitions as in Figure A.1, we can obtain $\vec{\mathbf{a}}_O$:

$$\begin{aligned}\vec{\mathbf{a}}_{O,r} &= \vec{\mathbf{a}}_{I,r} - \vec{\boldsymbol{\alpha}}_{O,r} \times \begin{bmatrix}0\\ l_{I,rx}\\ h_s\end{bmatrix}\frac{1}{g} - \vec{\boldsymbol{\omega}}_{O,r} \times \left(\vec{\boldsymbol{\omega}}_{O,r} \times \begin{bmatrix}0\\ l_{I,rx}\\ h_s\end{bmatrix}\right)\frac{1}{g} \\ &= \begin{bmatrix}a_{I,r,x} - a_{I,r,y}h_s + a_{I,r,z}l_{I,rx} - h_s\omega_{I,r,x}\omega_{I,r,z} - l_{I,rx}\omega_{I,r,x}\omega_{I,r,y}\\ l_{I,rx}\omega_{I,r,x}^2 + a_{I,r,y} + a_{I,r,x}h_s - \omega_{I,r,z}\left(h_s\omega_{I,r,y} - l_{I,rx}\omega_{I,r,z}\right)\\ h_s\omega_{I,r,x}^2 + a_{I,r,z} - a_{I,r,x}l_{I,rx} + \omega_{I,r,y}\left(h_s\omega_{I,r,y} - l_{I,rx}\omega_{I,r,z}\right)\end{bmatrix}\end{aligned} \tag{A.19}$$

[5]Complementary filtering, see `http://www.pieter-jan.com/node/11` for a brief explanation, last accessed on October 21st, 2021.

[6]Kalman filtering for balancing a hoverboard, an implementation: `https://globaljournals.org/GJRE_Volume19/2-Control-Unit-for-a-Two-Wheel.pdf`, last accessed on October 21st, 2021.

Equation A.19 is presented with the rear IMU as its measurement source, but the same principle holds for the front IMU, with the only change that $\vec{\mathbf{r}}_{O\rightarrow I,f} = [0, h_s, l_{I,rx} + l_{cx}]^T$. The $\frac{1}{g}$ term is present to make sure the units of the terms in Equation A.19 agree.

Now, the linear accelerations of point O (in the $\hat{x}_R, \hat{y}_R, \hat{z}_R$ coordinate system) and the accelerations from rotational motions are isolated, such that the estimate for the orientations of the bicycle from accelerometer only become more accurate. Obtaining angle estimates for ϕ and θ is performed with a number of assumptions. Obtaining an orientation estimate from an accelerometer is based on the notion that there is always a measurable gravitational acceleration present. However, not all three angles ϕ, θ and ψ can be obtained[7]. Mathematically, obtaining this orientation is based on the assumption that the coordinate system gravity acts in (X, Y, Z), which can be rotated towards the sensor coordinate system of the IMU's $(\hat{x}_R, \hat{y}_R, \hat{z}_R)$. The rotation matrix for this operation is:

$$\vec{\mathbf{R}}_{acc}^{-1} = \vec{\mathbf{R}}_{x}^{-1}(\phi)\vec{\mathbf{R}}_{\hat{y}_R}^{-1}(\theta)\vec{\mathbf{R}}_{z}^{-1}(\psi) \tag{A.20}$$

Where:

$$\vec{\mathbf{R}}_{x}^{-1}(\phi) = \begin{bmatrix} 1 & 0 & 0 \\ 0 & \cos(\phi) & -\sin(\phi) \\ 0 & \sin(\phi) & \cos(\phi) \end{bmatrix}$$

$$\vec{\mathbf{R}}_{\hat{y}_R}^{-1}(\theta) = \begin{bmatrix} \cos(\theta) & 0 & -\sin(\theta) \\ 0 & 1 & 0 \\ \sin(\theta) & 0 & \cos(\theta) \end{bmatrix}$$

$$\vec{\mathbf{R}}_{z}^{-1}(\psi) = \begin{bmatrix} \cos(\psi) & \sin(\psi) & 0 \\ -\sin(\psi) & \cos(\psi) & 0 \\ 0 & 0 & 1 \end{bmatrix}$$

What holds true, is that $\vec{\mathbf{a}}_r$ must be equal to the gravity vector, when the system is at rest. This results in:

$$\vec{\mathbf{a}}_r = \mathbf{R}_{acc}^{-1}\vec{\mathbf{g}} \tag{A.21}$$

or:

$$\vec{\mathbf{a}}_r = \begin{bmatrix} \cos(\theta)\cos(\psi) & \cos(\theta)\sin(\psi) & -\sin(\theta) \\ \cos(\psi)\sin(\theta)\sin(\phi) - \cos(\phi)\sin(\psi) & \cos(\phi)\cos(\psi) + \sin(\theta)\sin(\phi)\sin(\psi) & \cos(\theta)\sin(\phi) \\ \sin(\phi)\sin(\psi) + \cos(\phi)\cos(\psi)\sin(\theta) & \cos(\phi)\sin(\theta)\sin(\psi) - \cos(\psi)\sin(\phi) & \cos(\theta)\cos(\phi) \end{bmatrix} \begin{bmatrix} 0 \\ 0 \\ 1 \end{bmatrix}$$

which results in the following, where the measurement $\vec{\mathbf{a}}_r$ has been normalized:

$$\frac{1}{\sqrt{a_{r,x}^2 + a_{r,y}^2 + a_{r,z}^2}} \begin{bmatrix} a_{r,x} \\ a_{r,y} \\ a_{r,z} \end{bmatrix} = \begin{bmatrix} -\sin(\theta) \\ \cos(\theta)\sin(\phi) \\ \cos(\theta)\cos(\phi) \end{bmatrix} \tag{A.22}$$

So, finally:

$$\theta_{a,r} = \sin^{-1}\left(\frac{-a_{r,x}}{\sqrt{a_{r,x}^2 + a_{r,y}^2 + a_{r,z}^2}}\right) \tag{A.23}$$

and:

$$\phi_{a,r} = \tan^{-1}\left(\frac{a_{r,y}}{a_{r,z}}\right) \tag{A.24}$$

[7] `https://www.nxp.com/docs/en/application-note/AN3461.pdf`, last accessed October 21st, 2021.

Early measurement with this system show that large deviations occur due to parasitic sensor behaviour: if the bicycle undergoes a certain sustained cornering manoeuvre, the bicycle tends to be rolled with a certain angle. However, since the sensors are now tilted as well, the measurement for the pitch angle ϕ increases due to an angular velocity around the $\hat{x}_R$ axis. For this addition will be compensated later on. The accelerations of the front and rear accelerometer, as well as the angular velocities of the front and rear gyroscope are added and weighted with a weighing factor $w_a = \frac{1}{2}$:

$$\vec{\mathbf{a}}_{O,\hat{x}_R\hat{y}_R\hat{z}_R} = \vec{\mathbf{a}}_{O,f}\,(1 - w_a) + \vec{\mathbf{a}}_{O,r} w_a \tag{A.25}$$

$$\vec{\boldsymbol{\omega}}_{O,\hat{x}_R\hat{y}_R\hat{z}_R} = \vec{\boldsymbol{\omega}}_{O,f}\,(1 - w_a) + \vec{\boldsymbol{\omega}}_{O,r} w_a \tag{A.26}$$

The estimates for the roll and pitch angles from these compounded accelerations according to Equation A.23 and Equation A.24 are filtered with a moving-mean filter, with a width of $\frac{1.5}{T_s}$ samples. Since we try to derive a time-invariant algorithm for the , which merges data from the accelerometer and the gyroscope, a weighing factor is first devised based on accelerometer measurements. In basic terms, the weighing factor is based on the randomness of accelerations without the estimated gravity term, at a certain moment in a range of measurements. We can derive a mathematical factor for this, based on the moving standard deviation, which computes the standard deviation for a slice of acceleration measurements. If this standard deviation is high, chances are that the number of vibrations and non-gravity accelerations is high, so the computation of orientation of the bicycle from the accelerometer is not reliable. The algorithm will then favour the gyroscope measurements. There is a certain transition range between orientation from acceleration and orientation from gyroscope measurements, based on the cumulative distribution function of a normal distribution. This distribution was picked due to the fact that once $x \to \infty$, the value of the distribution approaches 1, so there are no jumps in the computed signal due to a function not having the horizontal asymptote equal to 1. Mathematically, the dynamic weighing factor can be described as follows:

$$\vec{\mathbf{S}}_{a,i} = \sqrt{\frac{1}{k-1}\sum_{k=1}^{n}\left(\vec{\mathbf{a}}_{O,\hat{x}_R\hat{y}_R\hat{z}_R,k} - \vec{\boldsymbol{\mu}}_{a,i}\right)^2} \tag{A.27}$$

Where $k = i - \frac{n}{2}, i - \frac{n}{2} + 1, i - \frac{n}{2} + 2, ..., i - \frac{n}{2} + n$ are the instances in a signal slice of length n, centred around measurement instance i and μ_i is the average of signal slice i, using the same instances k. $i = 2, 3, ..., n_{max}$; n_{max} being the total number of measurements. The acceleration used in the weighing factor is compensated with gravity as if the bicycle were at rest:

$$\vec{\mathbf{a}} = \vec{\mathbf{a}}_{O,\hat{x}_R\hat{y}_R\hat{z}_R} - \vec{\mathbf{g}}_{eq} = \vec{\mathbf{a}}_{O,\hat{x}_R\hat{y}_R\hat{z}_R} - \begin{bmatrix}0\\0\\1\end{bmatrix} \tag{A.28}$$

For each of the two accelerometer sensors, there are three possible scenarios, based on the magnitude of the weighing factor. These lower and upper limits of the transition range between accelerometer and gyroscope measurements are determined arbitrarily, with the center between the limits Δ_w, and the half-width between the center and either the upper or lower limit $\delta_w\Delta_w$.

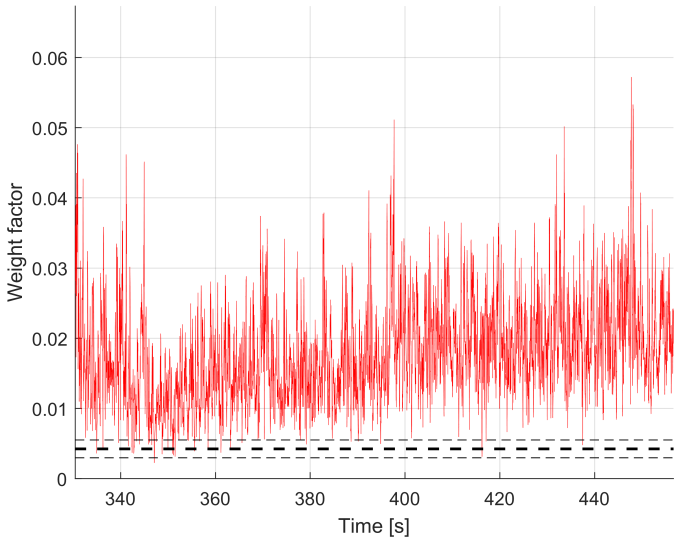

Figure A.5: Moving standard deviation of acceleration vector, with limits of width Δ_w.

The first scenario is that the weighing factor is too high to be in the transition range, and too high to be trusted for an accurate estimation of the orientation of the bicycle. In that case, the following holds true:

$$\|S_{a,r,i}\| > \Delta_w(1+\delta_w) \tag{A.29}$$

Then, the estimate for the orientation of the bicycle is the result of numerical integration of the measured angular velocity $\vec{\boldsymbol{\omega}}_{O,\hat{x}_P\hat{y}_P\hat{z}_P}$, which is measured in the bicycle $\hat{x}_R, \hat{y}_R, \hat{z}_R$ coordinate system. In order to measure in the world X, Y, Z coordinate system, the coordinate system $\hat{x}_R, \hat{y}_R, \hat{z}_R$ where measurement of $\vec{\boldsymbol{\omega}}_{I,r}$ takes place has to be rotated back to the X, Y, Z coordinate system, using the previous orientation estimation:

$$\vec{\mathbf{R}}_i = \vec{\mathbf{R}}_x(\phi_{\omega,i})\vec{\mathbf{R}}_y(\theta_{\omega,i}) \tag{A.30}$$

$$\vec{\boldsymbol{\omega}}_{O,\hat{x}_P\hat{y}_P\hat{z}_P} = \vec{\mathbf{R}}_i\vec{\boldsymbol{\omega}}_{O,\hat{x}_R\hat{y}_R\hat{z}_R} \tag{A.31}$$

Using this transformed angular velocity, we can use numerical integration, using Simpson's rule with a window of three points[8], to obtain an estimation of the rotation angles from the gyroscope measurements:

$$\vec{\boldsymbol{\omega}}_{O,\hat{x}_P\hat{y}_P\hat{z}_P,i-\frac{1}{2}} = \frac{1}{2}\left(\vec{\boldsymbol{\omega}}_{O,\hat{x}_P\hat{y}_P\hat{z}_P,i} - \vec{\boldsymbol{\omega}}_{O,\hat{x}_P\hat{y}_P\hat{z}_P,i-1}\right) + \vec{\boldsymbol{\omega}}_{O,\hat{x}_P\hat{y}_P\hat{z}_P,i-1} \tag{A.32}$$

$$\theta_i = \left(\omega_{O,\hat{y}_P,i-1} + 4\omega_{r,\hat{y}_P,i-\frac{1}{2}} + \omega_{r,\hat{y}_P,i}\right)\frac{\Delta t}{6} + \alpha_{HP}\theta_{i-1} \tag{A.33}$$

$$\phi_i = \left(\omega_{O,\hat{x}_P,i-1} + 4\omega_{r,\hat{x}_P,i-\frac{1}{2}} + \omega_{r,\hat{x}_P,i}\right)\frac{\Delta t}{6} + \alpha_{HP}\phi_{i-1} \tag{A.34}$$

Where the filtering constant $\alpha_{HP} = 1 - \frac{T_s}{10}$ is introduced, since early measurements showed that a bias in the angular velocity vector, however small, almost always introduces a bias to the estimated roll angle θ. Under the assumption that the equilibrium position of the bicycle is upright, and for θ, we are more interested in short-term rotations, the filtering constant α_{HP} makes sure the roll angle estimate converges to zero over a longer period of time, without affecting short term rotations.

[8]See `https://en.wikipedia.org/wiki/Simpson%27s_rule` for an overview, last accessed on October 21st, 2021.

The second scenario is that the weighing factor is low enough that the accelerometer can be used for the orientation estimate of the bicycle. In that case, the following holds true:

$$\|S_{a,i}\| < \Delta_w(1-\delta_w) \tag{A.35}$$

Where we can then use Equation A.25 in combination with Equation A.23 and Equation A.24 (processed with a moving-mean filter) to obtain the estimates for the bicycle's orientation with respect to gravity.

Finally, the most intricate situation, is where the weighing factor falls in the transition range between accelerometer and gyroscope estimations. To transition between these two measurements, the cumulative distribution function (CDF) of a normal distribution is used. This normal distribution is defined as with standard deviation $\sigma = \frac{\Delta_w \delta_w}{3}$ and average $\mu = \Delta_w$. The normal distribution is denoted $\mathcal{N}_w$. When the magnitude of the weighing factor falls between the upper and lower limits of the transition range, the following holds true:

$$\Delta_w(1-\delta_w) \leq \|S_{a,i}\| \geq \Delta_w(1+\delta_w) \tag{A.36}$$

The estimates for the orientation of the bicycle then become:

$$\theta_i = (1-w_{st})\left[\text{CDF}(\mathcal{N}_w, S_{a,i})\theta_{\omega,i} + (1-\text{CDF}(\mathcal{N}_w, S_{a,i}))\theta_{a,i}\right] + w_{st}\theta_{i-1} \tag{A.37}$$

With:

$$\theta_{\omega,i} = \left(\omega_{O,\hat{y}_P,i-1} + 4\omega_{O,\hat{y}_P,i-\frac{1}{2}} + \omega_{O,\hat{y}_P,i}\right)\frac{\Delta t}{6} + \alpha_{HP}\theta_{i-1}$$

$$\theta_{a,i} = \sin^{-1}\left(\frac{-a_{O,\hat{x}_R}}{\sqrt{a^2_{O,\hat{x}_R} + a^2_{O,\hat{y}_R} + a^2_{O,\hat{z}_R}}}\right)$$

A static weight factor is also introduced here, to further reduce sudden jumps in the orientation estimate. This weight factor acts as a low-pass filter, with $w_{st} = 0.99$.

The angle that has not been discussed so far, is the yaw angle of the bicycle ψ. Since only two geometric angles can be obtained from the accelerometer measurements, we have to rely on only the gyroscope and remove the sensor drift by applying a high-pass filter. This is no great problem, since we are interested in the harmonic motions of the bicycle under the influence of a rider, and long-term rotations, like those after making a corner with a bicycle, are not important in the scope of this study. The estimate for the yaw angle then becomes:

$$\psi_i = \left(\omega_{O,\hat{z}_P,i-1} + 4\omega_{O,\hat{z}_P,i-\frac{1}{2}} + \omega_{O,\hat{z}_P,i}\right)\frac{\Delta t}{6} + \psi_{i-1} \tag{A.38}$$

Using the rotation matrix computed in Equation A.30, we can rotate the the measurements taken in the local frame to the world-fixed frame, by rotating the coordinate system in which the measurements were taken backwards with $-\phi, -\theta$. In other words, rotate the measurements with the inverse of the inverse of $\vec{\mathbf{R}}_i$, which is in turn equal to $\vec{\mathbf{R}}_i$ (see Equation A.30). Using this, the gravitational component can now be removed more accurately from the accelerometer measurements so far, using:

$$\vec{\mathbf{a}}_{O,\hat{x}_P\hat{y}_P\hat{z}_P} = g\vec{\mathbf{R}}_i\left(\vec{\mathbf{a}}_r - \vec{\mathbf{R}}_i^{-1}\begin{bmatrix}0\\0\\1\end{bmatrix}\right) \tag{A.39}$$

where $g = 9.81\ \frac{m}{s^2}$ is Earth's gravitational acceleration. Now that we have the accelerations, we can use this to compute some resulting parameters, namely the instant velocity of the origin, $\vec{\mathbf{v}}_O$, and the instant displacements of the origin, $\vec{\mathbf{r}}_O$. These are approximated as numerical integrations of one another, since:

$$\vec{\mathbf{r}}_O = \frac{\partial \vec{\mathbf{v}}_O}{\partial t} = \frac{\partial^2 \vec{\mathbf{a}}_{O,XYZ}}{\partial t^2} \tag{A.40}$$

We can compute $\vec{\mathbf{v}}_O$ and $\vec{\mathbf{r}}_O$ numerically, again with Simpson's Rule:

$$\vec{\mathbf{v}}_{O,i} = \vec{\mathbf{v}}_{O,i-1} + \left(\vec{\mathbf{a}}_{O,i-1} + \vec{\mathbf{a}}_{O,i-\frac{1}{2}} + \vec{\mathbf{a}}_{O,i}\right)\frac{\Delta t}{6} \tag{A.41}$$

$$\vec{\mathbf{r}}_{O,i} = \vec{\mathbf{r}}_{O,i-1} + \left(\vec{\mathbf{v}}_{O,i-1} + \vec{\mathbf{v}}_{O,i-\frac{1}{2}} + \vec{\mathbf{v}}_{O,i}\right)\frac{\Delta t}{6} \tag{A.42}$$

where $\vec{\mathbf{a}}_{O,i-\frac{1}{2}}$ and $\vec{\mathbf{v}}_{O,i-\frac{1}{2}}$ are computed in a similar fashion as in Equation A.32.

Appendix B

Derivation of Bicycle Model

We reuse Figure A.4 for context:

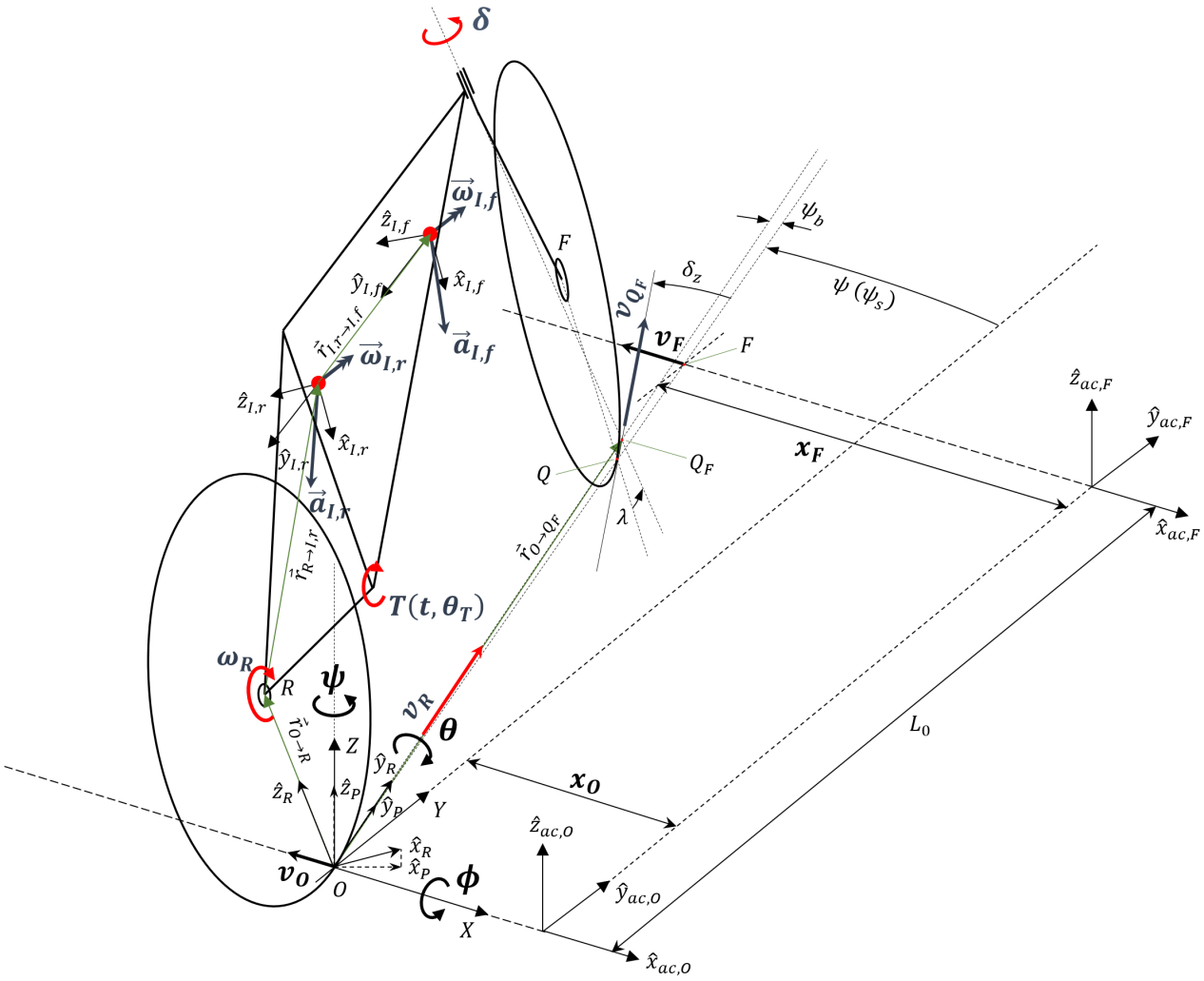

Figure B.1: Coordinate system, with sensors placed in the bicycle. Indicated are several coordinate systems, observed sensor values and coordinates of the simulator as well.

The required velocities for the vehicle model v_O, v_F are first determined in the $(\hat{x}\hat{y}\hat{z})_R$ coordinate system, where the rear wheel velocity v_R points in the direction of point Q_F. We can use rotation matrices to obtain the coordinates of point Q_F with respect to points Q and O. Rotation θ occurs around the $\vec{r}_{O\to Q}$ axis, as per the physical constraints of the mechanical setup. Obtaining the vectors which locate Q and Q_F is the first order of business. In unrotated orientation ($\psi = 0$, which is assumed for the initial calculations), the coordinates are the following:

$$\vec{\mathbf{r}}_{O\to Q,0} = \begin{bmatrix} 0 \\ w \\ 0 \end{bmatrix}, \quad \vec{\mathbf{r}}_{Q\to Q_F,0} = \begin{bmatrix} 0 \\ c \\ 0 \end{bmatrix} \tag{B.1}$$

And in general:

$$\vec{\mathbf{r}}_{O\to Q_F} = \vec{\mathbf{r}}_{O\to Q} + \vec{\mathbf{r}}_{Q\to Q_F} \tag{B.2}$$

Since rotation of the front wheel does not occur around the world Z-axis, but around the tilted steering hub, we need to follow some extra steps to obtain the rotated orientation of the front steering assembly. First, we define a rotation around a coordinate system with its origin at Q, oriented as $(\hat{x}\hat{y}\hat{z})_P$ (when the steering wheel is not rotated, $\delta = 0$). See Figure B.2.

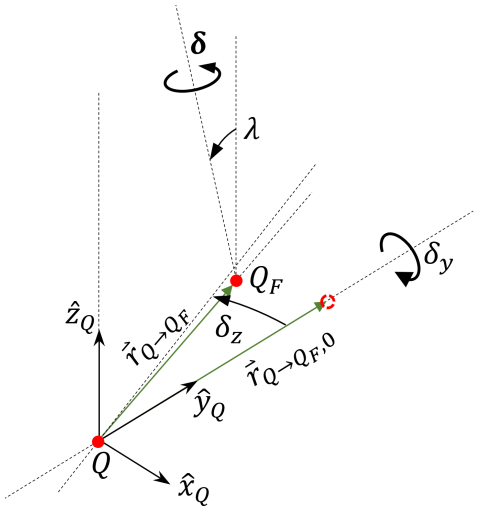

Figure B.2: Close-up of the front wheel ground contacts. Indicated are points Q and Q_F, where Q_F's initial position is denoted as a dashed-line circle. δ_z and δ_y are a result of steering angle δ.

Since the measurement system on the bicycle (see Appendix A) measures the steering angle δ on the bicycle directly, finding the relation between the also-measured δ_z and δ can provide useful for the verification of sensor values. Using that the location of Q_F with respect to Q can also be found by using a rotation around the steering axis, and relating that to the method used in Equation B.9, the following relation can be defined:

$$\vec{\mathbf{R}}_x^{-1}(-\lambda)\vec{\mathbf{R}}_y(\delta)\vec{\mathbf{R}}_x^{-1}(\lambda)\vec{\mathbf{r}}_{Q\to Q_F,0} = \vec{\mathbf{R}}_y(\delta_y)\vec{\mathbf{R}}_z(\delta_z)\vec{\mathbf{r}}_{Q\to Q_F,0} \tag{B.3}$$

Where $\vec{\mathbf{R}}_x, \vec{\mathbf{R}}_y$ are three-dimensional rotation matrices around a Cartesian right-handed coordinate system, the rotation axis indicated by the subscript. In words, the rotation of the steering axis, aligned with the rotated coordinate system located at point Q_F rotated around the local $\hat{x}$ axis with angle λ should provide the same location as the sequential rotation around the $\hat{z}_Q$ and $\hat{y}_Q$ axes with angles δ_z and δ_y, respectively. Equation B.3 then produces a number of equations, from which δ and δ_x can be obtained:

$$\cos(\delta_y)\sin(\delta_z) = \sin(\delta)\cos(\lambda) \tag{B.4}$$

$$\cos(\delta_z) = \sin(\lambda)^2 + \cos(\delta)\cos(\lambda)^2 \tag{B.5}$$

$$\sin(\delta_y)\sin(\delta_z) = -\cos(\lambda)\sin(\lambda) + \cos(\delta)\cos(\lambda)\sin(\lambda) \tag{B.6}$$

Using Equation B.5, the actual steering angle δ becomes:

$$\delta = \cos^{-1}\left(\frac{\cos(\delta_z) - \sin(\lambda)^2}{\cos(\lambda)^2}\right) \tag{B.7}$$

Consequently, δ_y can be obtained as:

$$\delta_y = \sin^{-1}\left(\frac{(\cos(\delta) - 1)\cos(\lambda)\sin(\lambda)}{\sin(\delta_z)}\right) \tag{B.8}$$

Consequently, we can derive the location of point Q_F with respect to point Q as in Equation B.9.

$$\vec{\mathbf{r}}_{Q\to Q_F,(\hat{x}\hat{y}\hat{z})_Q} = \vec{\mathbf{R}}_y(\delta_y)\vec{\mathbf{R}}_z(\delta_z)\vec{\mathbf{r}}_{Q\to Q_F,0} = \begin{bmatrix} -c\cos(\delta_y)\sin(\delta_z) \\ c\cos(\delta_z) \\ c\sin(\delta_y)\sin(\delta_z) \end{bmatrix} \tag{B.9}$$

Due to the roll angle of the bicycle (θ), the location vector in Equation B.9 becomes the following in the $(\hat{x}\hat{y}\hat{z})_P$ coordinate system:

$$\vec{\mathbf{r}}_{Q\to Q_F,(\hat{x}\hat{y}\hat{z})_P} = \vec{\mathbf{R}}_y(\theta)\vec{\mathbf{r}}_{Q\to Q_F,(\hat{x}\hat{y}\hat{z})_Q} = \begin{bmatrix} -c\sin(\delta_z)\cos(\theta)(\cos(\delta_y) - \sin(\delta_y)) \\ c\cos(\delta_z) \\ c\sin(\delta_z)\cos(\theta)(\cos(\delta_y) + \sin(\delta_y)) \end{bmatrix} \tag{B.10}$$

c and w are the bicycle's trail and wheelbase, respectively. $\vec{\mathbf{r}}_{O\to Q_F}$ then becomes:

$$\vec{\mathbf{r}}_{O\to Q_F,(\hat{x}\hat{y}\hat{z})_P} = \begin{bmatrix} -c\sin(\delta_z)\cos(\theta)(\cos(\delta_y) - \sin(\delta_y)) \\ c\cos(\delta_z) + w \\ c\sin(\delta_z)\cos(\theta)(\cos(\delta_y) + \sin(\delta_y)) \end{bmatrix} \tag{B.11}$$

We can now compute the angles ψ_b by computing the angle between two vectors based on the following dot product relation:

$$\cos(\psi_b) = \frac{\vec{\mathbf{r}}_{O\to Q_F} \cdot \vec{\mathbf{r}}_{O\to Q}}{\|\vec{\mathbf{r}}_{O\to Q_F}\| \cdot \|\vec{\mathbf{r}}_{O\to Q}\|} \tag{B.12}$$

But, since Equation B.12 is ambiguous in sign, we need to premultiply both angles with the negative sign of the dot product of the rotation plane's normal (Z-axis) and the two vectors we try to find the angle between (indicated as s_n). In the case of ψ_b, these are:

$$s_{n,\psi_b} = -\frac{\hat{n} \cdot (\vec{\mathbf{r}}_{O\to Q_F} \times \vec{\mathbf{r}}_{O\to Q})}{\|\hat{n} \cdot (\vec{\mathbf{r}}_{O\to Q_F} \times \vec{\mathbf{r}}_{O\to Q})\|} \tag{B.13}$$

Since we are interested in the rotations in the XY-plane, we can set the Z-values to zero when computing ψ_b and δ_z from the above relations. The projection of $\vec{\mathbf{r}}_{Q\to Q_F}$ on the XY-plane is then used. The difference in Z-position of point Q_F due to rotation of the steering wheel is then disregarded in the computation of ψ_b. What follows is:

$$\psi_b = \frac{\sin(\delta_z)\cos(\theta + \delta_y)}{|\sin(\delta_z)\cos(\theta + \delta_y)|} \cdot \cos^{-1}\left(\frac{w + c\cos(\delta_z)}{\sqrt{|c\sin(\delta_z)\cos(\theta + \delta_y)|^2 + |w + c\cos(\delta_z)|^2}}\right) \tag{B.14}$$

With these angles, we can now compute the velocities for the front and rear wheels, first in the $(\hat{x}\hat{y}\hat{z})_R$ coordinate system, under the boundary condition that the forwards front wheel velocity must be equal to the rear wheel velocity (both along $\vec{\mathbf{r}}_{O\to Q_F}$). This condition comes from the assumption that the steering wheel assembly and the rear bicycle frame are rigidly connected. The coordinate system in which v_R is measured, must also be rotated to the $(\hat{x}\hat{y}\hat{z})_R$ coordinate system, hence the rotation matrix in the equations below:

$$\vec{\mathbf{v}}_{O,(\hat{x}\hat{y}\hat{z})_R} = \vec{\mathbf{R}}_z^{-1}(-\psi_b)\begin{bmatrix} 0 \\ v_R \\ 0 \end{bmatrix} = \begin{bmatrix} -\sin(\psi_b)v_R \\ \cos(\psi_b)v_R \\ 0 \end{bmatrix} \tag{B.15}$$

And, using that the magnitude of the $\hat{y}_R$ component of v_Q is equal to the $\hat{y}_R$ component of v_O, but that v_Q is rotated with δ_z due to the steering wheel being rotated:

$$\vec{\mathbf{v}}_{Q,(\hat{x}\hat{y}\hat{z})_R} = \vec{\mathbf{R}}_z^{-1}(-\delta_z) \begin{bmatrix} 0 \\ \frac{\cos(\psi_b)v_R}{\cos(\delta_z)} \\ 0 \end{bmatrix} = \begin{bmatrix} -\frac{\cos(\psi_b)\sin(\delta_z)v_R}{\cos(\delta_z)} \\ \cos(\psi_b)v_R \\ 0 \end{bmatrix} \tag{B.16}$$

From relative motion analysis, these velocities are related as:

$$\vec{\mathbf{v}}_{Q,(\hat{x}\hat{y}\hat{z})_R} = \vec{\mathbf{v}}_{O,(\hat{x}\hat{y}\hat{z})_R} + \vec{\boldsymbol{\omega}}_{O,(\hat{x}\hat{y}\hat{z})_R} \times \vec{\mathbf{r}}_{O\to Q} \tag{B.17}$$

where $\vec{\boldsymbol{\omega}}_{O,(\hat{x}\hat{y}\hat{z})_R}$ are the transformed angular velocities from the world XYZ-frame.

$$\vec{\boldsymbol{\omega}}_{O,(\hat{x}\hat{y}\hat{z})_R} = \vec{\mathbf{R}}_y^{-1}(\theta) \begin{bmatrix} \dot{\phi} \\ \dot{\theta} \\ \dot{\psi} \end{bmatrix} = \begin{bmatrix} \cos(\theta)\dot{\phi} - \sin(\theta)\dot{\psi} \\ \dot{\psi} \\ \cos(\theta)\dot{\psi} + \sin(\theta)\dot{\phi} \end{bmatrix} \tag{B.18}$$

Which gives us a number of equations from which the the yaw rate of the bicycle around the world Z-axis can be obtained, with the notion that points Q_F and O always make contact with the surface the bicycle is riding on, such that the bicycle never rotates upward with respect to the road, i.e. $\dot{\phi} = \phi = 0$. Solving the first equation from combining Equation B.17 and Equation B.18:

$$\dot{\psi} = \frac{v_R \sin(\delta_z - \psi_b)}{w \cos(\theta)\cos(\delta_z)} \tag{B.19}$$

The computed value for $\dot{\psi}$ will come in later when comparing the derived equation to measurements on the bicycle, where we can measure $\dot{\psi}$ directly. Finally, the $(\hat{x}\hat{y}\hat{z})_R$ coordinate system is rotated back to the world XYZ-frame, such that the measurements occur with respect to the correct coordinate system:

$$\vec{\mathbf{v}}_{O,XYZ} = \vec{\mathbf{R}}_z^{-1}(-\psi)\vec{\mathbf{v}}_{O,(\hat{x}\hat{y}\hat{z})_R} = \begin{bmatrix} -\sin(\psi_b + \psi)v_R \\ \cos(\psi_b + \psi)v_R \\ 0 \end{bmatrix} \tag{B.20}$$

$$\vec{\mathbf{v}}_{Q,XYZ} = \vec{\mathbf{R}}_z^{-1}(-\psi)\vec{\mathbf{v}}_{Q,(\hat{x}\hat{y}\hat{z})_R} = \begin{bmatrix} -\frac{\sin(\delta_z+\psi)\cos(\psi_b)v_R}{\cos(\delta_z)} \\ \frac{\cos(\delta_z+\psi)\cos(\psi_b)v_R}{\cos(\delta_z)} \\ 0 \end{bmatrix} \tag{B.21}$$

Now that the velocities of the ground contact points O and Q are known, we can translate those to the points that are actually actuated in the bicycle simulator. For O, this corresponds with the rear support point of the simulator. For Q, we need to translate the velocity to point F, which are connected along $\vec{\mathbf{r}}_{O\to F}$, defined as:

$$\vec{\mathbf{r}}_{O\to F,XYZ} = \begin{bmatrix} -\frac{L_0\sin(\psi)}{\cos(\psi)} \\ L_0 \\ 0 \end{bmatrix} \tag{B.22}$$

And relating the velocities as:

$$\vec{\mathbf{v}}_{F,XYZ} = \vec{\mathbf{v}}_{O,XYZ} + \vec{\boldsymbol{\omega}}_{O,XYZ} \times \vec{\mathbf{r}}_{O\to F,XYZ} \tag{B.23}$$

Where $\vec{\boldsymbol{\omega}}_{O,XYZ}$ is defined as $\left[0, \dot{\theta}, \dot{\psi}\right]^T$, since $\dot{\phi} = 0$:

$$\vec{\mathbf{v}}_{F,XYZ} = \begin{bmatrix} -L_0\dot{\psi} - \sin(\psi_b + \psi)v_R \\ \cos(\psi_b + \psi)v_R - \frac{L_0\dot{\psi}\sin(\psi)}{\cos(\psi)} \\ \frac{L_0\sin(\psi)\dot{\theta}}{\cos(\psi)} \end{bmatrix} \tag{B.24}$$

The control setpoints of the rear and front wheel velocity in the X-directions should then be the following, respectively:

$$\vec{\mathbf{v}}_{O,X} = -\sin(\psi_b + \psi)v_R \tag{B.25}$$

$$\vec{\mathbf{v}}_{F,X} = -\frac{L_0 \sin(\delta_z - \psi_b)v_R}{w\cos(\theta)\cos(\delta_z)} - \sin(\psi_b + \psi)v_R \tag{B.26}$$

Now comes the point the differentiation between virtual and physical parameters of the simulator become relevant. Since both actuators have a limited range of motion, the physical yaw rate and linear velocities will have to be electronically limited at some point. The current yaw angle of the setup (ψ_s) can be directly derived, using Equation B.27:

$$\frac{L_0 \sin(\psi_s)}{\cos(\psi_s)} = x_F - x_O \Leftrightarrow \psi_s = \tan^{-1}\left(\frac{x_F - x_O}{L_0}\right) \tag{B.27}$$

Two parameters are used to denote the yaw angle of the setup, ψ_s and ψ, with the difference that ψ_s is the yaw angle of the bicycle with respect to the physical setup, thus with respect to the XYZ coordinate system, and ψ is measured virtually. In other words, ψ denotes the total amount of rotation the bicycle has undergone due to sustained steering, which can in a later stage be used for a digital visualisation of the bicycle's motion. But for now, this parameter is only supplementary, and aids in the verification of ψ_s. Using ψ_s, the velocity setpoints in Equation B.25 and Equation B.26 become:

$$\vec{\mathbf{v}}_{O,X} = -\sin(\psi_b + \psi_s)v_R \tag{B.28}$$

$$\vec{\mathbf{v}}_{F,X} = -\frac{L_0 \sin(\delta_z - \psi_b)v_R}{w\cos(\theta)\cos(\delta_z)} - \sin(\psi_b + \psi_s)v_R \tag{B.29}$$

Appendix C

System Identification & Coherence Data Processing

Grey-Box State-Space System Estimation

The first method of data comparison is based on the fitting of a linear State-Space model to the defined in- and outputs above. The model matrices, and the frequency responses for different cycling situations can be compared qualitatively and visually. The prediction of these models is done with MATLAB's SSEST function, an approximated state-space representation of the measured data. In broad terms, SSEST functions as described below. These descriptions are adapted from MATLAB's function descriptions.

SSEST: An algorithm which minimizes the prediction error in a state-space model. The state-space system that is going to be estimated is dependent on its states ($\mathbf{x}(t)$), the inputs ($\mathbf{u}(t)$), the outputs ($\mathbf{y}(t)$), and the prediction error of the model ($\mathbf{e}(t)$) and are related to each other through the derivative of the states ($\dot{\mathbf{x}}(t)$) and the $\mathbf{A}, \mathbf{B}, \mathbf{K}, \mathbf{C}$ and $\mathbf{D}$ matrices, defined as:

$$\begin{aligned} \dot{\mathbf{x}}(t) &= \mathbf{A}\mathbf{x}(t) + \mathbf{B}\mathbf{u}(t) + \mathbf{K}\mathbf{e}(t) \\ \mathbf{y}(t) &= \mathbf{C}\mathbf{x}(t) + \mathbf{D}\mathbf{y}(t) + \mathbf{e}(t) \end{aligned} \tag{C.1}$$

For a discrete-time system, Equation C.1 becomes:

$$\begin{aligned} \mathbf{x}(kT_s + T_s) &= \mathbf{A}\mathbf{x}(kT_s) + \mathbf{B}\mathbf{u}(kT_s) + \mathbf{K}\mathbf{e}(kT_s) \\ \mathbf{y}(kT_s) &= \mathbf{C}\mathbf{x}(kT_s) + \mathbf{D}\mathbf{u}(kT_s) + \mathbf{e}(kT_s) \end{aligned} \tag{C.2}$$

With T_s the sample time of the system, and $k = 1, 2, ...$ the sampling indices. The sizes of the matrices are dependent on the number of states (n_k), the number of inputs (n_i) and the number of outputs (n_j) for a certain model. The state variables and inputs are defined as:

$$\mathbf{x} = \begin{bmatrix} a_{O,x_{\hat{P}}} \\ \psi \\ \dot{\psi} \end{bmatrix}, \quad \mathbf{u} = \begin{bmatrix} \delta \end{bmatrix}$$

Which allows us to define an $\mathbf{A}$ matrix valid for both input-output systems. $\mathbf{A}$ is initialised as:

$$\mathbf{A} = \begin{bmatrix} 0 & A_{a_{O,x_{\hat{P}}}\dot{\psi}} & A_{a_{O,x_{\hat{P}}}\dot{\psi}} \\ 0 & 1 & T_s \\ 0 & 0 & A_{\dot{\psi}\dot{\psi}} \end{bmatrix}$$

The second row of the $\mathbf{A}$-matrix is set to $[0 \quad 1 \quad T_s]$ since there is in essence a numerical integration step taking place from the yaw rate to obtain the next yaw angle. $\mathbf{B}$ has size $n_k \times n_i$, and is initialised as:

$$\mathbf{B} = \begin{bmatrix} B_{a_{O,x_{\hat{P}}}\delta} \\ B_{\psi\delta} \\ B_{\dot{\psi}\delta} \end{bmatrix}$$

The outputs $\mathbf{y}$ have size $n_j \times 1$, so matrices $\mathbf{C}$ and $\mathbf{D}$ have sizes $n_j \times n_k$ and $n_j \times n_i$, respectively. These matrices are defined as:

$$\mathbf{C} = \begin{bmatrix} 1 & 0 & 0 \\ 0 & 1 & 0 \\ 0 & 0 & 1 \end{bmatrix}$$
$$\mathbf{D} = \begin{bmatrix} 0 & 0 & 0 \end{bmatrix}$$

The $\mathbf{K}$ matrix has size $n_j \times n_k$, and is set fixed to zero to try to obtain a system which truly tries to predict system behaviour, without making use of the prediction error a part of the system, i.e. not trying to best fit the data, but find a system that produces output data only due to system dynamics. As a result of this decision, the produced $\mathbf{A}$ and $\mathbf{B}$ matrices can be compared qualitatively. The resulting full state-space system with free parameters is:

$$\begin{bmatrix} a_{O,x_{\hat{P}}} \\ \psi \\ \dot{\psi} \end{bmatrix}_{k+1} = \begin{bmatrix} 0 & A_{a_{O,x_{\hat{P}}}\dot{\psi}} & A_{a_{O,x_{\hat{P}}}\dot{\psi}} \\ 0 & 1 & T_s \\ 0 & 0 & A_{\dot{\psi}\dot{\psi}} \end{bmatrix} \begin{bmatrix} a_{O,x_{\hat{P}}} \\ \psi \\ \dot{\psi} \end{bmatrix}_k + \begin{bmatrix} B_{a_{O,x_{\hat{P}}}\delta} \\ B_{\psi\delta} \\ B_{\dot{\psi}\delta} \end{bmatrix} \begin{bmatrix} \delta \end{bmatrix}_k \tag{C.3}$$

$$\begin{bmatrix} a_{O,x_{\hat{P}}} \\ \psi \\ \dot{\psi} \end{bmatrix}_k = \begin{bmatrix} 1 & 0 & 0 \\ 0 & 1 & 0 \\ 0 & 0 & 1 \end{bmatrix} \begin{bmatrix} a_{O,x_{\hat{P}}} \\ \psi \\ \dot{\psi} \end{bmatrix}_k \tag{C.4}$$

Since the behaviour of the bicycle is velocity-dependent, this is initialised in the $\mathbf{A}$ and $\mathbf{B}$ matrices, more velocity-dependent parameters can be identified after the full system identification process by observing the computed matrices and the system response. The unknown parameters of the $\mathbf{A}$-matrix are set to the following: $A_{a_{O,x_{\hat{P}}}\dot{\psi}} = -v_R$ due to an expected relation between the forward velocity, sideways acceleration and the bicycle's yaw rate. The other unknown parameters are initially set to zero, but remain free since there can be relations between $\dot{\psi}$ and other parameters due to physical limitations in the simulator.

All unknown parameters of the $\mathbf{B}$-matrix are initialised at zero, except for $B_{\dot{\psi}\delta}$, which is initially set to the linearised version of Equation B.19, which approximates the relation between $\dot{\psi}$, v_R and δ. Initially, $B_{\dot{\psi}\delta} = \frac{v_R}{w} c \cos(\lambda)$, but is left free to be optimised to compensate for deviations in the measured velocity. v_R is taken as the average velocity of a certain windowed dataset, for when someone for example rides constantly at 5 km/h, it would be equal to $v_R = \frac{5}{3.6}\ \frac{m}{s}$.

The roll-steer relation of the bicycle-rider system is initialised as a first-order state-space system, derived similarly as the full system description above. This system is as follows:

$$\begin{bmatrix} \theta \end{bmatrix}_{k+1} = \begin{bmatrix} A_{\theta\theta} \end{bmatrix} \begin{bmatrix} \theta \end{bmatrix}_k + \begin{bmatrix} B_{\theta\delta} \end{bmatrix} \begin{bmatrix} \delta \end{bmatrix}_k \tag{C.5}$$

$$\begin{bmatrix} \theta \end{bmatrix}_k = \begin{bmatrix} 1 \end{bmatrix} \begin{bmatrix} \theta \end{bmatrix}_k \tag{C.6}$$

The parameters are initialised according to observations from the signals; $A_{\theta\theta} = 0$, $B_{\theta\delta} = -1$ since the signals seem to behave oppositely within the same order of magnitude. However, in the measurements of δ and θ, a phase delay seems to exist between them, dependent on the cadence of the cyclist. The state-space algorithm is therefore also initialised with an (empirically determined) input delay of $-\frac{0.1944}{f_T T_s}$ samples, where $f_T = \frac{\omega_T}{2\pi}$ is the cadence frequency of the user.

The process of finding a set of parameters which fit the input and output timeseries is done through a prediction error minimisation algorithm. The cost function which is minimised for a Single-Input-Single-Output (SISO) system is defined in [24]. In order to determine whether a certain state-space approximation was accurate enough, the models, and how they fit the original data, are compared based on three qualities:

1. NRMSE (Normalised Root Mean Squared Error): metric based on the difference between the model output and measured output:

$$\text{NRMSE} = \left(1 - \frac{\|y_{meas} - y_{model}\|}{\|y_{meas} - \overline{y_{meas}}\|}\right) \tag{C.7}$$

   where y_{meas} is the measured model output data (used to derive the model), y_{model} is the predicted response from the model and $\overline{y_{meas}}$ is the channel-wise mean of the measured model output data. The closer this value is to one, the better the model has predicted the measured output.

2. MSE (Mean Squared Error): the norm of the signal error between the model output and the measured output, defined as:

$$\text{MSE} = \frac{1}{N}\sum_{t=1}^{N} e^T(t)e(t) \tag{C.8}$$

with $e(t)$ the signal error which is minimised for model estimation and N the number of data samples in the estimation dataset. The larger the MSE is, the poorer the model estimation is.

3. FPE (Final Prediction Error): Akaike's FPE is defined as a metric dependent on the number of free parameters in the model prediction:

$$\text{FPE} = \det\left(\frac{1}{N}E^T E\right)\left(\frac{1+\frac{n_p}{N}}{1-\frac{n_p}{N}}\right) \tag{C.9}$$

where E is the N-by-n_y matrix of prediction errors, where n_y is the number of output channels, n_p is the number of free parameters in the model and N is the number of samples in the estimation dataset.

Due to the nature of these estimation qualities, the NRMSE is able to give an estimation quality metric for each output channel in the model, whereas the MSE only considers the model as a whole, thus only giving a metric for overall model quality. The same goes for the FPE.

Frequency-Dependent Coherence Between Measured Variables

The magnitude-squared coherence between two time-domain signals $x(t)$ and $y(t)$ is defined as [1]:

$$C_{xy}(f) = \frac{|G_{xy}(f)|^2}{G_{xx}(f)\,G_{yy}(f)} \tag{C.10}$$

Where f is a certain frequency, $G_{xy}(f)$ is the cross-spectral density between signals $x(t)$ and $y(t)$, and $G_{xx}(f)$ and $G_{yy}(f)$ are the autospectral densities of signals $x(t)$ and $y(t)$, respectively. The cross-spectral density for discrete time-domain signals x_n and y_n is defined as:

$$C_{xy}(f) = \sum_{n=-\infty}^{\infty} R_{xy}(\tau_n)\, e^{-i2\pi f \tau_n \Delta\tau} \tag{C.11}$$

Where R_{xy} is the cross-correlation of signals x_n and y_n. See [32] for further reading on this topic. The autospectral density of a discrete signal x_n is defined as [32]:

$$G_{xx}(f) = \lim_{N\to\infty}\frac{\Delta t^2}{T}\left|\sum_{n=-N}^{N} x_n e^{-i2\pi f_n \Delta t}\right|^2 \tag{C.12}$$

Where N are the window limits of a signal measurement as $-N \leq n \leq N$ for a total measurement period of $T = (2N+1)\,\Delta t$.

The magnitude-squared coherence is often used as a estimation tool for the power transferred between the input and output of a linear system. If at a given frequency, the phase of two signals are fixed to each other, the coherence between those signals can be high ([32]). In other words, when there exists a certain relation between two signals such that the time-domain signals follow each other well, a high coherence value close to 1 exists between those signals, over a certain measurement period.

Appendix D

Experimentation Procedure

D.1 Experiment Procedures

Measurement Procedure + Checklist

There are four (dependent on the number of indoor cycling experiments, apart from the one conducted on the new bicycle simulator) experiments to be conducted with the same person. This document describes the steps required for a good measurement.

Step 1: Affixing the measurement equipment to the bicycle.

In order to obtain correct measurements, the measurement board, on which two accelerometer-gyroscope combinations, a control board with two LEDs and a joystick, an analogue to digital converter and a Raspberry Pi are mounted to the bicycle. The Raspberry Pi has a breakout board for a battery pack and an expansion board which increases the number of I2C connections.

Additionally, the bicycle has to have a HALL sensor affixed to the rear seatstay tube, as well as a number of magnets affixed to spokes in the rear wheel for a velocity measurement. The closer the HALL sensor can be fixed to the centre of rotation, the less likely it is signal dropouts occur (due to lower linear velocity of the magnet).

Finally, the steer rotation sensor has to be fixed to the head tube of the bicycle. Pay attention that the braking and shifting cables do not push the block with the sensor on it aside too much as a result of steering, which could influence the signal. Ensure cables are connected correctly.

Fix the Garmin Edge 830 mounting system to the bicycle steering handles, if one is not already present.

Step 2: Calibrating the sensors.

Once the measurement board is loosely fixed to the bicycle frame, use the script <*InitialBalancer.py*> to enter calibration mode, to make sure the board is correctly aligned perpendicular to gravity. Put the bicycle on its two wheels, keep the steering wheel straight. The graph shows the onboard-computed pitch and roll angles of the board with respect to the gravity horizon. Start the script, watch the resulting graph, and move the sensor board around within the bicycle frame until both readings measure approximately zero. Tighten the screws which lock the orientation of the measurement board and fix the board to the frame using zip-ties.

Once the measurement board is in place in its final position and affixed properly, a number of measures have to be taken of the sensor locations. These are visible in the image below. Some are related to the measurement board, which should be fixed.

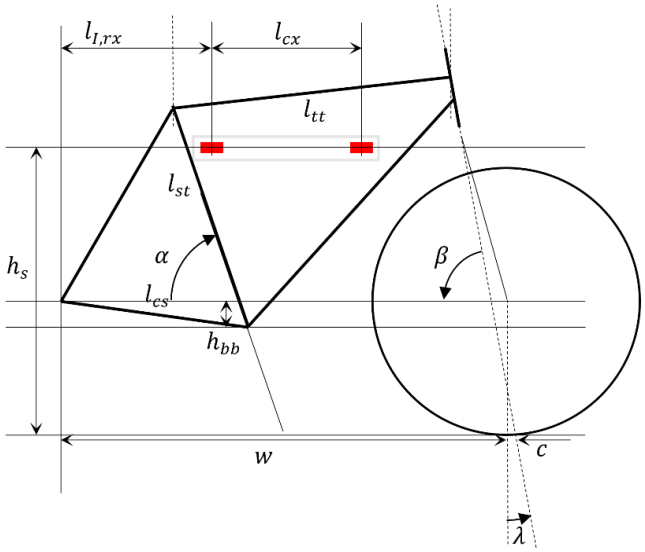

Some of these measures should be available through the manufacturer and standardized size of the bicycle, if the frame type is known. The important measures are h_s and $l_{I,rx}$, those will be used in computations after experiments.

The same goes for w, c and λ.

Step 3: Explain experiments to subject.

Take a moment to sit down with the participant to talk through the forms and questionnaire. Verify that the participant understands the questions and the scoring system. Double-check if he has any questions about the forms, such that he understands what the purpose of the questions is. Inform the participant of the risks and his rights, which are also described on the informed consent form.

The first experiment will be the performing of a number of manoeuvres outdoors. Explain the steps the cyclist has to perform on the bicycle outside. These are the following, in this order:

1. Constant cycling at incremental speeds, with the focus on cycling on that constant velocity (5, 10, 15, 20, 25, 30, 35 and 40 km/h). The participant is instructed to keep shifting gears to a minimum (but it is allowed in between velocities), find a comfortable transmission ratio for that velocity, and stay in it for the remainder of the velocity. The cyclist is also instructed that keeping the cranks stationary or rotating backwards should be kept to a minimum as well, for the purpose of cleaning up the pedal's velocity measurement. Keep to each velocity for one minute (which can be timed on the display of the Edge 530), less is allowed if the participant finds it too difficult or too unstable. The participant is able to view his own velocity on the Edge 530 display, as well. The participant is informed that consistency of the to-be maintained velocity is more important than actually cycling at <u>exactly</u> the prescribed velocity. This is allowed due to the results being velocity-normalised, anyway.

2. A zig-zagging manoeuvre performed at around 20-25 km/h. The participant is instructed to keep within half-width of the road, which is approximately the width of the working range of the simulator. This bound is for a fair comparison between outdoor zig-zagging and the simulator. The participant is again instructed to maintain this velocity for a minute.

3. Perform a section of standing up-cycling (or even a sprint). The participant is instructed to pick a velocity he thinks he will be able to maintain for one minute. If he misjudges and the required effort is too high, he is allowed to stop earlier than one minute. Again, the participant is instructed not to stop pedalling, and choose a correct transmission ratio beforehand.

Step 4: Outdoor measurements.

Turn on the Raspberry Pi system indoors, so errors can be identified and corrected before everything is hauled outside. Once the system goes into stand-by mode (red AND green LED on), the system is ready for measurements. Let the participant enter the first SSQ scores (15 minutes before experiments).

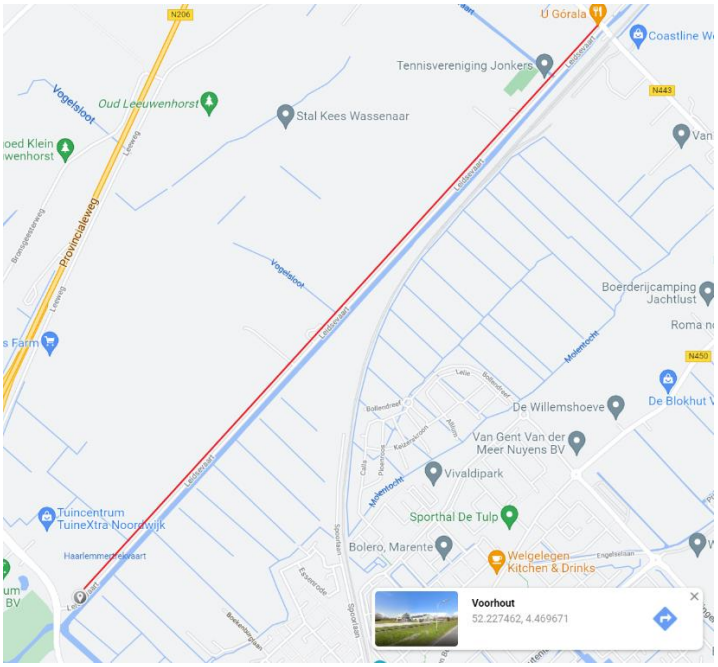

The participant is instructed to wear normal shoes (no clip pedals for safety), wear a crash helmet and comfortable clothes for high-effort cycling.

Take the bicycle outside to the testing location (image left, red line is a stretch of straight road about 2.5 km long), and turn on the Edge device. Verify the Rally pedals are both connected to the Edge. Don't start a measurement yet, start a warm-up round of about 10 minutes (which is the ride to the test location). This ride to the test location also serves as a ride to get used to the testing bicycle.

When everyone is ready for the first experiment, start by going to the RallyLog page on the Edge device, and verify both pedals are ready for logging. Hold down the joystick controller connected to the Pi until the green LED stops flashing slowly, and flashes quickly. Release. The first measurement has then been started. When the pedals are ready, start a measurement and verify that both pedals are logging data. Wait one minute, with nothing on the pedals, for the pedals to obtain their raw calibration values. This first section of data is later used by the *Titan-package*-tool to obtain noise data and compensation values.

Perform the calibration bump. Let either the rider or the executor of the experiment apply sudden bursts of force on the right pedal, which will be used in the data analysis stage. Letting the measured burst of force overlap with the jolt in acceleration signals makes sure the signals of the two measurement systems are aligned. The rider can then commence with the first step of the list of measurements.

After all numbered items in step 3, stop and save the Edge activity, which stops the pedals from logging data. Only after this, hold the joystick button sideways (towards the rear of the bike) until the red LED stops flashing. Then wait until both LEDs are on again, which indicates that experiment data has been recorded and saved from memory to flash.

When the final experiment has been completed, verify that it has been saved on both devices. The Pi can then be turned off by holding the joystick down for 10 seconds, and the Edge device put to sleep to save battery. Ride back to the Tacx building afterwards. First thing upon return, let the participant enter the subjective questionnaire form for outdoor cycling, and the centre column for SSQ. While the participant fills out the forms, the pedals on the bicycle can be exchanged for another pair, since the data has to be downloaded from them during experiments. This allows for the set of pedals used in the first experiment be reused in the third (during the static setup experiments), since only two sets of pedals are available for use.

Step 4: Indoor experiments, bicycle simulator

Step 3 is, broadly speaking, repeated for the simulator experiments. Additional steps to be taken in experiments are described below.

First remove the wheel of the bicycle and affix the bicycle to the braking unit and front fork support of the simulator. Transfer the hall sensor from the bicycle frame to the simulator. The implementation of the Hall sensor can prove tricky, since it is sensitive to not detecting the magnets of the braking unit's magnets when affixed improperly. Verify it is working by rotating the flywheel of the braking unit while the Hall sensor is powered up. The sensor should flash red with every pulse it detects.

Affix the dead-man's switch to the bicycle steering handles. Verify it can be pulled loose with a considerable amount of force. Connect the electronics to the switch, and start up the simulator PC. Measure the current position of the simulator support points with respect to the ends of the actuators, and fill those out in the control algorithm, since absolute encoders have not been implemented in the system (yet). Verify all sensors of the simulator produce the data they are expected to produce (steer, roll angles, velocity measurement, position and velocity of the actuators). Verify the external monitor is placed with its stand against the simulator frame, letting the distance from screen to bicycle steering wheel become 70 cm.

Verify that the participant is understanding the safety procedures of the bicycle simulator. Instruct him to wear a crash helmet and put his hand through the dead-man's switch cord every time. Connect the trainer to the Tacx Desktop App for a visualization during experiments. Use the Flanders movie, since the slope is 0% almost everywhere, and the visual scene is similar to the one during outdoor experiments. Let the user again fill out the questionnaire forms ahead of time, directly after experiments and after 15 minutes. Chances are this column reproduces the values of the third column of SSQ scores from the outdoor experiments, if the experiments are performed consecutively.

After the first column of SSQ for the simulator has been filled out, let the participant first get used to the kinematic simulator.

Step 5: Getting used to the simulator, performing manoeuvres on simulator

Early experiments have shown that people need about 5 minutes to get used to the movement of the system, participants are allowed 15 minutes, as follows:

Set the user gain of the vehicle model to 0.8, which, from early trials, improves how people first get used to the system. It reduces the influences of people's stiff, jumpy steering response when they're not yet used to the simulator's motion. Instruct the participant what is, from experience, the easiest way of getting used to the simulator's motions: sit on the saddle, keep your legs on the floorboard. Use one leg to give yourself some (virtual) velocity by pushing and rotating the cranks a couple of times. Don't try to lift both legs just yet, first use the steering handles to get a feel for how the simulator responds to velocity and steering. Participants are told that increasing the velocity makes it easier to control the bicycle, as a real bicycle would, as well. All participants were able to get used to the simulator's motion within 15 minutes, although some struggled more than others. One participant did not get any instructions, see the main document for how that went.

Let the participant ride the simulator once he gets the hang of it for a minute or 10. Inform him that the response of the system will change when the simulator gain is set to 1. Let the participant stop and set the user gain to 1. Let the participant again get used to this motion for another five minutes. Then start the experiment steps as described in step 3. The standing up manoeuvre is not required and even discouraged, since it may feel unsafe to the participant, which can inhibit his movements in such a way that the motion is not realistic anymore. The simulator also seems to respond too aggressively during standing up cycling, which could be a result of the vehicle model not accounting for the cyclist's posture on the bicycle.

The participant is again able to monitor his velocity, now from the visualisation (since the Edge 830 uses GPS for its velocity estimate) in the upper-left corner of the screen. At lower speeds, this estimate for velocity (coming from the disassembled bicycle trainer) is inaccurate, so a velocity graph which measures the velocity of the rear wheel directly is displayed on the right-hand side of the monitor, taking up about 10% of the width of the screen. The bottom of the screen shows the estimated time of arrival (ETA, completion of the predetermined route) and current ride time, which indicates to the participant how long he has been riding a certain manoeuvre velocity.

After the experiments, let the participant fill out the required forms again, and prepare for the final experiments on the static setup. Same visual environment, different mechanical setup. Change out the pedals for the ones that have now been emptied of the raw files.

Step 5: Indoor experiments, static setup

The steps for data collection from steps 3 and 4 can be largely reproduced for the static simulator. Affix the bicycle, the Hall sensor, make sure the correct SSQ columns are filled out for the static setup. Make sure the distance of the external monitor to the bicycle steering handles is the same as on the simulator (70 cm). The visualisation will be reset to the start, and the bicycle resistance unit is again connected to the Tacx Desktop app.

The participants are now not allowed a getting-used-to stage of experiments, since no hardships are expected on the static setup. No participant showed trouble using the static setup, so experiments are immediately started when all sensors are affixed and working.

The manoeuvres are the same as in step 3, except for the zig-zagging motion. Standing up is back on the list of manoeuvres, since no problems are expected with standing up. No crash helmet is required but allowed if the participant wants to use it.

The visualisation is now the only source for velocity, since the graph displaying the lower velocities was only available during simulator experiments, as it was part of the drive algorithm. Experiments have shown that it is easier for participants to maintain very low speeds on the static setup, and the results are velocity-normalised afterwards anyway. This velocity estimate is accepted as being sufficient for now.

After concluding all manoeuvres, the final forms are filled out, including the questions of the second category (comparative questions) as well as the middle column of the SSQ for the static setup. After fifteen minutes, the final column of the SSQ is filled out. Then, experiments are concluded for the participant.

Step 6 describes the obtaining of measurement data from the sensors, applied three times for three experiments. These steps are for the experimenter only.

Step 6: Obtaining and removing data from sensors

The data on the Pi has been saved in a folder in the "Master TestSetup"-folder on the Pi desktop. denoting the time and date of the start of the measurement. This is an incorrect timestamp, due to the inability to connect the Pi to the network for time synchronization. In this folder, there are a number of subfolders "ExpX", where X is the experiment number. Such a folder is created by starting a new measurement in the same run with the Pi. In each of these folders, there is a .csv file with "Final" in the name, which contains the completed measurement data. There are other files present, but those are created as intermediate backup files, which can be recovered in case of unexpected failure.

Copy the entire folder to the analysis PC, into the current analysis folder, each finalized "ExpX" .csv file into a separate experiment subfolder, such that experiments are easily distinguished.

To remove the data from the pedals, and to speed up experiments, remove the current set of pedals from the bicycle, and screw on another. Two sets are available. Download the files from the first set using the DSIAntfs program. Wake up the pedals by rotating them a couple of times. Then, start the search for devices. The pedals should come up with different device addresses, and you can connect to one of them by double clicking.

A file browser appears, select the files with indices 5, 6, 14, 15, 16, 50, 60, 256 and everything above (2XX), and 65533. The copying process takes a long time, and is unstable, so keep checking on the process whether it is completed successfully. Once this is verified, disconnect from the pedal and repeat for the other pedal.

Select a path and download the files, repeat with each pedal. Remove the files from the pedals when they are downloaded, so the pedals can be reused for subsequent experiments.

You can convert these .fit files into .csv files using another tool provided by Garmin. This is called Titan-package. Place the files with indices 6, 14, 15, 16, 50, 60, 256, and 65533 in the "Index" folder within the Titan-package folder. Every file starting from 256 is a separate activity, so the conversion needs to be repeated for every activity, with file 256 replaced with 257, then 258, etc. Verify the "Output" folder is empty each time you convert the files. Use Windows Powershell to change to the Titan-package directory, to "Titan-debug" and execute the "Simulator.exe" through Powershell. This should take a moment, the process is complete once Powershell displays an elapsed time. The "Output" folder now contains a long list of Excel files.

Copy the following .csv files to the same experiment folders as with the Pi files: "L-AccelCadSample-XX…", "L-Position-XX…", "R-AccelCadSample-XX…" and "R-Position-XX…", with XX… being the timestamp of conversion.

Further data processing is described in other Appendices of the main document.

D.2 Subject Questionnaire

Subjective Questionnaire form

Participant number: ____

Cycling level indoor: ____, outdoor:____

Please fill out this form using only scores from 1 through 10, whole numbers only. 1 is complete disagreement, 10 is complete agreement.

Questions relating to cycling in each situation, to be answered directly after performing the required manoeuvres.

Outdoor cycling:

1. I felt like I was riding a bicycle	
2. I felt like I was riding *my* bicycle	
3. Steering felt natural during the ride	
4. Maintaining control of the bicycle was effortless	
5. Balancing the bicycle felt natural during the ride	
6. I felt like I was not restricted in rolling the bicycle beneath me.	
7. The forwards motion I experienced felt coupled to my pedaling cadence and power.	
8. I was focused more on the mechanical aspects and limitations of the bicycle than on the actual cycling.	
9. The velocity I was cycling at felt the same as the velocity of what I was seeing.	
10. I felt like I could ride the bicycle wherever I wanted on the road that I could see.	
11. I felt like I was in control of the bicycle.	
12. I felt comfortable during cycling.	
13. I felt safe during the ride.	
14. The ride was enjoyable.	
15. During cycling, I felt as if there was some aspect of cycling missing (if scored above 1, mention below what you think was missing)	

Room for open answers/notes:

Questionnaire related to the Simulator Sickness Questionnaire procedure:

I experienced (column 1) with a severity of (column 2):

	Before (-15 min.)	Directly after	After (+15 min.)
General discomfort			
Fatigue			
Headache			
Eyestrain			
Difficulty focusing			
Increased salivation			
Sweating			
Nausea			
Difficulty concentrating			
Fullness of head			
Blurred vision			
Dizzy (eyes open)			
Dizzy (eyes closed)			
Vertigo			
Stomach awareness			
Burping			

Bicycle simulator cycling:

1. I felt like I was riding a bicycle	
2. I felt like I was riding *my* bicycle	
3. Steering felt natural during the ride	
4. Maintaining control of the bicycle was effortless	
5. Balancing the bicycle felt natural during the ride	
6. I felt like I was not restricted in rolling the bicycle beneath me.	
7. The forwards motion I experienced felt coupled to my pedaling cadence and power.	
8. I was focused more on the mechanical aspects and limitations of the bicycle than on the actual cycling.	
9. The velocity I was cycling at felt the same as the velocity of what I was seeing.	
10. I felt like I could ride the bicycle wherever I wanted on the road that I could see.	
11. I felt like I was in control of the bicycle.	
12. I felt comfortable during cycling.	
13. I felt safe during the ride.	
14. The ride was enjoyable.	
15. During cycling, I felt as if there was some aspect of cycling missing (if scored above 1, mention below what you think was missing)	

Room for open answers/notes:

Questionnaire related to the Simulator Sickness Questionnaire procedure:

I experienced (column 1) with a severity of:

	Before (-15 min.)	During	After (+15 min.)
General discomfort			
Fatigue			
Headache			
Eyestrain			
Difficulty focusing			
Increased salivation			
Sweating			
Nausea			
Difficulty concentrating			
Fullness of head			
Blurred vision			
Dizzy (eyes open)			
Dizzy (eyes closed)			
Vertigo			
Stomach awareness			
Burping			

Static cycling:

1. I felt like I was riding a bicycle	
2. I felt like I was riding *my* bicycle	
3. Steering felt natural during the ride	
4. Maintaining control of the bicycle was effortless	
5. Balancing the bicycle felt natural during the ride	
6. I felt like I was not restricted in rolling the bicycle beneath me.	
7. The forwards motion I experienced felt coupled to my pedaling cadence and power.	
8. I was focused more on the mechanical aspects and limitations of the bicycle than on the actual cycling.	
9. The velocity I was cycling at felt the same as the velocity of what I was seeing.	
10. I felt like I could ride the bicycle wherever I wanted on the road that I could see.	
11. I felt like I was in control of the bicycle.	
12. I felt comfortable during cycling.	
13. I felt safe during the ride.	
14. The ride was enjoyable.	
15. During cycling, I felt as if there was some aspect of cycling missing (if scored above 1, mention below what you think was missing)	

Room for open answers/notes:

Questionnaire related to the Simulator Sickness Questionnaire procedure:

I experienced (column 1) with a severity of (column 2):

	Before (-15 min.)	During	After (+15 min.)
General discomfort			
Fatigue			
Headache			
Eyestrain			
Difficulty focusing			
Increased salivation			
Sweating			
Nausea			
Difficulty concentrating			
Fullness of head			
Blurred vision			
Dizzy (eyes open)			
Dizzy (eyes closed)			
Vertigo			
Stomach awareness			
Burping			

Questions relating to differences in cycling between situations, to be answered after performing the required manoeuvres on <u>all</u> setups.

1. Balancing cost more effort on the simulator than outside	
2. Delivering pedalling power cost more effort on the simulator compared to outside	
3. Steering the bicycle had the same result on the simulator, as outside	
4. The sideways velocity of the bicycle simulator felt natural, compared to outside	
5. The physical motion of the simulator influenced my cycling and balance positively	
6. The visualization presented on the simulator influenced my cycling and balance positively	

Other remarks given by the participant:

Appendix E

HREC Application Documents

E.1 HREC Application Checklist

Delft University of Technology
ETHICS REVIEW CHECKLIST FOR HUMAN RESEARCH
(Version 18.06.2020)

This checklist should be completed for every research study that involves human participants and should be submitted before potential participants are approached to take part in your research study. This also applies for students doing their Master-thesis.

In this checklist we will ask for additional information if need be. Please attach this as an Annex to the application.

The data steward of your faculty can help you with any issues related to the protection of personal data. Please note that research related to medical questions/health may require special attention. See also the website of the CCMO.

Please upload the documents (go to this page for instructions).

Thank you and please check our website for guidelines, forms, best practices, meeting dates of the HREC, etc.

I. Basic Data

Project title:	
Name(s) of researcher(s):	**Jelle Haasnoot**
Research period (planning)	**Weeks 18-24 2021**
E-mail contact person	**j.haasnoot@student.tudelft.nl**
Faculty/Dept.	**3mE**
Position researcher(s):[1]	**MSc Student**
Name of supervisor (if applicable):	**Arend Schwab, Riender Happee**
Role of supervisor (if applicable):	**Research supervisor**

II. A) Summary Research

In this study, 15 test subjects will be asked to participate in a study comparing a newly designed bicycle simulator to outside bicycling, as well as existing stationary indoor cycling equipment. This will be done by both performing measurements on the subjects' personal (racing) bicycle, and asking them a number of subjective questions about the quality of the newly designed bicycle simulator.

This new bicycle simulator will be different in the sense that it allows for more involvement of the cyclist in balancing and steering the bicycle, and the bicycle will respond to the cyclist's input as it would outside. At least, that is the goal.

The participants will be people already present in the company where the graduation project takes place, as well as (semi-)professional racing cyclists from the Netherlands, if they are available. The subjects will have different levels of cycling experience and preferences. To breach their normal cycling as little as possible, they are allowed to use their own bicycle and equipment.

(Please very briefly (100-200 words) summarise your research, stating the question for the research, who will participate, the number of participants to be tested and the methods/devices to be used. Please avoid jargon and abbreviations).

[1] For example: student, PhD, post-doc

B) Risk assessment & risk management

Please indicate if you expect any risks for the participants as a result of your research and, if so, describe these risks and how you will try to minimize them.

Risks:
The greatest risk of harm lies in the using of the new bicycle simulator. Effort will be taken to make the simulator respond in an at least predictable way, but subjects may still behave unpredictably, due to the experience being new, the response of the device not being as expected, or the feedback of the bodies' sensors not being recognized as cycling. Furthermore, there lies a certain risk in cycling outside, but the manoeuvres asked from the participants are not that unusual in the context of riding a racing bicycle. In addition to that, current COVID-19 regulations require measures to be taken to guarantee the participant's safety in that regard.

Mitigations:
A cycling helmet will be required in all experiments where motion is part of the design. This includes outdoor cycling and the newly designed motion platform. In addition to this, the participant will mount the bicycle on the newly designed motion platform from a pressure sensitive plate, which disables any electric motors. A dead man's switch will be put on the participant's wrist, so in the case of a catastrophic fall, the machine will be immediately disabled. Only if the cyclist feels confident enough to use his clip pedals, he will be allowed to do so. In general, this is not recommended, since the subject's feet can be used to stabilize sudden unexpected movements. In regards to risks caused by COVID-19, a 1.5 meter distance will be maintained, facemasks are mandatory and can only be taken off by the cyclist while the experiment takes place. Subjects will be asked whether they recently had cold symptoms, and will be asked to verify this in the informed consent form.

Please refer to the supplemented Safety & Mitigations report for a more detailed description of the device, its risks and undertaken mitigations.

III. Checklist

Question	Yes	No
1. Does the study involve participants who are particularly vulnerable or unable to give informed consent? (e.g., children, people with learning difficulties, patients, people receiving counselling, people living in care or nursing homes, people recruited through self-help groups).		x
2. Are the participants, outside the context of the research, in a dependent or subordinate position to the investigator (such as own children or own students)?[2]		x
3. Will it be necessary for participants to take part in the study without their knowledge and consent at the time? (e.g., covert observation of people in non-public places).		x
4. Will the study involve actively deceiving the participants? (For example, will participants be deliberately falsely informed, will information be withheld from them or will they be misled in such a way that they are likely to object or show unease when debriefed about the study).		x
5. Sensitive personal data • Will the study involve discussion or collection of personal sensitive data (e.g., financial data, location data, data relating to children or other vulnerable groups)? Definitions of sensitive personal data, and special cases thereof are provided here.		X
6. Will drugs, placebos, or other substances (e.g., drinks, foods, food or drink constituents, dietary supplements) be administered to the study participants?		x
7. Will blood or tissue samples be obtained from participants?		x
8. Is pain or more than mild discomfort likely to result from the study?		x
9. Does the study risk causing psychological stress or anxiety or other harm or negative consequences beyond that normally encountered by the participants in their life outside research?	x	
10. Will financial inducement (other than reasonable expenses and compensation for time) be offered to participants?		x
Important: if you answered 'yes' to any of the questions mentioned above, please submit a full application to HREC (see: website for forms or examples).		
11. Will the experiment collect and store videos, pictures, or other identifiable data of human subjects? [3]	x	
12. Will the experiment involve the use of devices that are not 'CE' certified?	x	

[2] **Important note concerning questions 1 and 2.** Some intended studies involve research subjects who are particularly vulnerable or unable to give informed consent .Research involving participants who are in a dependent or unequal relationship with the researcher or research supervisor (e.g., the researcher's or research supervisor's students or staff) may also be regarded as a vulnerable group . If your study involves such participants, it is essential that you safeguard against possible adverse consequences of this situation (e.g., allowing a student's failure to complete their participation to your satisfaction to affect your evaluation of their coursework). This can be achieved by ensuring that participants remain anonymous to the individuals concerned (e.g., you do not seek names of students taking part in your study). If such safeguards are in place, or the research does not involve other potentially vulnerable groups or individuals unable to give informed consent, it is appropriate to check the NO box for questions 1 and 2. Please describe corresponding safeguards in the summary field.

[3] Note: you have to ensure that collected data is safeguarded physically and will not be accessible to anyone outside the study. Furthermore, the data has to be de-identified if possible and has to be destroyed after a scientifically appropriate period of time. Also ask explicitly for consent if anonymised data will be published as open data.

Question	Yes	No
Only, if 'yes': continue with the following questions:		
➢ Was the device built in-house?	x	
➢ Was it inspected by a safety expert at TU Delft? (*Please provide device report, see: HREC website*)	x	
➢ If it was not built in house and not CE-certified, was it inspected by some other, qualified authority in safety and approved? *(Please provide records of the inspection).*		x
13. Has or will this research be submitted to a research ethics committee other than this one? (*if so, please provide details and a copy of the approval or submission).*		x

IV. Enclosures

Please, tick the checkboxes for submitted enclosures.

Required enclosures

- A data management plan reviewed by a data-steward.

Conditionally required enclosures

if you replied 'yes' to any of the questions 1 until 10:
- A full research application

If you replied 'yes' to questions 11:
- An Informed consent form

If you replied 'yes' to questions 12:
- A device report

If you replied 'yes' to questions 13:
- Submission details to the external HREC, and a copy of their approval if available.

Additional enclosures

- Any other information which you feel to be relevant for decisionmaking by the HREC.

V. Signature(s

Signature(s) of researcher(s)
Date: 14-07-2021

Signature (or upload consent by mail) research supervisor (if applicable)
Date:
14-7-2021

E.2 Full HREC Application

Research Ethics Application

Please fill in the checklist first if you have not done so already. Please complete this form digitally and send it the Ethics Committee.

Date of Submission:14-7-2021

Project Title: Kinematic Sway, Roll, Steer and Yaw Motion Verification of a Linear Actuator-Based Racing Bicycle Simulator.

Name(s) of researcher(s): Jelle Haasnoot

Name of supervisor (if applicable): Arend Schwab, Riender Happee

Contact Information

Department: 3mE

Telephone number: +316 13 29 49 29

E-mail address: j.haasnoot@student.tudelft.nl

Contact information of external partners (if applicable): Company supervisor: Jos Joffers, Jos.Joffers@garmin.com

Summary

Please provide a brief summary of the research.

In this study, 15 test subjects will be asked to participate in a study comparing a newly designed bicycle simulator to outside bicycling, as well as existing stationary indoor cycling equipment. This will be done by both performing measurements on the subjects' personal racing bicycle (if they don't own one, one will be provided), and asking them a number of subjective questions about the quality of the newly designed bicycle simulator.

This new bicycle simulator will be different in the sense that it allows for more involvement of the cyclist in balancing and steering the bicycle, and the bicycle will respond to the cyclist's input as it would outside. At least, that is the goal.

The participants will be people already present in the company where the graduation project takes place, as well as (semi-)professional racing cyclists from the Netherlands, if they are available. The subjects will have different levels of cycling experience and preferences. To breach their normal cycling as little as possible, they are allowed to use their own bicycle and equipment.

Research

R.1. What is the research question? Please indicate what scientific contributions you expect from the research.

"How does user-balanced bicycle simulation relate kinematically to outdoor cycling and other in-door cycling solutions, focusing on sway, roll and steer motion directions?". In this study, I will show a new method of performing kinematic bicycle simulation, which instead of reacting to force inputs of the cyclist and simulating motion through a model, I will relay the balancing and steering task to the user more directly. If proven functional, this method will open up a great number of new possibilities for studies in bicycle handling, safety and simulation, but simulation qualities, influences of visual fidelity and simulator sickness in general as well.

R.2. What will the research conducted be a part of?

☐Bachelor's thesis

☒Master's thesis
☐PhD thesis
☐Research shills training
Other, namely: Enter what the research is part of here.

R.3. What type of research is involved?
☒Questionnaire
☒Observation
☒Experiment
Other, namely: Enter the type of research here.

R.4. Where will the research be conducted?
☐Online
☐At the university
☒Off-campus / non-university setting: R&D Department Tacx B.V., De Boeg 2, Oegstgeest
Other, namely: Enter where the research will be conducted here.

R.5. On what type of variable is the research based?
Give a general indication, such a questionnaire scores, performance on tasks, etc.
The results of the research will be based on the coupling of certain degrees of freedom in a bicycle, which are measured in a number of tasks every test subject has to perform on several simulator types. In addition to this, questionnaire scores will be recorded to measure subjective differences between environments.

R.6. If the research is experimental, what is the nature of the experimental manipulation?
In between experiments, both the apparatus and environment on which the participant is performing certain tasks, and the tasks themselves will change, since it is expected the subjects will perform differently in different cycling situations due to increased balancing effort, changes in bicycle dynamics and other factors.

R.7. Why is the research socially important? What benefits may result from the study?
A new type of bicycle platform is proposed, which uses a more direct and intuitive method of subject – simulator interaction. This platform may in future research prove insight in human control behaviour on vehicle simulators, when a high level of involvement from the human is required. This can be useful for exercise, revalidation and rehabilitation purposes. Furthermore, a platform for the determination of simulator control parameters will be available to improve vehicle simulator quality, as well as other boundary conditions which apply in vehicle simulators.

R.8. Are any external partners involved in the experiment? If so, please name them and describe the way they are involved in the experiment.
Tacx B.V. is providing budget and materials to enable this study. It is also the initiator of this project.

Participants

Pa.1. What is the number of participants needed? Please specify a minimum and maximum.
Minimum: 4
Maximum: 20

Pa.2.a. Does the study involve participants who are particularly vulnerable or unable to give informed consent? *(e.g., children, people with learning difficulties, patients, people receiving counselling, people living in care or nursing homes, people recruited through self-help groups)*
No.

Pa.2.b. If yes and unable to give informed consent, has permission been received from caretakers/parents?
N/A

Pa.3. Will the participants (or legal guardian) give written permission for the research with an 'Informed Consent' form that states the nature of the research, its duration, the risk, and any difficulties involved? If no, please explain.
Yes.

Pa.4. Are the participants, outside the context of the research, in a dependent or subordinate position to the investigator (such as own children or students)? If yes, please explain.
No.

Pa.5. How much time in total (maximum) will a participant have to spend on the activities of the study?
In total, a maximum duration of four hours can be expected for the experiments.

Pa.6. Will the participants have to take part in multiple sessions? Please specify how many and how long each session will take.
Preferably not. But if in pilot runs, this proves impossible due to experiments being performed both outside and inside (for example, bad weather conditions on the agreed experiment day), one subject will perform in two sessions, one of a duration of one hour (outdoor experiment) and another taking up three hours (indoor experiments).

Pa.7. What will the participants be asked to do?
The participants will be asked to perform nine manoeuvres on their bicycle, which include starting up from rest, perform a slow zig-zagging manoeuvre, cycling at constant velocity (on three velocities), cycling with increased and decreased resistance (equivalent to cycling up and down a hill, with varying inclines), performing a sprinting manoeuvre and low-speed balancing. These will be performed in ascending order of difficulty, and if any rider is not able to perform a certain task, more difficult tasks will not be performed. All these manoeuvres will be performed in several environments: outdoor cycling, indoor cycling on the newly designed motion platform, and existing Tacx indoor cycling equipment.

Pa.8. Will participants be instructed to act differently than normal or be subject to certain actions which are not normal? *(e.g. subject to stress inducing methods)*
In essence, no. Some getting used to the other-than-usual experiment environments may be necessary. Inexperienced cyclists may experience more difficulty balancing a bicycle, because they are not used to a racing bicycle (if they don't own one).

Pa.9. What are the possible (reasonably foreseeable) risks for the participants? Please list the possible harms if any.
The greatest risk of harm lies in the using of the new bicycle simulator. Effort will be taken to make the simulator respond in an at least predictable way, but subjects may still behave unpredictably, due to the experience being new, the response of the device not being as expected, or the feedback of the bodies' sensors not being recognized as cycling. Furthermore, there lies a certain risk in cycling outside, but the manoeuvres asked from the participants are not that unusual in the context of riding a racing bicycle. In addition to that, current COVID-19 regulations require measures to be taken to guarantee the participant's safety in that regard.

Pa.10. Will extra precautions be taken to protect the participants? If yes, please explain.
A cycling helmet will be required in all experiments where motion is part of the design. This includes outdoor cycling and the newly designed motion platform. In addition to this, the participant will mount the bicycle on the newly designed motion platform from a pressure sensitive plate, which disables any electric motors. A dead man's switch will be put on the participant's wrist, so in the case of a catastrophic fall, the machine will be immediately disabled. Only if the cyclist feels confident enough to use his clip pedals, he will be allowed to do so. In general, this is not recommended, since the subject's feet can be used to stabilize sudden unexpected movements. In regards to risks caused by COVID-19, a 1.5 meter distance will be maintained, facemasks are mandatory and can only be taken off by the cyclist while the experiment takes place. Subjects will be asked whether they recently had cold symptoms, and will be asked to verify this in the informed consent form. Full risk analysis is available in the supplemented "Safety & Mitigations" document.

Pa.11. Are there any positive consequences for a participant by taking part in the research? If yes, please explain.
No.

Pa.12. Will the participants (or their parents/primary caretakers) be fully informed about the nature of the study? If no, please explain why and state if they will receive all information after participating.
Yes.

Pa.13. Will it be made clear to the participants that they can withdraw their cooperation at any time?
Yes, in the informed consent form.

Pa.14. Where can participants go with their questions about the research and how are they notified of this?
To the student, Jelle Haasnoot. In the informed consent form.

Pa.15. Will the participants receive a reward?
☐Travel expenses
☐Compensation per hour
☒Nothing
Other, namely: When subjects are employed by Tacx, and perform the experiment under working hours, they will receive their normal hourly payment. However, this is not related to the experiment.

Pa.16. How will participants be recruited?
Participants will be selected by availability and cycling experience among the working staff at Tacx B.V., students and academic staff from the TU Delft Bicycle Lab and Jelle Haasnoot's immediate acquaintances. Different levels of cycling experience are preferred, to be able to observe differences between participants' behaviour and reactions on the newly developed bicycle simulator.

Privacy

Pr.1. Are the research data made anonymous? If no, please explain.
Yes.

Pr.2. Will directly identifiable data (such as name, address, telephone number, and so on) be kept longer than 6 months? If yes, will the participants give written permission to store their information for longer than 6 months?
No.

Pr.3. Who will have access to the data which will be collected?
Only the student (Jelle Haasnoot) will have direct access to the raw data.

Pr.4. Will the participants have access to their own data? If no, please explain.
No. The measuring method produces data not very useful or insightful to the participants. They are welcome to ask for conclusions or processed results if they are interested, provided they work for Tacx B.V., since data is used for commercial purposes.

Pr.5. Will covert methods be used? *(e.g. participants are filmed without them knowing)*
No.

Pr.6. Will any human tissue and/or biological samples be collected? *(e.g. urine)*
No.

Documents

Please attach the following documents to the application:

- Text used for ads (to find participants);
- Text used for debriefings;
- Form of informed consent for participants;
- Form of consent for other agencies when the research is conducted at a location (such as a hospital or school).

E.3 Informed Consent Form for Applicants

Consent Form for [*name of study*]

Information for the participant about the experiments and procedures.

Date: 09-04-2021

Project: *Kinematic Sway, Roll, Steer and Yaw Motion Verificationof a Linear Actuator-Based Racing Bicycle Simulator*

This study is aimed to obtaining the performance and realism of a newly designed bicycle motion platform and comparing this to existing indoor cycling solutions and outdoor cycling. The main purpose of this comparison is the need to find a bicycle simulator which allows the user to use his muscles and cycling mannerisms as he would outdoors. Additionally, this study will aid in research on the topic of human-simulator interaction, provide insight in the possibility and quality of balancing an actively controlled system. In turn, this could provide useful in improving bicycle safety, cycling for revalidation and quantifying and improving indoor exercise quality.

You will be asked to perform a number of cycling manoeuvres, which are the same in all cycling situations, as far as that is possible. For example, riding with the resistance of a 7.5% incline will be difficult on the road in the Netherlands. Those will be skipped.

You can withdraw from the experiments at any time, without having to give reason for it.

No identifiable personal data will be collected. You will be asked to state your biological sex, age, a short description of your cycling experience and weekly hours spent on cycling. These will be used to compare differences in the experiment results between cyclists. You will be given a participant number, and only Jelle Haasnoot has access to the person-participant number relation, should it be necessary. You are able to revoke your permission of this data storage at any time after the experiments have been conducted, and results been published.

The research data will be stored indefinitely, or as long as the repository allows, on both the TU Delft Research Repository and the Tacx CyclistBase database. Data will still be anonymised.

The contact information of the researcher is the following:

Jelle Haasnoot
jhaasnoot@tacx.nl
06 13 29 49 29

The contact information of the company supervisor and the daily supervisor are the following:

Company supervisor:
Jos Joffers
Jos.Joffers@garmin.com

Daily supervisor:
Arend L. Schwab
A.L.Schwab@tudelft.nl

The contact information of the data protection officer, 3mE, TU Delft is the following:

Yasemin Türkyilmaz-van der Velden
Y.Turkyilmaz-vanderVelden@tudelft.nl

Complaints about the experiment, data handling or other matters can be filed with either the researcher or the company supervisor.

Please tick the appropriate boxes	**Yes**	**No**
~~Taking part in the study~~		
I have read and understood the study information dated 09-04-2021, or it has been read to me. I have been able to ask questions about the study and my questions have been answered to my satisfaction.	□	□
I consent voluntarily to be a participant in this study and understand that I can refuse to answer questions and I can withdraw from the study at any time, without having to give a reason.	□	□
I understand that taking part in the study involves the collection of my cycling behaviour as sensor data, which is collected and stored anonymously. My age, biological sex and cycling experience will be used as dataset indicators. My subjective opinion, in the shape of a list of scoreable questions queried by the conductor of the experiment, will be recorded as well. Only the experiment conductor (Jelle Haasnoot) will have access to the recorded data.	□	□
Risks associated with participating in the study		
I understand that taking part in the study involves the following risks: • Unexpected behaviour by the simulator can cause the risk of falling and discomfort. Precautions have been taken to minimize damage, should a fall occur. • Discomfort as a result of a high level of physical exertion in certain cycling manoeuvres (high-power cycling)	□	□
I confirm that I have been informed about the risks of the simulator and know which parts I'm not supposed to touch or come near to.	□	□
Use of the information in the study		
I understand that information I provide will be used for the publication of a research paper, describing the experiments and outcomes of this study. In addition to that, the information will be used to improve existing indoor cycling equipment within Tacx, and will be added to a cyclists' database for comparison in the future.	□	□
I understand that personal information collected about me that can identify me, such as, will not be shared, and is only available to the researcher to inform participants of developments within the project and the experiments they participated in.	□	□
Future use and reuse of the information by others		
I give permission for the recorded sensor data and questionnaire scores that I provide to be archived a Tacx database, so it can be used for future research and learning. Personal data (name, phone number, e-mail address) will be anonymised after a three-month grace period, and stored out-of-reach of persons other than the project supervisors (Arend Schwab, Jos Joffers), or Jelle Haasnoot.	□	□

Signatures

_____	_____	_____
Name of participant [printed]	Signature	Date

I have accurately read out the information sheet to the potential participant and, to the best of my ability, ensured that the participant understands to what they are freely consenting.

_____	_____	_____
Jelle Haasnoot	Signature	Date

Study contact details for further information: Jelle Haasnoot, jhaasnoot@tacx.nl or +31613294929.

E.4 Data Management Plan

Bicycle Simulator Data Management Plan

0. Administrative questions

1. Name of data management support staff consulted during the preparation of this plan.

My faculty data steward, Yasemin Türkyilmaz-van der Velden, has reviewed this DMP on May 11th 2021.

2. Date of consultation with support staff.

2021-05-11

I. Data description and collection or re-use of existing data

3. Provide a general description of the type of data you will be working with, including any re-used data:

Type of data	**File format(s)**	**How will data be collected (for re-used data: source and terms of use)?**	**Purpose of processing**	**Storage location**	**Who will have access to the data**
Numerical data recorded from kinematic sensors	.csv and .fit files	Sensor system during experiments located on the bicycle	To compare cycling mannerisms between different cycling situations	TU Delft OneDrive, company PC, secure company back-up server	Project team and the company. Information can be destributed on request, in anonymised form.
Pseudonymized age (at time of study), indoor and outdoor cycling experience (in km/year) and gender, related to a participant number.	.xslx file	At the start of the experiment, by query	To identify and correlate certain bicycle mannerisms to age or cycling experience	TU Delft OneDrive, company PC, secure company back-up server	Project team and the company. Information can be destributed on request, in anonymised form
Pseudonymized subjective scoring data on the new bicycle simulator (graded 1 - 5)	.xlsx file	Survey during experiments	To identify differences between objective and subjective realism.	TU Delft OneDrive, company PC, secure company back-up server	Project team and the company. Information can be destributed on request, in anonymised form.
Informed consent forms.	Scanned .pdf files	At the start of the experiment	Participant consents to participating in the experiments.	TU Delft OneDrive	Student + back-up contacts
Participant number to name and contact information translational table	.xlsx file	At the start of the experiment, by query	Possibility for contacting post-experiment	TU Delft OneDrive	Student + back-up contacts

4. How much data storage will you require during the project lifetime?

- < 250 GB

II. Documentation and data quality

5. What documentation will accompany data?

- README file or other documentation explaining how data is organised

III. Storage and backup during research process

6. Where will the data (and code, if applicable) be stored and backed-up during the project lifetime?

- OneDrive
- Another storage system - please explain below, including provided security measures

The data is stored locally on a company PC after performing an experiment, and is backed up daily by performing a data upload to the company data server. This server is accessible by others within the company, so data will be stored encrypted and pseudonimyzed. The server is protected and only accessible through a VPN connection to the company network or local access, which is only possible when the user has company credentials. Personal information will only be stored on OneDrive.

IV. Legal and ethical requirements, codes of conduct

7. Does your research involve human subjects?

- Yes

8A. Will you work with personal data? (information about an identified or identifiable natural person)

If you are not sure which option to select, ask your Faculty Data Steward for

advice. You can also check with the privacy website or contact the privacy team: privacy-tud@tudelft.nl

- Yes

8B. Will you work with any types of confidential or classified data or code as listed below? (tick all that apply)

If you are not sure which option to select, ask your Faculty Data Steward for advice.

- Yes, data related to competitive advantage (e.g. patent, IP)

9. How will ownership of the data and intellectual property rights to the data be managed?

For projects involving commercially-sensitive research or research involving third parties, seek advice of your Faculty Contract Manager when answering this question. If this is not the case, you can use the example below.

This is an internship project carried in a company. It includes data used for gaining a competitive advantage. The terms are agreed upon in the TU Delft - Company - Student graduation agreement "Graduation Agreement at a Company", and the conditions therein.

10. Which personal data will you process? Tick all that apply

- Data collected in Informed Consent form (names and email addresses)
- Signed consent forms
- Gender, date of birth and/or age
- Email addresses and/or other addresses for digital communication
- Telephone numbers
- Names and addresses

11. Please list the categories of data subjects

Company employees and acquaintances who are willing to participate

12. Will you be sharing personal data with individuals/organisations outside of

the EEA (European Economic Area)?

- No

15. What is the legal ground for personal data processing?

- Informed consent

16. Please describe the informed consent procedure you will follow:

All study participants will be asked for their written consent for taking part in the study and for data processing before the start of the experiments.

17. Where will you store the signed consent forms?

- Same storage solutions as explained in question 6

18. Does the processing of the personal data result in a high risk to the data subjects?

If the processing of the personal data results in a high risk to the data subjects, it is required to perform a Data Protection Impact Assessment (DPIA). In order to determine if there is a high risk for the data subjects, please check if any of the options below that are applicable to the processing of the personal data during your research (check all that apply).
If two or more of the options listed below apply, you will have to complete the DPIA. Please get in touch with the privacy team: privacy-tud@tudelft.nl to receive support with DPIA.
If only one of the options listed below applies, your project might need a DPIA. Please get in touch with the privacy team: privacy-tud@tudelft.nl to get advice as to whether DPIA is necessary.
If you have any additional comments, please add them in the box below.

- None of the above applies

22. What will happen with personal research data after the end of the research project?

- Personal research data will be destroyed after the end of the research project

Personal data will be kept for three months after the finishing of the project. This date still has to be determined, but it will be the day the final presentation on the graduation project is given.

V. Data sharing and long-term preservation

30. How much of your data will be shared in a research data repository?

- < 100 GB

32. Under what licence will be the data/code released?

- Other - please explain

Not applicable. Data will not be uploaded to a public repository.

VI. Data management responsibilities and resources

33. Is TU Delft the lead institution for this project?

- Yes, leading the collaboration

This is an graduation project, taking place at the company Tacx B.V., under the supervision of a company supervisor and thesis supervisor from TU Delft: Arend L. Schwab.

34. If you leave TU Delft (or are unavailable), who is going to be responsible for the data resulting from this project?

The (latest) company supervisor (Jos Joffers, Jos.Joffers@garmin.com) or the thesis supervisor from TU Delft: Arend L. Schwab (A.Schwab@tudelft.nl).

35. What resources (for example financial and time) will be dedicated to data management and ensuring that data will be FAIR (Findable, Accessible, Interoperable, Re-usable)?

Not applicable. The data is not suitable for sharing in a repository due to its confidential nature.

E.5 Data Processing Agreement with Tacx B.V.

Verwerkersovereenkomst

inzake Verwerking Persoonlijke Data in Experimenten
Afstuderen Fietssimulator

tussen

Technische Universiteit Delft

en

Tacx B.V.

VERWERKERSOVEREENKOMST

Tussen:

TECHNISCHE UNIVERSITEIT DELFT, gevestigd te 2628CN DELFT, Stevinweg 1, vertegenwoordigd door Jelle Haasnoot,

hierna te noemen: "**Verwerkingsverantwoordelijke**",

en

Tacx B.V., gevestigd te 2343 HK Oegstgeest, De Boeg 2, vertegenwoordigd door Jos Joffers,

hierna te noemen: "**Verwerker**".

INHOUD

Overwegende:

A. Partijen hebben op 09-06-2021 een overeenkomst gesloten met kenmerk DPATacxTU met betrekking tot het verwerken van data van testpersonen in het afstudeeronderzoek van Jelle Haasnoot. Ter uitvoering van de Overeenkomst verwerkt Verwerker ten behoeve van Verwerkingsverantwoordelijke Persoonsgegevens;
B. In het kader van het uitvoeren van de Overeenkomst is Tacx B.V. aan te merken als Verwerker in de zin van de AVG en is Technische Universiteit Delft aan te merken als Verwerkingsverantwoordelijke in de zin van de AVG;
C. Partijen wensen zorgvuldig en in overeenstemming met de AVG en andere Toepasselijke wet- en regelgeving betreffende de Verwerking van Persoonsgegevens om te gaan met de Persoonsgegevens die ter uitvoering van de Overeenkomst verwerkt (zullen) worden;
D. Partijen wensen in overeenstemming met de AVG en andere Toepasselijke wet- en regelgeving betreffende de Verwerking van Persoonsgegevens hun rechten en plichten ten aanzien van de Verwerking van Persoonsgegevens van Betrokkenen Schriftelijk vast te leggen in deze Verwerkersovereenkomst

Komen het volgende overeen

1 DEFINITIES

In deze Verwerkersovereenkomst hebben de met hoofdletter geschreven begrippen de in dit artikel opgenomen betekenis. Waar de definitie in dit artikel in het enkelvoud is opgenomen, wordt ook het meervoud daaronder begrepen en vice versa, tenzij uitdrukkelijk anders vermeld of uit de context anders blijkt.

1.1 **AVG**: de Verordening (EU) 2016/679 van het Europees Parlement en de Raad van 27 april 2016 betreffende de bescherming van natuurlijke personen in verband met de Verwerking van Persoonsgegevens en betreffende het vrije verkeer van die gegevens en tot intrekking van Richtlijn 95/46/EG (algemene verordening gegevensbescherming).
1.2 **Betrokkene**: de geïdentificeerde of identificeerbare natuurlijke persoon op wie de Persoonsgegevens betrekking hebben, zoals bedoeld in artikel 4 onder 1) AVG.
1.3 **Bijlage**: een bijlage bij deze Verwerkersovereenkomst, die een integraal onderdeel vormt van deze Verwerkersovereenkomst.
1.4 **Bijzondere categorieën Persoonsgegevens**: Persoonsgegevens waaruit ras of etnische afkomst, politieke opvattingen, religieuze of levensbeschouwelijke overtuigingen, of het lidmaatschap van een vakbond blijken, en genetische gegevens, biometrische gegevens met het oog op de unieke identificatie van een persoon, of gegevens over gezondheid, of gegevens met betrekking tot iemands seksueel gedrag of seksuele gerichtheid, zoals bedoeld in artikel 9 AVG.
1.5 **Derde**: een natuurlijke persoon of rechtspersoon, een overheidsinstantie, een dienst of een ander orgaan, niet zijnde de Betrokkene, noch de Verwerkingsverantwoordelijke, noch de Verwerker, noch de personen die onder rechtstreeks gezag van de Verwerkingsverantwoordelijke of de Verwerker gemachtigd zijn om Persoonsgegevens te verwerken, zoals bedoeld in artikel 4 onder 10) AVG.

1.6 **Dienst**: de op grond van de Overeenkomst te leveren dienst(en) door Verwerker aan Verwerkingsverantwoordelijke.

1.7 **Inbreuk in verband met Persoonsgegevens**: een (vermoeden van een) inbreuk op de beveiliging die per ongeluk of op onrechtmatige wijze leidt tot de vernietiging, het verlies, de wijziging of de ongeoorloofde verstrekking van of de ongeoorloofde toegang tot doorgezonden, opgeslagen of anderszins verwerkte Persoonsgegevens, zoals bedoeld in artikel 4 onder 12) AVG.

1.8 **Medewerker**: de door Verwerker ingeschakelde werknemers en andere personen waarvan de werkzaamheden onder zijn verantwoordelijkheid vallen en die worden ingeschakeld door Verwerker ter uitvoering van de Overeenkomst.

1.9 **Ontvanger**: een natuurlijke persoon of rechtspersoon, een overheidsinstantie, een dienst of een ander orgaan, al dan niet een Derde, aan wie/waaraan de Persoonsgegevens worden verstrekt, zoals bedoeld in artikel 4 onder 9) AVG.

1.10 **Overeenkomst**: de overeenkomst die tussen Verwerkingsverantwoordelijke en Verwerker is gesloten en op grond waarvan Verwerker Persoonsgegevens ten behoeve van de uitvoering van deze overeenkomst voor Verwerkingsverantwoordelijke verwerkt.

1.11 **Persoonsgegeven**: alle informatie over een Betrokkene; als identificeerbaar wordt beschouwd een natuurlijke persoon die direct of indirect kan worden geïdentificeerd, met name aan de hand van een identificator zoals een naam, een identificatienummer, locatiegegevens, een online identificator of van een of meer elementen die kenmerkend zijn voor de fysieke, fysiologische, genetische, psychische, economische, culturele of sociale identiteit van die natuurlijke persoon, zoals bedoeld in artikel 4 onder 1) AVG.

1.12 **PIA**: de gegevensbeschermingseffectbeoordeling (privacy impact assessment) die vóór de Verwerking ten aanzien van het effect van de beoogde verwerkingsactiviteiten op de bescherming van Persoonsgegevens wordt uitgevoerd, zoals bedoeld in artikel 35 AVG.

1.13 **Schriftelijk**: op schrift gesteld of langs de elektronische weg, zoals bedoeld in artikel 6:227a van het Burgerlijk Wetboek.

1.14 **Sub-verwerker**: een andere verwerker, waaronder maar niet beperkt tot groepsmaatschappijen, zustermaatschappijen, dochtermaatschappijen en hulpleveranciers, die Verwerker inschakelt om voor rekening van de Verwerkingsverantwoordelijke specifieke verwerkingsactiviteiten te verrichten.

1.15 **Toepasselijke wet- en regelgeving betreffende de Verwerking van Persoonsgegevens**: de toepasselijke wet- en regelgeving en/of (nadere) verdragen, verordeningen, richtlijnen, besluiten, beleidsregels, instructies en/of aanbevelingen van een bevoegde overheidsinstantie betreffende de Verwerking van Persoonsgegevens, tevens omvattende toekomstige wijziging hiervan en/of aanvulling hierop, inclusief lidstaatrechtelijke uitvoeringswetten van de AVG en de Telecommunicatiewet.

1.16 **Toezichthoudende autoriteit**: één of meer onafhankelijke overheidsinstanties die verantwoordelijk is of zijn voor het toezicht op de toepassing van de AVG, teneinde de grondrechten en fundamentele vrijheden van natuurlijke personen in verband met de Verwerking van hun Persoonsgegevens te beschermen en het vrije verkeer van Persoonsgegevens binnen de Unie te vergemakkelijken, zoals bedoeld in artikel 4 onder 21) en artikel 51 AVG. In Nederland is dit de Autoriteit Persoonsgegevens.

1.17 **Verwerkersovereenkomst**: de onderhavige overeenkomst inclusief Bijlagen, zoals bedoeld in artikel 28 lid 3 AVG.

1.18 **Verwerking**: een bewerking of een geheel van bewerkingen met betrekking tot Persoonsgegevens of een geheel van Persoonsgegevens, al dan niet uitgevoerd via

geautomatiseerde procedés, zoals het verzamelen, vastleggen, ordenen, structureren, opslaan, bijwerken of wijzigen, opvragen, raadplegen, gebruiken, verstrekken door middel van doorzending, verspreiden of op andere wijze ter beschikking stellen, aligneren of combineren, afschermen, wissen of vernietigen van gegevens, zoals bedoeld in artikel 4 onder 2) AVG.

2 VOORWERP VAN DE VERWERKERSOVEREENKOMST

2.1 De Verwerkersovereenkomst vormt een aanvulling op de Overeenkomst en vervangt eventuele eerder gemaakte afspraken tussen Partijen ten aanzien van de Verwerking van Persoonsgegevens. Bij tegenstrijdigheid tussen de bepalingen uit de Verwerkersovereenkomst en de Overeenkomst, prevaleren de bepalingen uit de Verwerkersovereenkomst.

2.2 De bepalingen uit de Verwerkersovereenkomst gelden voor alle Verwerkingen die plaatsvinden ter uitvoering van de Overeenkomst. Verwerker brengt Verwerkingsverantwoordelijke onverwijld op de hoogte indien Verwerker reden heeft om aan te nemen dat Verwerker niet langer aan de Verwerkersovereenkomst kan voldoen.

2.3 Verwerkingsverantwoordelijke geeft Verwerker opdracht en instructies om de Persoonsgegevens te verwerken namens de Verwerkingsverantwoordelijke. De instructies van Verwerkingsverantwoordelijke zijn nader omschreven in de Verwerkersovereenkomst en de Overeenkomst. Verwerkingsverantwoordelijke kan naar redelijkheid Schriftelijk aanvullende of afwijkende instructies geven.

2.4 Verwerker verwerkt de Persoonsgegevens uitsluitend in opdracht van Verwerkingsverantwoordelijke en op basis van de instructies van Verwerkingsverantwoordelijke. Verwerker verwerkt de Persoonsgegevens uitsluitend voor zover de Verwerking noodzakelijk is ter uitvoering van de Overeenkomst, nimmer ten eigen nutte, ten nutte van Derden en/of voor reclamedoeleinden c.q. andere doeleinden, tenzij een op Verwerker van toepassing zijnde Unierechtelijke of lidstaatrechtelijke bepaling Verwerker tot Verwerking verplicht. In dat geval stelt Verwerker Verwerkingsverantwoordelijke voorafgaand aan de Verwerking Schriftelijk op de hoogte van deze bepaling, tenzij die wetgeving deze kennisgeving om gewichtige redenen van algemeen belang verbiedt.

2.5 Verwerker en Verwerkingsverantwoordelijke leven de AVG en andere Toepasselijke wet- en regelgeving betreffende de Verwerking van Persoonsgegevens na. Verwerker stelt de Verwerkingsverantwoordelijke onmiddellijk in kennis indien naar mening van Verwerker een instructie van Verwerkingsverantwoordelijke inbreuk oplevert op de AVG en/of andere Toepasselijke wet- en regelgeving betreffende de Verwerking van Persoonsgegevens.

2.6 Indien Verwerker in strijd met de Verwerkersovereenkomst en/of de AVG en/of andere Toepasselijke wet- en regelgeving betreffende de Verwerking van Persoonsgegevens het doel en de middelen van de Verwerking van Persoonsgegevens bepaalt, wordt Verwerker voor die Verwerkingen als Verwerkingsverantwoordelijke beschouwd.

3 VERWERKING VAN PERSOONSGEGEVENS

3.1 Voorafgaand aan het sluiten van de Verwerkersovereenkomst informeert Verwerker Verwerkingsverantwoordelijke in Bijlage A volledig en naar waarheid over de Verwerkingen die Verwerker ter uitvoering van de Overeenkomst uitvoert, tenzij in Bijlage A is opgenomen dat

Verwerkingsverantwoordelijke de betreffende informatie in deze Bijlage opneemt. Verwerker is uitsluitend tot de in Bijlage A gespecificeerde Verwerkingen gerechtigd.

4 VERLENEN VAN BIJSTAND EN MEDEWERKING

4.1 Verwerker verleent Verwerkingsverantwoordelijke alle benodigde bijstand en medewerking bij het doen nakomen van de op Partijen rustende verplichtingen op grond van de AVG en andere Toepasselijke wet- en regelgeving betreffende de Verwerking van Persoonsgegevens.
Verwerker verleent Verwerkingsverantwoordelijke in ieder geval bijstand met betrekking tot:

(i) De beveiliging van Persoonsgegevens;
(ii) Het uitvoeren van controles en audits;
(iii) Het uitvoeren van PIA's;
(iv) Voorafgaande raadpleging van de Toezichthoudende autoriteit;
(v) Het voldoen aan verzoeken van de Toezichthoudende autoriteit of een andere overheidsinstantie;
(vi) Het voldoen aan verzoeken van Betrokkenen;
(vii) Het melden van Inbreuken in verband met Persoonsgegevens.

4.2 Onder het verlenen van bijstand en medewerking met betrekking tot het voldoen aan verzoeken van Betrokkenen, worden in ieder geval de volgende verplichtingen voor Verwerker verstaan:

4.2.1 Verwerker neemt alle redelijke maatregelen om ervoor te zorgen dat Betrokkene zijn rechten kan uitoefenen.

4.2.2 Indien een Betrokkene met betrekking tot de uitvoering van zijn rechten direct contact opneemt met Verwerker, dan gaat Verwerker hier – behoudens uitdrukkelijke andersluidende instructie van Verwerkingsverantwoordelijke – niet (inhoudelijk) op in, maar bericht Verwerker dit onverwijld aan Verwerkingsverantwoordelijke met een verzoek om nadere instructies.

4.2.3 Indien Verwerker de Dienst rechtstreeks aanbiedt aan Betrokkene, is Verwerker verplicht om Betrokkene namens de Verwerkingsverantwoordelijke te informeren over de Verwerking van de Persoonsgegevens van Betrokkene op een wijze die in overeenstemming is met de rechten van Betrokkene.

4.3 Onder het verlenen van bijstand en medewerking met betrekking tot het voldoen aan verzoeken van de Toezichthoudende autoriteit of een andere overheidsinstantie, worden in ieder geval de volgende verplichtingen voor Verwerker verstaan:

4.3.1 Indien Verwerker een verzoek of een bevel van een Nederlandse en/of buitenlandse overheidsinstantie ontvangt met betrekking tot Persoonsgegevens, waaronder maar niet beperkt tot een verzoek van de Toezichthoudende autoriteit, informeert Verwerker Verwerkingsverantwoordelijke onverwijld, voor zover dat wettelijk is toegestaan. Bij de behandeling van het verzoek of bevel neemt Verwerker alle instructies van Verwerkingsverantwoordelijke in acht en verleent Verwerker alle redelijkerwijs benodigde medewerking aan Verwerkingsverantwoordelijke.

4.3.2 Indien het Verwerker wettelijk is verboden om te voldoen aan zijn verplichtingen op grond van artikel 4.3.1, behartigt Verwerker de redelijke belangen van Verwerkingsverantwoordelijke. Hieronder wordt in ieder geval verstaan:

4.3.2.1 Verwerker laat juridisch toetsen in hoeverre: (i) Verwerker wettelijk verplicht is om aan het verzoek of bevel te voldoen; en (ii) het Verwerker daadwerkelijk is verboden om aan zijn verplichtingen jegens Verwerkingsverantwoordelijke op grond van artikel 4.3.1 te voldoen.

4.3.2.2 Verwerker werkt alleen mee aan het verzoek of bevel indien Verwerker hiertoe wettelijk verplicht is en waar mogelijk maakt Verwerker (in rechte) bezwaar tegen het verzoek of bevel of het verbod om Verwerkingsverantwoordelijke hierover te informeren of de instructies van Verwerkingsverantwoordelijke op te volgen.

4.3.2.3 Verwerker verstrekt niet meer Persoonsgegevens dan strikt noodzakelijk om aan het verzoek of bevel te voldoen.

4.3.2.4 Verwerker onderzoekt indien sprake is van doorgifte in de zin van artikel 9 de mogelijkheden om te voldoen aan de artikelen 44 tot en met 46 AVG.

5 TOEGANG TOT PERSOONSGEGEVENS

5.1 Verwerker beperkt de toegang tot Persoonsgegevens aan Medewerkers, Sub-verwerkers, Derden en andere Ontvangers van Persoonsgegevens tot een noodzakelijk minimum.

5.2 Verwerker verschaft uitsluitend toegang aan die Medewerkers voor wie ter uitvoering van de Overeenkomst deze toegang tot Persoonsgegevens noodzakelijk is. De categorieën Medewerkers zijn in Bijlage A gespecificeerd.

5.3 Verwerker verschaft Sub-verwerkers geen toegang tot Persoonsgegevens zonder voorafgaande algemene of specifieke Schriftelijke toestemming van Verwerkingsverantwoordelijke. Algemene Schriftelijke toestemming voor het inschakelen van Sub-verwerkers is slechts verleend indien dit expliciet in Bijlage A is opgenomen. Specifieke toestemming voor het inschakelen van Sub-verwerkers is slechts verleend aan Sub-verwerkers die in Bijlage A zijn gespecificeerd.

5.4 Verwerker licht Verwerkingsverantwoordelijke in geval van algemene Schriftelijke toestemming voor het inschakelen van Sub-verwerkers uiterlijk drie (3) maanden voorafgaand aan beoogde veranderingen inzake de toevoeging, vervanging of wijziging van Sub-verwerker(s), Schriftelijk in, waarbij de Verwerkingsverantwoordelijke de mogelijkheid wordt geboden tegen deze veranderingen bezwaar te maken. Partijen treden hierop in onderhandeling.

5.5 De algemene of specifieke toestemming van Verwerkingsverantwoordelijke voor het inschakelen Sub-verwerkers laat de verplichtingen voor Verwerker voortvloeiende uit de Verwerkersovereenkomst, waaronder maar niet beperkt tot artikel 9, onverlet. Verwerkingsverantwoordelijke kan zijn algemene of specifieke Schriftelijke toestemming voor het inschakelen van Sub-verwerkers intrekken, indien Verwerker niet of niet langer voldoet aan de verplichtingen uit de Verwerkersovereenkomst, de AVG en/of andere Toepasselijke wet- en regelgeving betreffende de Verwerking van Persoonsgegevens.

5.6 Verwerker verstrekt op eerste verzoek van Verwerkingsverantwoordelijke een overzicht van de door Verwerker ingeschakelde Sub-verwerkers aan Verwerkingsverantwoordelijke.

5.7 Verwerker legt de in de Verwerkersovereenkomst opgenomen verplichtingen op aan de door Verwerker ingeschakelde (rechts)personen, waaronder maar niet beperkt tot Medewerkers en/of Sub-verwerkers. Verwerker draagt er zorg voor dat de door Verwerker ingeschakelde (rechts)personen, waaronder maar niet beperkt tot Medewerkers en/of Sub-verwerkers, de in

de Verwerkersovereenkomst opgenomen verplichtingen naleven door middel van een Schriftelijke overeenkomst.

5.8 Verwerker brengt Verwerkingsverantwoordelijke onverwijld op de hoogte indien Verwerker en/of door Verwerker ingeschakelde (rechts)personen, waaronder maar niet beperkt tot Medewerkers en/of Sub-verwerkers, in strijd handelen met de Verwerkersovereenkomst en/of de met Verwerker gesloten Schriftelijke overeenkomst zoals bedoeld in artikel 5.7.

5.9 Verwerker verstrekt op verzoek van Verwerkingsverantwoordelijke een afschrift van de Schriftelijke overeenkomst tussen Verwerker en de door Verwerker ingeschakelde (rechts)personen, waaronder maar niet beperkt tot Medewerkers en/of Sub-verwerkers.

5.10 Verwerker blijft ten aanzien van de Verwerkingsverantwoordelijke volledig verantwoordelijk en volledig aansprakelijk voor het nakomen van de verplichtingen door de door Verwerker ingeschakelde (rechts)personen, waaronder maar niet beperkt tot Medewerkers en/of Sub-verwerkers, voortvloeiende uit de AVG en/of andere Toepasselijke wet- en regelgeving betreffende de Verwerking van Persoonsgegevens en de verplichtingen voortvloeiende uit de Overeenkomst en de Verwerkersovereenkomst.

6 BEVEILIGING

6.1 Verwerker treft passende technische en organisatorische maatregelen om een op het risico afgestemd beveiligingsniveau te waarborgen, opdat de Verwerking aan de vereisten van de AVG en andere Toepasselijke wet- en regelgeving betreffende de Verwerking van Persoonsgegevens voldoet en de bescherming van de rechten van Betrokkenen is gewaarborgd. Verwerker treft hiertoe tenminste de technische en organisatorische maatregelen die zijn opgenomen in Bijlage B.

6.2 Bij de beoordeling van het passende beveiligingsniveau houdt Verwerker rekening met de stand van de techniek, de uitvoeringskosten, alsook met de aard, de omvang, de context en de verwerkingsdoeleinden en de qua waarschijnlijkheid en ernst uiteenlopende risico's voor de rechten en vrijheden van personen, vooral als gevolg van de vernietiging, het verlies, de wijziging of de ongeoorloofde verstrekking van of ongeoorloofde toegang tot doorgezonden, opgeslagen of anderszins verwerkte gegevens, hetzij per ongeluk hetzij onrechtmatig.

6.3 Verwerker legt zijn beveiligingsbeleid Schriftelijk vast. Op verzoek van Verwerkingsverantwoordelijke verschaft Verwerker inzage in het beveiligingsbeleid van Verwerker.

6.4 Het aansluiten bij een goedgekeurde gedragscode als bedoeld in artikel 40 AVG of een goedgekeurd certificeringsmechanisme als bedoeld in artikel 42 AVG kan worden gebruikt als element om aan te tonen dat de in dit artikel bedoelde vereisten worden nageleefd.

7 AUDIT

7.1 Verwerker is verplicht periodiek een onafhankelijke, externe deskundige een audit te laten uitvoeren ten aanzien van de organisatie van Verwerker, teneinde aan te tonen dat Verwerker aan het bepaalde in de Overeenkomst, de Verwerkersovereenkomst, de AVG en andere Toepasselijke wet- en regelgeving betreffende de Verwerking van Persoonsgegevens voldoet.

7.2 Verwerker verricht tenminste een keer per twee jaar een periodieke audit, zoals bedoeld in artikel 7.1. Indien Bijzondere categorieën Persoonsgegevens worden verwerkt, verricht Verwerker tenminste eenmaal per jaar een periodieke audit zoals bedoeld in artikel 7.1.

7.3 Verwerker is enkel niet gehouden tot het verrichten van een periodieke audit zoals bedoeld in artikel 7.1, indien Verwerker uitsluitend Persoonsgegevens verwerkt met een laag risico en uitdrukkelijk in Bijlage A is opgenomen dat Verwerker niet gehouden is tot het verrichten van een periodieke audit. Verwerkingsverantwoordelijke stelt vast of er sprake is van een laag risico.

7.4 Verwerker is verplicht de bevindingen van de onafhankelijke, externe deskundige, op verzoek aan Verwerkingsverantwoordelijke ter beschikking te stellen in de vorm van een verklaring, waarin de deskundige een oordeel geeft over de kwaliteit van de door Verwerker getroffen technische en organisatorische beveiligingsmaatregelen met betrekking tot de Verwerkingen die Verwerker ten behoeve van Verwerkingsverantwoordelijke verricht.

7.5 Verwerkingsverantwoordelijke heeft het recht om op zijn verzoek een audit te laten uitvoeren door een door Verwerkingsverantwoordelijke gemachtigde (rechts)persoon, ten aanzien van de organisatie van Verwerker, teneinde aan te tonen dat Verwerker aan het bepaalde in de Overeenkomst, de Verwerkersovereenkomst, de AVG en andere Toepasselijke wet- en regelgeving betreffende de Verwerking van Persoonsgegevens voldoet.

7.6 De kosten van de periodieke audit komen voor rekening van Verwerker. De kosten van de audit op verzoek van Verwerkingsverantwoordelijke komen voor rekening van Verwerkingsverantwoordelijke, tenzij uit de bevindingen van de audit blijkt dat Verwerker de bepalingen uit de Overeenkomst en/of de Verwerkersovereenkomst en/of de AVG en/of andere Toepasselijke wet- en regelgeving betreffende de Verwerking van Persoonsgegevens niet is nagekomen. Deze bepaling laat de overige rechten van Verwerkingsverantwoordelijke, waaronder het recht op schadevergoeding, onverlet.

7.7 Indien tijdens een audit wordt vastgesteld dat Verwerker niet aan het bepaalde in de Overeenkomst en/of de Verwerkersovereenkomst en/of de AVG en/of andere Toepasselijke wet- en regelgeving betreffende de Verwerking van Persoonsgegevens voldoet, neemt Verwerker onverwijld alle redelijkerwijs noodzakelijke maatregelen om te zorgen dat Verwerker hieraan alsnog voldoet. De bijbehorende kosten komen voor rekening van Verwerker.

8 INBREUK IN VERBAND MET PERSOONSGEGEVENS

8.1 Verwerker informeert Verwerkingsverantwoordelijke zonder onredelijke vertraging en uiterlijk binnen 24 uur na kennisneming, over een Inbreuk in verband met Persoonsgegevens of een redelijk vermoeden van een Inbreuk in verband met Persoonsgegevens. Verwerker informeert Verwerkingsverantwoordelijke via de contactpersoon en de contactgegevens van Verwerkingsverantwoordelijke zoals opgenomen in Bijlage A en ten minste ten aanzien van hetgeen is opgenomen in Bijlage C. Verwerker garandeert dat de verstrekte informatie volledig, correct en accuraat is.

8.2 Indien en voor zover het voor Verwerker niet mogelijk is om alle informatie uit Bijlage C gelijktijdig te verstrekken, kan de informatie zonder onredelijke vertraging en uiterlijk binnen 24 uur na het ontdekken, in stappen worden verstrekt aan Verwerkingsverantwoordelijke.

8.3 Verwerker heeft adequaat beleid en adequate procedures ingericht om Inbreuken in verband met Persoonsgegevens in een zo vroeg mogelijk stadium te detecteren, Verwerkingsverantwoordelijke hierover uiterlijk binnen 24 uur te informeren, hierop adequaat en onmiddellijk te reageren, (verdere) onbevoegde kennisneming, wijziging, en verstrekking dan wel anderszins onrechtmatige Verwerking te voorkomen of te beperken en herhaling hiervan te voorkomen. Op verzoek van Verwerkingsverantwoordelijke verschaft Verwerker informatie over en inzage in dit door Verwerker ingerichte beleid en deze door Verwerker ingerichte procedures.

8.4 Verwerker houdt Schriftelijk een register bij van alle Inbreuken in verband met Persoonsgegevens die betrekking hebben op of verband houden met de (uitvoering van de) Overeenkomst, met inbegrip van de feiten omtrent de Inbreuk in verband met Persoonsgegevens, de gevolgen daarvan en de getroffen corrigerende maatregelen. Op verzoek van Verwerkingsverantwoordelijke verschaft Verwerker Verwerkingsverantwoordelijke een afschrift van dit register.

9 DOORGIFTE VAN PERSOONSGEGEVENS

9.1 Persoonsgegevens mogen enkel worden doorgegeven aan derde landen of internationale organisaties indien sprake is van een passend beschermingsniveau en Verwerkingsverantwoordelijke hiervoor specifieke Schriftelijke toestemming heeft verleend. Deze specifieke Schriftelijke toestemming is slechts verleend indien dit is opgenomen in Bijlage A. Verwerker is uitsluitend gerechtigd tot deze in Bijlage A gespecificeerde doorgiften aan derde landen of internationale organisaties, tenzij een op Verwerker van toepassing zijnde Unierechtelijke of lidstaatrechtelijke bepaling Verwerker tot Verwerking verplicht. In dat geval stelt Verwerker Verwerkingsverantwoordelijke voorafgaand aan de Verwerking Schriftelijk op de hoogte van deze bepaling, tenzij die wetgeving deze kennisgeving om gewichtige redenen van algemeen belang verbiedt.

9.2 Verwerkingsverantwoordelijke kan aan de Schriftelijke toestemming, zoals bedoeld in artikel 9.1, nadere voorwaarden verbinden, waaronder maar niet beperkt tot het aantonen dat aan de vereisten zoals opgenomen in artikel 9.3 is voldaan.

9.3 Verwerkingsverantwoordelijke kan Verwerker slechts toestemming verlenen voor een doorgifte van Persoonsgegevens aan derde landen of internationale organisaties indien, ofwel:

(i) Een adequaatheidsbesluit overeenkomstig artikel 45 lid 3 AVG is genomen ten aanzien van het betreffende derde land of de betreffende internationale organisatie; ofwel

(ii) Passende waarborgen overeenkomstig artikel 46 AVG met inbegrip van bindende voorschriften zoals bedoeld in artikel 47 AVG, zijn getroffen ten aanzien van het betreffende derde land of de betreffende internationale organisatie; ofwel

(iii) Aan één van de specifieke voorwaarden uit artikel 49 lid 1 AVG is voldaan ten aanzien van het betreffende derde land of de betreffende internationale organisatie.

10 VERTROUWELIJKHEID VAN PERSOONSGEGEVENS

10.1 Alle Persoonsgegevens worden als vertrouwelijke gegevens gekwalificeerd en dienen als zodanig te worden behandeld.

10.2 Partijen houden alle Persoonsgegevens geheim en maken deze op geen enkele wijze verder intern of extern bekend, behalve voor zover:
(i) Bekendmaking en/of verstrekking van de Persoonsgegevens in het kader van de uitvoering van de Overeenkomst of Verwerkersovereenkomst noodzakelijk is;
(ii) Enig dwingendrechtelijk wettelijk voorschrift of rechterlijke uitspraak Partijen tot bekendmaking en/of verstrekking van die Persoonsgegevens verplicht, waarbij Partijen eerst de andere Partij hiervan op de hoogte stellen;
(iii) Bekendmaking en/of verstrekking van die Persoonsgegevens geschiedt met voorafgaande Schriftelijke toestemming van de andere Partij.

10.3 Overtreding van artikel 10.1 en/of artikel 10.2 wordt beschouwd als een Inbreuk in verband met Persoonsgegevens.

11 AANSPRAKELIJKHEID EN VRIJWARING

11.1 Verwerker is aansprakelijk voor alle schade die voortvloeit uit of verband houdt met het niet nakomen van de Verwerkersovereenkomst en/of de AVG en/of andere Toepasselijke wet- en regelgeving betreffende de Verwerking van Persoonsgegevens.

11.2 Verwerker vrijwaart Verwerkingsverantwoordelijke voor alle aanspraken, boeten en/of maatregelen van derden, daaronder begrepen Betrokkenen en de Toezichthoudende autoriteit, die jegens Verwerkingsverantwoordelijke worden ingesteld of opgelegd wegens een schending van de Verwerkersovereenkomst en/of de AVG en/of andere Toepasselijke wet- en regelgeving betreffende de Verwerking van Persoonsgegevens door Verwerker en/of door Verwerker ingeschakelde (rechts)personen, waaronder maar niet beperkt tot Medewerkers en/of Sub-verwerkers.

11.3 Verwerker draagt zorg voor afdoende dekking van de aansprakelijkheid door middel van een aansprakelijkheidsverzekering. Op verzoek van Verwerkingsverantwoordelijke geeft Verwerker Verwerkingsverantwoordelijke inzage in (de polis van) deze aansprakelijkheidsverzekering van Verwerker.

12 WIJZIGING

12.1 Verwerker is verplicht Verwerkingsverantwoordelijke onmiddellijk te informeren over voorgenomen wijzigingen in de Dienst, de uitvoering van de Overeenkomst en de uitvoering van de Verwerkersovereenkomst die betrekking hebben op de Verwerking van Persoonsgegevens. Hieronder wordt in ieder geval verstaan:
(i) Wijzigingen die invloed (kunnen) hebben op de te verwerken (categorieën) Persoonsgegevens;
(ii) Wijziging van de middelen waarmee de Persoonsgegevens worden verwerkt;
(iii) Het inschakelen van andere Sub-verwerkers;
(iv) Wijziging in de doorgifte van Persoonsgegevens aan derde landen en/of internationale organisaties.

12.2 Indien een wijziging met betrekking tot de Verwerking van Persoonsgegevens of een audit daartoe aanleiding geeft, treden Partijen op eerste verzoek van Verwerkingsverantwoordelijke in overleg over het wijzigen van de Verwerkersovereenkomst.

12.3 Verwerker is pas gerechtigd tot het uitvoeren van een wijziging in de Dienst, een wijziging in de uitvoering van de Overeenkomst, een wijziging in de uitvoering van de Verwerkersovereenkomst en/of een wijziging die aanpassing van Bijlage A tot gevolg heeft, indien Verwerkingsverantwoordelijke daaraan voorafgaand Schriftelijk toestemming voor deze wijziging(en) heeft gegeven.

12.4 Wijzigingen die betrekking hebben op de Verwerking van Persoonsgegevens mogen nooit tot gevolg hebben dat Verwerkingsverantwoordelijke niet kan voldoen aan de AVG en/of andere Toepasselijke wet- en regelgeving betreffende de Verwerking van Persoonsgegevens.

12.5 In geval van nietigheid of vernietigbaarheid van één of meer bepalingen van de Verwerkersovereenkomst, blijven de overige bepalingen onverkort van kracht.

13 DUUR EN BEËINDIGING

13.1 De duur van de Verwerkersovereenkomst is gelijk aan de duur van de Overeenkomst. De Verwerkersovereenkomst is niet los van de Overeenkomst te beëindigen. Bij beëindiging van de Overeenkomst eindigt de Verwerkersovereenkomst van rechtswege en vice versa.

13.2 Verwerkingsverantwoordelijke is gerechtigd de Verwerkersovereenkomst op te zeggen, indien Verwerker niet voldoet of niet langer kan voldoen aan de Verwerkersovereenkomst en/of de AVG en/of andere Toepasselijke wet- en regelgeving betreffende de Verwerking van Persoonsgegevens, zonder dat Verwerker aanspraak maakt op enige schadevergoeding. Bij de opzegging neemt Verwerkingsverantwoordelijke een redelijke opzegtermijn in acht, tenzij de omstandigheden onmiddellijke opzegging rechtvaardigen.

13.3 Binnen een maand nadat de Overeenkomst eindigt, vernietigt en/of retourneert Verwerker alle Persoonsgegevens en/of draagt Verwerker deze over aan Verwerkingsverantwoordelijke en/of een andere door Verwerkingsverantwoordelijke aan te wijzen partij, naar gelang de keuze van Verwerkingsverantwoordelijke. Alle bestaande (overige) kopieën van Persoonsgegevens, zich al dan niet bevindende bij door Verwerker ingeschakelde (rechts)personen, waaronder maar niet beperkt tot Medewerkers en/of Sub-verwerkers, worden hierbij aantoonbaar permanent verwijderd, tenzij opslag van de Persoonsgegevens Unierechtelijk of lidstaatrechtelijk is verplicht.

13.4 Verwerker bevestigt op verzoek van Verwerkingsverantwoordelijke Schriftelijk dat Verwerker aan alle verplichtingen uit artikel 13.3 heeft voldaan.

13.5 Verwerker draagt de kosten voor vernietiging, retournering en/of overdracht van de Persoonsgegevens. Verwerkingsverantwoordelijke kan nadere eisen stellen aan de wijze van vernietiging, retournering en/of overdracht van de Persoonsgegevens, waaronder eisen aan het bestandsformaat.

13.6 Verplichtingen uit de Verwerkersovereenkomst die naar hun aard bestemd zijn om na beëindiging van de Verwerkersovereenkomst voort te duren, blijven na beëindiging van de Verwerkersovereenkomst voortduren.

14 TOEPASSELIJK RECHT EN GESCHILLENBESLECHTING

14.1 De Verwerkersovereenkomst en de uitvoering daarvan worden beheerst door Nederlands recht.

14.2 Alle geschillen, die tussen Partijen ontstaan in verband met de Verwerkersovereenkomst, zullen worden voorgelegd aan de bevoegde rechter in de plaats waar Verwerkingsverantwoordelijke gevestigd is.

<NAAM>
<FUNCTIE>
<LEVERANCIER>

<NAAM>
<FUNCTIE>
Technische Universiteit Delft

Paraaf :

Paraaf TUD:

Bijlage A: Specificatie Verwerking Persoonsgegevens

Over de Dienst van Verwerker wordt in deze Bijlage het volgende uiteengezet:

- Categorieën Betrokkenen
- De te verwerken (categorieën) Persoonsgegevens;
- Groepen medewerkers en hun verwerkingen;
- Bewaartermijnen;
- Getroffen beveiligingsmaatregelingen;
- Ingeschakelde hulpleveranciers;
- Contactgegevens.

Indien Verwerker meerdere separate diensten aanbiedt aan Verwerkingsverantwoordelijke, is het mogelijk de informatie op te nemen in separate Bijlage(n), welke als volgt genummerd worden: "Bijlage A1", "Bijlage A2", etc..

Deze Bijlagen worden aan de Verwerkersovereenkomst gehecht.

Bijlage A: Verwerking persoonlijke identificatiegegevens

Versienummer **001** Datum laatste aanpassing: **13-07-2021**

Omschrijving van de Verwerking
Bij de experimenten bij het afstudeeronderzoek van Jelle Haasnoot worden enkele persoonsgegevens een aantal maanden bewaard. Dit onderzoek omvat het ontwerpen en verifiëren van een nieuw testplatform voor fietssimulaties, waarbij zowel numerieke meetdata als subjectieve scores worden verzameld voor de vergelijking tussen binnen en buiten fietsen. Het gaat hier om de naam, telefoonnummer en e-mailadres. Tijdens het onderzoek wordt deze persoonlijke data gepseudonimiseerd, en wordt meetdata verzameld en gekoppeld aan een persoonsnummer. Na aflopen van de bewaartermijn wordt data geanonimiseerd. De persoonlijke gegevens zullen allèèn worden opgeslagen op het OneDrive systeem beschikbaar gesteld door de TU.

Doeleinden van de Verwerking *(in te vullen door Verwerkingsverantwoordelijke)*
De persoonsgegevens die worden opgeslagen zijn de naam, het telefoonnummer en het e-mailadres van de testpersoon, om contact met testpersonen na afronding van de experimenten mogelijk te maken. Het bedrijf en de afstudeerbegeleider hebben beide aangegeven geen interesse te hebben in de data na afronding van het onderzoek, dus de data wordt puur opgeslagen om contact op te nemen, mocht er iets mis zijn met de data, of toestemming nodig zijn voor andere verwerkingen.

Categorieen betrokkenen *(in te vullen door Verwerkingsverantwoordelijke)*
Persoonlijke identificatiegegevens; naam, telefoonnummer en e-mailadres.

Categorie Persoonsgegevens *(in te vullen door Verwerkingsverantwoordelijke)*	**Risicoklasse**	**Bewaartermijn**
Persoonlijke identificatiegegevens	**I**	3 maanden na afronding onderzoek

Frequentie verrichten van audit *(in te vullen door Verwerkingsverantwoordelijke)*
Gezien de korte bewaartermijn, geen.

Paraaf **:** Paraaf TUD:

Groepen functies/medewerkers en hun verwerkingen
(in te vullen door Verwerker)

Vermeld de categorieen Medewerkers (functierollen/functiegroepen) die toegang hebben tot Persoonsgegevens (categorieen) en vermeld welke verwerkingen zij ten aanzien van de Persoonsgegevens mogen uitvoeren en vanuit welk land die Verwerking plaats vindt.

Groep functies/medewerkers	Categorie Persoonsgegevens	Soort Verwerking	Land van Verwerking
Student	Persoonlijke identificatiegegevens	**Inzien, wijzigen**	Nederland
Daily supervisor (Arend L. Schwab, A.Schwab@tudelft.nl)	Persoonlijke identificatiegegevens	**Inzien (bij afwezigheid student)**	Nederland
Company supervisor (Jos Joffers, Jos.Joffers@garmin.com)	Persoonlijke identificatiegegevens	**Inzien (bij afwezigheid student)**	Nederland

Toestemming inzet Sub-verwerkers
(in te vullen door Verwerkingsverantwoordelijke, aankruisen wat van toepassing is)

Verwerkingsverantwoordelijke heeft Verwerker:
- □ Algemene toestemming gegeven voor het inschakelen van Sub-verwerkers.
- □ Specifieke toestemming gegeven voor het inschakelen van de hierna opgenomen Sub-verwerkers

Sub-verwerkers
(in te vullen door Verwerker)

Sub-verwerker die door Verwerker wordt ingeschakeld voor het Verwerken van Persoonsgegevens	(categorie) Persoonsgegevens die Sub-verwerker verwerkt	Soort Verwerking	Land van Verwerking	Vestigings-land Sub-verwerker
N.v.t.				

Toestemming Doorgifte
(in te vullen door Verwerkingsverantwoordelijke)

Verwerkingsverantwoordelijke heeft Verwerker:
- □ Specifieke toestemming gegeven voor de hierna opgenomen doorgiften aan derde landen of internationale organisaties

Paraaf **:** Paraaf TUD:

Doorgiften
(in te vullen door Verwerker)

Beschrijving doorgifte	Entiteit die de Persoonsgegevens doorgeeft + land	Entiteit die de Persoonsgegevens ontvangt + land	Doorgifte-mechanisme
N.v.t.			

Contactgegevens

Bij vragen over deze Bijlage en/of de geleverde Dienst, kan contact worden opgenomen met:

	Verwerkingsverantwoordelijke	Verwerker
Naam	Jelle Haasnoot	Jos Joffers
Functie	Student	Team Lead ME
E-mailadres	j.haasnoot@student.tudelft.nl	jos.joffers@garmin.com
Telefoonnummer	0613294929	0627531719

Voor het melden van een Inbreuk in verband met Persoonsgegevens in artikel 8 kan contact worden opgenomen met:

	Verwerkingsverantwoordelijke	Verwerker
Naam	Jelle Haasnoot	Jos Joffers
Functie	Student	Team Lead ME
E-mailadres	j.haasnoot@student.tudelft.nl	jos.joffers@garmin.com
Telefoonnummer	0613294929	0627531719

Bijlage B: Beveiligingsmaatregelen

Versienummer **001**, Datum laatste aanpassing: **09-06-2021**

Uitwerking van de door Verwerker getroffen beveiligingsmaatregelen *(in te vullen door Verwerker)*
De opgeslagen persoonsgegevens zijn alleen toegankelijk op de OneDrive locatie beschikbaar gesteld door de TU. Ook is het bestand versleuteld met een wachtwoord, wat alleen de student en de afstudeerbegeleiders (van TU en bedrijf) zullen hebben.

Certificaten waarover Verwerker beschikt:
(in te vullen door Verwerker)

Certificaten	**Organisatieonderdeel / dienst waarop certificaat betrekking heeft**	**Geldigheidsduur certificaat**	**Verklaring van toepasselijkheid**
N.v.t.			

Kwalificaties waaraan Verwerker voldoet: *(in te vullen door Verwerker)*
N.v.t. ?

Bijlage C: Melding Inbreuk in verband met Persoonsgegevens

Versienummer **001,** Datum laatste aanpassing: **09-06-2021**

Als Verwerker de Verwerkingsverantwoordelijke moet informeren op grond van artikel 6, zal zij de volgende gegevens moeten verschaffen:

Contactgegevens melder

Naam	
Functie	
E-mailadres	
Telefoonnummer	

Gegevens over het Datalek

Geef een samenvatting van het incident waarbij de inbreuk op de beveiliging van Persoonsgegevens zich heeft voorgedaan
Van hoeveel personen zijn Persoonsgegevens betrokken bij de inbreuk?
☐ Aantal: ☐ Minimaal: ☐ Maximaal:
Omschrijf de groep mensen van wie Persoonsgegevens zijn betrokken bij de inbreuk
Wanneer vond de inbreuk plaats? (Kies een van de opties en vul waar nodig aan)
☐ Op (datum): ☐ Tussen (begindatum periode) en (einddatum periode): ☐ Nog niet bekend
Wat is de aard van de inbreuk ? (U kunt meerdere mogelijkheden aankruisen)
☐ Lezen (vertrouwelijkheid) ☐ Kopieren ☐ Veranderen (integriteit) ☐ Verwijderen of vernietigen (beschikbaarheid) ☐ Diefstal ☐ Nog niet bekend

Paraaf **:** Paraaf TUD:

Om welke categorieen Persoonsgegevens gaat het? (U kunt meerder mogelijkheden aankruisen)
☐ Naam -, adres - en woonplaatsgegevens ☐ Telefoonnummers ☐ E - mailadressen of andere adressen voor elektronische communicatie ☐ Toegangs - of identificatiegegevens (bijvoorbeeld inlognaam/wachtwoord of klantnummer) ☐ Financiële gegevens (bijvoorbeeld rekeningnummer, creditcardnummer) ☐ Burgerservicenummer (BSN) of sofinummer ☐ Paspoortkopieën of kopieën van andere legitimatiebewijzen ☐ Geslacht, geboortedatum en/of leeftijd ☐ Bijzondere Persoonsgegevens (bijvoorbeeld ras, etniciteit, criminele gegevens, politieke overtuiging, vakbondslidmaatschap, religie, seksuele leven, medische gegevens) ☐ Overige gegevens, namelijk (vul aan):
Welke gevolgen kan de inbreuk hebben voor de persoonlijke levenssfeer van de betrokkenen? (U kunt meerdere mogelijkheden aankruisen)
☐ Stigmatisering of uitsluiting ☐ Schade aan de gezondheid ☐ Blootstelling aan (identiteits)fraude ☐ Blootstelling aan spam of phishing ☐ Anders, namelijk (vul aan):

Vervolgacties naar aanleiding van het Datalek

Welke technische en organisatorische maatregelen heeft uw organisatie getroffen om de inbreuk aan te pakken en om verdere inbreuken te voorkomen?

Technische beschermingsmaatregelen

Zijn de Persoonsgegevens versleuteld, gehasht of op een andere manier onbegrijpelijk of ontoegankelijk gemaakt voor onbevoegden? (Kies een van de volgende opties en vul waar nodig aan.)
☐ Ja ☐ Nee ☐ Deels, namelijk: (vul aan)
Als de Persoonsgegevens geheel of deels onbegrijpelijk of ontoegankelijk zijn gemaakt, op welke manier is dit dan gebeurd? (Beantwoord deze vraag als u bij de vorige vraag gekozen heeft voor optie a of optie c. Als u gebruik heeft gemaakt van encryptie, licht dan ook de wijze van versleutelen toe.)

Internationale aspecten

Heeft de inbreuk betrekking op personen in andere EU-landen? (Kies een van de volgende opties)
☐ Ja ☐ Nee ☐ Nog niet bekend

E.6 Device Safety & Mitigations Report

Kinematic Sway, Roll, Steer and Yaw Motion Verification of a Linear Actuator-Based Racing Bicycle Simulator

Risks & Mitigations Report

In this report, a description of the newly developed bicycle simulator for Jelle Haasnoot's graduation project is first described, after which risks, and accompanying mitigations of the device are discussed.

Origin and purpose

The device that is being discussed in this document has been designed for the purpose of investigating a new, freer and more involved method of using an indoor cycling simulator. Existing, static indoor cycling solutions have existed for several decades now and have been proven to be safe and secure so far. Below, some examples of existing solutions are given:

The newly designed indoor cycling trainer will add degrees of freedom in the roll, steer and yaw directions of the bicycle. This, in theory, provides the cyclist with the ability to balance and position the bicycle as he or she would during outdoor cycling. This in turn should provide a more realistic experience, as well as a more realistic transfer of power to the bicycle, increasing training efficiency and realism. Some solutions, which add this capability, also already exist and have been proven to be usable, although with more getting used to the limited motion and new training environment:

What this newly designed simulator will add is the ability to increase the resistance power the cyclist has to provide, as well as implement the ability to alter the device reaction profile in order to increase objective and subjective realism, compared to outdoor cycling.

Device description

The developed bicycle simulator is a device which electronically acts upon the inputs given by a cyclist, which uses it. The system (as designed now) is portrayed in the image below:

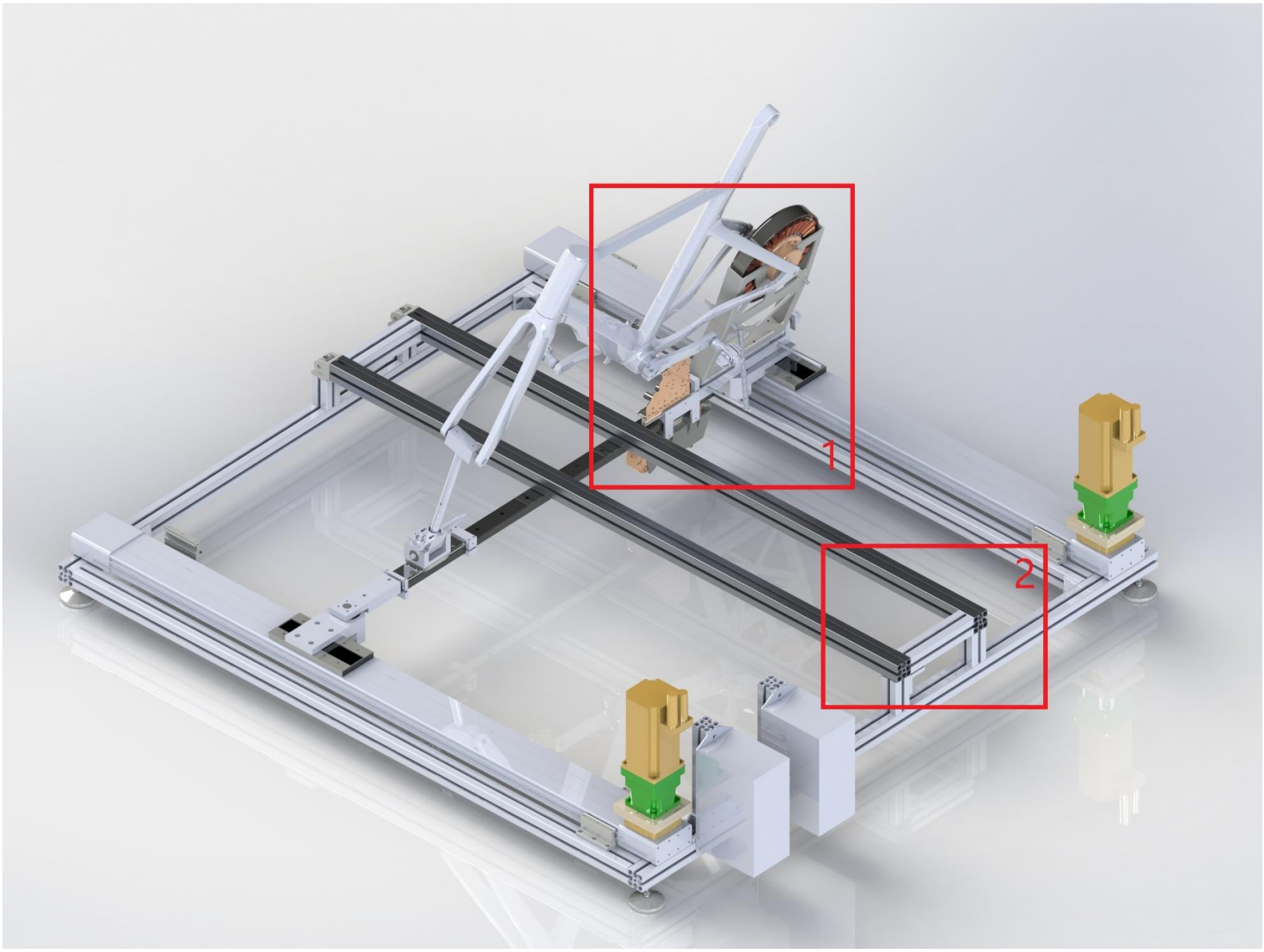

The system consists of two large electromechanical actuators, which are internally driven by a toothed belt and pulley system. Each of these actuators is capable of delivering a force in actuator direction of 1870 N (at standstill), and has the ability to move the positioner cart at max. $50\frac{m}{s^2}$ and $5\frac{m}{s}$. The actuators are provided as a completed and assembled system (more extensive data given further on in this document). The user of the bicycle is able to control the bicycle by rolling the bicycle as well as steering the bicycle steering wheel, of which the data will be recorded by potentiometer rotation sensors.

The realization of the system is visible in the image below:

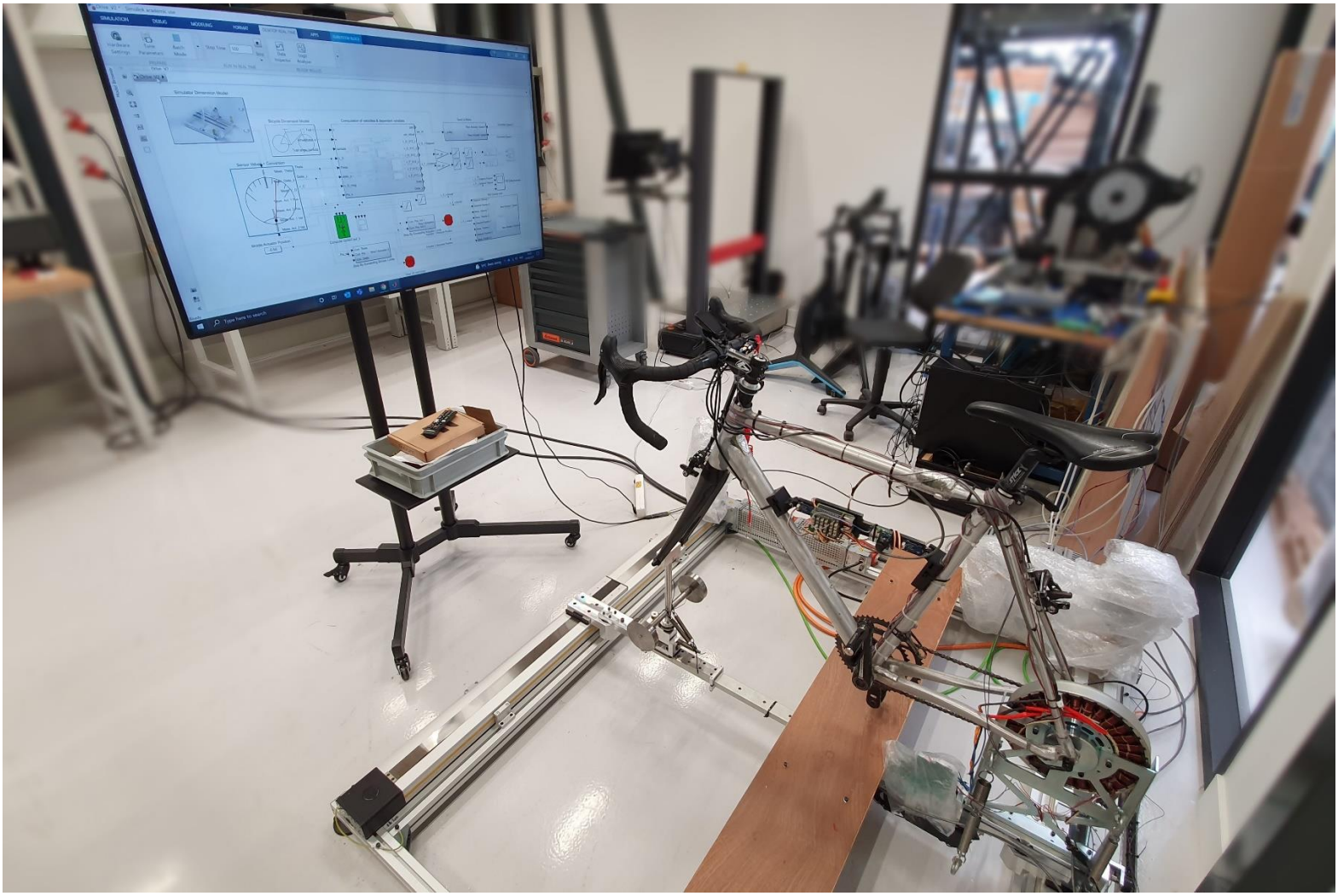

Where additional measures have been implemented to reduce the risk of injury, should the participant of the experiments fall of the bicycle. Unfortunately, not all (parts of the) elements of the device could be wrapped, due to overheating risks.

The test subject is able to put his foot down on the wooden plank, mounted to the set-velocity-0-button, described in closeup view 2 below.

All aluminium frame parts have been electronically connected, such that they are always grounded. The wires are visible in the bottom-left corner of the device, and are applied as such on every corner of the device. It has been verified that the frame parts are all connected electrically with a multimeter.

Closeup 1:

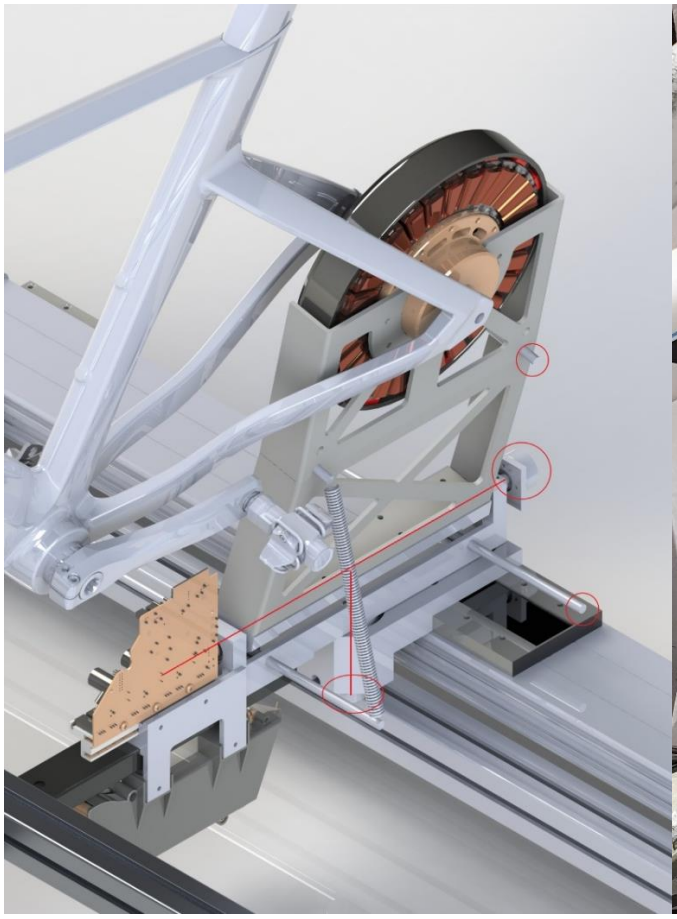

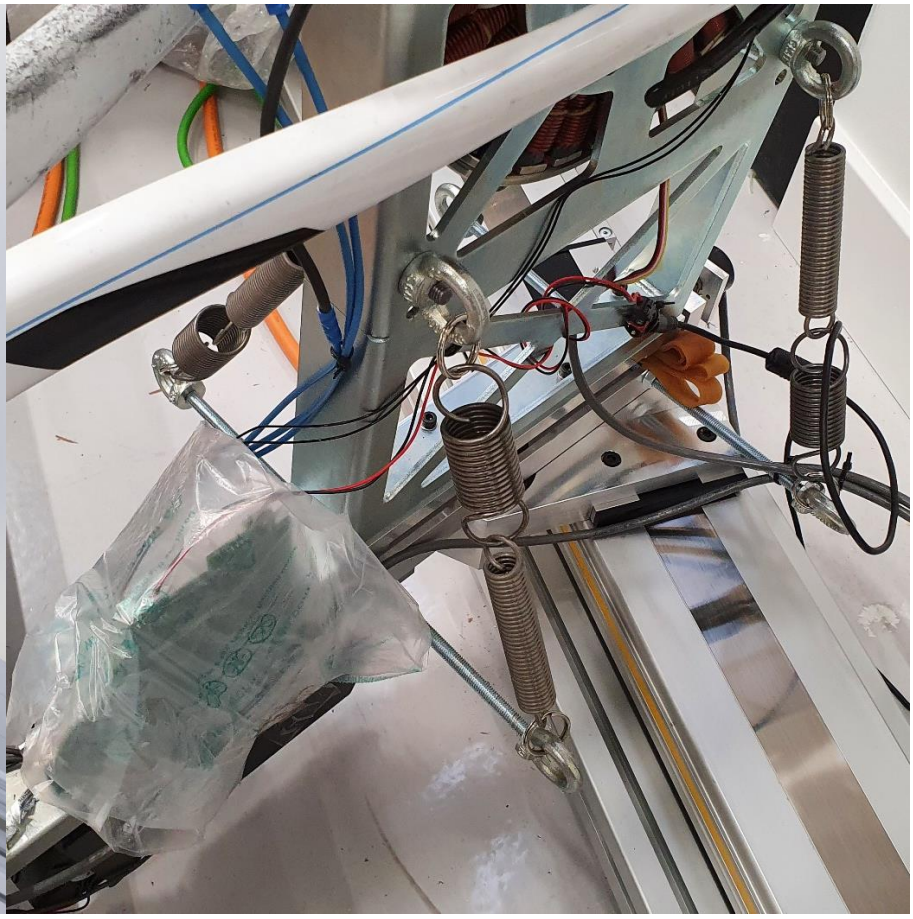

This closeup provides a more detailed overview of the rear of the system. Indicated are the roll and yaw axis, which are free degrees of freedom, as well as the roll and yaw potentiometer sensors. Two coiled springs are connected on both sides of the mounting plate, of which only one is shown for clarity. The mounting points of the other spring on this side of the system are indicated as well.

These springs increase stability of the system, compensate for the added weight of the electric motor, as well as aid the cyclist in keeping the bicycle upright. The springs can be replaced with stiffer ones, if necessary.

In between the mounting points of the rear axis of the bicycle, a disassembled Neo 2T braking motor is mounted. Accompanying this motor, the electronic control board, as well as the braking resistor are mounted in front of and below the rotating assembly. These have been covered by layers of plastic, to prevent electric shocks when touching the equipment (which will be advised to the participants NOT to do during the experiments).

The roll of the system is physically limited at 15 degrees from the vertical position, with plastic stopper blocks installed as indicated here on the right:

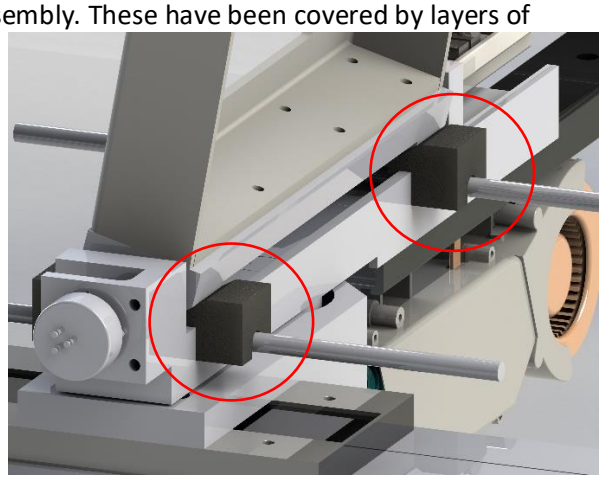

Closeup 2:

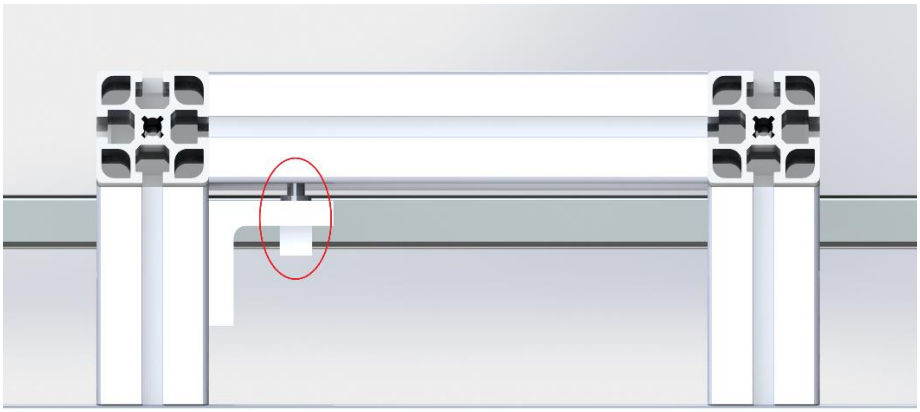

In this closeup, one of the safety features of this device is shown. It portrays an on/off switch which is deactivated when someone steps on the platform beneath the bicycle, triggering the Safe Torque Off feature built-in within the actuators.

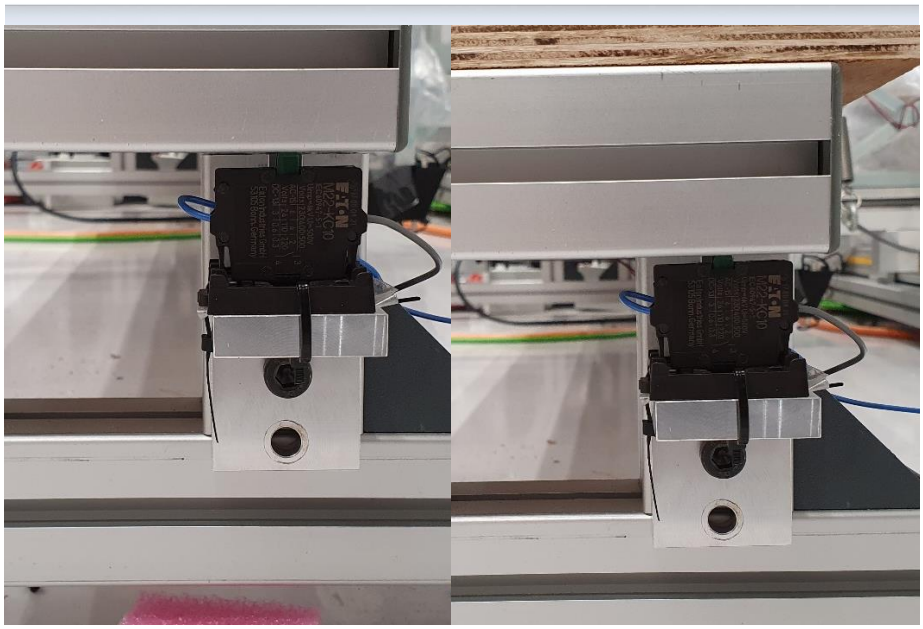

The realization of this system is visible here, where a switch is pressed in the right figure, and depressed in the left. The circuit is closed when the switch is pressed, thus setting both X12/10 inputs on 'high' (see next page). The switch type changed to "Normally-Closed", due to the way the halt-function works.

Control hierarchy and functions

In this section, an overview of the control scheme and its safety functions is presented. First on hardware level, then on software level.

The basic control scheme on hardware level will be as follows:

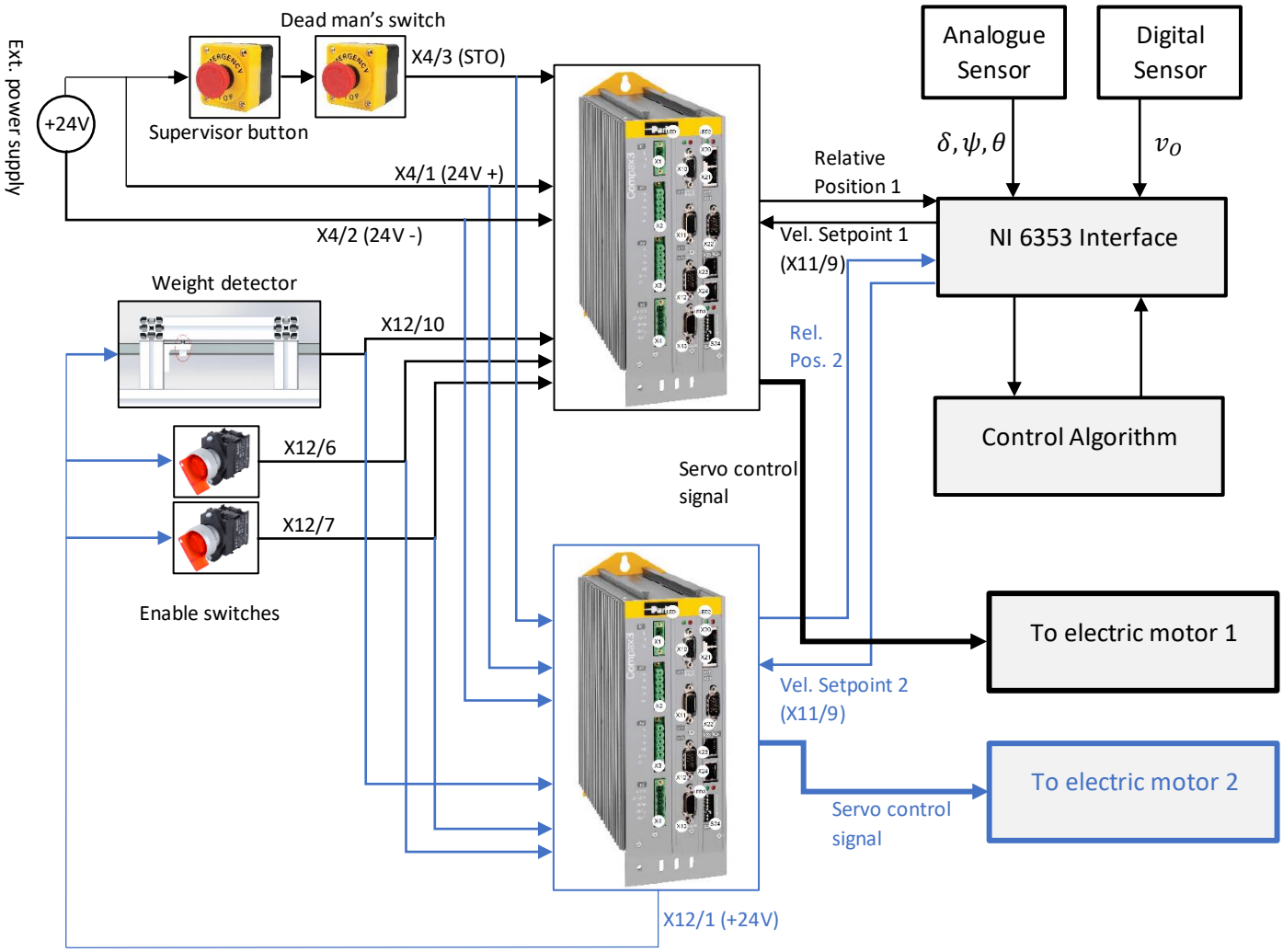

All relevant hardware components, and the main control algorithm outline, will be described in the section below.

Actuator data (2 units):

Additional information is supplemented in Parker Belt Driven Positioners.pdf

Model type: Parker OSPE32BHD

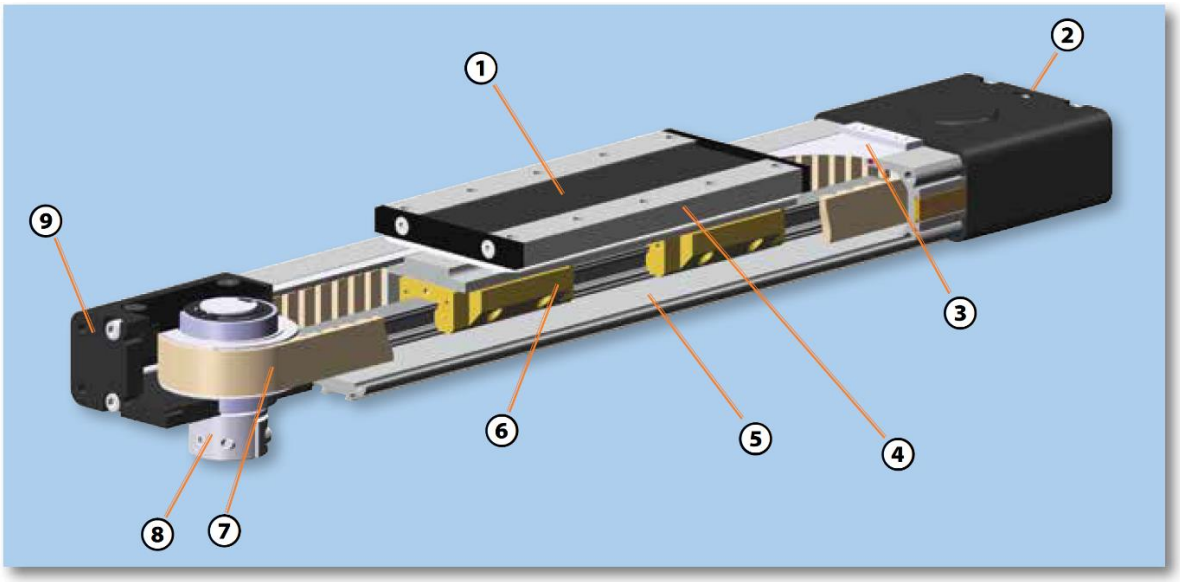

Internal works of the actuator. Belt-driven, ball-bearing cart with high stiffness in all directions.

Thrust capabilities:

Force-delivery in actuator direction, dependent on current velocity:

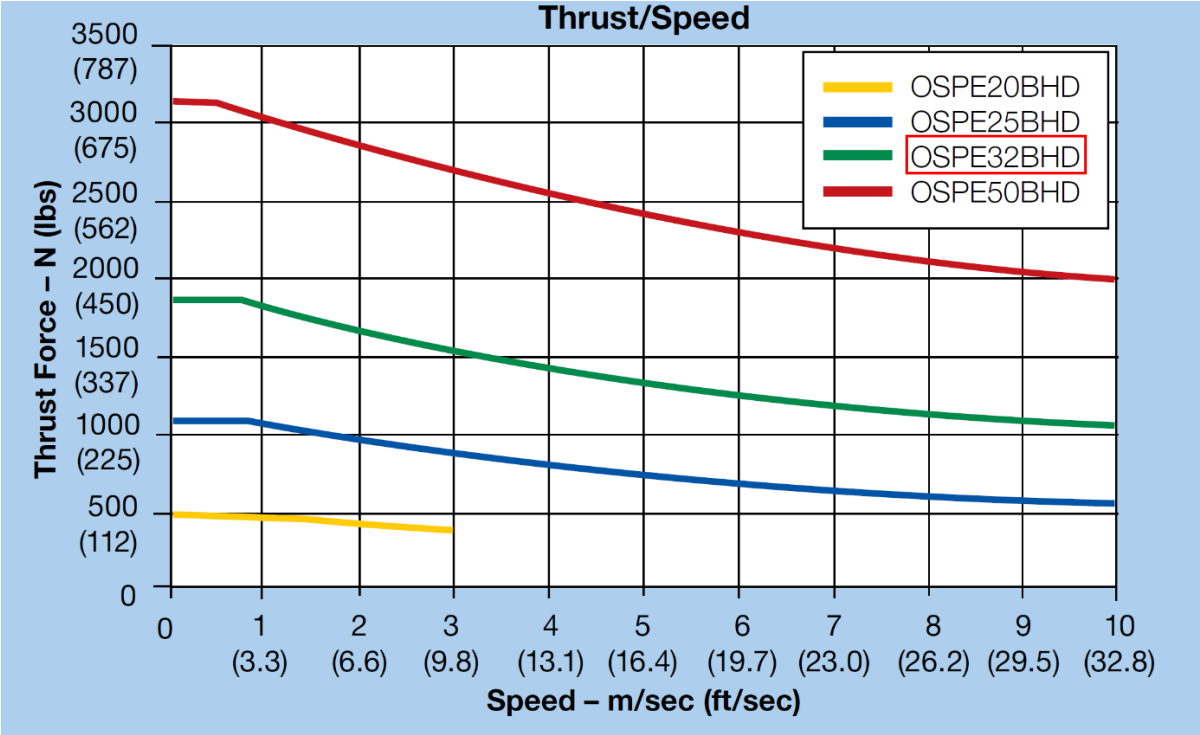

Max. acceleration	$\pm 50 \frac{m}{s^2}$
Max. velocity	$\pm 5 \frac{m}{s}$
Max. force	$F_x = 1850\ N$
Effective stroke	$1200\ mm$
Inertia (total)	$4540\ kgmm^2$
Belt drive radius	$0.0382\ m$

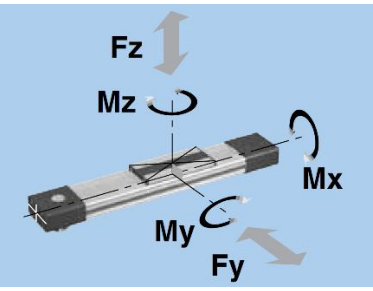

Other capabilities:

Max. load on cart, non-drive directions	$F_y = 5000\ N, F_z = 10{,}000\ N$
Max. moments on cart	$M_x = 120\ Nm, M_y = 1000\ Nm, M_z = 1400\ Nm$

Electric servomotor capabilities (2 units)

Model type: Parker SMH 100 56 06 519S2I64A64

Additional information is supplemented in 192_061013_SMB_SMH_Motoren.pdf

Relevant capabilities:

Stall torque	$6\ Nm$
Stall current	$5.9\ A$
Nominal torque	$2.5\ Nm$
Nominal speed	$5600\ tpm$
Nominal current	$2.4\ A$
Max. torque	$18\ Nm$

Due to the built-in gearbox in the actuators ($i = 1{:}\,8$), the maximum velocity and force that can be delivered to the actuator are changed to:

Stall torque	$42\ Nm$
Nominal torque	$20\ Nm$
Nominal speed	$700\ tpm$
Max. torque	$144\ Nm$

Such that the linear capabilities of the actuators themselves change to the following, with limitiations set in the motor controllers at:

Max. velocity	$\pm 2.8002\ \frac{m}{s}$, limited at $\pm 2 \frac{m}{s}$ in drive configuration
Max. acceleration	Limited at $10 \frac{m}{s^2}$ in control algorithm
Max. force	$F_x = 3770\ N$, limited at $942\ N$ in drive configuration

The maximum current to the motors already has to be limited to at least 50% of its max. current (at standstill), such that the force transferred to the actuator doesn't surpass the max. allowed force on the actuator. This is possible in the configuration of the motor controllers. It is limited to even less, to prevent the actuators to apply their max. force to the setup and increase pinching risks. If the device does not act as required with these limits, they are gradually increased if necessary.

Controller/frequency inverter (2 units):

Model type: Parker Compax3S C3 S075 V4 F10 I10 M00

Selected for the ability to control axis velocity based on analog signal. This enables full configuration of closed-loop response of actuators. Positional feedback signal is received through an encoder simulation, which produces A, A/, B, B/, N and N/ square-wave signals at a certain configurable resolution, which limits the max. measurable velocity of one actuator.

Additional information is supplemented in 192_120013_Compax3_Catalog.pdf

Relevant properties:

Max. cont. current delivery	$7.5\ A$
Max. peak current delivery (<5s)	$15\ A$
Power (each)	$6.2\ kVA$
Safe-Torque-Off (STO) functions	2, max. 3 ms reaction time
Setpoint voltage scan frequency	$8\ kHz$
Setpoint voltage resolution	+/- 10V, 14-bit
Encoder simulation resolution	User-configurable

Internal control model of frequency inverter:

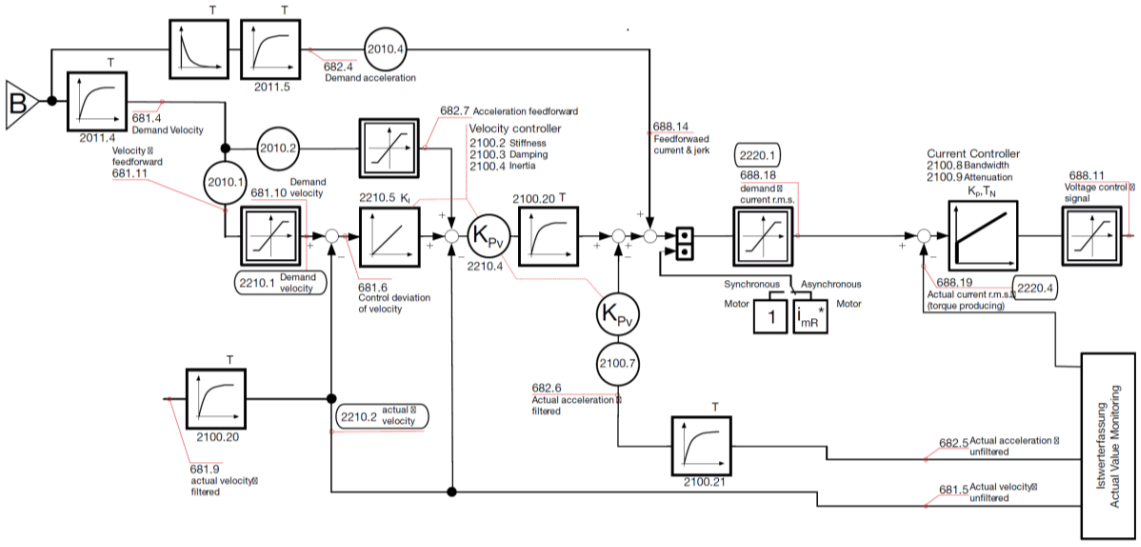

With configurable gains and filtering properties on how to react to input velocity signal. Configuration is possible through RS-232 connection to PC, with software delivered with frequency inverter.

The main safety function of both frequency controllers is based on the inputs in their X4-plug. The third input of that plug (X4/3) is used for enabling the power supply to the drive. If no +24V voltage is present on X4/3, the drives cannot start up. Furthermore, whilst already in operation, when the +24V signal is removed from X4/3, both drives will disengage and come to an effective standstill. In-between the 24V supply voltage and the X4/3 inputs on both frequency inverters, both safety switches will be placed in series. If one of them is interrupted (either the Dead Man's switch or the

emergency stop button), both drives will stop immediately. Manual acknowledgement of the emergency stop, or a complete restart of the system is then necessary to re-engage the drives.

In addition to two safety functions (STO), two high digital input signals are required to set the motors in motion:

X12/6	Energize motor, deactivate motor holding brake
X12/7	Enable setpoint value (given by analogue input)

Which are all connected to rotary independent on/off switches, which are split and applied to the corresponding inputs of both frequency inverters. An additional digital input is used (X12/10) on both devices, which is connected to the weight-detector. This digital input tells the drives to keep their current position and set the speed of the actuator 0. The response to an already moving system will have to be evaluated; if response times or decelerations are unsatisfactory, the weight-detector switch will also function as an interruptor in the STO-circuit.

All sensor signal cables (in the least the analogue ones) are shielded to reduce EMF- and other noise influences.

Hardware interface/control signal generation:

Model type: National Instruments PCIe 6353

Selected for high number of digital in/outputs, as well as analogue inputs and outputs.

Input-output capabilities:

Number of analogue inputs	16 differential, 32 single-ended
Analogue input resolution/sampling rate (max.)	16-bit/1 MS/s (multichannel, aggregate)
Number of analogue outputs	4
Analogue output resolution/frequency (max.)	16-bit/1.25 MS/s (when 4 channels in use)
Digital in/outputs	48 total, of which 16 are PFI-lines
Counter inputs	4

This board is Matlab – Simulink Desktop Real Time compatible, which enables the use of Simulink for the control scheme of the system. This PCIe expansion card will be used on a Dell Precision 5820 workstation, equipped with an Intel Core i9-10920X 12-core CPU, and 128 GB of system memory.

Matlab/Simulink Control Algorithm + safety functions.

In general, the control scheme will look like this (sub-functions excluded):

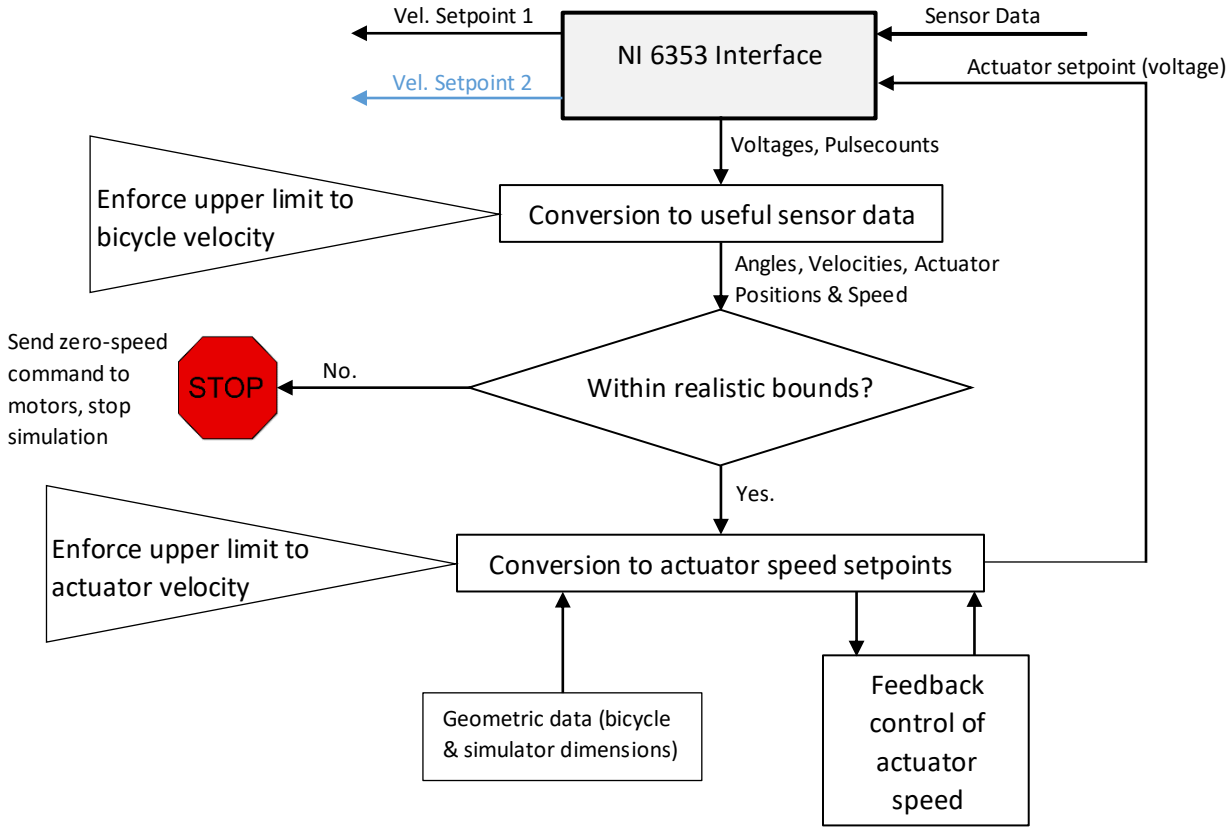

In practice, the control system will look like the control system on the next page (turned clockwise).

This snapshot still includes the feedback of already measured values back to the input, since the system has not been completed yet, so simulated data must be used to test the control algorithm.

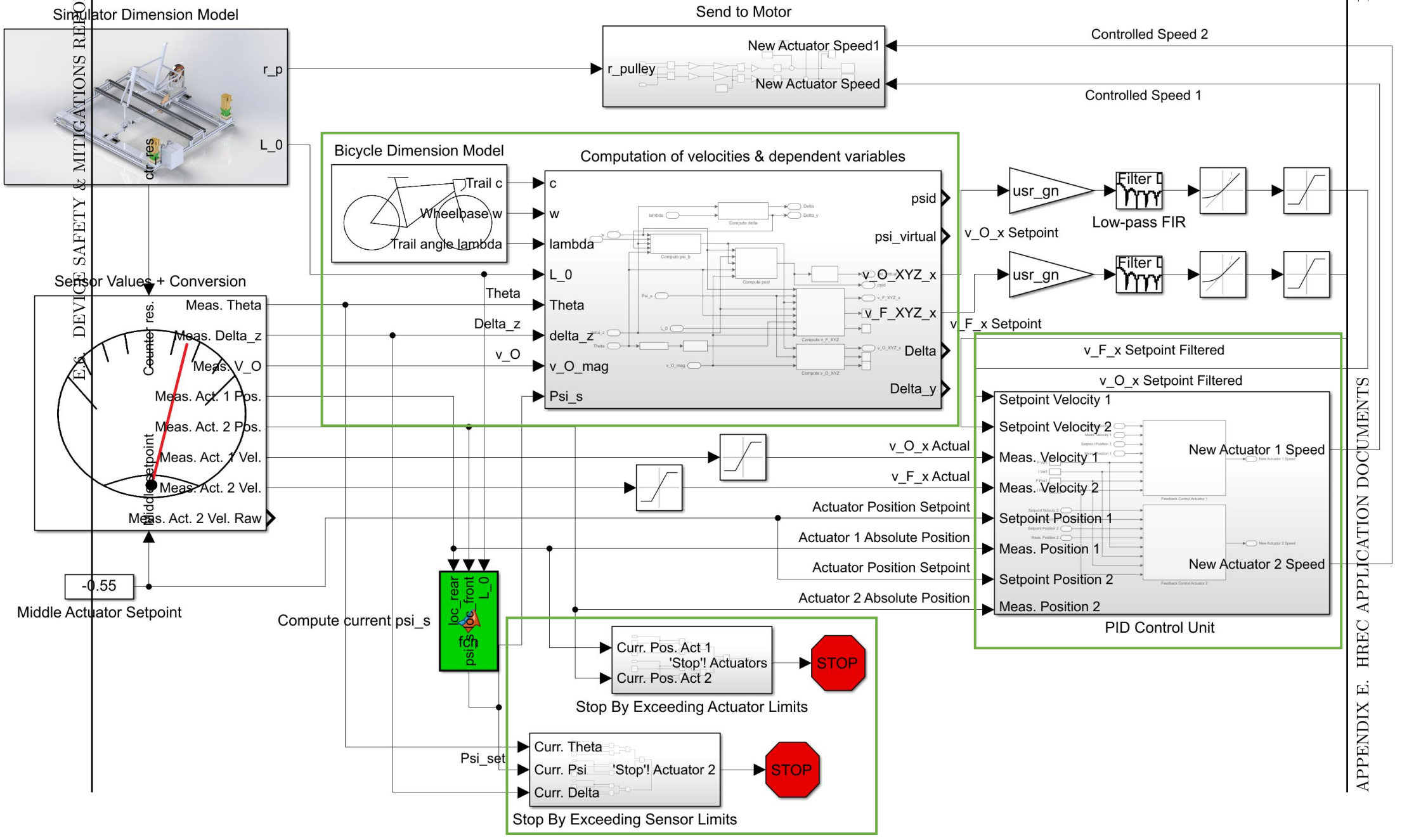
Simulator Dimension Model
r_p
L_0
ctr_res
Send to Motor
r_pulley
New Actuator Speed1
New Actuator Speed
Controlled Speed 2
Controlled Speed 1
Bicycle Dimension Model
Trail c
Wheelbase w
Trail angle lambda
Computation of velocities & dependent variables
c
w
lambda
L_0
Theta
delta_z
v_O_mag
Psi_s
psid
psi_virtual
v_O_XYZ_x
v_F_XYZ_x
Delta
Delta_y
usr_gn
Filter D
Low-pass FIR
v_O_x Setpoint
v_F_x Setpoint
Sensor Values + Conversion
Meas. Theta
Meas. Delta_z
Meas. V_O
Meas. Act. 1 Pos.
Meas. Act. 2 Pos.
Meas. Act. 1 Vel.
Meas. Act. 2 Vel.
Meas. Act. 2 Vel. Raw
Counter res.
Middle Setpoint
Theta
Delta_z
v_O
-0.55
Middle Actuator Setpoint
Compute current psi_s
loc_rear
loc_front
L_0
psi_s
v_F_x Setpoint Filtered
v_O_x Setpoint Filtered
v_O_x Actual
v_F_x Actual
Actuator Position Setpoint
Actuator 1 Absolute Position
Actuator Position Setpoint
Actuator 2 Absolute Position
Setpoint Velocity 1
Setpoint Velocity 2
Meas. Velocity 1
Meas. Velocity 2
Setpoint Position 1
Meas. Position 1
Setpoint Position 2
Meas. Position 2
New Actuator 1 Speed
New Actuator 2 Speed
PID Control Unit
Curr. Pos. Act 1
'Stop'! Actuators
Curr. Pos. Act 2
STOP
Stop By Exceeding Actuator Limits
Psi_set
Curr. Theta
Curr. Psi
'Stop'! Actuator 2
Curr. Delta
STOP
Stop By Exceeding Sensor Limits

The important safety blocks are indicated with green squares. These are the following:

- At the bottom of the control system, from left to right, there are two safety features which set the motors to standstill and stop the system from running. These are triggered when any of the sensor values for the roll, yaw or steer angle of the bicycle (left block) or the linear position of the actuator cart (right block) exceed the limits set to the specific value. Zero or saturated voltage are out of these limits, so when a sensor loses connection or shorts, the system is stopped. The limits, which can be changed when they appear to strict, or too loose are the following:

$-11.5° < \theta < 11.5°$ (the setup is physically limited in its roll freedom at $\pm 15°$)
$-45° < \psi < 45°$
$-45° < \delta < 45°$
Position rear actuator $-0.55 < x_O < 0.55$ w.r.t. actuator center.
Position front actuator $-0.55 < x_F < 0.55$ w.r.t. actuator center.

  These limits refer to the deviation of the zero-position, which is the bicycle pointing straight forward, fully upright, with the steering wheel aligned parallel with the bicycle frame.

- From the center block, the setpoints of the velocity of both the front (v_F_x) and rear (v_O_x) are computed from the vehicle model. These are limited with saturation blocks to not exceed realistic values. The limit for all velocities are now set to $1.4\frac{m}{s}$. In front of each saturation block, there is a rate limiter block, which limits the acceleration of all velocity setpoints to $10\frac{m}{s^2}$.

- The bottom-right block indicates the digital controller section of the control algorithm. Using a PID-controller, the current velocity of the setup is compared to the velocity setpoint, after which a control signal is created based on the error between the two. This controller should eliminate, or at least minimize, dynamics introduced to the system due to the physical control hardware. If this controller is not sufficient, the internal controller values of the Compax3S units are also changed to what the control system requires (more/less aggressive behavior, etc.).

The sensor value for the velocity the bicycle is virtually travelling at, by measuring the rear wheel velocity of the disassembled trainer, is also limited with a saturation block within the *Sensor Values + Conversion* block.

All saturation and emergency stops have been tested with pre-recorded data, and function as intended. Once the system is complete, the real-world effects of these safety features will have to be verified, by intentionally triggering the safety functions.

Risks, possible causes and mitigations per category

In the following section, the foreseeable risks presented to the user and bystanders of the device will be described. For each risk, one or multiple mitigation methods are presented.

Risk: falling off/capsizing the bicycle

The greatest risk of bringing harm to the user of the simulator is the one where the user falls off the bicycle. This can have a number of causes:

Unpredictable reaction of the control algorithm

The algorithm controlling the setup has a number of components in them. In a logical order, these are sensor signal → control algorithm → control signal → conversion to actuator speed. Any of these components can behave incorrectly due to outside factors.

Mitigation steps in this control sequence are the following:

- Rotation sensors have to produce a realistic value for it to be accepted by the control system. For example, the available rotation range for the yaw sensor is -45 to 45 degrees, offset from the middle of the mechanical angle of the potentiometer. If the sensor loses connection, it will produce a zero-angle value, which the control algorithm will detect and ignore, and the system is stopped. If the sensor's connection is completely lost, this will result in control unresponsiveness, and the system is stopped.

  All sensor signals are routed with shielded cables, to minimize electromagnetically induced signal noise.

- The control algorithm limits the maximum output that can be given as a control signal. The control algorithm will output an actuator velocity control signal, which is limited to a maximum velocity and acceleration, determined from pilot measurements.

  In addition to that, a low-pass filter is applied to the output control signal (before the *PID Control Unit* block), such that sudden movements, as well as input signal noise, are not propagated to the output signal of the system.

Unpredictable behavior of the human subject

The user of the system can, within the correct functioning of the control algorithm, still with or without intention drive the system into dangerous situations. The user may still need to get used to the system control behavior, as well as the unusual environment in which he is using a bicycle.

Mitigation steps in the unpredictable behavior of the cyclist are the following:

- The user of the setup is notified of the risks of using an unusual system as this before using it. He is made attentive of the safety features the device has, and how they are used. The user is instructed not to intentionally test the capabilities of the system, but stay within the confines of the experiment.

- The user is allowed a short while (15 minutes) of free cycling on the simulator, to get used to its behavior. He is also instructed to not use his clip pedals, but step loosely on the pedals of the bicycle, so he can use his legs to stabilize himself if the bicycle still reacts unpredictably.

- A mechanical stop (damper, secondary spring) is in place, which limits the roll angle of the system to a certain degree, determined in pilot experiments, as well as measurements from outdoor cycling.

- The participant is able to put his foot down to enable the zero-velocity setpoint (X12/10 on the control hardware), making the system stop. This is not an emergency stop, to prevent the system requiring a full restart after the cyclist just touching the board. However, if from experiments it proves necessary to make this function into a emergency shutoff function, the button will be placed in series with the emergency switches.

Should the cyclist fall of the simulator, in spite of all these mitigations, he is obligated to wear a cycling helmet at all times. The cyclist will wear a tethered dead-man's switch, which also triggers a safe-torque-off function when it is torn from its socket. In addition to that, the experiment supervisor stands by an emergency switch, which triggers an emergency stop of the system.

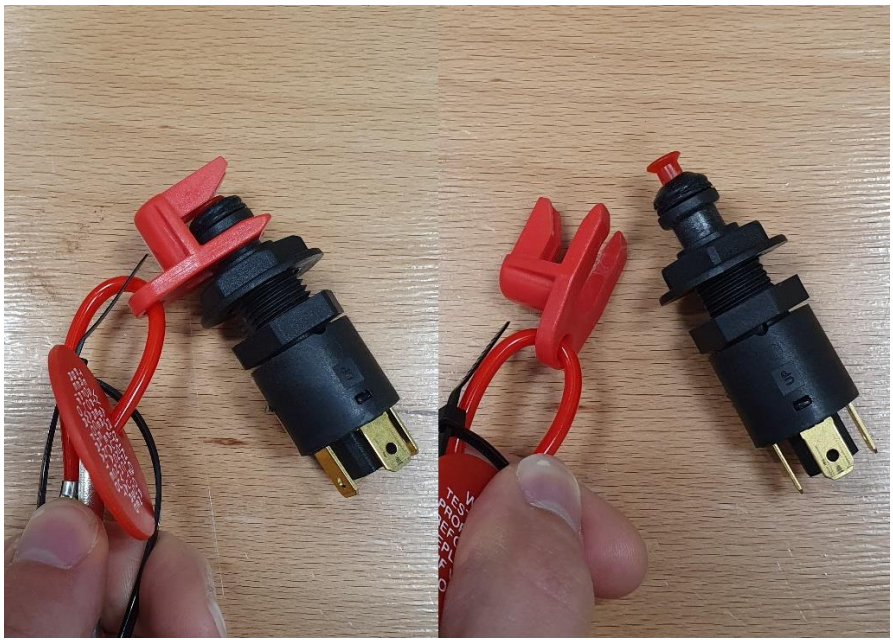

Verification steps for mitigations:

For the risk of falling of the device, the verification steps of the safety features are the following:

- Intentionally try to destabilize the device when the proposed safety features are in place.
- Intentionally try to surpass the force, velocity and acceleration limits built into the control algorithm.

Risk: Pinching of body parts between moving mechanical parts

When the device is not in use, and starts moving its mechanical parts nonetheless, the risk exists that someone gets his body parts caught between two parts in a pinching movement.

Mitigation steps with this risk are the following:

- The device cannot start moving when the dead-man's switch is not connected. Either the user or the mechanic working on the device has to wear the switch when near the device. So when not applied, the machine cannot start moving.

- The actuators are limited through software to always leave a gap between components (for example, between the rear electric motor and the rear of the bicycle construction). This limit can be enabled in the control algorithm based on the absolute encoder values, transmitted through the frequency controllers of the electric motors.

- When the device is in use, the user is instructed to only step on the platform beneath the bicycle (with the second interrupt switch connected to it), such that his legs do not come near the moving parts, should they still be moving.

- The experiment supervisor stands ready with the emergency stop button, should a dangerous situation still present itself.

- Bystanders are instructed to stay away from the device, and not step over indicative yellow tape on the floor, indicating a safe zone for the device.

- The actuators are current-limited, such that they cannot provide their max. force. This limit is set to $700\ mA$ per actuator, and will have to be verified to be sufficient to still let the actuators function as required.

Verification steps for mitigation steps:

- Measure smallest gaps when the system is in its extremes, put there by the control algorithm. These should largely exceed common leg and ankle dimensions.

Risk: Sharp edges

The device has custom-made parts in it. This means that potentially, one of these parts could have unfinished edges on them.

Mitigation steps with this risk are the following:

- The parts the user of the setup can (intentionally) come into contact with, have rounded edges (as for example in the platform beneath the bicycle, which is constructed from aluminium profiling with rounded edges).

- All custom-made parts are inspected before assembly, deburring and breaking sharp edges if they still exist.

Verification steps for mitigation steps:

- Inspection by multiple persons in trying to find sharp edges

Risk: Electric shock or malfunctioning

The device runs on high voltage, and has a number of sensors which run low-voltage wires. These introduce the risk for electric shock. In addition to that, the disassembled indoor trainer (Neo 2T) introduces a number of exposed electrical components, which give the risk of electric shock when touched.

Mitigation steps with this risk are the following:

- The actuator set, which run on high voltage, are CE-certified. We can assume these are safe when used correctly. Installation is supervised and checked by a qualified electrical engineer, especially the high-voltage lines.

- The frame and other interconnected, conducting components are grounded through the frame using the 380VAC ground line.

- The Neo 2T components are out of reach for the cyclist when the device is in use, and the user and bystanders are instructed not to touch these components. The components themselves are grounded via the support frame. The Neo 2T control board will be covered by a piece of plastic, to prevent access to electronic components.
- The user and bystanders are instructed not to touch any components when the device is in use, apart from the safety features. This is also verified in the Informed Consent form.

- A fire extinguisher is always at hand during experiments.

Verification steps for mitigation steps:

- Try to find remaining charges by measuring voltages across commonly touched parts on the setup, and a common ground while the system is on. If no voltages are found on conducting parts, the system passes.

Risk: High touch temperature

The device includes components that produce heat when used intensively. These can be hot to the touch, and cause pain or discomfort.

Mitigation steps with this risk are the following:

- The electric motors for the linear actuator have warning signs on them, warning the user for hot components.

- The disassembled indoor trainer is sold normally with an exposed metal disk, which can be hot to the touch, but doesn't surpass the prescribed temperature limits.

- The user and bystanders are instructed not to touch any components when the device is in use, apart from the safety features.

Verification steps for mitigation steps:

- Check whether surfaces remain below acceptable touch temperatures during extensive use of the device.
- Always let the user of the simulator only use the installed floorboard to step on, such that the pinching risk is minimized.

Risk: physical fatigue and exertion

The device is designed to let the user apply a high power, which is also part of the experiments. This could result in fatigue and discomfort of the user.

Mitigation steps with this risk are the following:

- The user of the device can quit the experiment any time he or she wants, without having to give a reason for it.

Verification steps for mitigation steps:

- Since fatigue and heavy exertion is part of the process, it only need to be checked whether the level of exertion remains acceptable. I.e. what one would expect during outdoor cycling.

Risk: motion sickness

Since this device involves a moving platform with the usual other sensory cues for cycling (wind, noise, moving visual environment, increased stress levels, among others), users are at an increased risk of experiencing motion sickness. This is unfortunately inherent to moving simulators, and one person can be affected more than the other.

Mitigation steps with this risk are the following:

- The user of the device can quit the experiment any time he or she wants, without having to give a reason for it.

- The user is repeatedly questioned about his or her experience on the bicycle. If he or she indicates the simulator is causing discomfort to the extent continuing or focusing on the experiment becomes difficult, the control algorithm can be altered to reduce the motion strength (although this is a last resort, since it was designed for realism).

Verification steps for mitigation steps:

- Motion sickness levels differ from person to person. A certain level of it is acceptable, but if no participant is able to finish experiments, the control algorithm will have to be altered. This can be verified in early trials.

Verification steps of safety procedures and mitigation steps.

For the discussed risks, certain mitigation steps are proposed. The steps which can be verified to be working, will be verified to be working before performing any experiments. The results of these tests are delivered to the Ethics Committee when required.

At the time of writing this report, the device is not yet fabricated. However, the mitigation steps described in this report are intended to be built into the device once it is being assembled, and as stated above, fully tested before allowing experiments to take place.

Appendix F

Literature Study

Delft University of Technology

Literature Survey
ME56010

Human Motion Perception in Vehicle Simulators: An Introductory Review

Authors:
Jelle Haasnoot (4473639)

July 28, 2021

Starting date: August 18th, 2020

MSc Thesis Advisors: Dr.ir. Arend L. Schwab
Dr.ir. Riender Happee
Professor: Dr.ir. Volkert van der Wijk
Company Supervisor: Martin Smits

Abstract

In this literature review, we study the question of how humans perceive motion in vehicle simulators. An overview of human motion perception mechanisms is provided, as well as a short introduction to human motion perception in real-world driving. Humans perceive motion across vehicle simulators dependent on two main factors: (1) How, and through which motion sensors the intended motion is presented to them and (2) what the level of involvement and type of task in the simulator is. Literature suggests strategies like application of washout filters and tilt coordination to influence the effectiveness of motion cueing, but also suggests a significant influence of involvement on motion perception, where boundary conditions like visual fidelity, as well as subjective differences affect motion perception and performance in vehicle simulators as well. Further research is required for an increase in perceived motion accuracy, through motion algorithms and validation, more added motion cues, experiments on active involvement and subjective preconditions.

Acknowledgements

I would like to thank Ksander de Winkel for his feedback and sincere interest in the creation of a complete overview of literature on the topic of human motion perception, Bernard Westerhof for providing his knowledge of applied motion perception in a motorcycle simulator, and Dr.ir. Riender Happee for his time and feedback as well. I would like to thank Marco Grottoli for sharing his personal experiences, as well. And last but not least, Dr.ir. Arend L. Schwab and Dr.ir. Riender Happee for their enthusiasm and constructive support.

Contents

List of Figures

Summary

Vehicle simulators have been a prevalent method of performing research in on human behaviour in simulators, to develop and transfer skills to trainees of vehicle drivers, and study new vehicles within a safe, grounded and controllable environment. One variable within vehicle simulators is the human, and his/her perception of the movement introduced to the motion platform. With an incentive from Tacx, an indoor bicycle trainer producer, this literature study was conducted on the topic of human motion perception in vehicle simulators, where the main research question to be answered is: *How is motion perceived by humans across vehicle simulators?* This literature review provides a constructive overview of how humans perceive motion in general, with an introduction to the human sensory system and how it is used and stimulated in a vehicle simulator environment.

Humans perceive motion through sensors mainly categorised into two main motion sensor systems: visual and inertial (vestibular and proprioceptive sensors), with a third category containing miscellaneous motion sensors (auditory, somatosensory and efference copy). Each motion sensor has its own individual detection threshold and dynamic response, and are combined with a variable weighting, depending on past experience and sensor source. In real-world driving, humans seem to depend mostly on optical cues for velocity and heading estimation.

From literature, it appears that humans perceive motion in vehicle simulators mainly based on two factors; how the intended motion is cued to them, and what the level of involvement and type of task is, in a particular vehicle simulator. On the first subject, there are some wide-applied methods of making use of a simulator's limited motion range and the human motion perception system to simulate sustained movements, while in fact remaining stationary. These are, mainly: the use of washout algorithms, where low-frequency content (i.e. slow accelerations, constant velocities) of an intended motion is removed and return-to-zero algorithms are used, below the human's motion perception thresholds. A second method is the use of tilt coordination, where humans are tilted physically to stimulate the vestibular system with gravity to feign constant linear acceleration - although limitations apply due to the properties of the same vestibular system. The mentioned methods are typically applied to most vehicle simulator types (automobile, motorcycle, aeroplane).

The level of involvement and type of motion task have been proven to influence motion perception thresholds, as well as simulator sickness and immersion levels in the vehicle simulator. The extent to which active involvement qualitatively affects motion perception, is a research branch where the effects could be studied more in the future, as well as in more vehicle simulator types. Great care must be taken when designing the visual cueing system in a vehicle simulator, since this can significantly affect the perception of motion, but also quality of experience and performance in vehicle simulators.

List of Definitions

In this report, the convention for the terminology of movements of the human person and the vehicle are the same as they usually are in ship motion: roll, pitch and yaw for rotations and heave, surge and sway for translations. See Figure 1 for a visualisation:

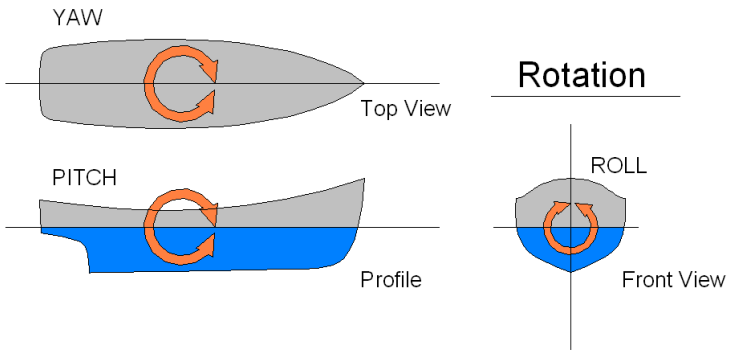

(a) Rotational definitions

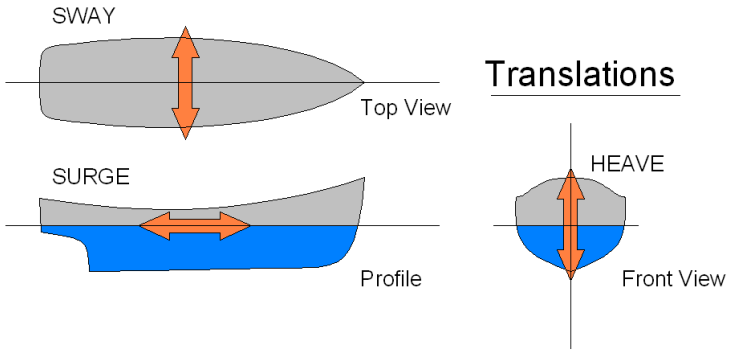

(b) Translational definitions

Figure 1: Rotational and translational definitions. Image source: Jmvolc (2006)

Introduction

Vehicle simulators become more and more prevalent in many societal developments. They are used for research on several modalities, including the development of new vehicles, studying human behaviour within them and training vehicle operators in a safe, grounded and controllable environment.

For the Delft University of Technology (TU Delft), one of the topics of interest considering vehicle simulators is how humans perceive motion within them. Intuitively, human motion perception appears to be a very subjective topic, since every person is unique. Academic staff at the TU Delft, Dr.ir. Arend L. Schwab in particular, are very interested in the mechanisms of human motion perception in vehicle simulators. Therefore, the main research question we will try to answer in this literature review is the following: *How is motion perceived by humans across vehicle simulators?*. Consequently, the title of this literature review is:

Human motion perception in vehicle simulators.

This literature review has come to be because of my affiliation with Tacx B.V., and their ever-expanding search for bicycle simulator realism. Coinciding with my graduating year on the TU Delft, we constructed a MSc thesis assignment for the development of a racing bicycle simulator with lateral freedom of motion.

In order to provide a constructive overview of human motion perception in vehicle simulators, and provide background knowledge on the topic of human motion perception in general, the layout of this literature review is the following:

First of all, human motion perception. In section 1.1, the physical mechanisms of motion perception are introduced and covered in their functional sense. Following that, methods of combining and weighting of the signals from these different sensors for the perception of motion are discussed in section 1.2. The applied use of the motion sensory system in vehicles is reviewed in section 1.3, with additional mechanisms of motion perception prevalent in vehicles.

When we understand how this perception of movement works in reality, we need to understand how that translates to simulator environments. How is motion perceived in vehicle simulators? This will be discussed by category of vehicle simulator in section 2.1. Since real vehicles are translated into (simplified) models applied in virtual reality, there are certain boundary conditions for the accurate, but also comfortable and immersive experience in vehicle simulators. Disruptive and influential properties of vehicle simulators will be discussed in section 2.2. Due to the length of this literature review, chapters 1 & 2 will be summarised in the final section of the respective chapters. These are recommended for fast readers with little time.

Finally, an overview is given of the collected information, and several knowledge gaps on the topic of human motion perception in vehicles will be pointed out. This will be done in chapter 3.

Chapter 1

Perception of Movement

In order to understand how motion perception of humans works in vehicle simulators, we will first review how motion perception works in humans, in the real world. To fulfill this knowledge, we need to look into the sensory systems of the human being. What sensors are there to perceive motion, and how do these combine into a logical signal to the brain which translates the stream of information into the actual perception of motion?

While we, engineers, like to describe every process of data conversion from input to output through simple, all-covering models, that is beyond the scope of this literature review. Many studies cover the modelled responses of individual, and even integrated motion sensors in the human body (see Valente Pais (2013), Nash et al. (2016) or Wendel (2019) for overviews of literature on modelled descriptions of the to-be-discussed motion sensors) but we will discuss the motion sensors as they are and function, and we will not try to describe them as modelled blocks. What is also beyond the scope of this review is the neurological process that goes on beyond the perception of motion, unless it is relevant for the topic at hand. Many sources exist which provide reviews on these neurological processes, including DeAngelis and Angelaki (2012) and Britton and Arshad (2019). We will view the motion perception mechanisms as black-box processes, which convert a certain stimulus into a certain perceived displacement, rotation, acceleration or other quantifiable result.

Methods of motion perception will be discussed in section 1.1, as a function of stimulus type (inertial, visual, or other) and where necessary, subdivided in different motion perception sensors for the same type of stimulus. After that, a short overview of research will be given which describes the methods of integration of all these separate motion perception sensors. It can be found in section 1.2. Following that, a translation of the knowledge we gathered up to that point is applied to vehicle driving. The way different sensors are used while driving, as well as some additional side issues with motion perception in real-world vehicles are described in section 1.3.

Finally, when all relevant information has been reviewed, we try to draw some conclusions based on the collected information and try to identify gaps in the information which could support new research in this area of research. This can be found in the final section, section 1.4. We will then, in the subsequent chapter 2, discuss the application and motion perception within vehicle simulators.

1.1 Motion Perception in the Human Body

Motion of the human body can be perceived in a number of ways. We focus on the perception of movement within the human body, where many different sensors contribute to this motion perception. Therefore, in order to provide a structured overview, we will split up the perception of motion within humans in three categories:

1. Inertial motion perception, where human self-motion is perceived purely based on sensors which are able to translate acceleration and jerk into perceived motion.
2. Visual motion perception, where humans detect self-motion and velocity based on the visual input they receive.
3. Other methods of motion perception. These include tactile, auditory and efferent copy as self-motion cues.

How these different categories of motion sensors integrate, and how they act while driving, follows in section 1.2 and section 1.3, respectively.

1.1.1 Inertial Motion Perception

One of the main sensor systems that perceives inertial self-motion of the human body is the vestibular system (Howard (1968)). The vestibular system comprises of two sensors which detect both linear and angular acceleration. See Figure 1.1 for a visual representation of the whole sensory system:

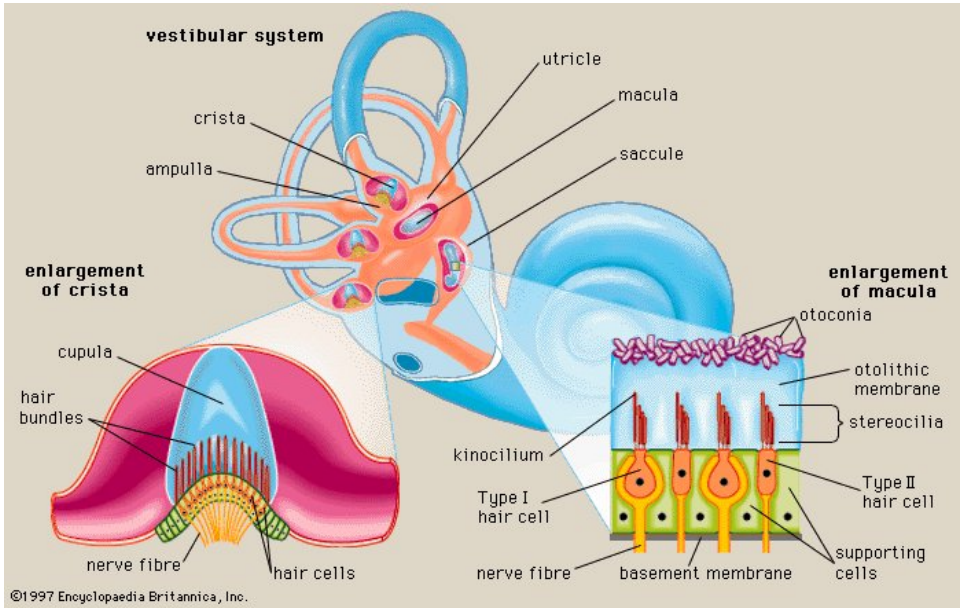

Figure 1.1: The Vestibular System, as represented by Encyclopædia Britannica (1997). Indicated are the three semicircular canals, and the otoliths.

The vestibular system is located in the inner-ear, near the cochlea (also visible in Figure 1.1), where sound coming from the eardrum and auditory ossicles[1] is being translated. For a more complete, but compact review of the vestibular system, and a more neurologically in-depth explanation on the processing of vestibular signals, please refer to the works by Britton and Arshad (2019).

[1]The ossicles (also called auditory ossicles) are three bones in either middle ear. They serve to transmit sounds from the air to the fluid-filled labyrinth (cochlea).

Linear Motion Perception Through the Vestibular System

Linear acceleration is mainly sensed through the otolith structure (DeAngelis and Angelaki (2012)), a part of the vestibular system located near the base of the semicircular canals (see Figure 1.1). In short terms, the otolith system consists of a layer of small, calcium-carbonate particles on top of a viscous gel layer, which in turn is penetrated with small hair cells (see Figure 1.2). Difference in acceleration deforms hair cells which penetrate a viscous gel layer, which transfer electrical signals to the brain where linear acceleration or direction of gravity is sensed (Britton and Arshad (2019)). In the vestibular system, two of these otolith structures are present, one oriented horizontally and the other vertically, but the system is able to perceive linear acceleration in the direction of all three dimensions, and is also able to estimate head orientation when a gravity field is present (Gray (2020), Britton and Arshad (2019)).

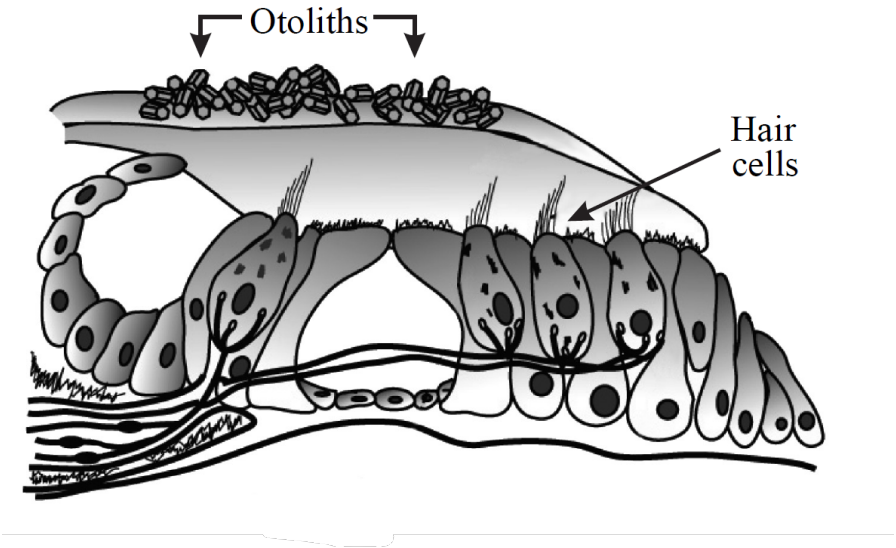

Figure 1.2: Diagram of otolith organ (Dunbar (2004)). Indicated are the otolith particles upon the viscous gel layer and the hair cells.

Limitations exist, however, for the perception of linear motion solely from the vestibular system. Accelerations are perceived only when reaching a certain threshold. In fact, many motion sensors in the human body do. However, these thresholds usually indicate a transition range of not perceivable motion to fully perceivable motion, and therefore, discrete motion perception thresholds are not generally used (Gundry (1978), Heerspink et al. (2005)). The ability to sense linear acceleration only from a certain threshold has experimentally been confirmed by several studies, including Kingma (2005), Benson et al. (1986) and more recently, Soyka et al. (2011). First of all, Soyka et al. presents a review of past studies researching linear acceleration perception thresholds through the vestibular system. A graphic overview of the vestibular linear acceleration detection thresholds, in both anterior-posterior (surge) and lateral (sway) directions, is given in Figure 1.3.

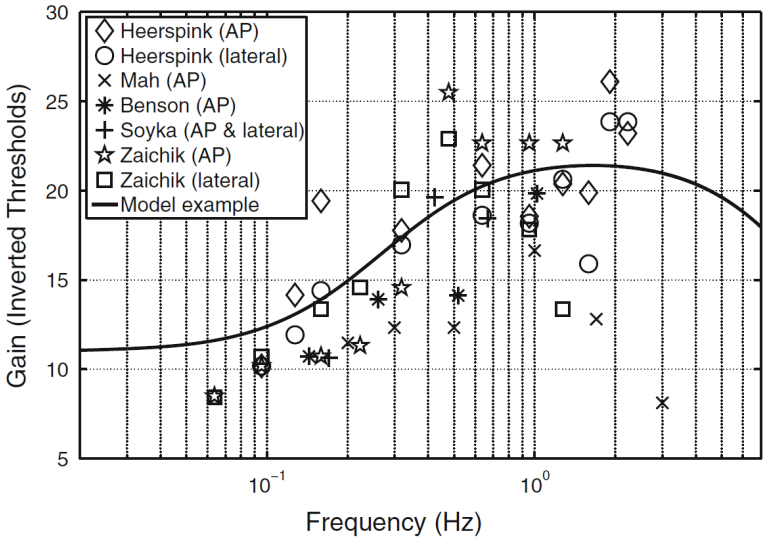

Figure 1.3: Anterior-posterior (AP) and lateral motion detection thresholds of the vestibular system, as presented by Soyka et al. (2011). For the complete list of references referred to in the legend, please refer to the original source. The inverted acceleration thresholds, now referred to as *Gain*, is presented as a function of acceleration input frequency, where a sinusoidal acceleration curve is inferred.

From this data, it becomes clear that when following a certain sinusoidal acceleration profile, the faster you accelerate, the easier it becomes do detect that acceleration through the vestibular system. Which seems to be contradicted by more recent work on linear acceleration perception thresholds (de Winkel et al. (2020)). de Winkel et al. found that there actually seems to be no dependency of jerk amplitude on motion perception thresholds. This discrepancy is explained by de Winkel et al. by showing that there is in fact a frequency dependency when considering jerk influences, below 1 Hz. Above 1 Hz motions, the dependency of perception threshold on jerk intensity or frequency disappears. In Figure 1.3, this jerk-frequency dependency manifests itself in the decrease of perception sensitivity below 1 Hz.

The decrease in perception thresholds in Figure 1.3 at higher (> 2 Hz) frequencies is predicted by Soyka et al. due to the physical limitations of the otolith system, which cannot follow high-frequency accelerations or is even damaged at these high frequencies. This is yet to be experimentally confirmed. Soyka et al. (2011) expands on the existing research on translational acceleration thresholds and includes acceleration profile dependencies on the acceleration detection threshold, at low frequencies ($<$ 0.67 Hz). They found that trapezoidal profiles elicit the lowest perception thresholds, while triangular profiles are perceived the hardest, with sinusoidal profiles in between. Which, in these experiments, translates to highest-to-lowest jerk levels, respectively. These measured perception mechanisms are approximated into LTI-systems, as well.

Some additional sources, which provide useful information not shown in Figure 1.3, are: Heerspink et al. (2005) presents frequency-dependent motion perception thresholds based purely on vestibular stimulation for all 6 degrees of motion. Influences of subject age on the linear acceleration perception thresholds are studied by Kingma (2005), where he found a dependency on age with anterior-posterior acceleration, but none for lateral.

Another shortcoming of relying on the vestibular system alone for sense of linear motion, is the inability to differentiate between translational acceleration and tilt of the otolith sensors with respect to a gravitational field (Angelaki and Dickman (2000)). In fact, in the absence of visual cues, there is often the impression in the observer that the person is tilted, instead of being accelerated (as studied in for example Previc et al. (1992), see DeAngelis and Angelaki (2012) for an overview). An example of where this could become a serious issue, is with aircraft pilots, who can mistakenly compensate for a linear acceleration by pitching the aircraft downwards (DeAngelis and Angelaki (2012)). On the other hand, this tilt can in fact be used to simulate linear acceleration, while in fact only rotating the observer (Groen and Bles (2004)). More on this subject in chapter 2.

On top of that, constant velocity is not encoded by the vestibular system, due to the physical properties of the otolith system (DeAngelis and Angelaki (2012), Valente Pais (2013)). When there is no acceleration present, the orientation of the hair cells does not change, so even while moving at a constant velocity, no acceleration (or motion, for that matter) is perceived through the vestibular system - theoretically. In reality, other motion sensors like the visual system will in fact perceive constant velocity (e.g. Van Boxtel et al. (2006)).

The inability of the vestibular system to encode constant velocity accurately is represented clearly in results by Siegle et al. (2009) (see Figure 1.4). Multiple experiments were conducted, where in one of them, subjects were put on a motion platform at the end of a robotic arm, and were presented with a visual target. They were asked to point towards that target, and close their eyes when they were moved along certain profiles. Subjects had to indicate whether they had reached the target, and their perceived location was measured continuously by recording their pointing direction.

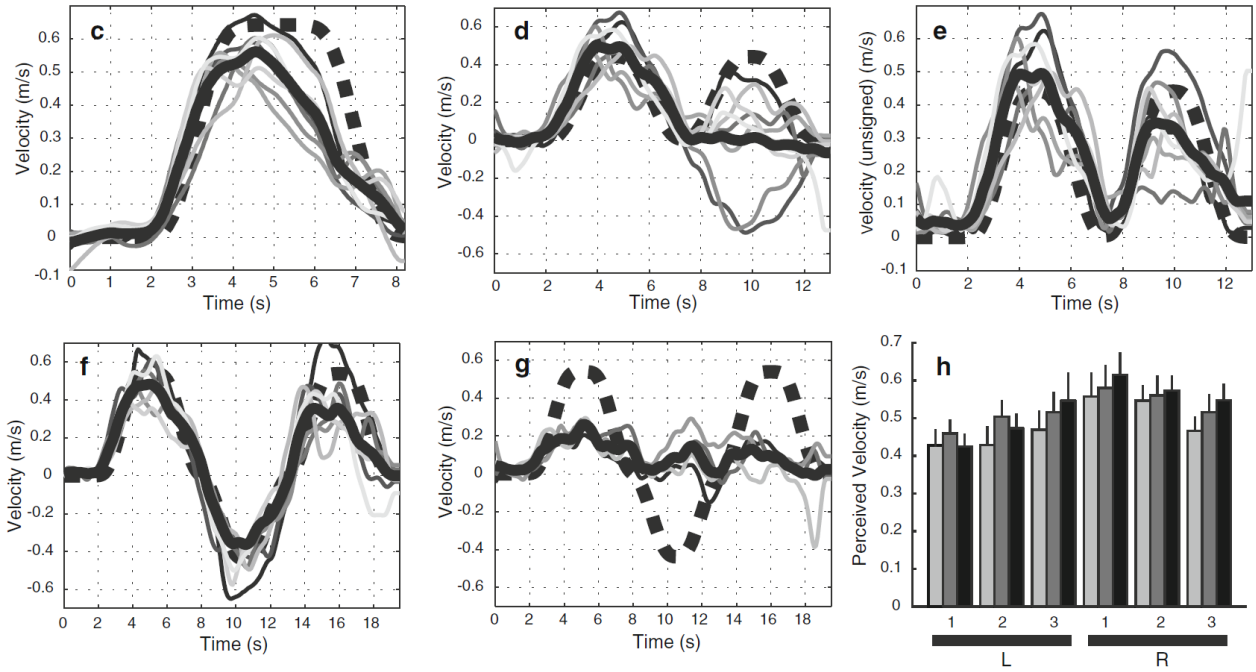

Figure 1.4: Velocity interpretation for three different motion profiles. Dashed line is actual velocity, solid black line is perceived velocity. Other lines are individual subject averages. Final figure shows starting point and velocity magnitude dependency (range 0.54, 0.64, 0.75 $\frac{m}{s}$, light to dark bars). From Siegle et al. (2009).

In places of the motion profile where the motion device moves at constant velocity, the perceived velocity gradually declines. In the second and third velocity profiles, perceived velocity between peaks also decreases significantly. Often, changes in direction of the velocity were not perceived or even misperceived as motion in the other direction in the experiments.

Harris et al. (2001) also presents results based on the singular perception of movement based on vestibular input, as a function of stimulus reference. Interestingly, subjects were able to estimate the distance travelled based on an inertial reference location alone fairly accurately, while results differed quite a lot when subjects were presented with their target only visually (similar to Siegle et al. (2009)). Differences in the magnitude of underestimations of travelled distance and velocity between Harris et al. (2000) and Siegle et al. (2009) can be explained through differences in method and experiment design; in the former, no involvement of the test subject apart from pressing a button was needed, whereas in the latter, subjects had to continuously point at where they thought the target was, which indicates some active involvement as well as some proprioceptive and efferent copy motion cues were present (see subsection 1.1.3 for definitions). In Siegle et al. (2009), subjects were deprived more actively of other motion cues, like vibration and sound.

Angular Motion Perception Through the Vestibular System

The second part that is of importance in detecting motion of the human head through the vestibular system are the semicircular canals. There are three of these semicircular canals in the vestibular system, one for detecting rotation about each of the world's three axes. A visual representation of these channels is given in Figure 1.1. These semicircular canals operate in a similar, slightly more complicated way than the otolith structure does. These semicircular canals are hollow, and filled with fluid. When angular acceleration of these channels occurs, the fluid remains stagnant and is pressed against the cupula or, conversely, gains momentum and presses against the other side of the cupula when deceleration occurs (see Figure 1.5 for a visual indication of the cupula). It is again permeated by hair cells, which turn the movement of the cupula into neurological information (Dunbar (2004), Khan and Chang (2013)).

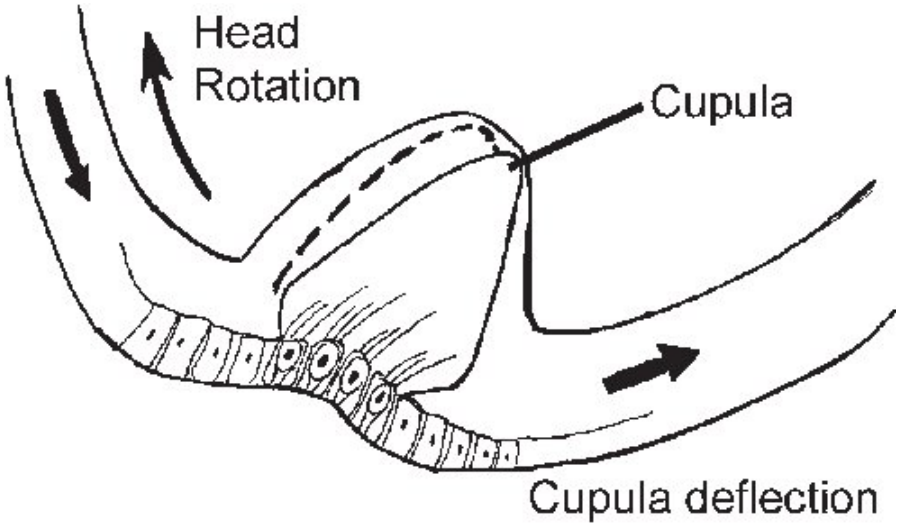

Figure 1.5: Diagram of the cupula, as represented by Khan and Chang (2013). Indicated is the cupula, penetrated by hair cells.

As with linear motion perception. there are certain thresholds for the actual detection of angular motion based on vestibular data alone. A study which has looked into existing research on the topic of the perception thresholds of rotational movement based on vestibular data alone is that performed by Nash et al. (2016). He compared existing research results (Benson et al. (1989), Grabherr et al. (2008), Soyka et al. (2012)) and produced the overview visible in Figure 1.6 for the perception thresholds of angular velocity.

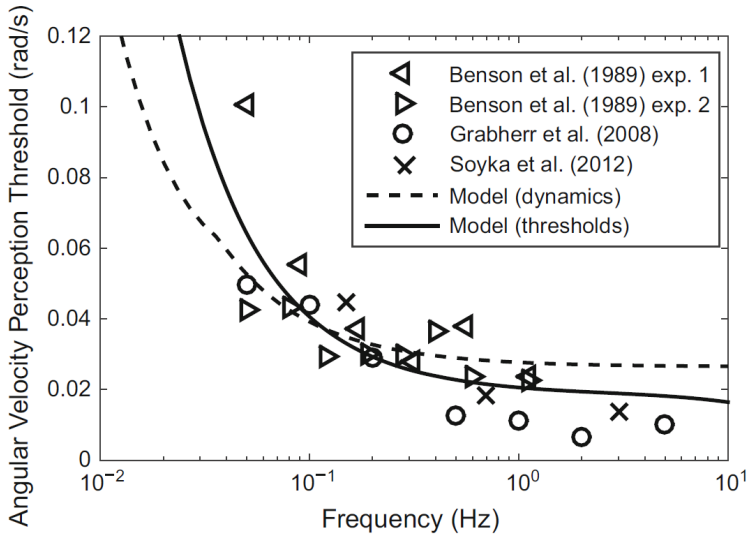

Figure 1.6: The results as presented by Nash et al. (2016). The graph represents data from several sources and models. Data from Benson et al. (1989), Soyka et al. (2012) and Grabherr et al. (2008) is represented, as well as a theoretical model of the semicircular canals. The frequency indicated on the horizontal axis represents the frequency of the sinusoidal input of angular velocity applied to the test subjects. The vertical axis represents the angular velocity threshold.

The represented data in Figure 1.6 is the mean of the data that followed from experiments. What is also notable here is that there is a perception "floor" apparent at input frequencies larger than approximately 0.5 Hz. This means that there is a somewhat constant minimum angular velocity necessary to be able to notice said angular acceleration, at velocity profiles faster than 0.5 Hz. In addition to that, no dependency of the rotation perception thresholds on the rotation axis is represented here, while in fact it has been shown that there certainly is one (Heerspink et al. (2005), confirmed more recently by Suri and Clark (2020), although experiment design and to-be-measured variable differed (angular acceleration vs. tilt angle as a function of frequency, respectively), which makes comparison of absolute data more difficult).

Motion Perception through Proprioception

Proprioception is another method of perceiving motion in the human body. Proprioception refers to the sense of self-movement and of positioning the body in general (Harris et al. (2001), Tuthill and Azim (2018)). Proprioception originates from proprioceptors, which are mechanosensory neurons located within muscles, tendons and joints (Tuthill and Azim (2018)). There are several types of proprioceptive sensors, which are split in three main categories. A short description is given below, for a more in-depth (neurological) review, see Tuthill and Azim (2018) or Proske and Gandevia (2012) (where the latter includes experimental verification experiments of the proprioceptive sensors).

- Muscle spindles, located within muscle tissue. Split into two sections, groups Ia and II, which sense muscle length and velocity, and static muscle length, respectively.
- Golgi tendon organs, located between at muscle-tendon interface. As group Ib, they sense muscle tension force.
- Joint receptors, located within joints. Split into four types, these proprioceptors act as limit sensors within the joint.

The role of the proprioceptive system in self-motion perception has been established by multiple studies. For example, during a remembered-target task, test subjects performed better when they were free to use combined vestibular and neck proprioceptive motion inputs, instead of just vestibular inputs alone (Blouin et al. (1998)). Similarly, another study found that reducing the amplitude of an applied stimulus also reduced the vestibular-only motion detection, but the reduced amplitude did not result in reduced proprioceptive motion cues (Nakamura and Bronstein (1995)). In that same study, the conclusion was that the detection of head turns was predominantly determined by somatosensory[2] inputs.

In general, the somatosensory sensor system transduces the magnitude and the direction of the inertial stimulation directly (Zaichik et al. (1999)). In that regard, the sensory data it produces is similar to that which the vestibular system produces. Both these systems, however, do not process the same input as the same motion, which also appears from results by Zaichik et al. (1999) (see Figure 1.7 on the next page). It appears that kinesthetic sensors have a higher acceleration perception threshold than for example the vestibular system for low acceleration frequencies. What is also interesting, is that tactile feedback (which originates from proprioception originating from muscles and skin tissue) is the toughest to be stimulated through acceleration, while the vestibular system is the easiest to stimulate.

[2]The somatosensory system is a component of the nervous system that detects and allows for perception of the modalities (sense) of pain, temperature, head and body position (called proprioception), head and body movement (called kinesthesia) and touch (Jacobs (2011)).

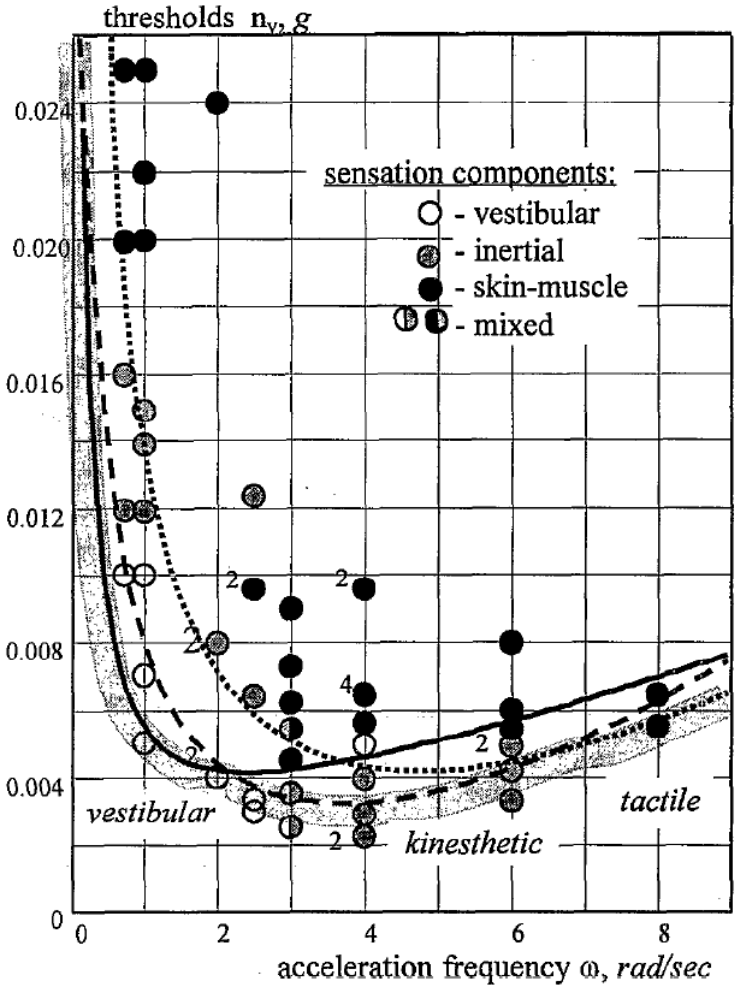

Figure 1.7: Results from Zaichik et al. (1999). Indicated are different perception thresholds, as a function of acceleration frequency. "Inertial" is the kinesthetic sensation.

1.1.2 Visual Motion Perception

Perception of movement also relies heavily on visual input. The visual system determines the position and orientation of the observer with respect to the observable world, but in addition to that, also provides velocity information to the observer (Van Boxtel et al. (2006), Van de Grind (1988)). The visual self-motion perception system is often considered to be a velocity sensor, thus dependent on velocity amplitude and direction (Van der Steen (1998), Bos et al. (2002), Bos et al. (2004)).

One of the main methods of perceiving self-motion from just visual cues for the human body is the processing of optic flow (Lappe et al. (1999)). Optic flow is the (apparent) movement of the surrounding scene relative to the observer, without the observer following the movement of these surroundings with his eyes. This already introduces a complication for the perception of self-motion from visual cues, since the observer, in reality, constantly moves his eyes to accompany the optic flow. These eye-movements are referred to as retinal flow (Lappe et al. (1999)). First optic flow will be discussed, after which influences of retinal movements and compensatory strategies will be added.

Optic flow

Optic flow was first widely recognised when Gibson (1950) described that the visual translational motion in the "optic array surrounding a moving observer" radially expands out of a single point along the direction of the heading of the observer. Gibson recognised that optic flow was a powerful signal to control the observer's movement. A visualisation of optic flow is given in Figure 1.8. Optic flow alone is not enough for the observer to get information about the absolute distance to an object, but rather to compare spatial intervals and for time measurements relative to the object and observer (Kemeny and Panerai (2003)).

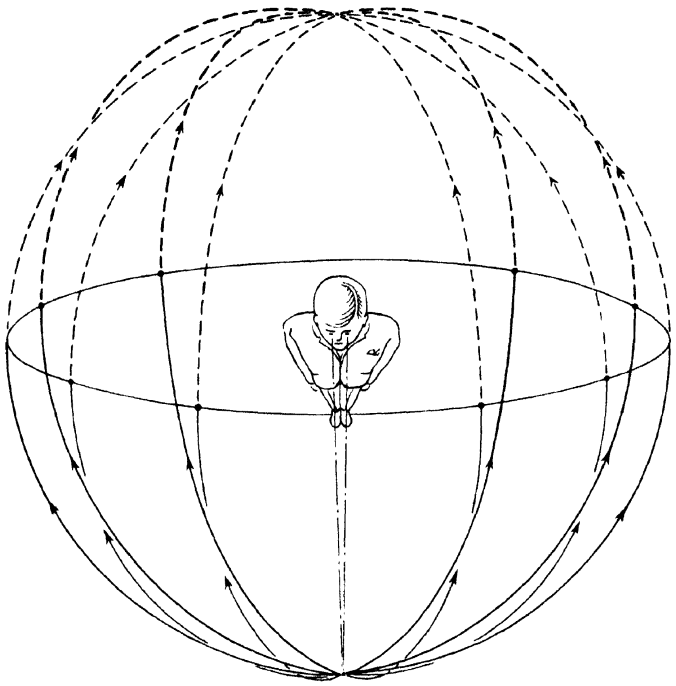

Figure 1.8: "The directions of Deformations in the Visual Field during Forward Locomotion[3], as Projected on a Spherical Surface around the Head", as presented by Gibson (1950)

[3]Locomotion: The ability to move from place to place, or the act of doing so (Wiktionary (2020)).

Optic flow information can be integrated by the observer to obtain an estimation of travelled distance, quite accurately (Kemeny and Panerai (2003)). An additional study which shows the accuracy of this estimation is presented in Harris et al. (2001) (adapted from Redlick et al. (2001)). In these experiments, subjects were shown a visual target in a virtual environment as a reference, and the virtual environment started moving. Subjects had to indicate whether they had reached the target, based on optic flow alone. Harris et al. (see Figure 1.9) showed that for very low accelerations (i.e. near-constant velocity), distance estimations are inaccurate, but become more accurate with increasing acceleration, showing a transition period over the range of frequencies where vestibular motion perception usually starts to take place (Gundry (1978)).

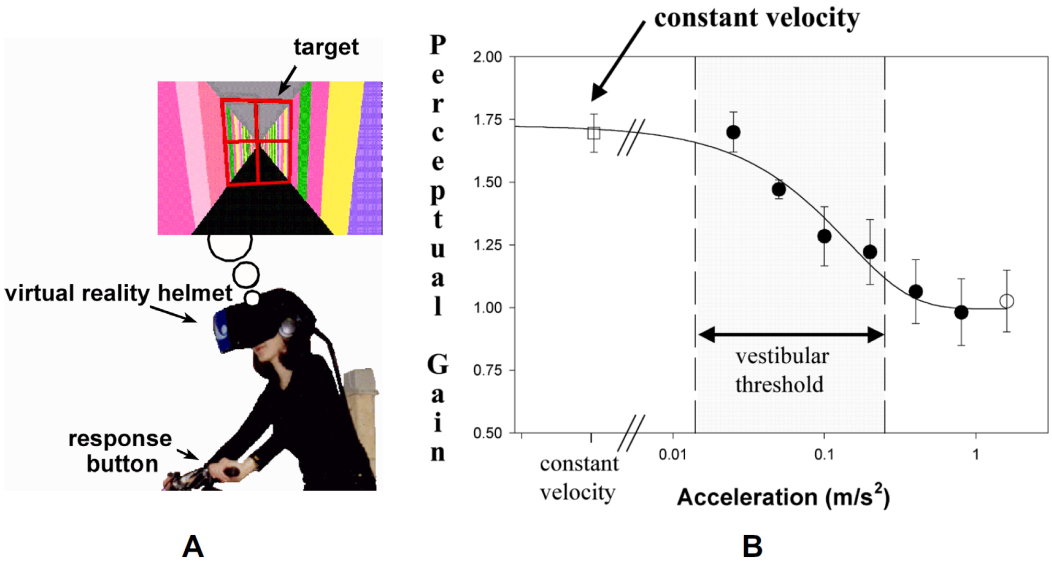

Figure 1.9: Experimental setup and perceptual results for a vection-based localisation task. Perceptual gain refers to the ratio of perceived distance (target distance) over optic flow distance. From Harris et al. (2001).

An interesting explanation is given for the overestimation of moved distance based on optic flow alone by Redlick et al.; it could be that this is a manifestation of a safety mechanism, where collision with obstacles is less likely when the remaining distance to those obstacles is underestimated. The transition to accurate estimations could be due to the internal change of strategy of distance estimation. However, a discrepancy in research results exists for the under- or overestimation of displacement based purely on optic flow; Frenz et al. (2007) also investigated displacement estimation based on optic flow. In Frenz's study, in all cases of visual variations, almost all test subjects kept constructively underestimating the distance they travelled. Which is, interestingly enough, contradicting the overestimation of displacement in Redlick et al. (2001) - in case of constant velocity. Redlick et al. reports an overestimation of 70% for constant velocities, whereas Frenz et al. reports an underestimation of 25% (average, over all visual fidelity conditions). In case of Redlick et al., the refresh rate of the head-mounted display was low, around 25 Hz, the field-of-view of the display was lower in most of the experiments, and no stereoscopic cues were applied. The virtual environment represented a colourful corridor, with very clear visual intervals, whereas Frenz et al. applied dot clouds and a simulated gravelled surface. The lack of clear visual reference, as well as differences in visual display quality could explain this large difference in displacement estimation. In section 2.2, the influences of visual cue fidelity will be described more qualitatively.

More studies tend to lean towards motion underestimation through optic flow. Kemeny and Panerai (2003) list a number of studies which point to velocity estimation from optic flow as being underestimated due to reduced image contrast, texture or luminance, which may manifest itself in drivers' underestimation while driving at night or in foggy weather (Gegenfurtner (1999) and Snowden (1998), respectively).

Retinal movements

As stated before, retinal movements can complicate the perception of motion and the estimation of heading from the observer's perspective. Several studies (reviewed by DeAngelis and Angelaki (2012)) suggest a dependency of the interpretation of optic flow on movements of the eye and head (Banks et al. (1995), Crowell (1998), among others). An example of this mix-up of cues is visible in Figure 1.10.

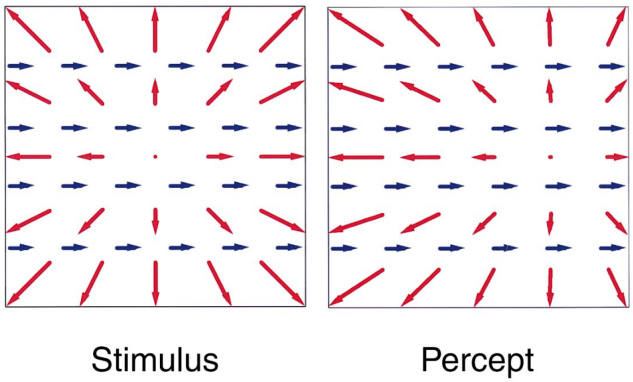

Figure 1.10: An illusion of optic flow - Lappe et al. (1999).

In Figure 1.10, the stimulus presented to the observer is two-fold: there is an optic flow component (red arrows) as well as an unidirectional motion (blue arrows). The overlapping of these cues results in the imaginary focus of expansion[4] being shifted a certain amount to the right (and is perceived as such) (Duffy and Wurtz (1993)). The described case is not the only combination of conflicting cues, which can result in erronous interpretations of self-motion. A larger overview of the dependencies of optic flow interpretation on retinal movements and compensation, is illustrated in Figure 1.11.

[4]Focus of Expansion was coined by Gibson (1950), where he suggested optic flow originates from a single point (see Figure 1.8). Gibson (1950) suggested that heading is estimated by localising this point.

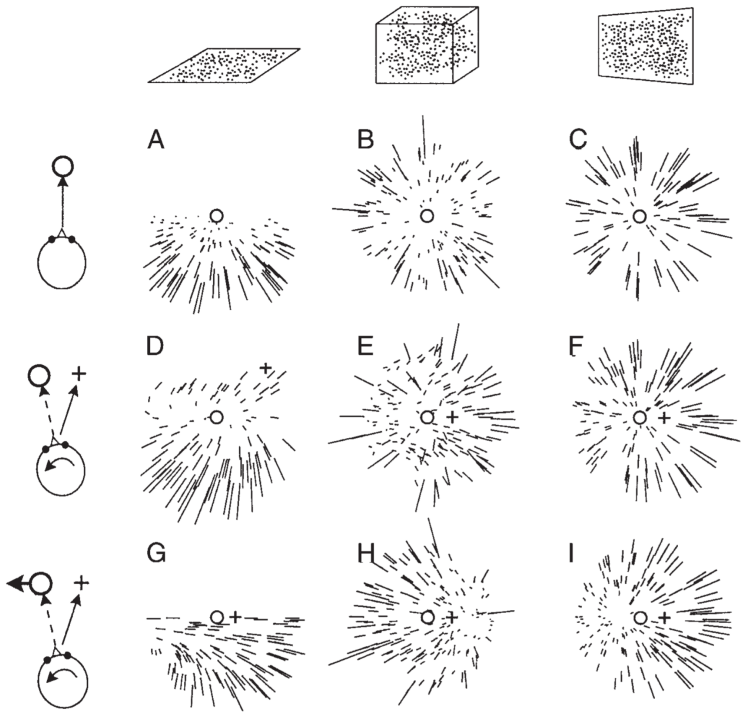

Figure 1.11: Motion of particle charts, depending on certain orientations and movement directions, as presented by Lappe et al. (1999).

The columns in Figure 1.11 represent the surrounding of the observer; in **A**, the observer moves over a plane of dots, in **B**, the observer moves through a box of dots and in **C**, the observer looks at a surface of dots. The stripes should be interpreted as streaks of motion-blur: dots which have been smeared out due to motion of the observer. Situations **A** through **C** represent a purely translational movement towards the target. The circle represents the direction of gaze of the observer. The confusing situations however, occur when the observer introduces eye- and eye-head movements. The heading of the observer is indicated by the cross. In situation **F**, the observer can mistakenly experience the motion as a pure forward motion, when this is in fact not the case (Warren Jr. and Hannon (1990), Royden et al. (1994)). In addition to that, when the object at which the observer is gazing is also being moved, the observer may experience the movement to be in a curve-like path, but in reality, only translational movement occurs. These situations of movement are also sometimes confused by the observer (Royden et al. (1994), Royden (1994)).

Although, as described above, many confusing situations may occur, the way humans compensate for self-motion with eye-movements, or change the way optic flow information is interpreted, is largely successful. This is likely due to the fact that the brain has access to other, internal information which can be used to compensate the perception of motion (e.g. efference copy) (DeAngelis and Angelaki (2012)). A more in-depth review of these compensatory mechanisms for movement perception is presented by Warren (2003), as suggested by DeAngelis and Angelaki (2012).

Combined and Other strategies for Visual Motion Perception

Combining optic flow and retinal movements results in an interpretation of the observer's current heading. The essence of heading perception in for example vehicle driving lies in the ability to differentiate between a simulated eye rotation (i.e., a perception of rotation due to a retinal movement) and an actual curve in the current heading of the observer. One method of decreasing the aforementioned error behaviour is the use of extraretinal (e.g. vestibular) information to differentiate between the two cases (Royden (1994), DeAngelis and Angelaki (2012)). Another method of discriminating between self-rotation and curved heading, is the use of motion parallax. The objects in the observer's field of view move, dependent on the observer's self-motion. For example, objects close to the direct line of sight move inward relative to the retinal flow, towards the point of gaze of the observer. This is referred to as motion parallax. In Figure 1.12 an example of the concept of motion parallax is given. Motion parallax is used as a heading estimation mechanism in the sense that, if the self-motion were to be completely rotational, all objects in view would move at the same apparent velocity. If not, that means a certain curved heading is attained (Lappe et al. (1999)).

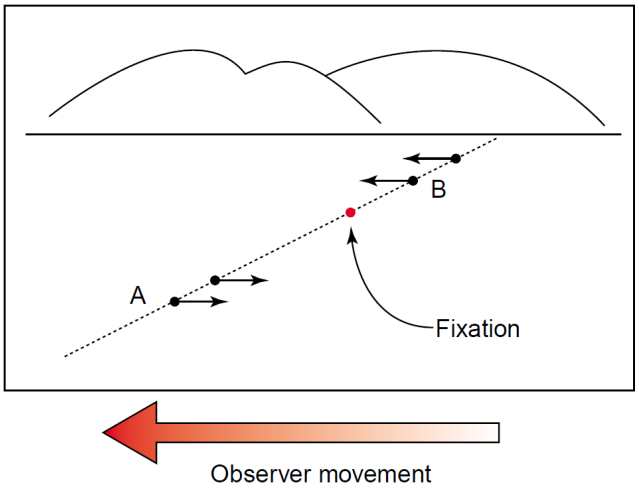

Figure 1.12: Motion parallax (Kemeny and Panerai (2003)).

One important aspect in perceiving self-motion based on the distance and velocity of objects in the observer's field of view, is the ability to estimate the distance to these objects. This is usually done (up to a certain distance) in the observer by making use of binocular disparity. Binocular disparity is a means of perception of depth, and is based the lateral positional difference between the two retinal projections of a certain point in space on both eyes (Qian (1997)). Disparity as a means of distance estimation is limited to a range of a few meters, and has shown to be effective for distances up to 30 meters (van Hofsten (1976), Loomis and Knapp (1999)). Therefore, it is accepted that in situations which exceed this distance to objects for motion perception, like in vehicle driving, optic flow is the main mechanism of motion perception (Regan and Beverly (1982), Jamson (2010)).

As with the inertial methods of motion perception, certain thresholds exist for the perception of motion through visual cues. One such study is the one performed by Bigler (2013) (as represented in Nash et al. (2016)). The results given in Figure 1.13 follow from a study where a certain optic signal was superimposed on an already constant velocity, after which the thresholds of perception of this change in constant motion was measured.

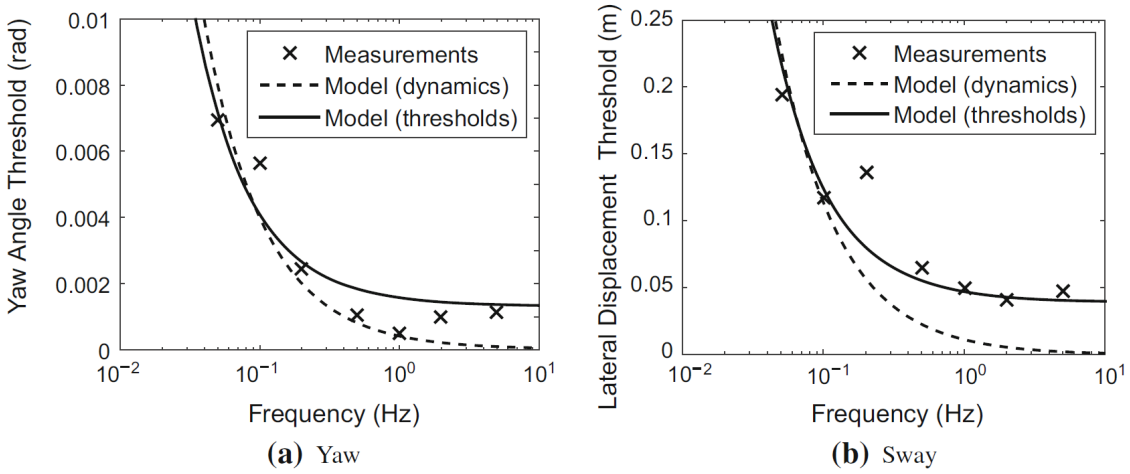

Figure 1.13: Results from Bigler (2013), as represented by Nash et al. (2016). Given are the visual motion perception threshold measurements for both yaw and lateral displacements, as a function of input frequency. A representation of optic sensor dynamics and thresholds models is given as well.

These are interesting results, since from a visual motion profile point of view, yaw and sway motions are similar, where sway introduces perspective dependency while yaw gives a uniform magnitude of optic flow. Which could explain the higher magnitudes for the perception of sway motion through visual cues.

Vection

The method of creating the sense of motion in the observer, using optic flow, is called vection; when optic flow occurs in the absence of other sensory cues, this can invoke the sense of movement (Gurnee (1931), Brandt et al. (1973), Valente Pais (2013)) and even postural adjustments (van Asten et al. (1988), Chardonnet et al. (2017)). An example of visually-induced sense of motion, which daily commuters may have experienced themselves already, is the illusion of self-movement when - while seated in a train - a train next to theirs departs. The movement of the other train gives the illusion of movement in the opposite direction (Valente Pais (2013)). An aspect of vection is that it is usually regarded as a slow process; the perception of self-motion after an onset in visual motion stimulation is not instantaneous (for example, Seno et al. (2018), Mergner and Becker (1990) and Brandt et al. (1973), see Nash et al. (2016) for an overview of time delays in motion perception systems). This means that certain patterns of optic flow are perceived as moving surroundings or objects initially, only to be recognised as self-motion after a short time delay. Interestingly enough, vection is experienced faster when conflicting vestibular stimuli are absent. In other words, vestibular signals that cohere with the visual cues result in the visual motion to be processed faster (Young et al. (1973), Berthoz et al. (1975)).

One interesting aspect of vection is its dependency of its subjective strength on exposure time. One study showed that, when subjects were subjected to certain vection patterns, for different durations, longer exposure resulted in higher vection strength ratings (Seno et al. (2018)). More recent work on this topic is lacking, where implementation of this effect into threshold and (simulator) performance could produce different results than those that are already available. In addition to that, active workloads also seem to influence the perceived magnitude of magnitude of vection (Seno et al. (2011a), where also a number of previous supporting studies are indicated), where increased required attention in active tasks reduces the susceptibility to vection. Furthermore, the direction of vection also influences the perceived strength of the vection, where oblique angles reduce perceived vection magnitude, vection onset latency and vection duration (Fujii and Seno (2020), results obtained with a dot cloud stimulus).

1.1.3 Miscellaneous Methods of Motion Perception

Apart from the perception of self-motion through inertial and visual motion cues, other methods of motion perception still exist. These include the efference copies, the perception of motion through auditory cues and tactile feedback (which does not include inertial tactile feedback, like feeling pressure on skin and muscles when accelerating).

Motion Perception Through Efference Copies

A final category of methods of motion perception are the efference copies. Efference copies are essentially copies of movement commands given by the brain, with which to compare the sensory stimuli obtained through other sensors (Britton and Arshad (2019), Bridgeman (1995)). Furthermore, the gain of the efference copy mechanism is less than 1, resulting it having to be supplemented by other motion perception mechanisms (Bridgeman (1995)). Having a copy of efferent commands allows the brain to prepare for the consequences of an intended motion before it has occurred. A mismatch between the sensory data from other sensors and the efferent commands is also believed to be one of the major causes of motion sickness (Oman (1998)) and to contribute to cybersickness (Lo and So (2001)). Having an an efference copy of a motor command also enables the discrimination between self-generated and passive motion (Britton and Arshad (2019)). The effects of efference copy as a motion perception mechanism should therefore become visible when active tasks are introduced during a motion perception process. Which underscores the importance to differentiate between active and passive motion perception when considering other motion perception sensors.

Motion Perception Through Skin Sensations

One special case of somatosensory perception is the detection of airflow over the skin. At normal walking velocities, the flow of air over the skin is most likely too slow to be noticeable, thus not providing self-motion information. However, at faster speeds, this effect becomes much more prevalent Harris et al. (2001). A study pointed out that with birds, airflow can enhance their visual reflexes to movement (Gioanni and Sansonetti (1999)). The sense of air flowing over exposed skin is a form of tactile flow[5]. In humans, tactile flow by air flow has been shown to enhance the perception of self-motion in humans (Seno et al. (2011b)). Tactile flow is not believed to be combined with other cues of motion, unlike the combination of visual and vestibular cues to determine heading (Fetsch et al. (2009), Gu et al. (2008)) or orientation (MacNeilage et al. (2007)), but tactile flow seems to even dominate or enhance perceptual judgements, and can even serve as an emergency override over other available cues (Harris et al. (2017)).

[5]Tactile flow is the sense of changing tactile stimuli, similar to optic flow (Scilingo et al. (2008)). This can be achieved with for example airflow over exposed skin, but also through oscillating of a felt surface (by e.g. fingertips) (Harris et al. (2017))

Motion Perception Through Auditory Cues

Auditory cues as a means of motion perception may also be of influence next to (and combined with) visual, inertial and tactile information. In case of normal, non-vehicular situations, there are four main aspects of auditory cues which are the most relevant for the detection of moving sound sources (Rosenblum et al. (1987)):

1. Doppler frequency shifts
2. Binaural cues (interaural time and intensity changes), i.e. comparing audio cues recorded in both ears
3. Intensity changes
4. Reverberation (ratio of direct to reverberant energy)

For an in-depth description of these aspects of auditory motion cueing, Kapralos et al. (2004) gives an overview. In Kapralos et al., the results indicated that for motion perception, at low accelerations (closer to constant velocities, $< 0.1\frac{m}{s^2}$), combined audio and physical cues provided more accurate estimations of travelled distance. For these accelerations, the result did not differ much from physical cues only. But, for higher accelerations, physical motion only became more erroneous, while combined physical and auditory, and auditory cues only, became the most accurate. These results were in accordance with earlier research (Lutfi and Wang (1999), Perrot et al. (1993)).

Carlile and Leung (2016) reviews studies on the perception of motion through auditory cues, on multiple levels; the perception of a moving sound source, the perception of self-motion through auditory cues and the neurological encoding of auditory motion. This review holds a lot of information which can greatly improve understanding of underlying auditory cue processing, but little practical application in the case of self-motion in either vehicles or simulators.

1.2 Integration of Motion Perception Sensors

The discussed methods of perceiving self-motion above all contribute to the general sense of self-motion of the observer; the fact that combining sensory data in humans improves motion perception and task performance, is well-established. The integration of different sensor values is essential to compute a complete image of position, orientation, motion and heading. Using one sensory input alone could result in false images, illusions of motion and loss of information (Britton and Arshad (2019)). Comparing sensory data to internal efference copy data allows a differentiation between passive motion (like in vehicle driving, to some extent) and self-generated motion to be made. The process of becoming "good" at combining sensory data, is a learning process, however (Ramkhalawansingh et al. (2016b)).

The contributions of two of the principal methods of perceiving motion, visual and vestibular, has been established as being dependent on experimental conditions rather than a continuous weighting (see Britton and Arshad (2019)). Being able to set a fixed value for the weighting and altering motion cueing accordingly, is therefore unlikely, and understanding the dynamic reweighting of combined sensory data may provide more insight in how to tune vehicle simulator motion to not cause misperceptions, or worse, simulator sickness.

Data from several studies suggests that the sensory inputs are integrated in a Bayesian[6]-optimal way. This, in turn, suggests that sensory data is integrated weighted with its respective reliability. Many studies support this premise, which are listed in the works of Fetsch et al. (2010), and Nash et al. (2016) as well. The latter source also provides insight in experimental data and mathematical models covering the topic of sensory integration.

An advanced manifestation of this Bayesian reasoning in motion sensor integration is the model of Causal Inference. In this context, this model suggests that the brain checks whether sensor information from different sensors originate from the same outside stimulus, and combines this multi-sensory information when this is the case. Sensory information is not split between sensor origin, in this case. If the information is not judged as coming from the same stimulus, sensor data is split, and an estimate of self-motion is based on one of the sources (de Winkel et al. (2017)). This reasoning of sensor choice and stimulus acceptance is susceptible to manipulation by drawing attention to the sensor you want the observer to use - experimentally found in certain visual-proprioceptive goal-directed actions, that is (Limanowski and Friston (2020)).

[6]Bayesian statistics is a system for describing epistemological uncertainty using the mathematical language of probability. [...] Bayesian statistical methods start with existing 'prior' beliefs, and update these using data to give 'posterior' beliefs, which may be used as the basis for inferential decisions. Spiegelhalter and Rice (2009)

An applied branch of research which also cover the topic of sensory integration, and sensor information acceptation, is the research that covers so-called "Coherence Zones". A coherence zone is a region of comparison between sensory information, where the information of sensors is decided upon as being coherent, and is accepted as a still providing the perception of an earth-stationary visual scene (Valente Pais (2013), but initially introduced by Van der Steen (1998)). A visualisation of a theoretical example of a coherence zone is given in Figure 1.14.

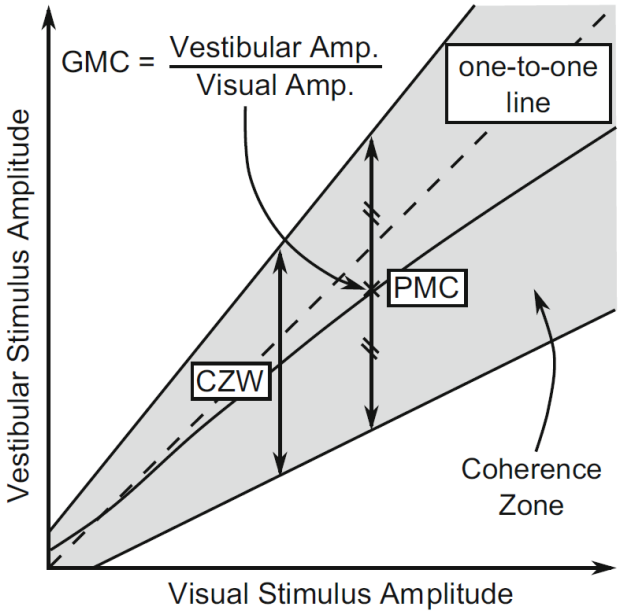

Figure 1.14: Theoretical example of a coherence zone between visual and inertial stimuli (Nash et al. (2016)). Terminology is given below figure.

Where the following terms are the meaning of the abbreviations in Figure 1.14:

- CZW: Coherence zone width; total difference between the limits of the coherence zone.
- PMC: Point of mean coherence; the point halfway between the limits of the coherence zone.
- GMC: Gain of mean coherence; the ratio of the vestibular amplitude over the visual amplitude which also represents the preferred gain between visual and vestibular cues. Follows the solid black line.

Coherence zones are an quantifiable metric for simulation environments, where a region of acceptance can be determined for any combination of (usually visual and vestibular) motion stimuli in a certain motion/vehicle simulator. These coherence zones, however, are usually not interchangeable between simulators, since they are dependent on task and platform (Valente Pais (2013), referring to Roark and Junker (1978), Hosman and van der Vaart (1978), Samji and Reid (1992)). Since the concept of coherence zones is a more simulator-related subject, and dependent on simulator vehicle type, more information and experimental results on this topic will be given in chapter 2.

1.3 Motion Perception and Heading Estimation in Real-World Vehicles

The information found in the previous sections gives a basis on which we can base some conclusions on which perception methods are influencing ones ability to perceive motion while in a vehicle. Basically, we can say that no cue can be disregarded while operating a vehicle, and that all different types of cues are codependent. Generally, when humans are asked to perform tasks on a certain motion axis, while being moved on another (Hosman and van der Vaart (1978), Samji and Reid (1992)), or when (driving) tasks are introduced, motion perception thresholds increase (Nash et al. (2016)). Therefore, the indifference threshold[7] should determine the limits of perception during tasks where motion occurs in multiple directions and through multiple motion sensors (Groen et al. (2006)).

In case of vehicle (automobile, in particular) driving, it is known and accepted that optic flow is considered one of the most important types of visual information for driving, but it is heavily influenced by eye-head and body movements (Regan and Beverly (1982), Jamson (2010)). Moving at a constant forward velocity is perceived through optic flow, but for the optic flow to not be blurry, a series of optokinetic movements are elicited both in simulated motion and car driving (Niemann et al. (1999), Authié and Mestre (2011), respectively). Furthermore, and as we have determined before, it is generally accepted that drivers in vehicle simulators (for example: Harris et al. (2000), Groeger et al. (1997), Jamson (2010), Will (2017) and Duncan (1995)) and real driving (Kemeny and Panerai (2003)) underestimate the velocity they travel at based on visual cues .

In addition to velocity estimation, heading determination enables drivers to follow certain paths and perform certain driving manoeuvres. Heading is not estimated based just on optic flow. Multiple visual motion perception strategies are used. In addition to the use of motion parallax (Lappe et al. (1999)) and the use of binocular disparity (Loomis and Knapp (1999)), the observer is able to estimate heading and motion based on active gaze strategies (Land (1992), Land and Lee (1994), Land and Horwood (1995)). These encompass the looking for objects on the observer's path, the edge of the road, or other oncoming objects. This requires a dissociation between observing moving objects and self-motion with respect to objects, and when these are difficult to distinguish, vestibular cues can facilitate this dissociation (Dokka et al. (2015), Crowell (1998)).

The use of these trajectory-gazing methods of heading and motion perception are quite dominant in the case of driving. Some sources even suggest that locomotion can be achieved using purely visual direction information, without using optic flow (Rushton (1998), Harris and Rogers (1999), Rogers and Dalton (1999)). A combination of optic flow and the use of gaze-fixation on present objects and indicators of trajectory has been viewed by Harris (2001) as redundant a system. When these road markings or apparent stationary objects are not (sufficiently) present, optic flow-based perception becomes more dominant.

[7] Indifference threshold: the threshold for perception of a stimulus in the presence of other congruent or incongruent stimuli (Groen et al. (2006)).

The occurrence and relation of active gaze strategies to upcoming bends is apparent in the research results from Land and Lee (1994). There appears to be a clear correlation between steer angle and gaze angle of the driver. In Figure 1.15 below, the steering behaviour of two drivers was evaluated.

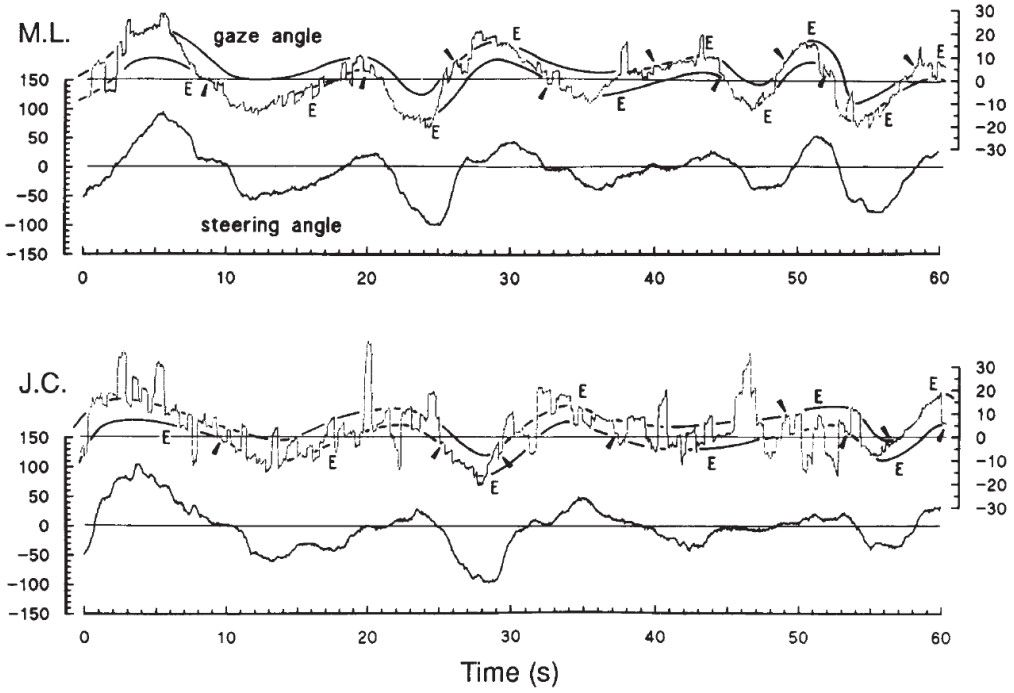

Figure 1.15: Driving test results from two drivers, M.L. and J.C. in Land and Lee (1994). The correlation between gaze angle and steering angle is apparent in both cases.

In Figure 1.15, the two smooth, solid lines on the gaze angle axis indicate the edges of the road, and the fluctuating line indicates the driver's gaze angle. Little arrows indicate the first clear saccade[8] to the tangent point preceding each bend. The E's indicate the point on the exit from each bend where the tangent point disappears.

Apart from the visual cues vehicle drivers usually experience, as they were discussed above, vestibular cues also factor in while driving. Kemeny and Panerai (2003) suggests that normal functioning of the vestibular system is necessary in many types of sensori-motor processes, e.g. for compensatory eye movements in optic flow and in postural control. With this notion, the dependence on active gaze and optic flow while driving implicates the importance of the vestibular system. It was also shown by Reymond et al. (2001) that lack of vestibular input to the motion perception resulted in the decrease of safety margins in the control of the lateral acceleration in curve driving. In other words, drivers were cornering bends faster in a vehicle simulator, when vestibular cues were not present. Conversely, the presence of vestibular input while driving in a driving simulator seems to also be important in the perception (or suppression of perception) of illusory self-tilt and illusory self-motion, as researched by Groen et al. (1999).

[8] A saccade is a rapid, jerky eye-movement of both eyes between two or more phases of fixation in the same direction Cassin and Solomon (1990). In this context, the first rapid eye-movement towards the edge of the road.

It should be noted that the tuning of these vestibular signals in a hypothetical vehicle simulator needs to be appropriate for the application, since they can also result in incorrect perception of motion. In real driving, false signals from the vestibular system were reported by Page and Gresty (1985) to be the precursor to inappropriate steering adjustments.

The above discussed research results primarily focus on car driving. For other vehicle applications, usually similar motion perception mechanisms are observed. In case of real-world motorcycle driving, Will (2017) presents results on the accuracy of velocity estimation, as well. The results are given in Figure 1.16 below.

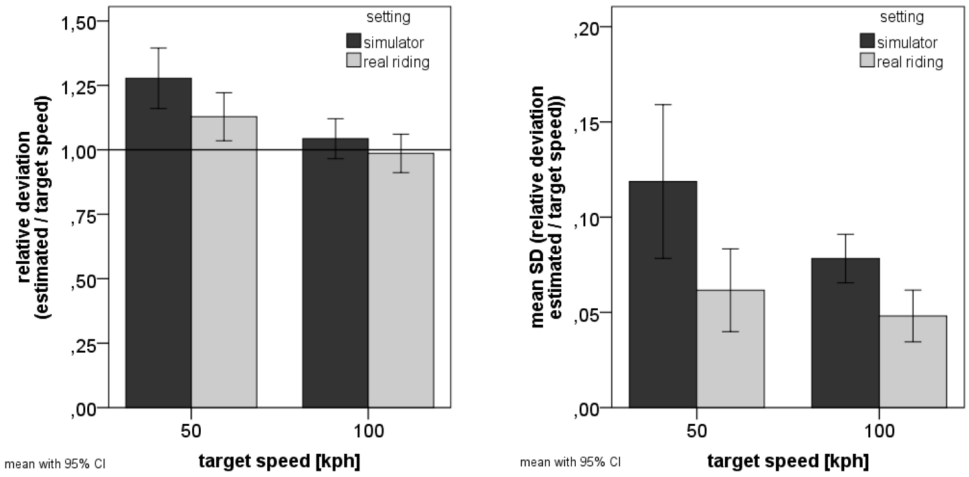

Figure 1.16: Results as presented by Will (2017). In this case, real-world driving self-motion estimation accuracy. On the left, the relative deviation between the correct score (= 1,00) and different target velocities and environments are given. On the right, the mean Standard Deviation between estimated and target speeds is given.

With these results, Will (2017) shows the underestimation of velocity on a motorcycle. What is interesting is that lower speeds are overestimated more than higher ones. In case of these experiments, because of the experiment being a real-world driving experiment, all motion cues are present in the motorcycle driver. Which confirms the intuitive hypothesis that speed estimations will be more accurate in reality than on simulators, due to not necessarily the inaccurate reproduction of all motion cues, but perhaps the incorrect interpretation or integration of these simulated motion cues.

Vansteenkiste et al. (2013) researches the gaze strategies on a bicycle, dependent on path width and velocity, and compares them with readily available models for pedestrian locomotion and car driving (see Schepers et al. (2013) for an expansion). A velocity-dependence of the distance on which is focused by the cyclist is apparent, which is partly in accordance with car driving strategies.

1.4 Summary & Discussion on Human Motion Perception

In the preceding chapter, we set out to discuss the motion perception mechanisms in humans; how and what type of motion (jerk, acceleration, velocity) is perceived through several different sensors in the human body, how those streams of information of different sensors is integrated into one percept of motion and how it is applied in normal vehicle driving in the real world.

1.4.1 Summary

To summarise, there are a number of methods through which the human body can detect motion:

- Inertial sensors: the vestibular system, which detects (angular) acceleration due to physical deformation of the sensors. Can be integrated for estimations of velocity and displacement estimations, although is rarely accurate, and often underestimated (Harris et al. (2001), Siegle et al. (2009), Heerspink et al. (2005)). In addition to the vestibular system, other sensors which detect motion through inertial effects are the proprioceptive sensors, located within muscles and joints (Tuthill and Azim (2018)).
- Visual sensors: usually based on optic flow and affected by retinal movements (Lappe et al. (1999)) and regarded as a velocity sensor (Van der Steen (1998), Bos and Bles (2002)), but also used for position and orientation determination (Van Boxtel et al. (2006), Van de Grind (1988)). Optic flow uses the visual flowing by of the outside world to estimate current self-motion velocity (Gibson (1950), Kemeny and Panerai (2003)). Velocity and distance estimation from optic flow is usually underestimated (Harris et al. (2000), Groeger et al. (1997), Jamson (2010), Duncan (1995), Kemeny and Panerai (2003)). Retinal movements are also used to estimate heading, compensate for head- and body movements (DeAngelis and Angelaki (2012)) and is usually supplemented with other sensory information to reduce perception errors (Royden (1994)). Visual stimuli can be used to induce the sense of motion, called the process of vection (Gurnee (1931), Brandt et al. (1973), Valente Pais (2013)).
- Other motion sensors: including efference copy, which are internal copies of motor commands (Britton and Arshad (2019), Bridgeman (1995)), somatosensory sensors, which provide information through skin sensations (Seno et al. (2011b), Harris et al. (2017)) and auditory cues, which aid in localisation and motion perception as well (Rosenblum et al. (1987), Kapralos et al. (2004)).

It appears that every method of motion perception (especially the first two categories, although research on those topics is more prevalent) in the human body is subject to certain perception thresholds. These thresholds depend on many factors, including most importantly the sensor type, but also the individual, motion profile, direction and magnitude (Soyka et al. (2011), Siegle et al. (2009), Heerspink et al. (2005), Nash et al. (2016), Zaichik et al. (1999), Bigler (2013)). One commonality across sensors is that the motion perception thresholds usually require a minimum magnitude of stimulus above certain stimulus frequencies.

Integration of motion perception sensors is where in normal situations, the complete perception of motion becomes critical. Humans obtain motion data from several sensors, originating from the same stimulus, and then have to combine this into a complete percept of motion. Usually, sensor data is weighted based on the environmental conditions (Britton and Arshad (2019)) and one of the more accepted theories to date is that the brain incorporates the reliability of motion sensors in a Bayesian-optimal way (Fetsch et al. (2009), Nash et al. (2016) for a review). One more expansion upon this theory is the one of causal inference (CI), where sensor data is judged whether it comes from the same stimulus through different motion sensors, and is thereafter combined when it is judged as being so (de Winkel et al. (2017)). Coherence zones provide a constructive and visual method to determine in what combination of visual and vestibular stimuli, this combination is still judged as coherent and therefore useful (Van der Steen (1998), Valente Pais (2013)). Coherence zones become especially useful in describing vehicle simulators.

In vehicle driving, motion sensor data is used from several motion sensors. Optic flow is regarded as the main source of motion information, but is heavily influenced by eye-head and body movements (Regan and Beverly (1982), Jamson (2010)). Heading and motion perception in vehicles seems to rely the most on these active gazing strategies to obtain information about heading and velocity based on the visual environment (Land and Horwood (1995), Land and Lee (1994)). If the environment is lacking sufficient fixation points to base heading and velocity estimations on, optic flow becomes more dominant in motion perception (Rushton (1998), Harris and Rogers (1999)).

1.4.2 Discussion

Overall, we need to be careful when describing and measuring human motion sensor dynamics. As we have shown in this chapter, there is a strong dependency of motion perception thresholds distinguishing between active and passive participation of the subject. Available studies suggest are lacking in the influence of active involvement in human motion perception. This could be a result of the difficulty of measuring the perception through a single sensor, while letting the subject perform tasks, which in turn introduces factors like expectation, efference copy and proprioceptive motion perception. In the next chapter, we may be able to expand on the topic of active involvement a bit more, since we will not try to investigate single sensory systems.

For the sake of comparability, many studies on motion perception thresholds use the same motion profiles, which is another topic of interest which could be explored more in-depth (although some studies already exist, including Soyka et al. (2011)). With this same reasoning, not much research has been done on the effects of prolonged exposure to certain stimuli. For vection, temporal effects have been studied and showed to be influential, even after short periods of time (Seno et al. (2018)). This could have implications for other motion sensors as well, or at least, the subjective experience of motion. After next chapter, we may truly indicate what the topics of new avenues of research are with respect to applied motion perception in humans.

Chapter 2

Movement Perception in Vehicle Simulation

Now that we are making the jump from real-world motion perception in humans and the application of the mechanisms of motion perception in vehicles to virtual simulation of vehicles, there are a number of things we need to consider. Since the freedom of motion is subjective to the vehicle that is attempted to be simulated, the perception of motion in that particular vehicle simulator may vary as well compared to other vehicle simulators. Therefore, the motion perception in vehicle simulators is categorised on vehicle type, starting with the most to-be simulated degrees-of-freedom, the flight simulator, in section 2.1.

We usually try to achieve the most realistic feeling or most accurate representation of real-world vehicle driving. Whether this will result in a one-to-one copy of outside vehicle dynamics and motion cues, this chapter will point out. Because increasing realism or, conversely, decreasing it because of limitations in the availability of motion cues in a vehicle simulator can have negative effects on both the immersion and the feeling of presence in a simulator, and the induction of motion sickness, or as it will be used in this chapter, simulator sickness. Therefore, we will discuss these influences in section 2.2.

When this information has all been processed and organised, we may be able to draw conclusions on how we best apply the gathered information. This is done in section 2.3.

2.1 Vehicle Simulators by Vehicle Category

As became clear in chapter 1, movement is perceived through a number of different sensor systems, and a combination of their signals. It is a complicated process to induce a sense of movement in a vehicle simulator based on just one sensory system - albeit visual, vestibular or other. It is usually a combination of these sensors which results in the accurate perception of movement, and that complicates things. As we've seen in chapter 1, the integration of different sensory systems is dependent on the application environment and task. Below, human motion perception in vehicle simulators is described as a function of vehicle type.

2.1.1 Flight Simulators

Flight simulators represent one of the more advanced categories of vehicle simulator platforms. Due to the larger number of degrees of freedom in flying, the motion platform and the motion cueing algorithms become more intricate compared to ground-based vehicle simulators. Or at least, that is the expectation. We will find out below how humans perceive motion in flight simulators, as a function of motion cue type, intensity and combination.

Figure 2.1: Delft University of Technology SIMONA Research Flight Simulator (image source: of Technology (2020)).

Several studies have suggested that sufficient realism is required for the training and transfer of new skills from simulator to reality (Meyer et al. (2012), see Hays et al. (1992) for a review of past studies on training effectiveness). The determination of what is "realistic" can be defined in a number of ways, where one could argue that mechanical fidelity (i.e. one-to-one representation of reality in a simulator) is the most realistic. This may however, not be the most fitting definition, and several more exist (see Pool (2012) for a short review on fidelity definitions and applications). In this section (and chapter, unless indicated otherwise), we will focus on the human-centered motion perception, and its accompanying accuracy of task-performance as a factor within motion perception. Flight simulators as a concept are limited in their ability to recreate all movements of an aircraft for a sustained time due to their physical motion limitations. The creation of vestibular stimuli is thus limited and has to be simulated in other ways. In case of recreating linear accelerations, one such method is the

use of body rotation with respect to Earth's gravity field to fool the vestibular system into thinking it is accelerated (Groen and Bles (2004), DeAngelis and Angelaki (2012)). The use of this method of acceleration simulation is called tilt coordination, and has certain thresholds to be perceived as realistic. See Figure 2.2.

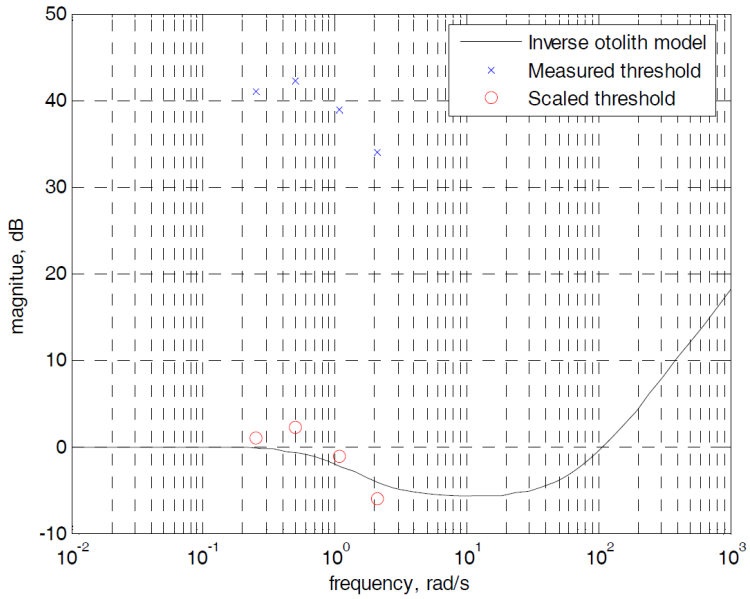

Figure 2.2: Tilt coordination: acceleration perception thresholds for realistic movements, plotted with absolute otolith acceleration threshold model, and scaled thresholds for comparison with otolith model (Groen and Bles (2004)).

These perception limits, however, are determined here for surge acceleration only. Sway and heave, are not included in these analyses, which is likely due to the physical properties of the otolith structure. Furthermore, tilt coordination can only be used to simulate acceleration up to 20 - 30°, thus only simulating accelerations up to 0.5g (Grottoli (2020), from Reymond and Kemeny (2000)). Tilt coordination in the roll direction has to be limited in rate to not be perceived as actual roll, which is mostly critical in flight (and motorcycle) simulators, and usually, a value of 3° per second is attained as a maximum roll rate for the motion not to be perceived as roll (Groen and Bles (2004), Grottoli (2020), Pretto et al. (2014)). There is however a dependency of this limit on the motion cueing algorithm, as Valente Pais et al. (2009a) points out, where 6° per second roll rate was not perceived as roll with certain motion cueing algorithms.

Tilt coordination is one application of simulating accelerations the simulation platform is unable to sustain. In the more general case, motion cueing algorithms need to suppress low-frequency components (i.e. high-pass filtering) of motion in order to not exceed physical limitations of the platform. These motion cueing algorithms are referred to as washout filters (Valente Pais (2013)), and know many variations, which are usually vehicle type-specific. These washout filters reduce low-frequency, continuous accelerations of the motion platform, and return the platform to its initial position, slowly (hence the term, "washout"). Many variants exist, where several include human motion perception models in order to compensate for human perceptual, and optimising the simulator motion towards optimal perception (Sivan et al. (1982), Dagdelen et al. (2009) and Asadi et al. (2016) include perceptual modelling, through predictive modelling techniques and linear quadratic regulator (LQR) methods), instead of accurate representation of real-world aeroplane movements (references based on Natal et al. (2019)). However, constructive validation of these algorithms, and their effects on motion perception in flight simulators is lacking (as of writing this review). Some literature is available of application of human perception-inclusive algorithms in driving simulators, which will be addressed in subsection 2.1.2.

An area of research within flight simulator motion perception where results appear to be scarce, are the influences of active control tasks on motion perception. Some experiments exist (Hosman and van der Vaart (1978), Samji and Reid (1992)), although, as Valente Pais et al. (2012) points out, the former does not include inertial motion feedback, and the latter studies motion perception thresholds on another degree-of-freedom than the one being controlled. Valente Pais et al. (2012) expands on this topic of research, but only on the motion detection in one direction (pitch of an aircraft). What they found was that perception thresholds increased in active tasks compared to passive ones, but not by a great amount. Which is interesting, because many works on motion perception have emphasised the dependency of motion perception on involvement and produced larger differences between passive and active measurements (as in Roark and Junker (1978), Hosman and van der Vaart (1978), Samji and Reid (1992)). The reasoning behind this difference in results is that there seems to be a large influence of small changes in experimental setup, and the measured and controlled degree of freedom differ. But, overall, the research points in the direction of increased motion perception thresholds when actively conducting flight control tasks.

Passive measurements on coherence zones, Valente Pais et al. (2012) concludes, may in the case of flight simulator applications be applied to active control cases under the condition that the control task is performed on another degree-of-freedom than the one the coherence zone applies to. This is not applicable to the case for control tasks on the same degree-of-freedom of motion that is stimulated through inertial cues, since in addition to perceptual fidelity, adequate performance and control behaviour the inertial motion feedback is important.

A critical factor in flight simulator motion perception is how the combined set of motion cues is perceived. The use of mechanically accurate visual motion cues is often implemented, since visual cues are not limited by physical properties of the flight simulator. To what extent inertial cues are introduced in addition to the visual cues determines whether the sensory information is accepted and perceived as accurate - which studies on the coherence zones (see section 1.2) in flight simulators have indeed pointed out.

There are several studies which look into the perceived intensity of the inertial motion cues in flight simulators. Intuitively, there would be the expectation that combined motion cues which represent reality accurately (i.e. a visual-inertial motion gain of one) is the method of eliciting the same motion perception in subjects in a flight simulator compared to real-world aircraft. However, this does not seem to be the case. Groen et al. (2001) found that while attempting to recreate a longitudinal acceleration with combined linear acceleration and rotation of the platform, as well as visual input, inertial motion gains smaller than one were perceived as "accurate". Inertial acceleration simulation with a gain of approximately 0.6 with respect to the visual input were reported. This experiment was performed, however, in a wide field-of-view environment, in a fighter jet cockpit. Only experienced pilots participated, and were not able to influence the behaviour of the simulator with the present controls. This sub-unity gain is reported in other studies as well: Correia Grácio et al. (2013b) describes a sub-unity optimal gain zone (determined with no interaction from pilots on movement, in a simulated passenger aircraft, sway motion only) and Groen et al. (2007) does report preferred lower inertial gains as well (again no interaction from pilots, in a fighter jet cockpit but virtual passenger plane, roll, yaw and pitch motions are considered).

A comparative case between flight simulators has been made in Correia Grácio et al. (2013b) as well. The coherence and optimal gain zones were determined for two separate vehicle simulators. It was investigated whether there was any difference between the simulators, which were both able to represent the same motion task through different motion algorithms accurately. In Figure 2.3, the results are shown.

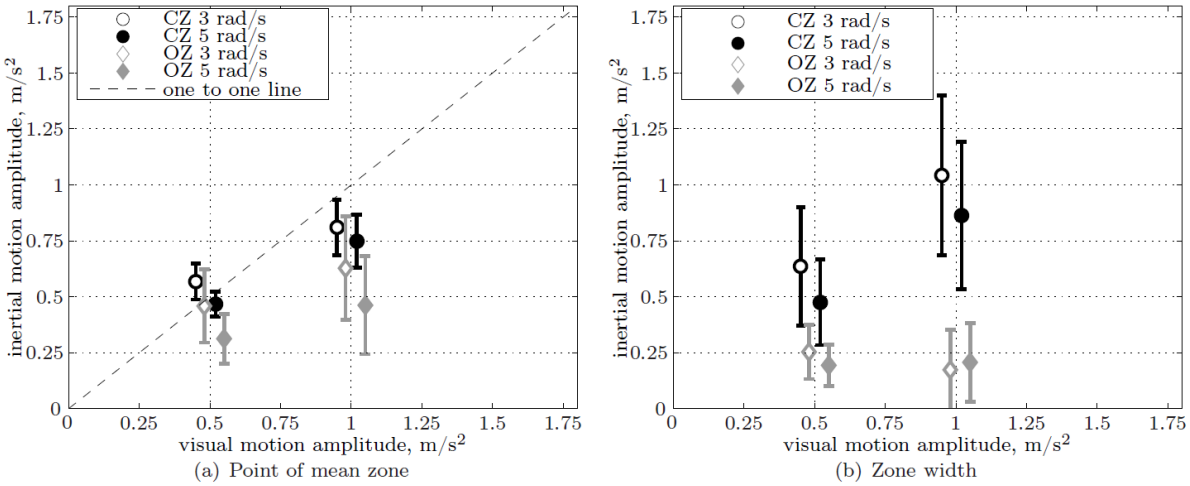

Figure 2.3: Coherence Zone (CZ) and Optimal Zone (OZ) for two different simulators. (a) denotes the mean point of the zones, (b) denotes the width of the zone, with 95% confidence intervals.

Interestingly, no significant difference was found between the two simulators. The signal-to-noise ratio difference between simulators was not large enough to state that they performed significantly differently. So we may conclude that so long as there are no large differences in motion setup (motion platform, cockpit layout, display fidelity) and motion cueing algorithms, the resulting coherence and optimal zones should not differ significantly, as well. This has been further supported in more recent work by Valente Pais et al. (2015), where a third flight simulator was introduced in the comparison. As in earlier work by Valente Pais et al., however, only sway motion was simulated, and subjects were isolated from auditory cues (like wind and engine noise), which has been proven in a helicopter to enhance performance significantly when combined with inertial motion (although the contribution is highly task-dependent) (Meyer et al. (2012)).

An exceptional case where obtaining consistent results in flight simulation becomes difficult, is where spatial disorientation simulation is concerned. Spatial disorientation is a dangerous occurrence among pilots where motion of the aircraft is misperceived due to changes or deprivations in motion cues (see Newman (2007) for an overview of different types of spatial disorientation and their causes). This is an area where the choice of "accurate" simulator performance becomes critical: will the simulator be exactly the same as real-world simulations, and will there only be intended deviations from that to simulate spatial disorientation? Or is it necessary to account for human motion perception in-between, and compensate for it?

This is where current literature is currently expanding upon, because spatial disorientation is one of the most important dangers in piloting where pilots should be prepared for intensively. History proves spatial disorientation to be the second-most prominent cause of aircraft crash incidents (Newman et al. (2012)). Thus, Newman et al. (2012) developed a modelling method which can be applied to centrifuge-based flight simulators, and this model is expanded upon by incorporating human motion perception mechanisms (McGrath et al. (2015)).

Other advances are also made in the direction of haptic feedback in the control mechanism of Unmanned Aerial Vehicles (UAVs) (Malik et al. (2020)) or even applying it in the control system of actual aeroplanes (van Baelen et al. (2018), although no applied test results were recorded; Zikmund et al. (2019), tested in small aircraft, no significant improvement, but setup lacked training and had deficiencies). Although the haptic feedback has not yet proven itself over a large number of control situations, this could be an avenue of increasing flight simulator immersion, increased involvement in the control of an aeroplane (either virtual or real) and actual aeroplane safety systems.

2.1.2 Automobile Simulators

Starting off on the ground-based vehicle simulators, automobile simulators are widely applied nowadays for research on drivers, driver-less cars and driving algorithms. The number of degrees-of-freedom to be simulated is reduced once more, now that we will focus on automobile (car) driving simulators. As opposed to the motorcycle and flight simulators, roll motion is not part of the usual motions a car makes under the control of a driver (in reality; in a simulator roll and pitch motions can be used for the feigning of linear acceleration through rotation: tilt coordination, as we have discussed previously). There is plenty of research considering the performance and motion perception within driving simulators. A short review of driving simulators and studies on motion perception within them is given in Valente Pais (2013). For a more recent, and more critical review of comparative studies between simulator and real-world driving, see Wynne et al. (2019). It is evident that the inclusion of (advanced) inertial motion in driving simulators positively affects human perception and performance, as well as reduce motion sickness (e.g. Bertollini et al. (2014), Pinto et al. (2008)). An example of a high-fidelity driving simulator, the Renault ULTIMATE driving simulator, is shown in Figure 2.4.

Figure 2.4: Renault ULTIMATE driving simulator. Used in Colombet et al. (2018), image source: VSimulation (2020).

In section 1.3, we have focused on some aspects that are of importance in the motion perception in humans while driving. The aforementioned section considered mainly car driving applications, and found that the indifference threshold should determine the limits of perception while driving (i.e. the motion perception thresholds in the presence of other stimuli). Optic flow is regarded as being the most important mechanism of motion perception while driving, combined with active gaze strategies of the driver. This does not mean that inertial cues are not important; they do aid in driving more safely. The velocity underestimation and variance are present in real driving, and, as it turns out, in car driving simulators (Ohta and Komatsu (1991), Ramkhalawansingh et al. (2016b)). The inclusion of visual motion parallax in car driving simulator environments does not seem to influence the experience of driver subjects for a certain driving task. In experiments performed by Hultgren et al. (2012), the inclusion of motion parallax did not even seem noticeable. Some earlier lab experiments support this notion, however inconsistently (as we described in subsection 1.1.2). In experiments by Frenz et al. (2007), the inclusion of pictorial depth cues and motion parallax, as well as stereoscopic visualisation, also did not increase the accuracy of distance estimations.

Although tilt coordination around the pitch axis is used in flight simulators mainly for the simulation of surge acceleration, it is more difficult to apply it there for the simulation of sway motion through roll motion, since roll is an actual movement an aeroplane can make when steered. In a car driving experiment, roll can be used to simulate lateral acceleration, and becomes harder to detect in the presence of other, sometimes conflicting cues. This is shown by Pretto et al. (2014), who performed experiments in a car driving simulator investigating roll motion perception thresholds in presence of other motion cues. The results were the following (Figure 2.5).

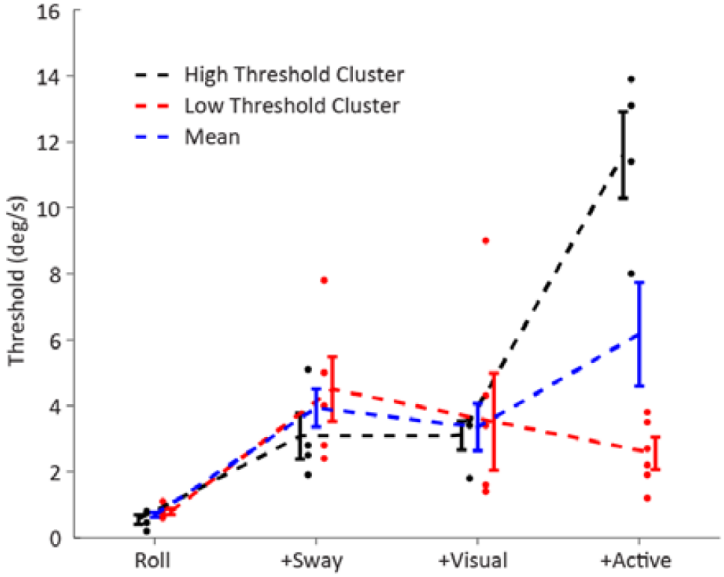

Figure 2.5: Roll motion perception thresholds under influence of other motions on different motion axes and motion perception mechanisms, from Pretto et al. (2014).

What these results show is that roll perception thresholds increase significantly with the addition of other motion cues, but become entirely unpredictable when active involvement of the driver is required. Which supports the notion that active control tasks are heavily influencing the motion perception thresholds on other, different motion axes, and supports the results found by Valente Pais et al. (2012), who found almost no difference between active and passive control cases - when considering control and perception on the same motion axis.

This higher rate is further supported in tilt coordination in pitch direction for acceleration and deceleration manoeuvres in car driving (Colombet et al. (2018)) and in roll direction as well (Fang et al. (2015)). But, as all these studies recognise, tilt coordination only works up to a certain point (i.e. rotation limit), where linear acceleration of the simulator setup has to take over in order to simulate certain movements accurately.

A study (Valente Pais et al. (2009b)) on a car simulator provides an interesting new tactic in the inertial motion cues, where none except for road rumble are used, and compared to a classical washout algorithm, as well as a new motion cueing algorithm. What is interesting, that in most situations, the rumble algorithm elicited subjective realism scores higher than the classical[1] motion algorithm, as well as in more driving-related rating topics. Although driver performance was not a recorded metric, simulator sickness occurrence was, and the rumble algorithm elicited the lowest incidence scores, but not significantly lower than the other two algorithms. The inclusion of human motion perception metrics in applied washout algorithms (as discussed in subsection 2.1.1) in driving simulators is still not widely applied, just like in flight simulators, but designs for these algorithms exist (in addition to those mentioned in subsection 2.1.1):

- Chen and Fu (2010) describes an optimal design process for a theoretical algorithm which includes human perception mechanisms (but not necessarily for car driving simulators).
- Aykent et al. (2011) looked into different washout algorithms (none that included human motion perception, however) and compared them based on subjective criteria. Adaptive algorithms performed slightly better than the classical algorithm.
- Asadi et al. (2019), who plan to validate the proposed fuzzy logic-based algorithm, with human motion perception implemented.
- Qazani et al. (2020), who applied a theoretical model with a neural network to estimate driving performance.

The above mentioned sources should include sufficient material and references for recent methods of motion cueing design, and in the near future, should be supplemented with validational experiments.

We have seen that the introduction of auditory cues to the driver in the vehicle simulator can improve the perception and estimation of velocity. In motorcycle simulator environments, this was proven by Will (2017). The improvement of combined visual and auditory cues with respect to only visual cues in speed perception in car simulators is corroborated by other other research (Horswill and Plooy (2008), Denjean et al. (2012), Ramkhalawansingh et al. (2016a)). All the aforementioned studies were performed in car driving simulators, in which the latter two allowed the subject to control the velocity they were going at, and let them estimate their velocity by controlling it. Only the latter two studies used large field-of-view displays, but also used computer-generated environments, while Horswill and Plooy (2008) used recorded footage, either sped-up or slowed down.

Although the addition of proprioception has had no significant addition to the performance of pilots in flight applications (due to the limited application so far), it appears that in driving simulation, for example force-feedback in steering improves the sense of realism of the simulator (Mourant and Sadhu (2002) (although setup was static) and Mohellebi et al. (2009), as cited by Will (2017)). Which is in line with the findings of Will, applying it to a motorcycle simulator, where driver performance and velocity estimation improved as well with the introduction of proprioceptive motion cues.

[1] Classic washout algorithm, a simple version of the washout filter (discussed in the previous section), with implementation of high-pass filtering and return-to-zero algorithm (Conrad and Schmidt (1970), Valente Pais (2013)).

2.1.3 Motorcycle Simulators

A third category of vehicle simulators are the motorcycle simulators. In addition to the movements a car makes under the influence of a driver, motorcycles are able to roll with respect to their contact point with the ground. Which makes them, in that respect, more related to flight simulators, apart from the possibility of pitching the vehicle (in order to steer it, not to simulate acceleration). Motorcycle drivers have the ability to steer the vehicle with direct feedback through the steering assembly, which results in an extra degree of freedom which can be simulated. For an overview of the current state-of-the-art of motorcycle simulators, see Grottoli (2020), and for a more in-depth review of existing literature considering motion cues and perception in driving simulators, see Will (2017) as well. An example of a motorcycle simulator system is shown in Figure 2.6 below:

Figure 2.6: Cruden Motorcycle Simulator, as used in Westerhof (2017)

As we have reviewed in section 1.3, the use of optic flow and active gaze in road-based vehicle driving for heading and velocity estimation is critical. Recreating these motion cues in motorcycle simulators seems to be the intuitive first step in recreating an accurately perceived motorcycle riding experience. However, a study by Will (2017) showed that the influence of other motion cues, including proprioceptive, auditory and vestibular ones, matter in the correct estimation of self-motion velocity. Influences of simulator qualities like display field-of-view, resolution etc. are discussed in section 2.2. In effect, velocity estimation on a motorcycle simulation increases significantly when introducing more motion cues in addition to visual cues. See Figure 2.7.

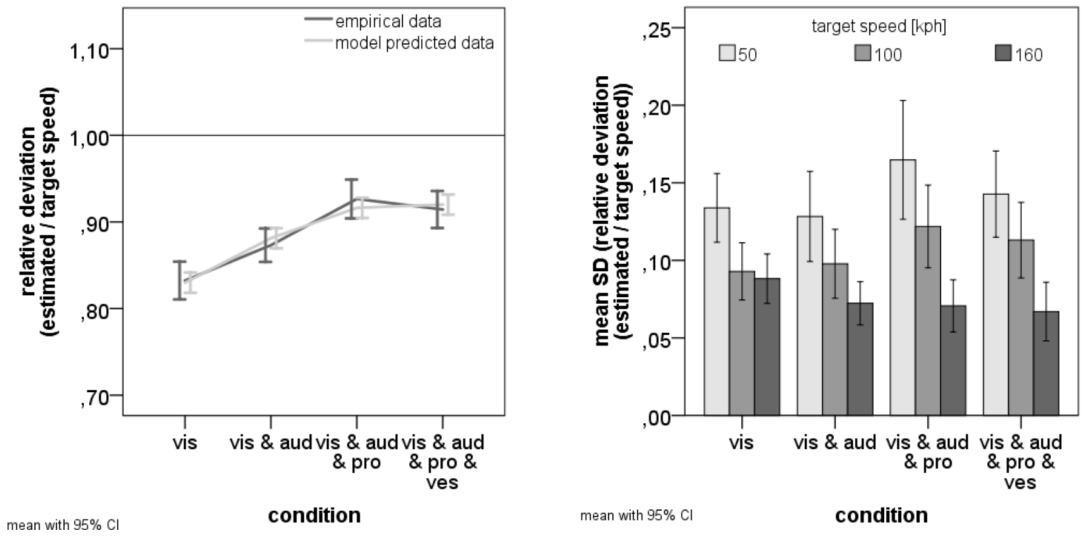

Figure 2.7: Results produced by Will (2017). On the left, the relative deviation from the perfect estimation (= 1,00) is given as a function of motion cues. On the right, the mean Standard Deviation is given as a function of motion cues. Three bars of data are represented, for three different velocities.

The velocity is judged more accurately at higher velocities, it appears, and the addition of several motion cues also improves the estimation of the velocity. What is important to note, is that Will (2017) used a motorcycle simulator with a wide (220°) field-of-view display, such that optic flow could be simulated in the subjects' entire field of view. Evidently, the velocity is underestimated the most by the test subjects when subjected to only visual cues. The inclusion of haptic and proprioceptive cues appears to have the greatest influence on velocity estimation, while the addition of vestibular cues does not affect the velocity estimation. As will be shown in the next section on automobile driving simulators, the impression that the addition of auditory cues in vehicle simulation improves velocity estimation performance found by Will, seems to be a common property among vehicle simulators.

However, the above results for velocity estimation do not include the active participation of the rider in controlling the velocity. As we have discussed, the introduction of active control tasks can influence the motion perception in vehicle simulators. Luckily, Will expands his research in that regard as well, and investigates the differences between active and passive control cases in Figure 2.8.

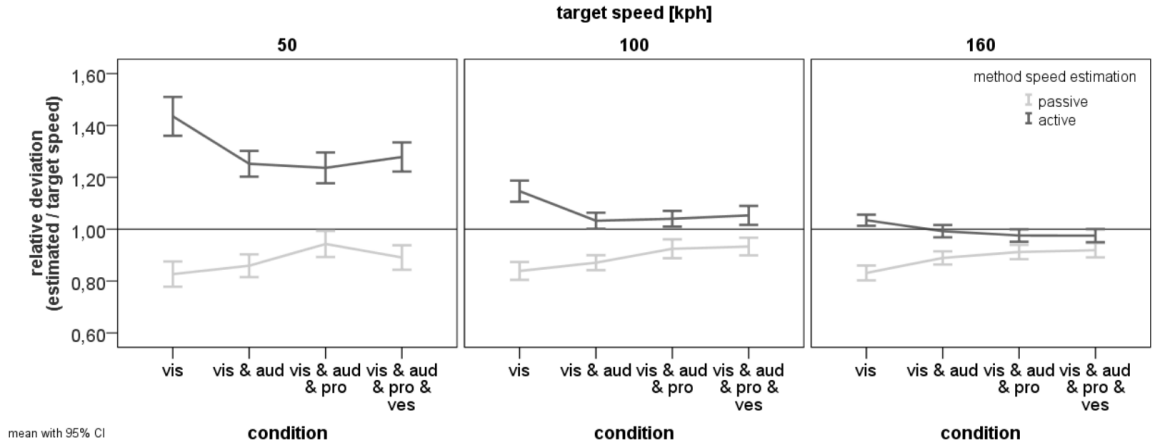

Figure 2.8: Results produced by Will (2017). Now, with users being able to influence the simulator's velocity, the mean deviation reduces to an almost perfect estimation at high velocities, but falls behind at lower velocities.

These results are in accordance with earlier research by What is important to note in both the passive and active results of Will (2017) is that the velocities at which the experiments were performed were relatively high. Extrapolating the trend observable in these results shows that at lower velocities, the error in estimation could really increase. The study by Grottoli (2020) could fill this gap of research results. Although this research was not pointed at velocity estimation and focused more on whether certain manoeuvres were executable. Underestimation of velocities was still present here, but still within the same levels Will (2017) reported - but no auditory or proprioceptive cues were present in Grottoli's research. Grottoli (2020) investigated influences of simulator motion and visual display type influences on driver performance at low velocities. Significantly less subjects were able to complete experiments using a HMD compared to an external display, due to simulator sickness occurrence. Furthermore, he found that motion of the platform only improved performance significantly in case of braking scenarios, but improved subjective realism experience within subjects.

A difficulty lies in letting a motorcycle simulator user perceive accurate cornering behaviour. Due to physical limitations of motion platforms, continuous accelerations are difficult to simulate, as was discussed in previous sections. Especially in motorcycle driving, where roll motion is usually accompanied by lateral acceleration - whereas in aeroplanes, independent roll is also possible. Washout filters can account for this for a certain period, but tilt coordination becomes difficult when lateral acceleration is absent with a tilted motorcycle simulator and compensation by balancing of the rider is necessary to not fall of the simulator. Westerhof (2017) reduced this problem by reducing physical tilt of the simulator to less than a quarter of the visual tilt, and did not include tilt coordination within the applied classic washout filter, similar to what Cossalter et al. (2010) used in the UNIPD motorcycle simulator. The latter study includes subjective ratings of the motorcycle simulator behaviour, with manual tuning of the washout algorithm to improve perceptual fidelity of the simulator. Grottoli (2020) used an adapted classic motion filter with adaptive washout, with tilt coordination implemented, but limited to a certain roll-rate for it not be be perceived as roll (the same reasoning for this limit as in subsection 2.1.1). In Shahar et al. (2014), participants were allowed to tune the motorcycle simulator parameters themselves, focused on roll parameters, with complete freedom. Participants were generally found to reduce the physical roll of the setup to a small fraction of the visual roll, although a dependency of this ratio was apparent. This setup, however, only simulated physical roll, and no other accelerations.

As with flight simulators, application and validation of advanced motion cueing algorithms which internally account for human perception is lacking.

2.1.4 Miscellaneous Vehicle Simulators

In this section, we will look into other appliances of vehicle simulators and the accompanying methods of motion perception. The vehicle simulators put into this category are applied less in day-to-day situations, or are very purpose-specific in their design.

As we have looked into visual motion perception quite in-depth up to this point, the results obtained in the majority of the studies consider the test subjects sitting down. This is logical considering their respective applications, but the effects of vehicle simulators where the user is usually standing up has not been considered yet in this literature review. One such application is a ship simulator. A quantitative study on the effects of visual pitch and roll in a ship simulator, as well as actual pitch and roll motion, reported an increase in postural sway under the influence of visual motion simulation of a ship (Murai et al. (2010)). Considering that sea sickness is a common occurrence, which has been related to (conflicting) motion cues in certain low-frequency ranges (Stoffregen and Smart (1998)), the similarity to simulator sickness is evident (Johnson (2005), but also, see section 2.2). The test setup and simulator used in Murai et al. (2010) is displayed in Figure 2.9.

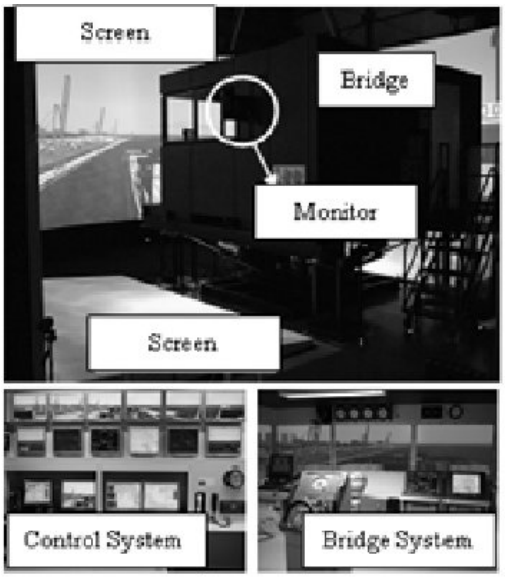

Figure 2.9: Ship bridge simulator used by Murai et al. (2010). No better quality image was available.

We mentioned that in automobile driving simulators, the effects of stereoscopic vision and motion parallax into the visual motion system did not really alter the experience, or driver performance. An application where it appears that stereoscopic vision becomes more important is when for the vehicle task at hand, accurate distance perception is necessary. One such application is the crane simulator, where it was shown by Juang et al. (2013) that performance of operators improved when kinesthetic vision[2] and stereoscopic visual cues were applied. Operator confidence and intuition improved significantly, as well.

[2]Kinesthetic vision is a visual rendering application where images on the screen are displayed with respect to the orientation and location of the observer's head. Stationary objects can be viewed from multiple angles, in practice, and a sense of depth and dimension is given to the displayed image (Juang et al. (2013)).

One type of vehicle simulator which requires a larger level of involvement is the bicycle simulator. Although many iterations of (research) bicycle simulator platforms exist (e.g. Hernández-Melgarejo et al. (2019), Dialynas et al. (2019), Yap et al. (2018)), the incorporation of motion is usually limited to the virtual environment (i.e. visual cues only). Some form of proprioception is usually applied in the steering mechanism of the bicycle simulators, to simulate correct steering torque, but studies focused on motion perception mechanisms in these cases is lacking. What we can theorise, comparing bicycle simulators to motorcycle simulators, is that the introduction of physical motion to the system will improve the overall experience and involvement, and could decrease sickness occurrence (but more on that in section 2.2). See Figure 2.10 for a visualisation of a bicycle research simulator:

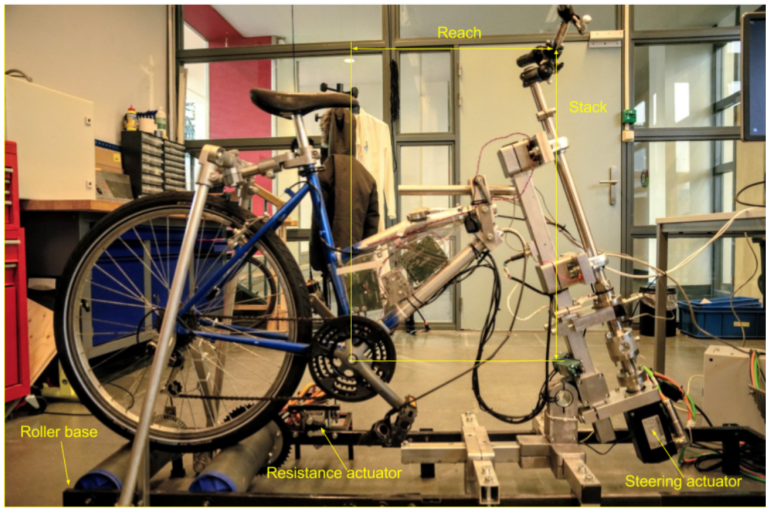

Figure 2.10: Bicycle simulator, from Dialynas et al. (2019)

Nog aanvullen

2.2 Simulator Sickness and Immersion: A Trade-off

The quality of experience and immersion in a vehicle simulator - especially those meant for exercise and gaming - are some of the most important aspects of vehicle simulators, apart from realism. What one tries to achieve in a vehicle simulator should not be impeded by factors like simulator sickness or a lack of immersion. In this section, we will discuss the possible causes for simulator sickness, how to resolve them, and how this affects the immersion in a vehicle simulator.

2.2.1 Cause for Simulator Sickness

Bertolini and Straumann (2016) provides an overview for several theoretical causes for simulator sickness (or motion sickness, these definitions are used interchangeably here). We will describe them briefly below. Several mathematical models exist for the prediction of motion sickness, which have been reviewed by Lewkowicz (2016), where he presents a constructive basis for a choice of motion sickness model.

Sensory Conflict - Perceptual Origin of Motion Sickness

The first theory states that conflict of motion stimuli alone is not sufficient to cause motion sickness. Motion sickness only occurs when the pattern of new, different motion signals is not coherent with the expectation based on previous experiences (Reason and Brand (1975)). The use of virtual environments induces a sense of self-motion, as we have seen in previous sections. When this apparent self-motion is perceived through visual cues, but not corroborated correctly by inertial or other motion sensors, simulator sickness is likely to occur. Conversely, by making sure that in a simulator these sensory inputs give the same information about the movement of the user, simulator sickness is likely to be reduced (Johnson (2005)). This notion is supported by multiple studies in the past, such as Oman (1982) and Reason (1978), among others (based on Reason and Brand (1975)). However, it has been shown more recently that only under the influence of vection only, motion sickness is not necessarily induced (Kuiper et al. (2019)). Which is contradicting the earlier found results, but explained by Kuiper et al. that subjective susceptibility to motion sickness, a different basis for motion sickness (loss of orientation with respect to gravity) or abstraction of the virtual environment. As well as the notion that motion sickness could be caused by inconsistent vection stimuli, instead of the constant one used here.

A further simplification of this theory is the subjective vertical conflict theory, where the subjective vertical of the observer and the vertical provided by motion sensors are not in accordance with each other (for example, Bles et al. (1998)). This theory, however, does not cover all cases, since there are incidents where sensory conflict does predict and explain motion sickness, while the subjective vertical does not (see Bertolini and Straumann (2016) for applied examples).

A third theory states that motion sickness is related to the difference between the yaw eigenvector of velocity storage[3] (where integration and coordination of self-motion perception signals takes place) and the actual vestibular velocity signal. This theory was designed specifically for head rotations, but it takes up several parallels with the subjective vertical conflict theory.

[3]Velocity storage is an internal process where velocity data is "stored", such that compensatory eye-movements are made with respect to the expected (or stored) velocity Raphan et al. (1979)

Postural Instability - Sensori-motor Origin of Motion Sickness

However, a fourth and unique theory exists: this theory points at postural instability as the cause of motion sickness (Riccio and Stoffregen (1991)). The notion for postural instability is that small perturbations of the subject's body are introduced at the same frequency range as the body's postural control system. This leads to postural instabilities, however small, and this can lead to motion sickness. According to Guignard and McCauley (1991) and Lawther and Griffin (1988), motion sickness occurs at frequencies in the range between 0.08 and 0.4 Hz, which is also a characteristic range of frequencies of oscillations in ships, trains and aircraft.

One experiment that corroborates these results, is another study performed by Stoffregen et al. (2000). They performed an experiment on a number of subjects which were all subjected to an optic flow pattern in the range of frequencies described above. A distinct categorisation was applied to the subjects beforehand, during and after the experiments, based on the Simulator Sickness Questionnaire designed by Kennedy and Lane (1993). Postural motion was also recorded beforehand and during the experiments. From the participants, those that were flagged as "at risk for motion sickness" did indeed get sick from the experiments. Those that weren't, did not. Preceding the motion sickness, in all cases, was an increase in postural motion and sway, which can in the future be used as an indicator for motion sickness that is being developed.

In more recent research (Groen and Bos (2008)), it was found that, in a vehicle simulator, the incidence of simulator sickness was dependent on the frequency of the mismatch between the motion cues in the simulator environment. Simulator sickness occurred more often at a mismatch frequency of 0.08 Hz than at 0.46 Hz, although this may also be due to differences in the experiment design. This frequency range is, in any case, the critical range for motion sickness as it was previously defined.

A number of shortcomings of this theory are the following: firstly, this theory already excludes situations where no postural control is required; while lying down or sitting, for example. Moreover, it assumes that motor control within the human body is ranked above the perception of being upright, which is a debated phenomenon, according to Bertolini and Straumann (2016).

2.2.2 Simulator Sickness and Immersion: Dependence on Stimulus Type

Can simulator sickness then be reduced by means of introducing (accurate) motion to the system? The first theory of causes of motion sickness suggests that it should, and a more recent study by Westerhof (2017) partially answers this question. He performed experiments on the Cruden Motorcycle simulator, a setup which consists of a hexapod-mounted motorcycle and a head-mounted display (HMD) system.

In this setup, a curve-driving trajectory was to be followed by test subjects, either with motion enabled or disabled. The results from the Simulator Sickness Questionnaire (Kennedy and Lane (1993)) showed that with motion of the platform enabled, all aspects of simulator sickness manifestations (Nausea, oculomotor discomfort and disorientation) did not change in a statistically significant manner, but suggests a decrease in discomfort with motion enabled. These results, however, were based on test subjects flagged as being at lower risk of simulator sickness. There was, however, a statistically significant increase in overall sense of presence, when motion was enabled in the experiments of Westerhof (2017). In experiments by Grottoli (2020), however, discomfort due to motion sickness was so high with a HMD, that a large portion of the test subjects dropped out before testing. The setup was altered to one with a small external monitor to be able to continue testing. Grottoli shows, in accordance with Westerhof (2017), that simulator sickness decreases with motion enabled in the simulator, but decreases more with no HMD system. In automobile driving (Aykent et al. (2014)), the addition of motion seems to decrease subjective motion sickness incidence as well.

Will (2017) did also incorporate both the simulator sickness and immersion factors in his research on the effects of motion stimuli. The categorisation of test subjects based on susceptibility to simulator sickness is absent here, but the size of the pool of subjects is larger. And, it should be noted, all participants were new to dynamic motorcycle simulators in Will's research - although no head-mounted display was used, but a large field-of-view projection system. In the results (shown in Figure 2.11), no significant difference between cues on influence on simulator sickness is visible (both in passive and active involvement of the rider). However, when comparing active and passive cases, an overall increase in SSQ scores was observed. In the active case, subjects were actively able to influence the velocity of the motorcycle simulator, whereas in the passive case, subjects only acted as observers at a predetermined velocity.

Subjective ratings on spatial presence, interface quality and involvement also raised significantly when more cues were introduced to the simulator. Especially the inclusion of proprioceptive and vestibular cues increased the involvement and presence of the riders. See Figure 2.11.

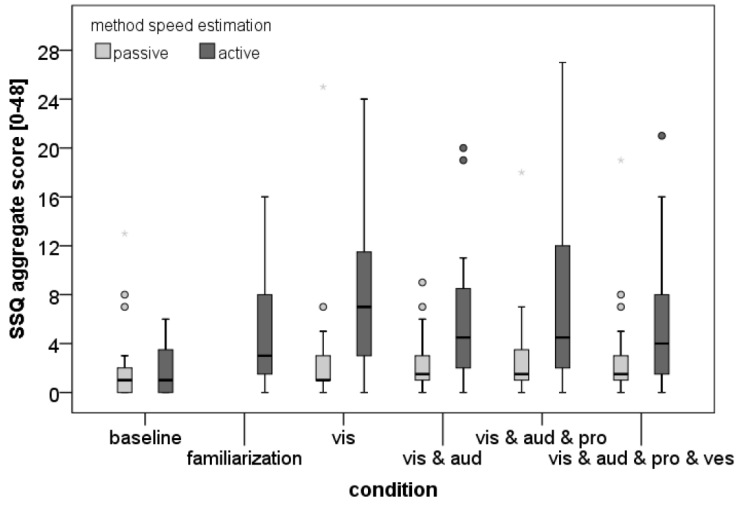

(a) Simulator Sickness Scores

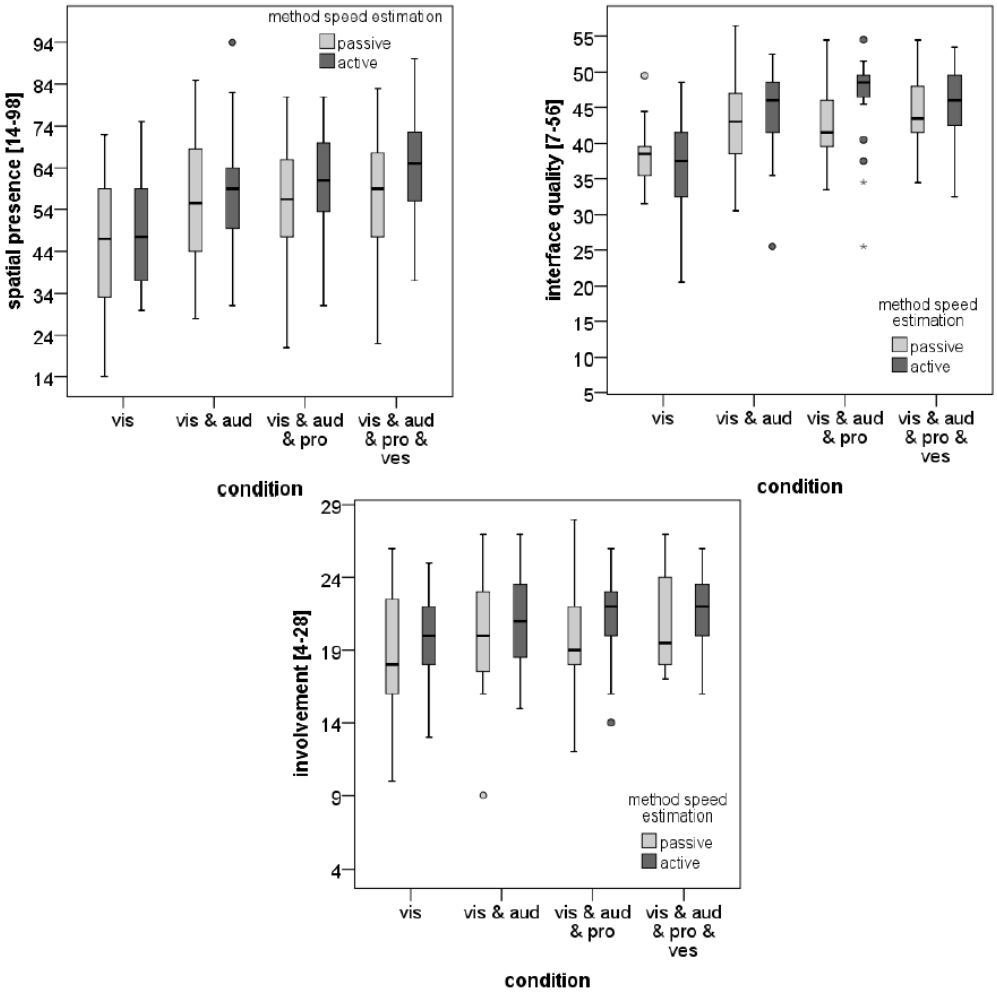

(b) Subjective Immersion Scores

Figure 2.11: Results from in Will (2017). Scores are given as a function of different motion cues, as well as the active and passive rider involvement cases.

It appears from these results that increased involvement of the user results in both the increased immersion and spatial presence, but increased sickness susceptibility as well.

On the topic of immersion and comfort of vehicle simulators, another subject-oriented study of the quality and accuracy of driving in a motion simulator is that performed by Berthoz et al. (2013). They looked into the influence of physical motion gain, compared to real-world driving, in a multi-track vehicle (which differentiates it from the researches by Will (2017) and Westerhof (2017)). Used were three different motion simulators, wherein subjects performed three distinct experiments. What they found was that a sub-unity motion gain is preferred by drivers (between 0.4 and 0.75), which is in accordance with earlier research (Greenberg et al. (2003), Correia Grácio et al. (2013b), Groen et al. (2007), although more recent studies have indicated higher gains are best employed: Fischer and Werneke (2008), Berger et al. (2010)). This preference for motion gains may be coupled to the underestimation of speed humans typically experience in vehicle simulators, such that the simulated and physical velocity match the underestimated model (Berthoz et al. (2013)). These gains only become noticeable by subjects at around 0.9 for translational movements, and 0.87 for tilting motion (Jamson (2010)). Influences of the fidelity of the visual feedback may also be a cause for the motion to be required to be scaled down, to maintain perceptual coherence.

2.2.3 Influences of Visual Fidelity

Visual cues are dependent on the way they are presented to us, as this section will point out. With visual cues, dependency on display refresh rate, resolution (pixel density), field of view and combinations thereof are more prevalent. In the section below, each of these categories is discussed briefly, and the effects of the variable in visual fidelity are discussed.

Field of View

Field-of-view (FOV) largely determines what portion of peripheral vision contributes to the motion perception in a virtual environment. Increasing the FOV is an effective method of increasing the sense of self-motion (Dichgans and Brandt (1978), Held et al. (1975)). Jamson (2000) found that there was a 120° horizontal field of view minimum for accurate speed perception. A study which looks into the effects of FOV on subjective sense of presence and dispersion is one by Been-Lirn Duh et al. (2001). The research group here looked into the effects of increasing FOV by subjecting the test subjects to an increasing field of view to stimulate the peripheral vision more and more. What they reported was a little bit of a counter-intuitive result. When the FOV angle increased, subjects reported a higher level of dispersion and had more difficulty trying to keep their balance. With greater field of view, the subjects received a greater amount of information through their peripheral vision, which apparently acted as more disturbing. In the Figure 2.12, the level of subjective dispersion as a function of FOV angle and different virtual environments is given.

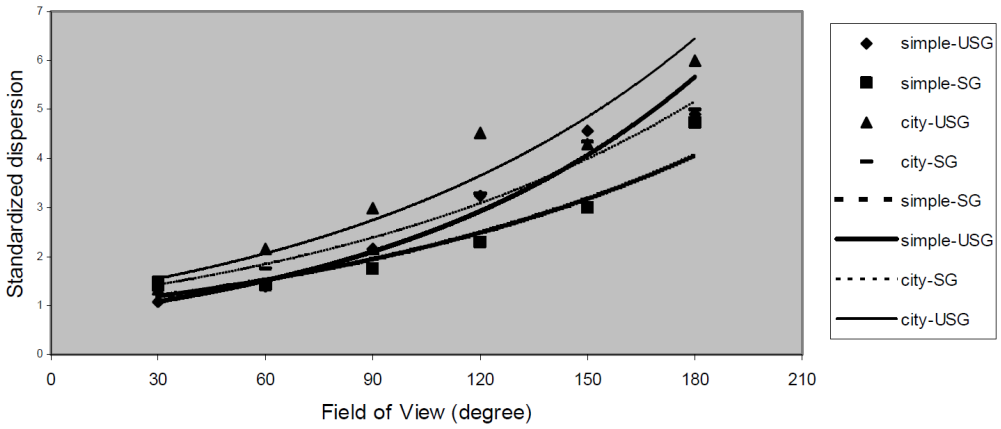

Figure 2.12: Dispersion as a function of FOV, as presented by Been-Lirn Duh et al. (2001). Different lines represent different scenes.

This suggests that higher FOV angles lead to more postural instability, which is a conclusion that is also supported by other studies (DiZio and Lackner (1997), Kenyon and Kneller (1993), Kennedy et al. (1989)). On the other hand, the widening of the FOV introduces a greater sense of immersion and conversely, a limited FOV may degrade the user's sense of presence (Prothero and Hoffman (1995)), but may also reduce simulator sickness (Lin et al. (2002), although research could expand on this topic with current technology). Field of view, together with additional size and depth cues, has been shown to affect the preferred visual motion cue gain with respect to inertial motion. With increasing field-of-view, visual gains decreased, but the visual gain also shows a dependency on motion direction (surge, sway and yaw) within the virtual scene (Correia Grácio et al. (2013a)). With yaw, a one-to-one visual gain was preferred, whereas with surge, the highest visual gains were set by subjects, averaging around 4. This difference in motion directions is explained through the optic flow content of different virtual reality movements, and their relation to depth perception.

Display Type - Head-mounted Display or Other

As discussed, the field-of-view size plays an important role in self-motion perception (velocity perception) (Kemeny and Panerai (2003)). This wide field of view can be achieved through a number of methods. The most prevalent options are the use of a large external digital monitors, projection screens and the use of a head-mounted displays. On the one hand, increasing the FOV increases immersion and improves user presence in the virtual environment, as we've seen, but on the other, simulator sickness can become more prevalent. One recent study that looked into the influences of different display types on simulator sickness is one performed by Mittelstaedt et al. (2018).

In this study, subjects were placed in a virtual environment and controlled a bicycle through different methods; either with a stationary bicycle ergometer or a gamepad controller. They were also put through the experiment with either a large screen display or a HMD as visual input device. What we would expect from the information presented in this section above is that the HMD will prove to be the most immersive experience (since it usually has the largest field of view), but also the one to be the likeliest to cause simulator sickness. In the previous section of this chapter, active involvement of the subjects was also suggested as a method to increase immersion, but this could also increase simulator sickness incidence. The results, again based on the Simulator Sickness Questionnaire by Kennedy and Lane (1993), are in agreement with this hypothesis. The results are presented in Figure 2.13 below.

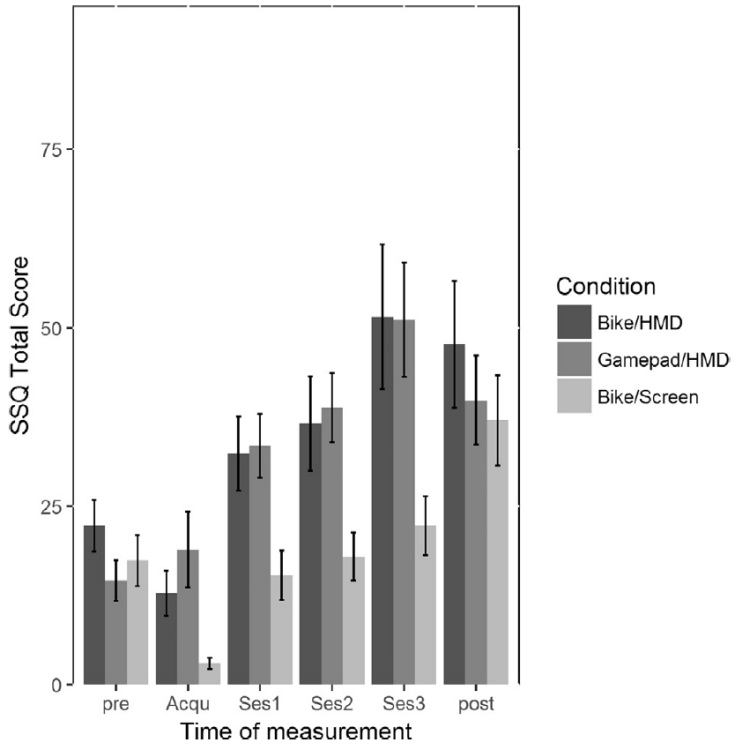

Figure 2.13: Experiment results as presented by Mittelstaedt et al. (2018). Subjects were queried at different stages of the experiment: Acqu = familiarization phase in VR, Ses1-Ses3 = three consecutive navigation sessions, post = after VR immersion

The results do not differ much between the bike and gamepad as input devices, combined with the HMD. Both score relatively high on the SSQ score. Using an external display resulted in lower scores of motion sickness during use, but afterwards still resulted in relatively high scores, which implies time-related effects in simulator sickness. It could be that the SSQ score are as high as they are because no physical motion was introduced to the users, which has been shown in vehicle simulators

to decrease motion sickness (see section 2.1). However, in Grottoli (2020), some subjects dropped out or were not able to complete motorcycle driving experiments on a motion platform with a HMD, but were able to with an external display. As found in the previously mentioned study by Westerhof (2017), simulator sickness can decrease significantly when motion is introduced to the user, but it does not disappear. In addition to that, according to Westerhof's research, sense of presence in the virtual reality environment also increased when motion was enabled for the motorcycle simulator users. However, the increase in presence was not as dramatic as the decrease in simulator sickness symptoms.

Overall, it is encouraging to see that more recent research, like those performed by Mittelstaedt et al. (2018) and Westerhof (2017), are still in agreement with earlier research by Been-Lirn Duh et al. (2001), in terms of the effects of field-of-view and display type. One recent study which benchmarks the performance of a vehicle simulator using an external monitor, and a HMD, compared to an actual real-world driving experiment is one by Parduzi et al. (2020). They found that performance of the driver between external display and HMD did not differ significantly, but that immersion factors did increase with the HMD. Simulator sickness, did not differ significantly in both cases, either, but this could be due to short experiment durations, as per Parduzi, or an increase in HMD quality and fidelity compared to earlier experiments. The HMD did however put more strain on the users, according to the Driver-Activity Load Index. Interestingly enough, the test subjects drove at lower speeds in the virtual environments, driving the slowest with the external monitor system. This could be a result of the now well-known issue of velocity underestimation in virtual environments based on visual cues. A similar series of experiments conducted by Benz et al. (2019) found similar results to Parduzi et al. (2020), where a comparison is made between a HMD and a projector-based visual system, within an actual real car simulator (i.e. a car on a test track, with simulated visual inputs). In Benz et al. (2019), both systems had similar display qualities, but the HMD was experienced as more simulator sickness-inducing, while presence was not significantly affected. This experiment can be used as a comparison between HMD and external displays, but translates less well for driving simulators, since the set of other motion cues (auditory, vestibular, proprioceptive and even efference copies) was equal to a real-world drive, due to the experiments taking place in a real car. On the other hand, it shows that with an ideal package of motion cues, simulator sickness is reduced greatly. This set of motion cues would have to be reproduced very accurately to be able to verify the results by Benz et al. in a driving simulator.

Display Refresh Rate and Delay

There are more factors that influence the experience someone has in a virtual environment. We have considered the display field of view and type, but not yet display fidelity (resolution, image quality) and display refresh rate. Since as we have seen in previous experiments, HMDs provide the best immersion, but also the highest risk of simulator sickness, the virtual display quality factors are evaluated for HMD displays.

Katsigiannis et al. (2019) provides results on this topic. Test subjects were subjected to a virtual cycling environment where they were able to control the speed of the bicycle by pedalling on the setup, and steer in the virtual environment using buttons. The virtual environment cycled between resolutions of the HMD display as well as the refresh rate of the HMD display. The results were the following:

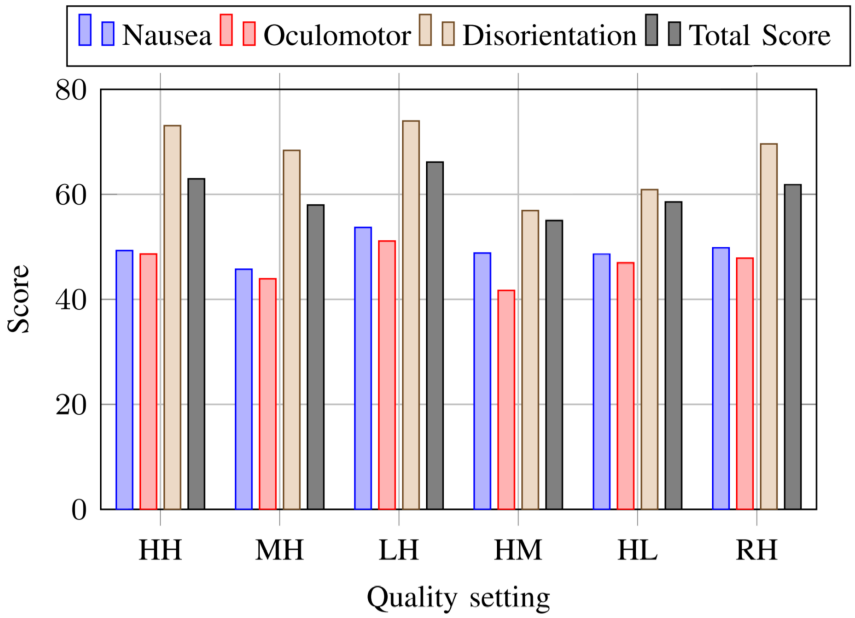

Figure 2.14: Average SSQ scores of participants. First letter in the indices indicates texture quality, ranging from H, M, L and R as 1024×1024, 512×512, 256×256 and random textures at 256×256 pixels, respectively. The second letter in the indices indicates display framerate, ranging from H, M and L as 60, 30 and 15 frames per second respectively.

From these results, Katsigiannis was not able to obtain statistically significant results which indicate one setting to result in less simulator sickness symptoms than the other. There were, however, significant differences in quality experience. Test subjects were asked to score the experience of the virtual environment in the same different configurations as described in Figure 2.14. The results are given in Figure 2.15.

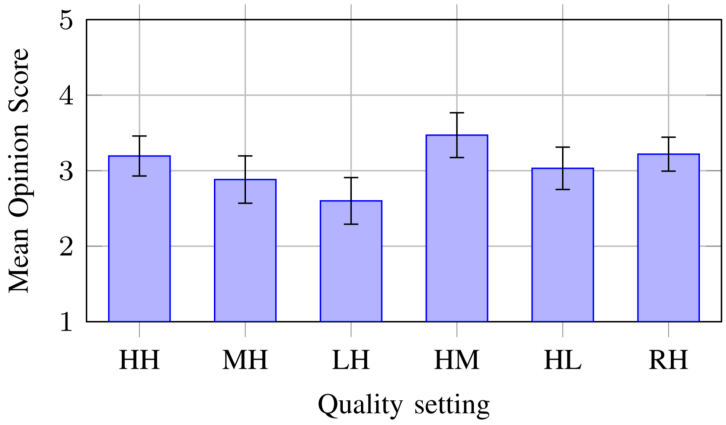

Figure 2.15: Mean rated scores with 95% confidence intervals. Users were able to rate the experience with a score from 1 to 5. From Katsigiannis et al. (2019).

It appears that the highest framerate settings are not necessary for the best experience of the virtual environment. However, having low texture quality at high framerates seems to be even more disruptive to the overall experience. This group of test subjects, however, also had individuals in them with prior simulator experience. Interestingly enough, subjects with regular virtual reality experiences indicated half the simulator sickness scores compared to those with no previous virtual reality experience. It appears that prior experience can reduce the experienced simulator sickness, so this suggests that there is a level of getting used to the environment, before the experience remains comfortable.

Latency effects in virtual environments are also influential on one's ability to handle tasks. Delay in the visual feedback can slow the response of the user and thereby decrease the user's ability to perform for example tracking and pursuit tasks (Foulkes and Miall (2000)). More recent work has also indicated that the frequency of visual feedback delay is the affecting factor in sickness in virtual environments, as opposed to the amplitude of the visual feedback delay (Kinsella et al. (2016)). Increasing variable latency can decrease the users' performance significantly, as became clear from the test results of Wilson et al. (2020), where the test subjects had to perform certain tasks either with constant or varying latency. Simulator sickness levels did not achieve as high a level as in previous studies, according to Wilson et al. (2020), but this may be due to the level of concentration required in performing the prescribed tasks. This is in accordance with other research on the same premise, that higher concentration levels result in lower levels of simulator sickness (Bos (2015), Matsangas et al. (2014)). This suggests that a higher level of involvement could be used as a method to decrease simulator sickness.

2.3 Summary on Vehicle Simulator Motion Perception

In this chapter, we set out to investigate the motion perception in humans in vehicle simulators. Several mechanisms of letting humans perceive motion while subjected to the limited availability of motion cues due to physical and electrical limitations were discussed, as well as limitations in human acceptance of motion. The found information is summarised below.

In the final chapter of this literature review, chapter 3, we will discuss the presented information, indicate differences and commonalities between real-world and vehicle simulator motion perception. Future topics of research will be implied.

Vehicle Simulator Motion Perception

Vehicle simulators are tools of research, transfer of skills and training, and generally profit from increased realism (Meyer et al. (2012), Hays et al. (1992)). One aspect all motion-based vehicle simulators have to deal with, is limited actuator range, thus limited motion space. A wide-applied method of incorporating this in the motion design, is the use of washout filters (Valente Pais (2013)). These motion algorithms are an expanding area of research, with more advanced models incorporating human motion perception dynamics for increased perceived realism (Sivan et al. (1982), Dagdelen et al. (2009), Asadi et al. (2016)). Experimental data on human motion perception with advanced motion cueing algorithms employed, is lacking.

A strategy to let humans perceive sustained linear accelerations across vehicle simulators is the use of tilt coordination, applied in flight simulators (Valente Pais (2013)), automobile driving simulators (Pretto et al. (2014), Valente Pais et al. (2012), Colombet et al. (2018), Fang et al. (2015)) and motorcycle simulators (Grottoli (2020)), although difficulties occur in the latter category due to absence of lateral acceleration forces, and tilt is reduced (in roll direction) to prevent falling off (Westerhof (2017), Cossalter et al. (2010), Shahar et al. (2014)). Tilt coordination rates and angles are usually limited to remain below motion perception thresholds for it to be effectively perceived as linear acceleration (Reymond et al. (2001), Groen and Bles (2004)), although there seems to be a dependency of this limit on motion cueing algorithm (Valente Pais et al. (2009a)) or presence of other motion cues and their direction (Valente Pais et al. (2012), Pretto et al. (2014), Colombet et al. (2018), Fang et al. (2015)). In general, motion perception thresholds increase in presence of motion on other motion axes.

Focusing on flight simulators, humans prefer an inertial motion with a gain lower than one compared to visual motion, in general (Groen et al. (2001), Groen et al. (2007), Correia Grácio et al. (2013a), Fischer and Werneke (2008), Berger et al. (2010)) with no active involvement of the subjects on platform motion. This preferred relation between motion cues manifests itself in coherence and optimal zones between flight simulators (Valente Pais et al. (2015)), which implicates a degree of transferability of coherence zones between flight simulators when motion pattern fidelity is similar. Simulated auditory cues in flight simulators have not been investigated greatly, although it has been proven in a helicopter simulator that auditory cues improve pilot performance significantly (Meyer et al. (2012)). The same goes for haptic and tactile motion cues, although it is an ongoing area of investigation in real aeroplanes (van Baelen et al. (2018), Zikmund et al. (2019)) or remote UAV control (Malik et al. (2020)).

Automobile simulators employ similar tactics to improve human motion perception and motion cue fidelity. One observed property across driving simulators - and real-world driving, see section 1.3 - including motorcycle simulators, is the underestimation of velocity (Ohta and Komatsu (1991), Ramkhalawansingh et al. (2016b)), where adding additional motion cues to visual ones usually improves the sense of realism and velocity perception accuracy (Horswill and Plooy (2008), Denjean et al. (2012), Ramkhalawansingh et al. (2016a), Mohellebi et al. (2009), Will (2017)). Although advanced

washout filters may improve motion perception, in certain driving tasks, just rumble can be perceived just as realistic as classic washout algorithms (Valente Pais et al. (2009a)). In addition to that, the addition of motion parallax, used for heading and velocity estimation in real driving (see section 1.3), to a driving simulator's visual system is usually not noticed by drivers, and therefore rarely necessary in certain cases (Hultgren et al. (2012)).

Active involvement in vehicle simulator motion has been determined to be of influence on motion perception in the simulator (Roark and Junker (1978), Hosman and van der Vaart (1978), Samji and Reid (1992)), although the motion axis of this active involvement is a factor, as well as the task, which can create large differences in motion perception between humans (Pretto et al. (2014)).

Simulator Sickness & Immersion Factors

Several origins of motion (or similarly, simulator) sickness have been theorised, the two most prevalent being the theory of sensory conflict (Reason and Brand (1975), Reason (1978), Oman (1982)) and the theory of postural instability (Riccio and Stoffregen (1991), Guignard and McCauley (1991), Stoffregen et al. (2000)). The first assumes simulator sickness is related to discrepancies between human motion sensors, whereas the latter is based on incoming motion having a frequency content similar to postural control mechanisms in humans.

Measurements on simulator sickness occurrence relate simulator sickness to various motion cueing variables in vehicle simulators:

- The introduction of physical simulator motion in addition to only visual cues reduces simulator sickness incidence (Aykent et al. (2014), Grottoli (2020), Westerhof (2017)).
- The introduction of auditory and proprioceptive motion cues improves immersion in a motorcycle simulator, although it does not necessarily reduce simulator sickness (Will (2017)).
- Active involvement of the user can decrease simulator sickness levels (Matsangas et al. (2014), Bos (2015), Wilson et al. (2020)), although this is dependent on task intensity, since Will (2017) did not report a decrease in simulator sickness with limited simulator control.

Visual fidelity plays an important role in simulator sickness and immersion as well; when comparing Head-Mounted Displays (HMDs) and external projection devices, HMDs usually cause higher levels of simulator sickness than external displays (Mittelstaedt et al. (2018), Westerhof (2017), Grottoli (2020)). The size of the display's field-of-view (FOV) influences immersion and simulator sickness incidence as well; increasing the available FOV (with for example a HMD) increases immersion, but also simulator sickness incidence (Been-Lirn Duh et al. (2001), DiZio and Lackner (1997), Prothero and Hoffman (1995)) and has been shown to affect optimal gain zones (Correia Grácio et al. (2013a)). However, recent studies have indicated less difference in simulator sickness between display types, which can be due to increasing HMD qualities (Parduzi et al. (2020), Benz et al. (2019)). Increasing the FOV assists correct velocity estimation (Kemeny and Panerai (2003), Jamson (2000)), which supports the premise from chapter 1 of basing velocity estimations on optic flow.

Increasing the texture quality (Katsigiannis et al. (2019), to some extent), resolution (theorised by differences in older and more recent research) and display refresh rate (Katsigiannis et al. (2019)) and decreasing latency variance (Kinsella et al. (2016), Wilson et al. (2020)) can reduce simulator sickness and increase subjective simulator quality and immersion.

Chapter 3

General Discussion and Conclusions

In this literature review, we studied the concept of human motion perception in vehicle simulators. For that purpose, we first described the mechanisms of motion perception as passive systems of sensors. These sensors have a certain threshold for motion perception, perceive motion in a certain time domain (position, velocity, acceleration) and combine their information with other sensors in certain ways. Then, the more active stimulation of the motion sensors was introduced in the form of vehicle simulators. We discussed several boundary conditions that are of importance in vehicle simulators, and moved to the effects of several motion cues on the experience and accuracy of vehicle simulators.

3.1 Discussion and Conclusion

To answer the posed research question at the start of this literature review, *"How is motion perceived accurately by humans in several types of vehicle simulators?"*, it appears there is no single, all-covering answer. As it turns out, human motion perception is a fluid concept in general, where motion sensors have individual thresholds, as well as combined thresholds, dependent on the motion axes. The motion sensors integrate with each other in a variable way, depending on the task and environment. Motion sensors are weighted, compared with each other, compared with expectations, and judged whether the information is coherent (thus accepted) or not.

In short, humans perceive motion in vehicle simulators dependent on two main factors: how the motion is presented to them and what the level and type of involvement in this motion is. On the former subject, many variables exist which can influence the way a certain intended motion is perceived. On an inertial motion level, tilt coordination proves a useful tool across vehicle simulator types, as well as the application of washout motion algorithms, but limitations exist, with the human motion perception system in particular. As for the effects of level of involvement in tasks in vehicle simulators, motion perception remains similar to passive motion perception for tasks on the motion axis that task is performed on, but becomes unpredictable when other motion axes are concerned.

Several motion perception properties are typically transferable across vehicle simulator types (car, motorcycle, aeroplane); velocity is generally underestimated, inertial motion cue intensity is usually preferred to remain below visual motion cue intensity, and may improve human performance in the vehicle simulator. Coherence zones are an important metric in vehicle simulators, which provide insight in this relation between motion cues, for a specific vehicle simulator. On the topic of display system, care must be taken in ensuring the correct level of fidelity as to not cause simulator sickness or increase levels of immersion, thus increasing the level of involvement. Enough literature exists to serve as guidelines for a choice of display properties, where high (virtual) quality, large field-of-view displays prove to be the most effective for the correct interpretation of motion cues, in most cases, if the simulator system allows it. The overview of information on simulator sickness provided in this literature is useful for initial design choices for vehicle simulators, but since this was not the main

subject in the scope of this literature review, this overview could be expanded upon.

Overall, we can say that the vehicle simulator as a concept is dependent on many factors. When performing experiments in them, the effects of boundary conditions which lie outside the human observer must not be neglected, since they largely influence how the motion cues presented to the observer are interpreted.

3.2 Further Research

For further research, there are several avenues where research can improve upon the state-of-the-art of the knowledge of human motion perception in vehicle simulators. The greatest being, in my opinion, researching the effects on motion perception in vehicle simulators where great human influence on motion is present, such as balancing acts, for example within bicycle simulators. Effects of conflicting motion cues on compensatory or balancing movements is particularly interesting in this regard. Research on passive motion perception is abundant, and, while more and more research is published on driving simulators, avenues of expansion remain open on the topic of the effects of efference copy and tactile/proprioceptive motion cues. More scientific studies pointed at motion perception in other types of vehicle simulators - next to automobile, motorcycle and aeroplane simulators - is a direction new research could go into as well, to study effectiveness of motion cueing and task involvement and type into greater detail. More relevant to Tacx, it may also be interesting to investigate differences in sports applications of vehicle simulators - either in driving (for e.g. Formula 1, MotoGP), flight (stunt pilots) or bicycling (e.g. Tour de France).

Recent studies have shown that motion cues which are not regarded as very important previously, turn out to be of greater influence on the motion perception in vehicle simulators than expected. One such example is the introduction of auditory motion cues. I expect this also to be the case with tactile and proprioceptive cues. It is recognised that it is tough to separate effects of individual inertial motion cues and efference copies, in the passive case and more so in the active case, which demands constructive understanding of the human motion perception system for further experiments.

Integrating human motion perception into the motion drive algorithms of simulators is a method of improving the accuracy and representability (of real-world vehicle motion) of perceived motion. While the theoretical models exist, little has been applied in perception-oriented experiments in several types of vehicle simulators. Further research has to produce experimental data on these motion algorithms, such that they can be optimised and the overall experience and the sense of actually driving or piloting the simulated vehicle can be achieved. Ideally, not only human vestibular models are added to these advanced motion drive algorithms, but also less prevalent motion cues, such as tactile, proprioceptive, auditory, or even efference copy. But experimental data on these latter sensory systems in certain vehicles (and vehicle simulators) is required for them to be accurately included in these motion drive algorithms.

More emphasis could be put on the influence of the individual, to study the effects of training, inexperience with vehicle simulators, and the experience with real-world vehicle driving. Some of the presented studies do include short mention of test subject demographics, but since we are considering vehicle simulators, a structured - maybe even standardised - categorisation of test subjects could be implemented more often to be able to judge the applicability of a certain vehicle simulation platform to a greater extent. A number of the presented studies have indicated a difference in motion stimulus interpretation between individuals.

With this literature review, I hope to have informed the reader about a large portion of the considerations to take into account when evaluating, designing or experimenting on vehicle simulators, as well as elevated the reader's understanding of human motion perception in general. With this information, I hope to have achieved a basis upon which new areas of research can be based.

Bibliography

Angelaki, D. and Dickman, J. (2000). Spatiotemporal processing of linear acceleration: primary afferent and central vestibular neuron responses. *Journal of Neurophysiology*, 84(4):2113–2132.

Asadi, H., Mohamed, S., and Lim, C. (2016). Robust optimal motion cueing algorithm based on the linear quadratic regulator method and a genetic algorithm. *IEEE Transactions on Systems, Man and Cybernetics*, 74(2):238–254.

Asadi, H., Mohammadi, A., Lim, C., Mohamed, S., Nahavandi, D., and Nahavandi, S. (2019). Increasing motion fidelity in driving simulators using a fuzzy-based washout filter. *IEEE Transactions on Intelligent Vehicles*, 99:1–1.

Authié, C. and Mestre, D. (2011). Optokinetic nystagmus is elicited by curvilinear optic flow during high speed curve driving. *Vision Research*, 51(16):1791–1800.

Aykent, B., Merienne, F., Chr, G., Paillot, D., and Kemeny, A. (2014). Motion sickness evaluation and comparison for a static driving simulator and a dynamic driving simulator. *Proceedings of the Institution of Mechanical Engineers Part D, Journal of Automobile Engineering.*

Aykent, B., Paillot, D., Merienne, F., Fang, Z., and Kemeny, A. (2011). Study on the influence of different washout algorithms on simulator sickness for a driving simulation task. *ASME 2011 World Conference on Innovative Virtual Reality, ASME*, pages 331–341.

Banks, M., Ehrlich, S., Backus, B., and Crowell, J. (1995). Estimating heading during real and simulated eye movements. *Vision Research*, 36(3):431–443.

Been-Lirn Duh, H., Jeng-Weei Lin, J., Kenyon, R., Parker, D., and Furness, T. (2001). Effects of field of view on balance in immersive environment. *Proceedings IEEE Virtual Reality 2001*, pages 235–240.

Benson, A., Hutt, E., and Brown, S. (1989). Thresholds for the perception of whole-body angular movement about a vertical axis. *Aviation, Space, and Environmental Medicine*, 60(3):205–213.

Benson, A., Spencer, M., and Scott, J. (1986). Thresholds for the detection of the direction of whole-body, linear movement in the horizontal plane. *Aviat. Space Environ. Med.*, 57(11):1088–96.

Benz, T., Riedl, B., and Chuang, L. (2019). Projection displays induce less simulator sickness than head-mounted displays in a real vehicle driving simulator. *In: 11th International Conference on Automotive User Interfaces and Interactive Vehicular Applications (AutomotiveUI '19), September 21–25, 2019, Utrecht, Netherlands.*

Berger, D., Schulte-Pelkum, J., and Bülthoff, H. (2010). Simulating believable forward accelerations on a stewart motion platform. *ACM Transactions on Applied Perception*, 7(1):5:1–5:27.

Berthoz, A., Bles, W., Bülthoff, H., Correia Grácio, B., Feenstra, P., Filliard, N., Hühne, R., Kemeny, A., Mayrhofer, M., Mulder, M., Nusseck, H., Pretto, P., Reymond, G., Schlüsselberger, R., Schwandtner, J., Teufel, H., Vailleau, B., Van Paassen, M., Vidal, M., and Wentink, M. (2013).

Motion scaling for high-performance driving simulators. *IEEE Transactions on Human-Machine Systems*, 43(3):265–276.

Berthoz, A., Pavard, B., and Young, L. (1975). Perception of linear horizontal self-motion induced by peripheral vision (linearvection). basic characteristics and visual- vestibular interactions. *Experimental Brain Research*, 23(5):471–489.

Bertolini, G. and Straumann, D. (2016). Moving in a moving world: A review on vestibular motion sickness. *Frontiers in Neurology*, 7:14.

Bertollini, G., Glaser, Y., Szczerba, J., and Wagner, R. (2014). The effect of motion cueing on simulator comfort, perceived realism and driver performance during low speed turning. *Driving Simulation Conference 2014, Paris, France, September 4-5*.

Bigler, R. (2013). *Automobile driver sensory system modeling*. PhD thesis, Cambridge University.

Bles, W., Bos, J., de Graaf, B., Groen, E., and Wertheim, A. (1998). Motion sickness: only one provocative conflict? *Brain Res Bull*, 47(5):481–7.

Blouin, J., Okada, T., Wolsley, C., and Bronstein, A. (1998). Encoding target-trunk relative position: cervical versus vestibular contribution. *Experimental Brain Research*, 122(1):101–7.

Bos, J. (2015). Less sickness with more motion and/or mental distraction. *Journal of Vestibular Research*, 25(1):23–33.

Bos, J. and Bles, W. (2002). Theoretical considerations on canal-otolith interaction and an observer model. *Biological Cybernetics*, 86:191–207.

Bos, J., Groen, E., and Nooij, S. (2004). Further thoughts on and calculations by spatial orientation and motion sickness modeling. *TNO Defense Technical Report TM-04-I005*.

Bos, J., Hosman, R., and Bles, W. (2002). Visual-vestibular interactions and spatial (dis)orientation in flight and flight simulation. *TNO Defense Technical Report TM-02-C009*.

Brandt, T., Dichgans, J., and Koenig, E. (1973). Differential effects of central versus peripheral vision on egocentric and exocentric motion perception. *Experimental Brain Research*, 16:476–491.

Bridgeman, B. (1995). A review of the role of efference copy in sensory and oculomotor control systems. *Annals of Biomedical Engineering*, 23:409–422.

Britannica, E. (1997). Vestibular system.

Britton, Z. and Arshad, Q. (2019). Vestibular and multi-sensory influences upon self-motion perception and the consequences for human behavior. *Front. Neurol.*, 10:63.

Carlile, S. and Leung, J. (2016). The perception of auditory motion. *Trends in Hearing*, 20:2331216516644254.

Cassin, B. and Solomon, S. (1990). *Dictionary of Eye Terminology*. Triad Publishing Company.

Chardonnet, J., Mirzaei, M., and Merienne, F. (2017). Features of the postural sway signal as indicators to estimate and predict visually induced motion sickness in virtual reality. *International Journal of Human-Computer Interaction*, 33(10):771–785.

Chen, S. and Fu, L. (2010). An optimal washout filter design for a motion platform with senseless and angular scaling maneuvers. *Conference: American Control Conference (ACC), 2010*.

Colombet, F., Fang, Z., and Kemeny, A. (2018). Pitch tilt rendering for an 8-dof driving simulator. *Driving Simulation Conference 2015 Europe VR, Sep. 2015, Tübingen, Germany*, pages 55–61.

Conrad, B. and Schmidt, S. (1970). Motion drive signals for piloted flight simulators. Technical report, Tech. rep. Washington: NASA.

Correia Grácio, B., Bos, J., van Paassen, M., and Mulder, M. (2013a). Perceptual scaling of visual and inertial cues. *Experimental Brain Research*, 232(2).

Correia Grácio, B., Valente Pais, A., van Paassen, M., Mulder, M., Kelly, L., and Houck, J. (2013b). Optimal and coherence zone comparison within and between flight simulators. *Journal of Aircraft*, 50(2):493–507.

Cossalter, V., Lot, R., and Rota, S. (2010). Objective and subjective evaluation of an advanced motorcycle riding simulator. *In: Symposium on the Dynamics and Control of Single Track Vehicles, 20 - 22 October 2010, Delft, The Netherlands.*

Crowell, J. t. (1998). Visual self-motion perception during head turns. *Nature Neuroscience*, 1(8):732–7.

Dagdelen, M., Reymond, G., Kemeny, A., Bordier, M., and Maïzi, N. (2009). Model-based predictive motion cueing strategy for vehicle driving simulators. *Control Engineering Practice*, 17(9):995–1003.

de Winkel, K., Katliar, M., and Bülthoff, H. (2017). Causal inference in multisensory heading estimation. *PLoS ONE*, 12(1).

de Winkel, K., Soyka, F., and Bülthoff, H. (2020). The role of acceleration and jerk in perception of above-threshold surge motion. *Experimental Brain Research*, 238:699–711.

DeAngelis, G. and Angelaki, D. (2012). *Visual-Vestibular Integration for Self-Motion Perceptions.* CRC Press/Taylor & Francis.

Denjean, S., Roussarie, V., Kronland-Martinet, R., Ystad, S., and Velay, J. (2012). How does interior car noise alter driver's perception of motion? multisensory integration in speed perception. *Acoustics.*

Dialynas, G., Schwab, A., and Happee, R. (2019). Design and hardware selection for a bicycle simulator. *Mechanical Sciences*, 10:1–10.

Dichgans, J. and Brandt, T. (1978). *Visual-vestibular interaction: Effects on self-motion perception and postural control. In: Held R., Leibowitz H.W., Teuber, H.L. (eds) Perception. Handbook of Sensory Physiology*, volume 8. Springer, Berlin, Heidelberg.

DiZio, P. and Lackner, J. (1997). Circumventing side effects of immersive virtual environments. *Design of computing system: Social and ergonomic considerations*, 2:893–896.

Dokka, K., DeAngelis, G., and Angelaki, D. (2015). Multisensory integration of visual and vestibular signals improves heading discrimination in the presence of a moving object. *The Journal of Neuroscience*, 35(40):13599–13607.

Duffy, C. and Wurtz, R. (1993). An illusory transformation of optic flow fields. *Vision Research*, 33:1481–1490.

Dunbar, B. (2004). Human vestibular system in space.

Duncan, B. (1995). Calibration trials of the trl driving simulator. trl report pa/3079/95. *Transport Research Laboratory, Crawthorne, U.K.*

Fang, Z., Colombet, F., Collinet, J., and Kemeny, A. (2015). Roll tilt thresholds for 8 dof driving simulators. *Driving Simulator Conference, Paris, France, September 4–5, 2014.*

Fetsch, C., DeAngelis, G., and Angelaki, D. (2010). Visual-vestibular cue integration for heading perception: Applications of optimal cue integration theory. *European Journal of Neuroscience*, 31:1721–9.

Fetsch, C., Turner, A., DeAngelis, G., and Angelaki, D. (2009). Dynamic reweighting of visual and vestibular cues during self-motion perception. *Journal of Neuroscience*, 29(49):15601–12.

Fischer, M. and Werneke, J. (2008). The new time-invariant motion cueing algorithm for the dlr dynamic driving simulator. *Proceedings of the Driving Simulation Conference (DSC Europe 2008)*.

Foulkes, A. and Miall, R. (2000). Adaptation to visual feedback delays in a human manual tracking task. *Experimental Brain Research*, 131(1):101–10.

Frenz, H., Lappe, M., Kolesnik, M., and Bührmann, T. (2007). Estimation of travel distance from visual motion in virtual environments. *ACM Trans. Appl. Percept.*, 4:3.

Fujii, Y. and Seno, T. (2020). The effect of optical flow motion direction on vection strength. *i-Perception*, 11(1).

Gegenfurtner, K. (1999). Seeing movement in the dark. *Nature*, 398:475–476.

Gibson, J. (1950). *The Perception of the Visual World*. Houghton Mifflin.

Gioanni, H. and Sansonetti, A. (1999). Characteristics of slow and fast phases of the optocollic reflex (ocr) in head free pigeons. *European Journal of Neuroscience*, 11(1):155–166.

Grabherr, L., Nicoucar, K., Mast, F., and Merfeld, D. (2008). Vestibular thresholds for yaw rotation about an earth-vertical axis as a function of frequency. *Experimental Brain Research*, 186:677–681.

Gray, L. (2020). *Neuroscience Online; Chapter 10: Vestibular System: Structure and Function*. The University of Texas Health Science Center at Houston (UTHealth).

Greenberg, J., Artz, B., and Cathey, L. (2003). The effect of lateral motion cues during simulated driving. *Proc. Driving Simul. Conf.*

Groeger, J., Carsten, O., Blana, E., and Jamson, E. (1997). Speed and distance estimation during simulated driving. *In: A.G. Gale, I.D. Brown, C.M. Haslegrave & S.P. Taylor (eds.), Vision in Vehicles VII*.

Groen, E. and Bles, W. (2004). How to use body tilt for the simulation of linear self motion. *Journal of Vestibular Research: Equilibrium & Orientation*, 14(5):375–85.

Groen, E. and Bos, J. (2008). Simulator sickness depends on frequency of the simulator motion mismatch: An observation. *PRESENCE: Teleoperators and Virtual Environments*, 17(6):584–593.

Groen, E., Clari, M., and Hosman, R. (2007). Perception model analysis of flight simulator motion for a decrab maneuver. *Journal of Aircraft*, 44(2):427–435.

Groen, E., Howard, I., and Cheung, B. (1999). Influence of body roll on visually induced sensation of self-tilt and rotation. *Perception*, 28(3):287–297.

Groen, E., Valenti Clari, M., and Hosman, R. (2001). Evaluation of perceived motion during a simulated takeoff run. *Journal of Aircraft*, 38(4).

Groen, E., Wentink, M., Valente Pais, A., Mulder, M., and van Paassen, M. (2006). Motion perception thresholds in flight simulation. *AIAA modeling and simulation technologies conference and exhibit, American Institute of Aeronautics and Astronautics, Reston, Virigina*, page e6254.

Grottoli, M. (2020). *Development and evaluation of a motorcycle riding simulator for low speed maneuvering*. PhD thesis, Delft University of Technology.

Gu, Y., Angelaki, D., and Deangelis, G. (2008). Neural correlates of multisensory cue integration in macaque mstd. *Nat. Neurosci.*, 11(10):1201–1210.

Guignard, J. and McCauley, M. (1991). *The accelerative stimulus for motion sickness. In: Crampton GH (ed.), Motion and Space Sick-ness*. FL: CRC Press, Inc.

Gundry, A. (1978). Thresholds of perception for periodic linear motion. *Aviat. Space Environ. Med.*, 49(5):679–86.

Gurnee, H. (1931). The effect of a visual stimulus upon the perception of bodily motion. *The American Journal of Psychology*, 42(1):26–48.

Harris, J. (2001). The future of flow? *Trends in Cognitive Sciences*, 5(1):7–8.

Harris, J. and Rogers, B. (1999). Going against the flow. *Trends in Cognitive Sciences*, 3(12):449–450.

Harris, L., Jenkin, M., and Zikovitz, D. (2000). Visual and non-visual cues in the perception of linear self motion. *Experimental Brain Research*, 135(1):12–21.

Harris, L., Jenkin, M., Zikovitz, D., Redlick, F., Jaekl, P., Jasiobedzka, U., Jenkin, H., and Allison, R. (2001). *Simulating Self-Motion I: Cues for the Perception of Motion*. Centre for Vision Research and Departments of Computer Science, Psychology and Biology, York University.

Harris, L., Sakurai, K., and Beaudot, W. (2017). Tactile flow overrides other cues to self motion. *Scientific Reports*, 7(1059).

Hays, R., Jacobs, J., Prince, C., and Salas, E. (1992). Flight simulator training effectiveness: A meta-analysis. *Military Psychology*, 4(2):63–74.

Heerspink, H., Berkouwer, W., Stroosma, O., van Paassen, M., Mulder, M., and Mulder, J. (2005). Evaluation of vestibular thresholds for motion detection in the simona research simulator. *AIAA Modeling and Simulation Technologies Conference and Exhibit, 15 - 18 August 2005, San Fransisco, California*.

Held, R., Dichgans, J., and Bauer, J. (1975). Characteristics of moving visual scenes influencing spatial orientation. *Vision Research*, 15(3):357–365.

Hernández-Melgarejo, G., Flores-Hernández, D., Luviano-Juárez, A., Castañeda, L., Chairez, I., and Di Gennaro, S. (2019). Mechatronic design and implementation of a bicycle virtual reality system. *ISA Transactions*, 97:336–351.

Horswill, M. and Plooy, A. (2008). Auditory feedback influences perceived driving speeds. *Perception*, 37(7):1036–43.

Hosman, R. and van der Vaart, J. (1978). Vestibular models and thresholds of motion perception: results of tests in a flight simulator. Technical report, Delft University of Technology.

Howard, I. (1968). *Handbook of Perception and Human Performance*, volume I. Wiley-Interscience.

Hultgren, J., Blissing, B., and Jansson, J. (2012). Effects of motion parallax in driving simulators. *Proceedings of the Driving Simulation Conference Europe 2012*.

Jacobs, K. (2011). *Encyclopedia of Clinical Neuropsychology*. Springer, New York, NY.

Jamson, A. (2010). *Motion Cueing in Driving Simulators for Research Applications*. PhD thesis, The University of Leeds.

Jamson, H. (2000). Driving simulation validity: issues of field of view and resolution. *Proc. Driving Simul. Conf.*, pages 57–64.

Jmvolc (2006). "three rotational degrees of freedom of a ship or boat" and "three linear degrees of freedom of a boat or ship".

Johnson, D. (2005). Introduction to and review of simulator sickness research. *U.S. Army Research Institute for the Behavioral and Social Sciences*.

Juang, J., Hung, W., and Kang, S. (2013). A crane simulator with kinesthetic and stereoscopic vision. *Advanced Engineering Informatics*, 27:506–518.

Kapralos, B., Zikovitz, D., Jenkin, M., and Harris, L. (2004). Auditory cues in the perception of self-motion. *Audio Engineering Society Convention Paper, 116th Convention*.

Katsigiannis, S., Willis, R., and Ramzan, N. (2019). A qoe and simulator sickness evaluation of a smart-exercise-bike virtual reality system via user feedback and physiological signals. *IEEE Transactions on Consumer Electronics*, pages 119–127.

Kemeny, A. and Panerai, F. (2003). Evaluating perception in driving simulation experiments. *Trends in Cognitive Science*, 7(1):31–37.

Kennedy, R. and Lane, N. (1993). Simulator sickness questionnaire: An enhanced method for quantifying simulator sickness. *International Journal of Aviation Psychology*, 3(3):203–220.

Kennedy, R., Lilienthal, M., Berbaum, K., Berbaum, D., and McCauley, M. (1989). Simulator sickness in u.s. navy flight simulators. *Aviation, Space and Environmental Medicine*, 60(1):10–6.

Kenyon, R. and Kneller, E. (1993). The effects of field of view size on the control of roll motion. *IEEE Transactions on Systems, Man, and Cybernetics*, 23(1):183–196.

Khan, S. and Chang, G. (2013). Anatomy of the vestibular system: A review. *Neurorehabilitation*, 32(3):437–43.

Kingma, H. (2005). Thresholds for perception of direction of linear acceleration as a possible evaluation of the otolith function. *BMC Ear, Nose and Throat Disorders*, 5:5.

Kinsella, A., Mattfield, R., Muth, E., and Hoover, A. (2016). Frequency, not amplitude, of latency affects subjective sickness in a head-mounted display. *Aerospace Medicine and Human Performance*, 87(7):604–609.

Kuiper, O., Bos, J., and Diels, C. (2019). Vection does not necessitate visually induced motion sickness. *Displays*, 58:82–87.

Land, M. (1992). Predictable eye-head coordination during driving. *Nature*, 359:318–320.

Land, M. and Horwood, J. (1995). Which parts of the road guide steering? *Nature*, 377:339–340.

Land, M. and Lee, D. (1994). Where we look when we steer. *Nature*, 369(6483):742–744.

Lappe, M., Bremmer, and F. van den Berg, A. (1999). Perception of self-motion from visual flow. *Trends in Cognitive Sciences*.

Lawther, A. and Griffin, M. (1988). Motion sickness and motion characteristics of vessels at sea. *Ergonomics*, 31(10):1373–1394.

Lewkowicz, R. (2016). Modelling motion sickness. *Pol. J. Aviat. Bioeng. Psychol.*, 22(3):32–42.

Limanowski, J. and Friston, K. (2020). Active inference under visio-proprioceptive conflict: Simulation and empirical results. *Scientific Reports*, 10(4010).

Lin, J., Duh, H. B., Abi-Rached, H., Parker, D., and Furness, T. (2002). Effects of field of view on presence, enjoyment, memory and simulator sickness in a virtual environment. *Proceedings of the IEEE Virtual Reality 2002 (VR'02).*

Lo, W. and So, R. (2001). Cybersickness in the presence of scene rotational movements along different axes. *Applied Ergonomics*, 32(1):1–14.

Loomis, J. and Knapp, J. (1999). Visual perception of egocentric distance in real and virtual environments. *L.J. Hettinger & M.W. Haas (eds.), Virtual and adaptive environments.*

Lutfi, R. and Wang, W. (1999). Correlated analysis of acoustic cues for the discrimination of auditory motion. *Journal of the Acoustical Society of America*, 106(2):919–928.

MacNeilage, P., Banks, M., Berger, D., and Bülthoff, H. (2007). A bayesian model of the disambiguation of gravitoinertial force by visual cues. *Experimental Brain Research*, 179(2):263–290.

Malik, H., Rasool, S., Maqsood, A., and Riaz, R. (2020). Effect of haptic feedback on pilot/operator performance during flight simulation. *Applied Sciences*, 10(11):3877.

Matsangas, P., McCauley, M., and Becker, W. (2014). The effect of mild motion sickness and sopite syndrome on multitasking cognitive performance. *Human Factors*, 56(6).

McGrath, B., Lawson, B., Newman, M., and Rupert, A. (2015). An algorithm to improve ground-based spatial disorientation training. *Proceedings of the American Institute of Aeronautics and Astronautics, 7 Jan., Virginia beach.*

Mergner, T. and Becker, W. (1990). *Perception and Control of Self Motion.* Lawrence Erlbaum Associates, Inc.

Meyer, G., Wong, L., Timson, E., Perfect, P., and White, M. (2012). Objective fidelity evaluation in multisensory virtual environments: Auditory cue fidelity in flight simulation. *PLoS ONE*, 7(9):e44381.

Mittelstaedt, J., Wacker, J., and Stelling, D. (2018). Effects of display type and motion control on cybersickness in a virtual bike simulator. *Displays*, 51:43–50.

Mohellebi, H., Kheddar, A., and Espié, S. (2009). Adaptive haptic feedback steering wheel for driving simulators. *IEEE Transactions on vehicular technology*, 58(4):1654–1666.

Mourant, R. and Sadhu, P. (2002). Evaluation of force feedback steering in a fixed base driving simulator. *Paper presented at the 46th Human Factors and Ergonomics Society Annual Meeting, Baltimore, MD.*

Murai, K., Hayashi, Y., and Matsumoto, T. (2010). Evaluation of body sway in artificial ship rolling and pitching. *3rd International Conference on Emerging Trends in Engineering and Technology*, pages 110–115.

Nakamura, T. and Bronstein, A. (1995). The perception of head and neck angular displacement in normal and labyrinthine-defective subjects: a quantitative study using a 'remembered saccade' technique. *Brain*, 118(5):1157–68.

Nash, C., Cole, D., and Bigler, R. (2016). A review of human sensory dynamics for application to models of driver steering and speed control. *Biological Cybernetics*, 110:91–116.

Natal, G., Arjoni, D., de Oliveira, W., Rodamilans, G., de Silva, E., Silveira, L., Villani, E., and Trabasso, L. (2019). Implementation analysis of a washout filter on a robotic flight simulator - a case study. *Journal of Aerospace Technology and Management*, 11:e0919.

Newman, D. (2007). An overview of spatial disorientation as a factor in aviation accidents and incidents, atsb transport safety investigation report - b2007/0063. Technical report, Australian Transport Safety Bureau.

Newman, M., Lawson, B., Rupert, A., and McGrath, B. (2012). The role of perceptual modeling in the understanding of spatial disorientation during flight and ground-based simulator training. *Proceedings of the American Institute of Aeronautics and Astronautics, 15. Aug., Minneapolis, MN*.

Niemann, T., Lappe, M., Büscher, A., and Hoffmann, K. (1999). Ocular responses to radial optic flow and single accelerated targets in humans. *Vision Research*, 39(7):1359–1371.

of Technology, D. U. (2020). Tu delft: Simona.

Ohta, H. and Komatsu, H. (1991). Speed perception in driving - comparison with tv observation. *Vision in Vehicles, III*.

Oman, C. (1982). A heuristic mathematical model for the dynamics of sensory conflict and motion sickness. *Acta Oto-Laryagologica*, 94(392):4–44.

Oman, C. (1998). Sensory conflict theory and space sickness: our changing perspective. *Journal of Vestibular Research*, 8(1):51–56.

Page, N. and Gresty, M. (1985). Motorist's vestibular disorientation syndrome. *J. Neurol. Neurosurg. Psychiatry*, 48(8):729–735.

Parduzi, A., Venrooij, J., and Marker, S. (2020). The effect of head-mounted displays on the behavioural validity of driving simulators. *Driving Simulation 2020 Proceedings*.

Perrot, D., Costantino, B., and Ball, J. (1993). Discrimination of moving events which accelerate or deccelerate over the listening interval. *Journal of the Acoustical Society of America*, 93:1053–1057.

Pinto, M., Cavallo, V., and Ohlmann, T. (2008). The development of driving simulators: towards a multisensory solution. *Le Travail Humain*, 71:62–95.

Pool, D. (2012). *Objective Evaluation of Flight Simulator Motion Cueing Fidelity Through a Cybernetic Approach*. PhD thesis, Delft University of Technology.

Pretto, P., Nesti, A., Nooij, S., Losert, M., and Bülthoff, H. (2014). Variable roll-rate perception in driving simulation. *Driving simulation conference*, 3(1):1–7.

Previc, F., Varner, D., and Gillingham, K. (1992). Visual scene effects on the somatogravic illusion. *Aviat. Space Environ. Med.*, 63:1060–1064.

Proske, U. and Gandevia, S. (2012). The proprioceptive senses: Their roles in signaling body shape, body position and movement, and muscle force. *Physiological Reviews*, 92(4):1651–1697.

Prothero, J. and Hoffman, H. (1995). Widening the field-of-view increases the sense of presence within immersive virtual environments. *Human Interface Technology Laboratory Tech. Rep., R-95-4*.

Qazani, M., Asadi, H., Mohamed, S., and Nahavandi, S. (2020). Prepositioning of a land vehicle simulation-based motion platform using fuzzy logic and neural network. *IEEE Transactions on Vehicular Technology*, 69(10):10446–10456.

Qian, N. (1997). Binocular disparity and the perception of depth. *Neuron*, 18:359–368.

Ramkhalawansingh, R., Keshavarz, B., Haycock, B., Shahab, S., and Campos, J. (2016a). Age differences in visual-auditory self-motion perception during a simulated driving task. *Frontiers in Psychology*, 7:595.

Ramkhalawansingh, R., Keshavarz, B., Haycock, B., Shahab, S., and Campos, J. (2016b). Examining the effect of age on visual-vestibular self-motion perception using a driving paradigm. *Perception*, 46:566–85.

Raphan, T., Matsuo, V., and Cohen, B. (1979). Velocity storage in the vestibulo-ocular reflex arc (vor). *Experimental Brain Research*, 35:229–248.

Reason, J. (1978). Motion sickness adaptation: A neural mismatch model. *Proceedings of the Royal Society of Medicine*, 71(11):819–829.

Reason, J. and Brand, J. (1975). *Motion sickness*. Academic Press.

Redlick, F., Jenkin, M., and Harris, L. (2001). Humans can use optic flow to estimate distance of travel. *Vision Research*, 41:213–219.

Regan, D. and Beverly, K. (1982). How do we avoid confounding the direction we are looking and the direction we are moving? *Science*, 215(4529):194–196.

Reymond, G. and Kemeny, A. (2000). Motion cueing in the renault driving simulator. *Vehicle System Dynamics*, 34(4):249–259.

Reymond, G., Kemeny, A., Droulez, J., and Berthoz, A. (2001). Role of lateral acceleration in curve driving: driver model and experiments on a real vehicle and a driving simulator. *Human Factors*, 43(3):483–95.

Riccio, D. and Stoffregen, T. (1991). An ecological theory of motion sickness and postural instability. *Ecol Psychol*, 3:195–240.

Roark, M. and Junker, A. (1978). The effects of closed loop tracking on a subjective tilt threshold in the roll axis. *Proceedings of the 14th Annual Conference on Manual Control, Los Angeles and Moffet Field, CA, USA, April 25-27*, pages 443–450.

Rogers, B. and Dalton, C. (1999). The role of (i) perceived direction and (ii) optic flow in the control of locomotion and for estimating the point of impact. *Invest. Ophthalmol. Vis. Sci.*, 40(764).

Rosenblum, L., Carello, C., and Pastore, R. (1987). Relative effectiveness of three stimulus variables for locating a moving sound source. *Perception*, 16:175–186.

Royden, C. (1994). Analysis of misperceived observer motion during simulated eye rotations. *Vision Research*, 34(23):3215–3222.

Royden, C., Crowell, J., and Banks, M. (1994). Estimating heading during eye movements. *Vision Research*, 34(23):3197–3214.

Rushton, S. t. (1998). Guidance of locomotion on foot uses perceived target location rather than optic flow. *Current Biology*, 8(21):1191–1194.

Samji, A. and Reid, L. (1992). The detection of low-amplitude yawing motion transients in a flight simulator. *IEEE Trans. Syst. Man. Cybern.*, 22(2):300–306.

Schepers, J., Den Brinker, B., De Waard, D., Twisk, D., Schwab, A., and Smeets, J. (2013). Studying the role of vision in cycling. *Accident Analysis and Prevention*, 59:466–468.

Scilingo, E., Sgambelluri, N., and Bicchi, A. (2008). *The Role of Tactile Flow in Processing Dynamic Haptic Stimuli. In: Bicchi, A., Buss, M., Ernst, M.O., Peer, A. (eds) The Sense of Touch and its Rendering.* Springer, Berlin, Heidelberg.

Seno, T., Ito, H., and Sunaga, S. (2011a). Attentional load inhibits vection. *Attention, Perception & Psychophysics*, 73:1467–1476.

Seno, T., Murata, K., Fujii, Y., Kanaya, H., Ogawa, M., Tokunaga, K., and Palmisano, S. (2018). Vection is enhanced by increased exposure to optic flow. *i-Perception*, 9(3):1–16.

Seno, T., Ogawa, M., Hiroyuki, I., and Sunaga, S. (2011b). Consistent air flow to the face facilitates vection. *Perception*, 40(10):1237–1240.

Shahar, A., Dagonneau, V., Caro, S., Israël, I., and Lobjois, R. (2014). Towards identifying the roll motion parameters of a motorcycle simulator. *Applied Ergonomics*, 45(3):734–740.

Siegle, J., Campos, J., Mohler, B., Loomis, J., and Bülthoff, H. (2009). Measurement of instantaneous perceived self-motion using continuous pointing. *Experimental Brain Research*, 195:429–444.

Sivan, R., Ish-Shalom, J., and Huang, J. (1982). An optimal control approach to the design of moving flight simulators. *IEEE Transactions on Systems, Man, and Cybernetics*, 12(6):818–827.

Snowden, R. (1998). Speed perception fogs up as visibility drops. *Nature*, 392:450.

Soyka, F., Giordano, P., Barnett-Cowan, M., and Bülthoff, H. (2012). Modeling direction discrimination thresholds for yaw rotations around an earth-vertical axis for arbitrary motion profiles. *Experimental Brain Research*, 220(1):89–99.

Soyka, F., Giordano, P., Beykirch, K., and Bülthoff, H. (2011). Predicting direction detection thresholds for arbitrary translational acceleration profiles in the horizontal plane. *Experimental Brain Research*, 209(1):95–107.

Spiegelhalter, D. and Rice, K. (2009). Bayesian statistics. *Scholarpedia*, 4(8):5230.

Stoffregen, T., Hettinger, L., Haas, M., Roe, M., and L.J., S. (2000). Postural instability and motion sickness in a fixed-base flight simulator. *Human Factors*, 42(3):458–469.

Stoffregen, T. and Smart, L. (1998). Postural instability precedes motion sickness. *Brain Research Bulletin*, 47(5):437–438.

Suri, K. and Clark, T. (2020). Human vestibular perceptual thresholds for pitch tilt are slightly worse than for roll tilt across a range of frequencies. *Experimental Brain Research*, 238:1499–1509.

Tuthill, J. and Azim, E. (2018). Proprioception. *Current Biology*, 28(5):194–203.

Valente Pais, A. (2013). *Perception Coherence Zones in Vehicle Simulation.* PhD thesis, Delft University of Technology, Faculty of Aerospace Engineering.

Valente Pais, A., Grácio, B., Kelly, L., and Houck, J. (2015). Comparison of flight simulators based on human motion perception metrics. *NASA Technical Reports Server - Report NASA TM–2015-21868.*

Valente Pais, A., Pool, D., de Vroome, A., van Paassen, M., and Mulder, M. (2012). Pitch motion perception thresholds during passive and active tasks. *Journal of Guidance, Control & Dynamics*, 35(3):904–918.

Valente Pais, A., Wentink, M., van Paassen, M., and Mulder, M. (2009a). Comparison of three motion cueing algorithms for curve driving in an urban environment. *Presence: Teleoperators & Virtual Environments*, 18(3):200–221.

Valente Pais, A., Wentink, M., van Paassen, M., and Mulder, M. (2009b). Comparison of three motion cueing algorithms for curve driving in an urban environment. *Presence Teleoperators & Virtual Environments*, 18(3):200–221.

van Asten, W., Gielen, C., and van der Gon, J. (1988). Postural adjustments induced by simulated motion of differently structured environments. *Experimental Brain Research*, 73:371–383.

van Baelen, D., Ellerbroek, J., van Paassen, R., and Mulder, M. (2018). Design of a haptic feedback system for flight envelope protection. *In Proceedings of the 2018 AIAA Modeling and Simulation Technologies conference: Kissimmee, Florida.*

Van Boxtel, J., Van Ee, R., and Erkelens, C. (2006). A single system explains human speed perception. *Journal of Cognitive Neuroscience*, 18(11):1808–19.

Van de Grind, W. (1988). The possible structure and role of neuronal smart mechanisms in vision. *Cognitive Systems*, 2(2):163–180.

Van der Steen, F. (1998). *Self-Motion Perception.* PhD thesis, Delft University of Technology, Faculty of Aerospace Engineering.

van Hofsten, C. (1976). The role of convergence in visual space perception. *Vision Research*, 16(2):193–198.

Vansteenkiste, P., Cardon, G., D'Hondt, E., Philippaerts, R., and Lenoir, M. (2013). The visual control of bicycle steering: The effects of speed and path width. *Accident Analysis and Prevention*, 51:222–227.

VSimulation (2020). Vsimulation: Projects.

Warren, W. (2003). Optic flow. *In: Chalupa, L.M. & Werner, J.S. (eds.): The visual neurosciences. Cambridge, MA: MIT PRess.*

Warren Jr., W. and Hannon, D. (1990). Eye movements and optical flow. *J. Opt. Soc. Am. Ser. A, Optics and image science*, 7(1):160–9.

Wendel, K. (2019). Bicycle-rider control identification: A literature review. Master's thesis, Delft University of Technology.

Westerhof, B. (2017). Evaluation of the cruden motorcycle simulator. Master's thesis, Delft University of Technology.

Wiktionary (2020). Wiktionary, the free dictionary.

Will, S. (2017). *Development of a presence model for driving simulators based on speed perception in a motorcycle riding simulator.* PhD thesis, Julius-Maximilians-Universität Würzburg.

Wilson, M., Beadle, S., Kinsella, A., Mattfield, R., Hoover, A., and Muth, E. (2020). Task performance in a head-mounted display: The impacts of varying latency. *Displays*, 61.

Wynne, R., Beanland, V., and Salmon, P. (2019). Systematic review of driving simulator validation studies. *Safety Science*, 117:138–151.

Yap, H., Tan, C., Taha, Z., Chang, S., Sivadas, C., and Wan, W. (2018). Design and development of a spatial immersive track cycling simulator. *Malaysian Journal of Movement, Health and Exercise*, 7(2).

Young, L., Dichgans, J., Murphy, R., and Brandt, T. (1973). Interaction of optokinetic and vestibular stimuli in motion perception. *Acta Oto-Laryngologica*, 76:24–31.

Zaichik, L., Rodchenko, V., Rufov, I., Yashin, Y., and White, A. (1999). Acceleration perception. *Proceedings of the AIAA Modeling and Simulation Technologies Conference and Exhibit, Portland (OR)*.

Zikmund, P., Dubnický, L., Horpatzká, M., Macík, M., and Jebáček, I. (2019). Flight test of pilot-aircraft haptic feedback system. *MATEC Web of Conferences*, 304:06005.